

AD-A065 144

PRATT AND WHITNEY AIRCRAFT GROUP WEST PALM BEACH FL 6--ETC F/6 21/5  
LO-FREQUENCY AUGMENTOR INSTABILITY STUDY.(U)

DEC 78 P L RUSSELL, G BRANT

F33615-76-C-2024

UNCLASSIFIED

PWA-FR-10397

AFAPL-TR-78-82

NL

1 of 3  
AD  
A065144



AFAPL-TR-78-82

**LEVEL** *IV*

*2*

ADA065144

# LO-FREQUENCY AUGMENTOR INSTABILITY INVESTIGATION

*study.*

P. L. Russell, G. Brant  
Pratt & Whitney Aircraft Group  
Division of United Technologies Corporation  
Box 2691, West Palm Beach, Florida 33402



December 1978

Final Report for Period 1 March 1976 Through 30 July 1978

Approved for Public Release: Distribution Unlimited

Prepared for

Air Force Aero Propulsion Laboratory  
Air Force Wright Aeronautical Laboratories  
Air Force Systems Command  
Wright-Patterson Air Force Base, Ohio 45433

DDC FILE COPY

79 02 27 004

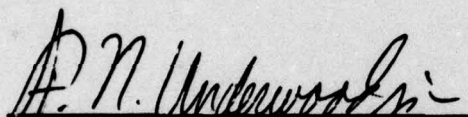


## NOTICE

When Government drawings, specifications, or other data are used for any purpose other than in connection with a definitely related Government procurement operation, the United States Government thereby incurs no responsibility nor any obligation whatsoever; and the fact that the Government may have formulated, furnished, or in any way supplied the said drawings, specifications, or other data, is not to be regarded by implication or otherwise as in any manner licensing the holder or any other person or corporation, or conveying any rights or permission to manufacture, use, or sell any patented invention that may in any way be related thereto.

This report has been reviewed by the Information Office (IO) and is releasable to the National Technical Information Service (NTIS). At NTIS, it will be available to the general public, including foreign nations.

This technical report has been reviewed and is approved for publication.

  
F. N. UNDERWOOD, Captain, USAF  
Project Engineer

  
JOSEPH E. HURST, Major, USAF  
Chief, Components Branch

FOR THE COMMANDER

  
ERNEST C. SIMPSON  
Director, Turbine Engine Division

Copies of this report should not be returned unless return is required by security considerations, contractual obligations, or notice on a specific document.

UNCLASSIFIED

SECURITY CLASSIFICATION OF THIS PAGE (When Data Entered)

REPORT DOCUMENTATION PAGE		READ INSTRUCTIONS BEFORE COMPLETING FORM	
1. REPORT NUMBER AFAPL TR-78-82	2. GOVT ACCESSION NO.	3. RECIPIENT'S CATALOG NUMBER 9	
4. TITLE (and Subtitle) LO-FREQUENCY AUGMENTOR INSTABILITY STUDY,		5. TYPE OF REPORT & PERIOD COVERED Final Report, 1 Mar 1976 to 30 July 1978,	
7. AUTHOR(s) P. L. Russell / G. Brant		6. PERFORMING ORG. REPORT NUMBER PWA - FR-10397	
9. PERFORMING ORGANIZATION NAME AND ADDRESS United Technologies Corporation Pratt & Whitney Aircraft Group Government Products Division West Palm Beach, FL 33402		8. CONTRACT OR GRANT NUMBER(s) F33615-76-C-2024	
11. CONTROLLING OFFICE NAME AND ADDRESS 11/15 Dec 78 12/23/78		10. PROGRAM ELEMENT, PROJECT, TASK AREA & WORK UNIT NUMBERS 16 3066 05 30	
14. MONITORING AGENCY NAME & ADDRESS (if different from Controlling Office) Air Force Aero Propulsion Laboratory (TBC) Wright-Patterson Air Force Base, Ohio 45433		12. REPORT DATE 12-15-78	
		13. NUMBER OF PAGES 212	
		15. SECURITY CLASS. (of this report) Unclassified	
		15a. DECLASSIFICATION/DOWNGRADING SCHEDULE	
16. DISTRIBUTION STATEMENT (of this Report) Approved for public release; distribution unlimited			
17. DISTRIBUTION STATEMENT (of the abstract entered in Block 20, if different from Report)			
18. SUPPLEMENTARY NOTES			
19. KEY WORDS (Continue on reverse side if necessary and identify by block number) Flameholder                      Afterburner Combustion Stability              Combustion Efficiency Augmentors                      Turbofan			
20. ABSTRACT (Continue on reverse side if necessary and identify by block number) With the advent of the mixed-flow afterburner in turbofan engines, a type of low-frequency instability known as rumble became a serious problem. Rumble occurs mainly at high fuel-air ratios and at flight Mach numbers and altitudes where low duct inlet air temperatures and pressures exist. 'Cut and try' methods of solution during engine development have been partially successful, but very expensive. To aid the development engineer in designing rumble-free afterburners an analytical model has been formed. The model was evolved in conjunction with and checked by two experimental programs. Rumble mechanisms investigated early in this			

DD FORM 1 JAN 73 1473 EDITION OF 1 NOV 65 IS OBSOLETE

UNCLASSIFIED

SECURITY CLASSIFICATION OF THIS PAGE (When Data Entered)

392 887 79 02 27 004 LB



UNCLASSIFIED

SECURITY CLASSIFICATION OF THIS PAGE(When Data Entered)

study involved system airflow dynamics, combustion efficiency oscillations, fuel vaporization and recirculation wake energy. The model was then refined and extended to include the mixed flow experienced in a turbofan augmentor. Predictions were made for the effects of altitude, fan stream fuel-air ratio, fan stream temperature, core stream fuel-air ratio, and fan duct pressure loss. The major conclusion from the modeling effort was that the efficiency falloff in the fan stream at high fuel-air ratio causes rumble. This was verified with engine altitude tests at NASA Lewis Research Center with several augmentor configurations. These tests included heat addition to the fan stream, fuel-air distribution changes and spraybar to flameholder length variation. The basic formulation of the model, the mixed flow augmentor model, predictions, and the experimental programs are discussed.

UNCLASSIFIED

SECURITY CLASSIFICATION OF THIS PAGE(When Data Entered)



## FOREWORD

This final report was prepared in accordance with Contract F33615-76-C-2024, Project No. 3066, Task No. 05, Lo-Frequency Augmentor Instability Study. The work was conducted under the direction of Captain F. N. Underwood, Project Engineer, TBC of the Air Force Aero Propulsion Laboratory. The Naval Air Propulsion Center cosponsored the contract and Mr. W. W. Wagner, was the Navy Program Monitor. This report, submitted 31 August 1978, presents the work conducted by Pratt & Whitney Aircraft Group, Government Products Division of United Technologies Corporation, Box 2691, West Palm Beach, Florida 33402, during the period 1 March 1976 through 31 July 1978. G. Petrino, R. Murphy and G. Brant were the principal investigators under the direction of P. L. Russell, the Program Manager for Pratt & Whitney Aircraft Group.

ACCESSION for	
NTIS	
DDC	White Section <input checked="" type="checkbox"/>
UNANNOUNCED	Buff Section <input type="checkbox"/>
JUSTIFICATION	<input type="checkbox"/>
BY	
DISTRIBUTION/AVAILABILITY CODES	
A	SPECIAL

## TABLES OF CONTENTS

Section		Page
I	INTRODUCTION.....	1
II	TECHNICAL DISCUSSION.....	2
	1. Phase I — Model Development.....	2
	2. Phase II — Model Refinement and Extension.....	54
	3. Phase III — Model Demonstration.....	87
	4. Phase IV — Swirl Augmentor Model Verification.....	120
	5. Results, Conclusions and Recommendations.....	130
	APPENDIX A.....	135
	APPENDIX B.....	145
	APPENDIX C.....	147
	APPENDIX D.....	165
	APPENDIX E.....	185
	REFERENCES.....	211

## LIST OF ILLUSTRATIONS

<i>Figure</i>		<i>Page</i>
1	Augmentor Rig Math Model Schematic.....	3
2	Typical Section of Augmentor Rig.....	3
3	Augmentor Efficiency Correlation from Reference 1.....	4
4	Ideal Temperature Rise for Constant Pressure Combustion of Hydrocarbon Fuels.....	4
5	Typical Combustion Temperature Profiles.....	5
6	Steps in Augmentor Combustion Process.....	10
7	Condition for Rumble.....	15
8	Open Loop Transfer Function Baseline Configuration.....	15
9	System Instability Study Test Rig.....	17
10	Rig Hardware.....	18
11	Inlet Case.....	19
12	Fuel Injection Case.....	19
13	Fuel Spraybars.....	20
14	Spray Direction and Pintel Location With Liquid Fuel Injectors.....	21
15	Combustion Case.....	21
16	Flame Holders.....	22
17	Transition Flange.....	23
18	Geometric Nozzle Area Extremes.....	24
19	Nozzle Actuator Assembly.....	25
20	Kistler Model 606A Installed in Water Cooled Adapter.....	28
21	Flameholder Skin Thermocouple Locations.....	28
22	Lo-Frequency Augmentor Instability Investigation Test Matrix.....	29
23	Lo-Frequency Augmentor Model and Flameholder Model Rig Tests.....	30
24	Typical Rumble Induced Blowout O-Graph Traces (50% Flameholder Blockage).....	33



## LIST OF ILLUSTRATIONS (Continued)

<i>Figure</i>		<i>Page</i>
25	Transfer Function and Phase Angle Data for Test Point 1, Baseline, Run Number 7.01, Data Point 22.....	34
26	Fuel Distribution Affects Combustion Stability.....	35
27	JP4 Fuel Air Distribution Used to Isolate Rumble Mechanisms.....	36
28	Rumble Amplitude Correlated With Fuel-Air Ratio and Stability Parameter, Test Point 1.....	38
29	The Effect of Cold Duct Length on Stability. A Comparison of Test Point 11 and Test Point 3.....	39
30	Comparison of Liquid JP4 Test Point 1 Fuel and Gaseous Methane Fuel Test Point 2 With Same Test Configuration.....	41
31	Effect of Increased Injector to Flameholder Length. A Comparison of Test Point 9 With Test Point 1.....	42
32	Effect of Turbulence Screen on Stability. A Comparison of Test Point 7 With Test Point 1.....	43
33	Rumble Amplitude Correlates With Blowout Parameter and Fuel-Air Ratio.	45
34	Predicted Onset of Rumble for Experimental Test Rig.....	46
35	Comparison of Model Prediction With Rig Data.....	47
36	Response of Airflow at Spraybars to Combustion Heat Release: Baseline Configuration.....	49
37	Response of Airflow at Spraybars to Combustion Heat Release, Screen 40 Inches Upstream of Flameholders.....	50
38	Open Loop Transfer Function Long Duct (Run 11.01) (Test Point 3).....	51
39	Open Loop Transfer Function Short Duct (Run 14.01) (Test Point 11).....	51
40	Pressure Waveform at 52 Hz.....	52
41	Velocity Waveform at 52 Hz.....	52
42	Density Waveform at 52 Hz.....	53
43	Temperature Waveform at 52 Hz.....	53
44	Rumble Model Flow Chart.....	56
45	Open Loop Transfer Function at 53,000 Feet Altitude and 0.8 Mach Number	57

# LIST OF ILLUSTRATIONS (Continued)

Figure		Page
46	Condition for Rumble.....	58
47	Rumble Rig Conditions for Temperature Gradient Study.....	59
48	Rig Response Without Gradient.....	59
49	Rig Response With Gradient.....	60
50	V-Gutter Rumble Model Schematic.....	62
51	Steps in Augmentor Combustion Process.....	63
52	The Effect of Fan Stream Fuel-Air Ratio and Altitude on Rumble.....	65
53	The Effect of Core Stream Fuel-Air Ratio on Lo-Frequency Rumble.....	66
54	The Effect of Low Core Stream Fuel-Air Ratio on Higher Mode Stability....	67
55	The Effect of High Core Stream Fuel-Air Ratio on Higher Mode Stability....	68
56	The Effect of Increased Fan Duct Pressure Loss.....	69
57	The Effect of Heat Addition to Fan Stream on Rumble.....	70
58	The Effect of Mixer on Stability.....	71
59	A Comparison of Engine Parameters at Various Flight Altitudes.....	73
60	Typical Swirl Augmentor Geometry.....	75
61	Typical Vorbix Augmentor Geometry.....	76
62	Full Swirl Augmentor Model Schematic.....	77
63	Vorbix Rumble Model Schematic.....	77
64	System Efficiency Characteristics for the Configuration With Swirlers Removed (Run 34) and for the Vorbix II Augmentor Configurations (Run 35, 38-40).....	78
65	Full Swirl Augmentor Efficiency Characteristic at High Fuel-Air Ratio.....	79
66	Open Loop Transfer Function and Phase as a Function of Frequency for the Full Swirl Nominal Case.....	79
67	Full Swirl With Uniform Combustion.....	80
68	Full Swirl With Fan Duct $\Delta P/P = 0$ .....	81



## LIST OF ILLUSTRATIONS (Continued)

<i>Figure</i>		<i>Page</i>
69	Core Heat to Fan Stream Flameholder Close-up — HB1.....	82
70	B/M Flameholder.....	83
71	Extended Mount Flameholder.....	83
72	Drafted Flameholder — RE1.....	84
73	Core Heat to Fan Stream Flameholder — HB1.....	84
74	Flameholder Configurations for FSER Verification Tests.....	85
75	Mixer Configurations for FSER Verification Tests.....	86
76	Local to Average Airflow Distribution for Engine P026 With B/M Augmentor	97
77	Relative Spraying Locations for FSER Test Program.....	98
78	Zone 3 Untailored B/M Fuel-Air Map.....	101
79	Zone 5 Untailored B/M Fuel-Air Map.....	101
80	Zone 3 Tailored B/M Fuel-Air Map.....	102
81	Zone 5 Tailored B/M Fuel-Air Map.....	102
82	Flameholder Combustion Model Predictions Data Point 195.....	105
83	Flameholder Combustion Model Predictions Data Point 195.....	106
84	Combined Augmentor Rumble/Flameholder Combustion Model Output.....	107
85	Rumble Model Output (Hand Calculated Z's).....	107
86	Rumble Model Output 0.003 Lag on $q'_{out}$ (Hand Calculated Z's).....	108
87	Combined Model Schematic.....	112
88	Input List for Five Model Combinations.....	113
89	Cross Section Sketch of Swirl Augmentor Compared to Conventional Augmentor.....	122
90	Swirl Augmentor With Cooling Liner Duct and Nozzle Installed.....	123
91	Swirl Augmentor Without Duct and Nozzle Installed.....	123
92	P072/Swirl Augmentor Scheme No. 1.....	125



## LIST OF ILLUSTRATIONS (Continued)

<i>Figure</i>		<i>Page</i>
93	P072/Swirl Augmentor Scheme No. 2.....	125
94	P072/Swirl Augmentor Scheme No. 3.....	126
95	P072/Swirl Augmentor Scheme No. 4.....	126
96	Swirl Augmentor Dynamic Pressure Traces.....	128
97	Rumble Data for Test Point Number 1 and 2 — Test Number 7.01.....	150
98	Rumble Data for Test Point Number 3 — Test Number 11.01.....	151
99	Rumble Data for Test Point Number 4 — Test Number 12.01.....	152
100	Rumble Data for Test Point Number 7 — Test Number 8.01 (5% $\Delta P$ Screen)	153
101	Rumble Data for Test Point Number 7 — Test Number 8.01 (2% $\Delta P/P$ Screen)	154
102	Rumble Data for Test Point Number 8 — Test Number 11.01 (5% $\Delta P/P$ Screen).....	155
103	Rumble Data for Test Point Number 9 — Test Number 9.01.....	156
104	Rumble Data for Test Point Number 10 — Test Number 10.01.....	157
105	Rumble Data for Test Point Number 11 — Test Number 14.01.....	158
106	FSER Duct Thermal Efficiency.....	161
107	FSER Duct Thermal Efficiency Near Blowout Limit.....	162
108	FSER Core Thermal Efficiency.....	162
109	Duct Thermal Efficiency With Heat Addition to Wake of Flameholder.....	163/164
110	Effect of Mixers on Duct Thermal Efficiency.....	163/164
111	Rumble Model Station Identification.....	166
112	Steps in Augmentor Combustion Process.....	178
113	Ideal Temperature Rise for Constant Pressure Combustion of Hydrocarbon Fuels.....	182
114	Location of a Core Streamtube in a Turbofan Engine Augmentor.....	186
115	Single Streamtube Logic Map.....	187

## LIST OF ILLUSTRATIONS (Continued)

<i>Figure</i>		<i>Page</i>
116	Duct Stream Wake Solution.....	189
117	Location of Typical Fan Duct Streamtube.....	190
118	Single Streamtube Geometry and Flow Inputs — Fan.....	191
119	External Heat Addition to Fan Duct Gutters.....	192
120	Location of a Core Streamtube in a Turbofan Engine Augmentor.....	195
121	Variation in Activation Energy With Inlet Temperature and Equivalence Ratio.....	200
122	External Heat Addition to Fan Duct Gutters.....	201
123	Schematic of Flame Spreading Analysis.....	203
124	Flame Speed for Monodisperse Tetralin Spray.....	205
125	Fictitious Temperature Rise vs Main Burner Fuel-Air Ratio.....	209
126	FSER P026 Instrumentation Locations.....	210

## LIST OF TABLES

<i>Tables</i>	<i>Page</i>
1      Lo-Frequency Augmentor Instability Study Rig Instrumentation Description	27
2      Revised Test Conditions.....	31
3      Summary of Parametric Study of Full Swirl Augmentor.....	80
4      Lo-Frequency Augmentor Instability Study FSER Instrumentation Description.....	89
5      FSER Test Program Run Log.....	92
6      Summary of FSER Test Results.....	99
7      Summary of Phase II Model Predictions and FSER Test Results.....	100
8      Summary of Fuel-Air Distribution for B/M and Tailored Sprayrings.....	103
9      Model Predictions vs FSER Test Results.....	104
10     Point-to-Point Comparisons Rumble Model vs FSER Test Results.....	109
11     Stability Summary at 1/45K FSER Test to Model Prediction.....	111
12     Combined Model Input Parameter Description.....	114
13     Rumble Model Tabular Output.....	116
14     Flameholder Combustion Model Output.....	118
15     P072 Swirl Augmentor Significant Performance Parameters.....	124
16     Sprayring Configuration.....	127
17     Model Predictions vs Swirl Augmentor SLS Results.....	129
18     Experimental Study Rig Data.....	150



## LIST OF SYMBOLS

### *English Symbols*

<u>Symbol</u>	<u>Definition</u>	<u>Typical Unit</u>
a	Reaction index in eq'n (138)	d'less
A	Area	in <sup>2</sup>
A	Dummy variable in eq'n (169)	d'less
A	Stirred reactor mass loading in eq'n (138)	gm-mole/sec
A <sub>s</sub>	Surface area	sq in.
B/D	Wake width per unit flameholder	d'less
B/M	Bill of Material	—
BPR	Bypass ratio, fan duct airflow/core airflow	d'less
C	Sonic velocity	in./sec
C	Activation energy constant in eq'n (137)	°K
C <sub>d</sub>	Drag coefficient	d'less
C <sub>p</sub>	Specific heat at constant pressure	Btu/lbm/°R
C <sub>v</sub>	Specific heat at constant volume	Btu/lbm/°R
C <sub>w</sub>	Wake shape factor in eq'n (133)	in <sup>2</sup> /in <sup>2</sup>
C <sub>i</sub>	Dummy variable in eq'n (116)	d'less
d	Diameter	in.
D <sub>v</sub>	Diffusion coefficient	in <sup>2</sup> /sec
f	Frequency	Hz
FA	Fuel-air ratio	d'less
FAP	Vitiated core stream fuel-air ratio at entry to augmentor	d'less
F/H	Flameholder	—
g <sub>c</sub>	Gravitational constant	ft-lbm/sec <sup>2</sup> /lb <sub>r</sub>
H	Enthalpy	Btu/lbm
h <sub>f</sub>	Film coefficient	Btu/in <sup>2</sup> sec°R
k	Reaction rate in eq'n (137)	d'less

# LIST OF SYMBOLS (Continued)

## English Symbols

<u>Symbol</u>	<u>Definition</u>	<u>Typical Unit</u>
$k$	Thermal conductivity in eq'n (121)	Btu/in <sup>2</sup> sec°R
$K$	Dummy variable in eq'n (101)	d'less
$K_1$	Recirculative coefficient	d'less
$l$	Axial length between stations	in.
$L$	Augmentor length	in.
$L/D$	Wake length per unit flameholder width	d'less
$m$	Mass	lbm
$\dot{m}$	Mass flowrate	lbm/sec
$M$	Mach number	d'less
$MB$	Main burner reference	d'less
$MW$	Molecular Weight	lbm/lb-mole
$n$	Pressure index	d'less
$n$	Reaction order in eq'n (138)	d'less
$N$	Flameholder width	in.
$Nu$	Nusselt number	d'less
$P$	Pressure	lbf/in <sup>2</sup> , psia, Pa
$\Delta P$	Pressure drop	lbf/in <sup>2</sup>
$PFSR$	Sprayring fuel pressure	lbf/in <sup>2</sup>
$Pr$	Prandtl number	d'less
$P_r$	Pressure ratio	d'less
$q'$	Volumetric heat release rate	Btu/sec/in <sup>3</sup>
$\dot{q}$	Heat flux	Btu/in <sup>2</sup> sec
$Q$	Heat release rate	Btu/sec
$R$	Gas constant	ft-lbf/lbm-°R
$R$	Resistance, defined by eq'n (10)	d'less

# LIST OF SYMBOLS (Continued)

<u>Symbol</u>	<u>Definition</u>	<u>Typical Unit</u>
Re	Reynold's number	d'less
r	Real part of a zero of characteristic function or LaPlace transform	d'less
S	Entropy	Btu/lbm/°R
St	Laminar flame speed	ft/sec
St	Turbulent flame speed	ft/sec
S/R	Spraying on spraybar	—
t	Time	sec
T	Temperature	°F, °R, °K
TFSR	Spraying fuel temperature	°F
u	Internal energy	Btu/lbm/°R
u'	RMS turbulence velocity fluctuation	ft/sec
U	Flameholder lip velocity	ft/sec
V	Velocity	ft/sec
v	Volume	in <sup>3</sup>
V <sub>o</sub>	Wake volume	litre
W	Mass flowrate	lbm/sec
w	Duct width	in.
WCOOL	Liner cooling flow/total engine flow	d'less
x	Axial distance	in.
Δx	Distance	in.
y	Stoichiometry factor in eq'n (138)	d'less
Δy	Flame penetration distance	in.
z	Defined in eq'n (106)	d'less
Z	Defined in eq'n (169)	d'less
ZEF	Normalized Efficiency Slope	d'less



# LIST OF SYMBOLS (Continued)

## Greek Symbols

<u>Symbol</u>	<u>Definition</u>	<u>Typical Unit</u>
$\alpha$	Flameholder Apex angle	degrees
$\beta$	Defined in eq'n (105)	d'less
$\beta_1$	Droplet vaporization coefficient	d'less
$\beta_2$	Droplet collective coefficient	d'less
$\beta_3$	Surface vaporization coefficient	d'less
$\beta_e, \beta_r, \beta_s$	Defined in eq'n (35)	d'less
$\Gamma$	Blockage ratio	d'less
$\tau_{DC}$	Drift delay from fuel spraying to flameholder	sec
$\tau$	Residence time	
$\tau'$	Nondimensionalized residence time	d'less
$\gamma$	Ratio of specific heats	d'less
$\epsilon$	Wake reaction efficiency	d'less
$\epsilon_0$	Turbulence intensity	d'less
$\eta$	Efficiency	d'less
$\theta_1, \theta_2, \theta_3$	Defined by equation (7)	d'less
$\lambda$	Latent heat of vaporization	Btu/lbm
$\nu$	Viscosity	lbf/in.
$x_o$	Oxygen concentrative	gm-mole/litre
$x_{o_2}$	Oxygen volume fraction	d'less
$x_f$	Fuel concentrative	gm-mole/litre
$\rho$	Density	lbm/in <sup>3</sup>
$\psi$	Stability parameter	d'less

## LIST OF SYMBOLS (Continued)

### *Special Symbols*

<u>Symbol</u>	<u>Definition</u>	<u>Typical Unit</u>
$\Delta$	Denotes change in a variable from its steady-state value	
c	Collected; combustion	
<i>Subscripts</i>		
v	Vapor; vaporized	
stoich	Stoichiometric	
S/B	Spraybar	
r	Recirculated	
OA	Overall	
M	Mixed conditions	
g	Gas	
fict	Fictitious	
F/H	Flameholder reference	
f	Fuel	
ext	External	
ex	Exit	
a	Air	
L	Liquid	
C	Fan stream values	
H	Core Stream	
1 through 11	Station numbers	
o	Subscript signifies stagnation state	
i	Subscript signifies ideal value	
t	Subscript signifies total (combined) value	
w	Wake reference	

## LIST OF SYMBOLS (Continued)

### Special Symbols (Continued)

<u>Symbol</u>	<u>Definition</u>	<u>Typical Unit</u>
<b>Superscripts</b>		
—	Average value	
.	Superscript denotes steady-state value	
'	Superscript denotes change in a variable divided by its steady-state value (e.g., $P' = \Delta P/P$ ), except for entropy, which is normalized by $C_v$ ( $S' = \Delta S/C_v$ )	



## SUMMARY

The principal objective of the Lo-Frequency Augmentor Instability Study was to develop a reliable analytical model that will predict the rumble stability limits and characteristics of turbofan engine augmentors. The one, most important difficulty in developing a model that accurately defines rumble is a clear understanding of the causes. A usable model must also apply to other than conventional V-gutter augmentors; without understanding and incorporating the fundamental rumble mechanisms, failure is imminent. To solve this problem the model was evolved in conjunction with and checked by three experimental programs. Rumble mechanisms investigated early in this study involved system airflow dynamics, combustion efficiency oscillations, fuel vaporization and recirculation wake energy. Rumble was identified as a system problem in which airflow dynamics couple with the combustion process. The model was then refined and extended to include the mixed flow experienced in a turbofan augmentor. Predictions were made for the effects of altitude, fan stream fuel-air ratio, fan stream temperature, core stream fuel-air ratio, and fan duct pressure loss. It was concluded from these analytical studies that the efficiency falloff in the fan stream at high fuel-air ratio is the driving mechanism for rumble. Thus to eliminate rumble the development engineer must decouple the airflow dynamics from the combustion process by (1) changing lengths or pressure drop in the cold duct or (2) choosing augmentor design parameters that will minimize or eliminate the decrease in combustion efficiency at high fuel-air ratio. This design philosophy was evaluated with engine altitude tests. These tests included heat addition to the fan stream, fuel-air distribution changes, increased fan duct pressure loss, and a baseline augmentor. The model did not accurately predict every observed test, but it did substantiate design trends would influence the occurrence of rumble. The system rumble model was extended to include the new Vorbix and Full Swirl Augmentor concepts. The treatment of these concepts were not as rigorous as for the V-gutter augmentor. Analytical representations of the combustion process in the newer concepts are not as well defined; there are no models available which will predict their steady-state combustion efficiency characteristics. Sea level swirl augmentor testing was used to provide combustion input to the rumble model. Based on the shape of the efficiency vs fuel-air ratio data the swirl augmentor was predicted to be rumble free at sea level conditions and an altitude of 50K feet at 0.8 Mach number for an 0.050 overall fuel-air ratio. Stable operation was demonstrated at the sea level condition.

## SECTION I

### INTRODUCTION

With the introduction of the mixed-flow augmentor in turbofan engines, a type of low-frequency instability known as rumble or chugging became a serious problem. Rumble is a periodic afterburning combustion instability (pressure oscillations fed by the combustion process) occurring usually at high fuel-air ratios at flight Mach numbers and altitudes when low duct inlet air temperatures and pressures exist. This instability usually leads to afterburner blowout and/or fan surge and engine stall. The frequency of oscillation usually lies between 30 and 200 Hz.

Data from engine programs and early rumble investigations suggest several possible mechanisms which regulate or cause low-frequency combustion instability in afterburners. They can be summarized under the following categories:

1. Longitudinal system dynamics
2. Combustion efficiency oscillations
3. Insufficient and/or nonuniform fuel vaporization
4. Low recirculation wake energy.

Even subtle changes in flameholder designs have altered the rumble characteristics of a turbofan engine. With some experience at hand, the design engineer has successfully produced "fixes" for unstable conditions. Redistribution of the fuel-to-air mixture ratio has worked, and deriching the fan duct has lessened rumble problems in the past. However, complete understanding of this combustion/dynamics problem has been inadequate to design rumble-free mixed flow afterburners with confidence.

The purpose of this 30-month research project was to devise a reliable empirical and analytical model that will aid afterburner designers. The program was conducted in four phases. In Phase I concurrent experimental and analytical studies were conducted. The analytical efforts to develop the rumble model were supported by and compared with the stability characteristics of the experimental rig. During the experimental program, several possible mechanisms were investigated on a boiler plate combustion system. In Phase II the model was computerized in a readily usable format and extended to a turbofan engine with a conventional V-gutter, the "Vorbix" and "Full Swirl" augmentors. Support hardware was designed and fabricated during this phase for the Full Scale Engine Research (FSER) model verification test program. During Phase III the Rumble Model computer program was combined with the Flameholder Combustion Model, Reference 1; and the FSER test program was conducted to substantiate the model. The model was used to investigate stability design improvements and to establish recommended development and test criteria for future engine programs. A User's Manual (CCD 1144-0.0) was prepared for the combined Augmentor Rumble/Flameholder Combustion Model computer program. In Phase IV the Full Swirl augmentor was tested at sea level to verify the rumble model formulated under Phase II. The test program was used to provide data on combustion efficiency and low-frequency instability for varied augmentor overall fuel-air ratio overall and fuel-air ratio distribution.



## SECTION II

### TECHNICAL DISCUSSION

#### 1. PHASE I — MODEL DEVELOPMENT

##### a. Background

In Phase I, experimental and analytical studies were conducted to verify the mechanisms initiating and sustaining low-frequency combustion instability (rumble) in augmentors. These studies were directed toward the development of an analytical model capable of predicting the conditions under which rumble would occur. The model could then be used to identify augmentor design modifications which would alter those conditions and thereby eliminate rumble.

During these studies, a rumble model was developed for a test rig, which was essentially a long, constant-area pipe containing spray rings and V-gutter flameholders. The rumble model was a formulation of dynamic acoustic and combustion equations. The acoustic equations described the longitudinal oscillation of the flowing, burning airstream as it responded to variations in the combustion efficiency. The dynamic combustion equations described how the longitudinal oscillation of the airstream would, in turn, cause variations in the combustion efficiency, leading to the unstable coupling of acoustic and combustion characteristics commonly called rumble.

As rig test results became available, they were incorporated into the model, and the model was refined and modified accordingly.

##### b. Model Formulation

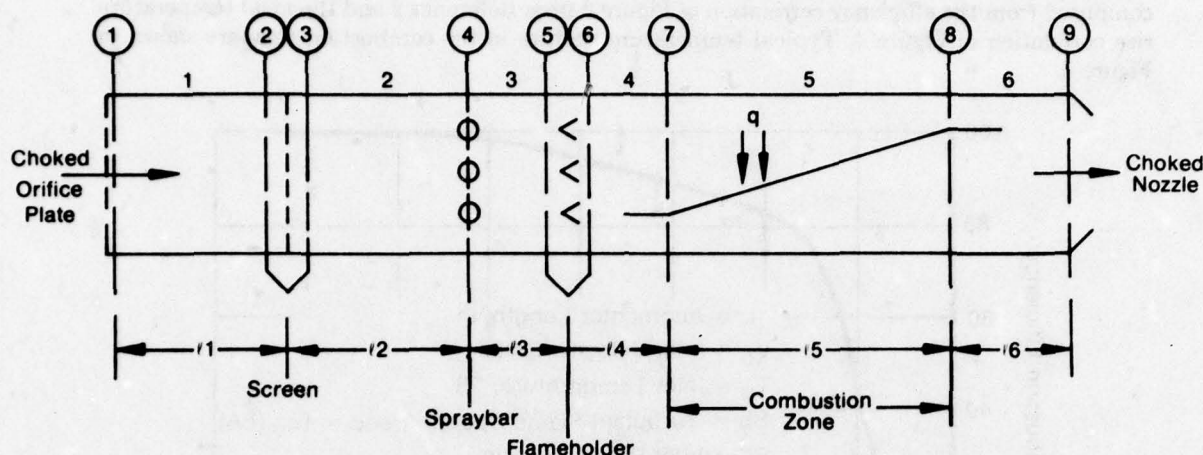
The augmentor math model consists of a set of time-dependent equations describing the longitudinal dynamics of the flowing airstream and of the axially distributed combustion process in the augmentor, coupled with a solution technique for determining stability. The equations are linearized, through the assumption of small perturbations, and transformed from the time domain to the Laplace transform "S" domain. The solution technique is based upon the Nyquist stability criterion and consists of determining whether the time response of the system to a small disturbance would display oscillatory behavior with a growing amplitude. The result is a determination of stability at a given operating point, which then allows identification of regions of operation which will cause rumble or changes to the augmentor to make it rumble-free.

##### (1) Model Description of the Experimental Rig

The augmentor rig, shown schematically in Figure 1, was for modeling purposes, and consisted of a long pipe fed by a choked inlet orifice plate (designated by station (1)) and discharging through a choked exhaust nozzle (station (9)). In a turbojet augmentor, station (1) would represent turbine discharge and station (9) the upstream face of the exhaust nozzle. In a turbofan duct augmentor, station (1) would represent fan discharge.

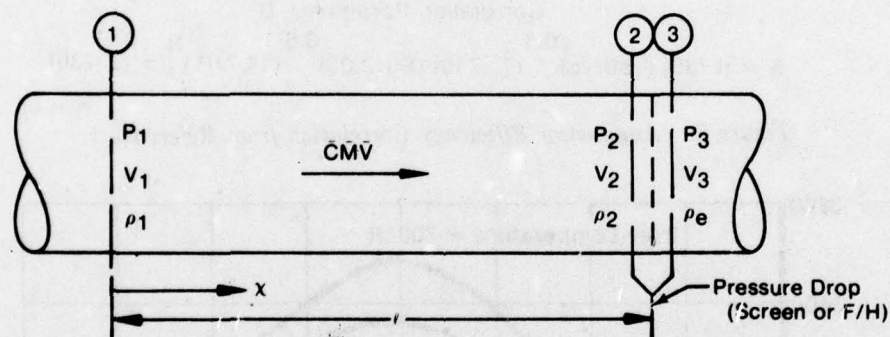
Fuel was supplied through spraybars at station (4). The resulting fuel-air mixture flowed over a set of flameholders between stations (5) and (6). For some tests a screen, see Figure 2, was inserted upstream of the spraybars between stations (2) and (3) to generate turbulence in the airstream.





FD 151402

Figure 1. Augmentor Rig Math Model Schematic



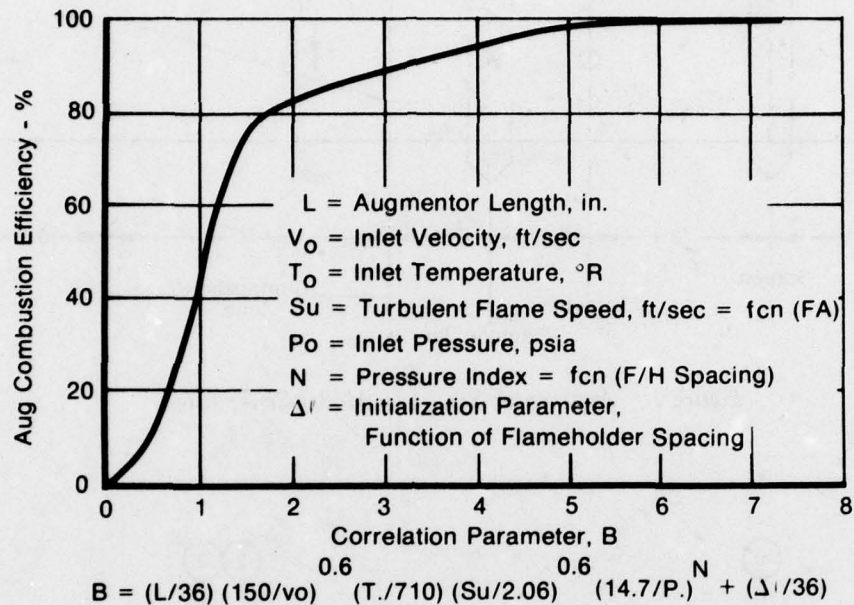
FD 151402

Figure 2. Typical Section of Augmentor Rig

The flameholders divided the augmentor into a cold upstream section and a hot downstream section. The cold section was at uniform pressure and temperature, except for a small pressure drop when the turbulence screen was in place.

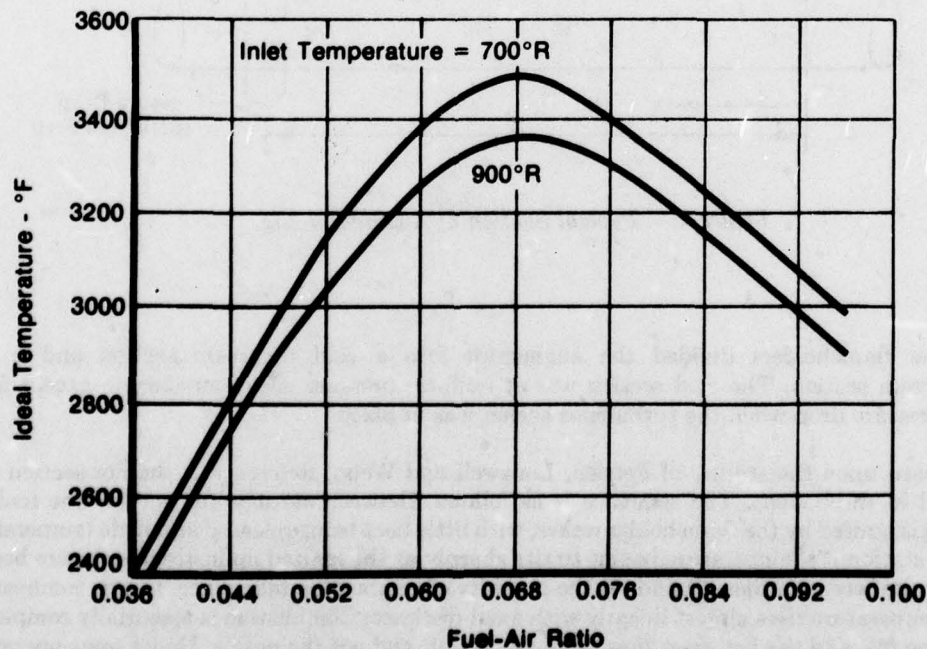
Based upon the studies of Petrien, Longwell and Weiss, Reference 2, the hot section was modeled in three steps. The sequence is as follows. Between stations (6) and (7) the fuel-air mixture is ignited by the flameholder wakes, with little heat being released and little temperature rise. At station (7) temperature begins to rise sharply as the ignited mainstream mixture begins burning. Between stations (7) and (8) the majority of combustion take place. In this combustion zone, temperature rises almost linearly with axial distance. Combustion is essentially completed at station (8), and the hot gases flow on to station (9) and out the nozzle. Under some operating conditions, combustion may not be completed before the fuel-air mixture reaches the nozzle. In this case station (8) would move back and become coincident with station (9). The locations of

the beginning and end of the combustion zone (stations (7) and (8)) and the temperature rise were computed from the efficiency correlation of Figure 3 from Reference 2 and the ideal temperature rise correlation of Figure 4. Typical temperature profiles in the combustion zone are shown in Figure 5.



FD 151401

Figure 3. Augmentor Efficiency Correlation from Reference 1



FD 151431

Figure 4. Ideal Temperature Rise for Constant Pressure Combustion of Hydrocarbon Fuels

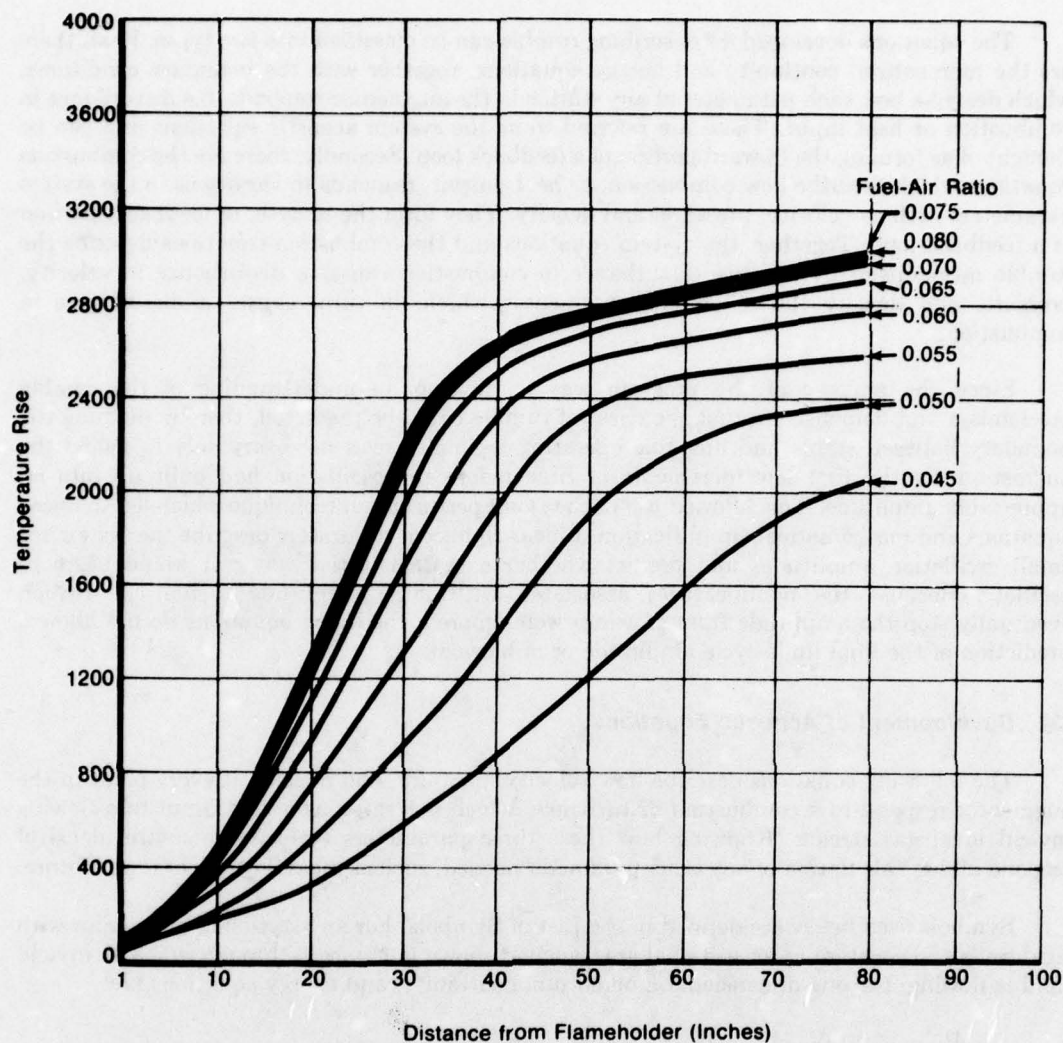


Figure 5. Typical Combustion Temperature Profiles

FD 151432

## (2) Modeling Approach

Since the frequency of rumble has long been associated with the relatively low-frequency longitudinal, or axial, modes of vibration of the air column in the augmentor, the model was formulated to take only the longitudinal dimension into account. Accordingly, each station in Figure 1 was considered to represent a plane over which the value of any parameter (such as velocity, pressure, or density) could be considered as uniform at any instant in time.

Motion pictures of rumble had shown a change in color of the burning gas during a cycle of oscillation, indicating that alternate hotter and cooler combustion products were being produced. These hot and cold combustion products could be seen drifting from the flameholder to the exhaust nozzle in a time span which matched, or was a multiple of, the period of oscillation of the rumble. Since flowrate out through the nozzle is dependent upon the temperature of the entering gas, it was important that the model treat the traveling combustion products, which were mathematically identified, as traveling entropy waves.



The equations developed for describing rumble can be classified into two types. First, there are the momentum, continuity and energy equations, together with the boundary conditions, which describe how each parameter at any station in the augmentor responds to a disturbance in combustion or heat input. These are referred to as the system acoustic equations and can be thought of as forming the forward portion of a feedback loop. Secondly, there are the combustion equations which describe how combustion, or heat output, responds to variations in the system parameters such as velocity, pressure, and density. They form the reverse, or feedback, portion of a feedback loop. Together, the system equations and the combustion equations describe the rumble mechanism, by which a disturbance in combustion causes a disturbance in velocity, pressure, and density throughout the augmentor which, in turn, causes a disturbance in combustion.

Since the purpose of the program was to develop an understanding of the rumble mechanism and demonstrate that the onset of rumble could be predicted, thereby defining the boundary between stable and unstable operating regions, it was necessary only to model the augmentor for the first few increments of time before the oscillation had built up into an appreciable amplitude. This allowed use of the small perturbation technique which led to linear equations and mathematical simplification. Linear equations accurately describe the system for small oscillation amplitudes and predict whether a system initially at rest would begin to oscillate. Because the nonlinearities associated with large amplitude oscillations (which eventually stop the amplitude from growing) were ignored, the linear equations do not allow a prediction of the final limit-cycle amplitude or of blowout.

### (3) Development of Acoustic Equations

The following equations describe how velocity, pressure, and density at every point in the augmentor respond to a combustion disturbance, which is treated as a heat input to a flowing inviscid ideal gas stream. Knowing how these three parameters (velocity, pressure, density) respond allows calculation of any other parameter needed, such as mass flowrate or temperature.

Symbols used below are defined in the List of Symbols. For any section of augmentor with rigid walls and constant cross-sectional area, such as shown in Figure 2, through which an inviscid fluid is flowing, the one-dimensional momentum, continuity, and energy equations are:

$$\begin{aligned} \frac{\partial P}{\partial x} + \rho V \frac{\partial V}{\partial x} + \rho \frac{\partial V}{\partial t} &= 0 \\ \rho \frac{\partial V}{\partial x} + V \frac{\partial \rho}{\partial x} + \frac{\partial \rho}{\partial t} &= 0 \\ q + \frac{PV}{\rho} \frac{\partial \rho}{\partial x} + \frac{P}{\rho} \frac{\partial \rho}{\partial t} &= \rho V \frac{\partial u}{\partial x} + \rho \frac{\partial u}{\partial t} \end{aligned} \quad (1)$$

For an ideal gas these equations reduce to the following nonlinear wave equations:

$$\begin{aligned} (V+C) \left[ \frac{1}{P} \frac{\partial P}{\partial x} + \frac{\gamma}{C} \frac{\partial V}{\partial x} \right] + \left[ \frac{1}{P} \frac{\partial P}{\partial t} + \frac{\gamma}{C} \frac{\partial V}{\partial t} \right] &= (\gamma-1) \frac{q}{P} \\ (V-C) \left[ \frac{1}{P} \frac{\partial P}{\partial x} - \frac{\gamma}{C} \frac{\partial V}{\partial x} \right] + \left[ \frac{1}{P} \frac{\partial P}{\partial t} - \frac{\gamma}{C} \frac{\partial V}{\partial t} \right] &= (\gamma-1) \frac{q}{P} \\ V \left[ \frac{1}{P} \frac{\partial P}{\partial x} - \frac{\gamma}{\rho} \frac{\partial \rho}{\partial x} \right] + \left[ \frac{1}{P} \frac{\partial P}{\partial t} - \frac{\gamma}{\rho} \frac{\partial \rho}{\partial t} \right] &= (\gamma-1) \frac{q}{P} \end{aligned} \quad (2)$$

The wave equations are linearized by the small perturbation substitutions:

$$\begin{aligned} P(x,t) &= \bar{P}(x) + \Delta P(x,t) \\ \rho(x,t) &= \bar{\rho}(x) + \Delta \rho(x,t) \\ C(x,t) &= \bar{C}(x) + \Delta C(x,t) \\ V(x,t) &= \bar{V}(x) + \Delta V(x,t) \\ q(x,t) &= \bar{q}(x) + \Delta q(x,t) \end{aligned} \quad (3)$$

Second order terms are neglected in making the substitutions. It is further assumed that mean values of the steady-state parameters  $\bar{P}(x)$ ,  $\bar{V}(x)$ ,  $\bar{C}(x)$  can be chosen so that  $\bar{P}$ ,  $\bar{V}$ ,  $\bar{C}$  can be considered constants, independent of  $x$ , i.e.,

$$\frac{d\bar{P}(x)}{dx} = \frac{d\bar{V}(x)}{dx} = \frac{d\bar{C}(x)}{dx} = 0 \quad (4)$$

To simplify notation the following substitutions are made which normalize the change in each variable by its steady-state value:

$$P' = \frac{\Delta P}{\bar{P}}, \quad V' = \frac{\Delta V}{\bar{V}}, \quad \rho' = \frac{\Delta \rho}{\bar{\rho}}, \quad q' = \frac{\Delta q}{\bar{q}} \quad (5)$$

For zero initial conditions the solution of equations (2) from a station (1) at  $x = 0$  to a station (2) at  $x = l$ , written in terms of the Laplace transform of each normalized variable, is:

$$\begin{aligned} P'_2 + \gamma \bar{M} V'_2 &= [P'_1 + \gamma \bar{M} V'_1] e^{\frac{-tS}{\bar{C}(1+\bar{M})}} + \theta_1 \\ P'_1 - \gamma \bar{M} V'_1 &= [P'_2 - \gamma \bar{M} V'_2] e^{\frac{-tS}{\bar{C}(1-\bar{M})}} + \theta_2 \\ P'_2 - \gamma \rho'_2 &= [P'_1 - \gamma \rho'_1] e^{\frac{-tS}{\bar{C}\bar{M}}} + \theta_3 \end{aligned} \quad (6)$$

where:

$$\begin{aligned} \theta_1 &= \frac{(\gamma-1)}{\bar{C}(1+\bar{M})} \int_0^l \left( \frac{\bar{q}}{\bar{P}} \right) q'(x,s) e^{\frac{-(l-x)S}{\bar{C}(1+\bar{M})}} dx \\ \theta_2 &= \frac{(\gamma-1)}{\bar{C}(1+\bar{M})} \int_0^l \left( \frac{\bar{q}}{\bar{P}} \right) q'(x,s) e^{\frac{-xS}{\bar{C}(1-\bar{M})}} dx \\ \theta_3 &= \frac{(\gamma-1)}{\bar{C}\bar{M}} \int_0^l \left( \frac{\bar{q}}{\bar{P}} \right) q'(x,s) e^{\frac{-(l-x)S}{\bar{C}\bar{M}}} dx \end{aligned} \quad (7)$$

In equations (6) the first equation describes downstream running waves of the form  $P' + \gamma \bar{M} V'$ , traveling at sonic speed plus throughflow velocity. The second equation describes upstream running waves of the form  $P' - \gamma \bar{M} V'$ , traveling at sonic speed minus throughflow velocity. The third equation describes entropy waves,  $P' - \gamma \rho'$ , drifting downstream at throughflow velocity.

The entropy waves become more apparent from the expression for the entropy of an ideal gas:

$$\frac{\Delta S}{C_v} = S' = P' - \gamma \rho' \quad (8)$$

The entropy waves are related to temperature by:

$$\gamma T' = S' + (\gamma - 1) P' \quad (9)$$

It is through equation (9) that the drifting hot and cold combustion products, or entropy waves, are accounted for in the rumble model. Temperature changes produced as the entropy waves strike the exhaust nozzle cause velocity changes which then travel back upstream at sonic speed.

Equations (6) are used throughout the augmentor between any two stations between which there is no discontinuity. Referring to Figure 1 they are applied between stations (1)-(2), (3)-(4), (4)-(5), (6)-(7), (7)-(8), and (8)-(9). Between stations (1) through (7) and between stations (8)-(9) there is little or no heat addition, and so  $\theta_1 = \theta_2 = \theta_3 = 0$  for these sections. The heat addition terms for the combustion zone, stations (7)-(8), are discussed in the following section.

Discontinuities occur at the turbulence screen and at the flameholders, which are modeled as small incompressible resistive pressure drops of zero length. The continuity and energy equations are also applied. Referring to Figure 1, the three normalized equations applied between stations (2)-(3) and again between stations (5)-(6) are:

$$\begin{aligned} P_2 - P_3 &= R V_2 \\ \rho_2 + V_2 &= \rho_3 + V_3 \\ P_2 - \rho_2 &= P_3 - \rho_3 \end{aligned} \quad (10)$$

where

$$R = 2 \frac{(P_2 - P_1)}{P_2}$$

Definition of the upstream and downstream boundary conditions complete the acoustic equations. At the upstream boundary station (1) mass flowrate is constant, and total temperature must equal the total temperature of the incoming air, which is also constant. The two upstream boundary conditions at station (1) are:

$$\begin{aligned} W' &= \rho' + V' = 0 \\ T' &= P' - t' = 0 \end{aligned} \quad (11)$$

The second upstream boundary condition in equations (11) indicates that entropy waves are produced by wave reflections at the inlet orifice plate. These drift downstream but are of minor importance compared to the entropy waves created in the combustion zone.



The downstream boundary condition is based upon the short choked nozzle just downstream of station (9), which requires that the flow parameter and Mach number at station (9) be constant. This leads to the condition at station (9) that:

$$V' = \frac{1}{2}T' = \frac{1}{2}(P' - \rho') \quad (12)$$

This completes the system acoustic equation development (except for evaluation of the heat addition terms in equations (7), which are covered in the following section, "Development of Combustion Equations"). These equations describe the response of pressure, velocity, and density throughout the augmentor to a disturbance in combustion. A list of equations is given in Appendix B.

#### **(4) Development of Combustion Equations**

Combustion equations used in the rumble model are based upon an extension of empirical steady-state processes to the case of time variant flow. A schematic of the steady-state processes is shown in Figure 6. The following steps occur:

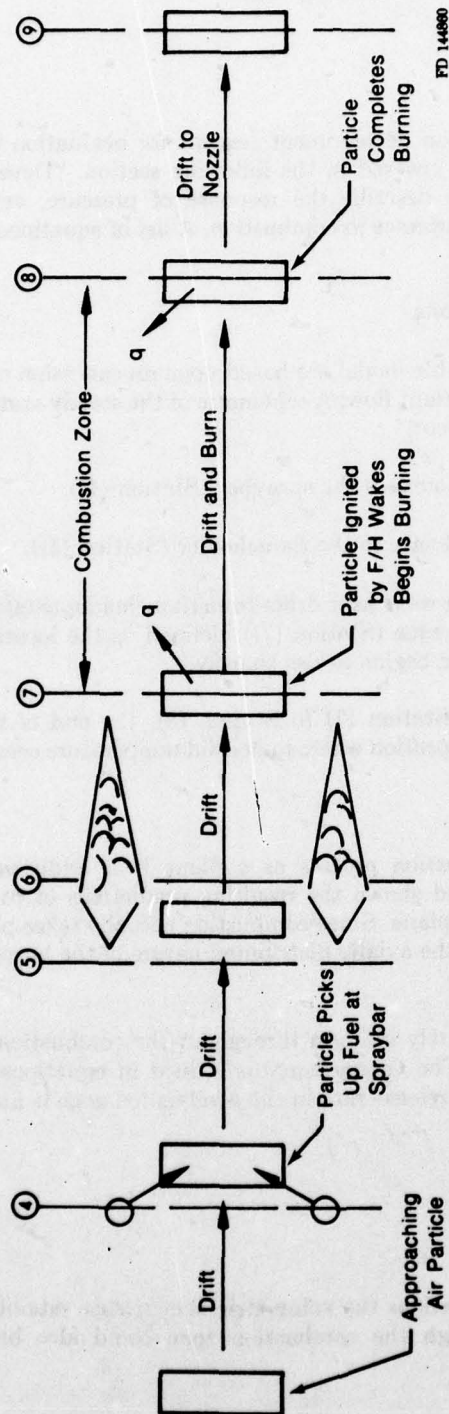
- Particle of air picks up fuel as it crosses the spraybar (Station (4)).
- Particle drifts at throughflow velocity to the flameholder (Station (5)).
- Particle is ignited by flameholder wake as it drifts from flameholder (Station (6)) to beginning of combustion zone (Station (7)), defined as the location where the bulk fluid temperature begins to rise sharply.
- Particle drifts and burns from Station (7) to Station (8), the end of the combustion zone, defined as the location where bulk fluid temperature ceases its sharp rise.

Experience with modeling the combustion process as a plane heat addition (with all combustion taking place in zero length) had shown the resulting predictions of rumble were sensitive to the axial location chosen for the plane. Since combustion actually takes place over a distance of 40 to 80 in., it was decided that the axially distributed nature of the burning should be accounted for.

At steady state, pressure is approximately uniform throughout the combustion zone and temperature rises approximately linearly. The energy equation (third in equations (1)) then states that the steady-state volumetric heat release rate in the combustion zone is independent of distance.

$$\frac{dP}{dx} = 0, \frac{dT}{dx} = \text{constant}, \frac{d\dot{q}}{dx} = 0 \quad (13)$$

It was assumed that for small perturbations the volumetric heat release rate of a burning particle of fuel-air mixture drifting through the combustion zone could also be taken as independent of distance.



FD 144880

Figure 6. Steps in Augmentor Combustion Process

Consider a stream of fuel-air mixture crossing the flameholder (Station (6)) at steady state. Numbered subscripts refer to station locations and sections in Figure 1. The rate at which this fluid stream will release heat in the combustion zone, and which can be considered the "potential" heat release rate of the stream at Station (6), is:

$$q_6 v = C_p W_6 T_1 \eta \quad (14)$$

A particle of fuel-air mixture in the stream crossing the flameholder will begin burning after a time delay  $t_d/V_6$ , which is the time required to drift from Station (6) to (7), while being ignited. When it begins burning at Station (7) the heat release rate of the particle will be:

$$q_7(t) = q_6(t - t_d/V_6) \quad (15)$$

At some station,  $x$  distance downstream of Station (7), the local heat release rate will become that of the particle after an additional time delay  $x/V_6$ , which is the time required to drift from Station (7) a distance  $x$  at mean average velocity  $V_6$ . Then at a location  $x$  in the combustion zone the heat release rate will be:

$$q(x,t) = q_7(t - x/V_6) \quad (16)$$

The ideal temperature rise,  $T_1$ , is a function only of the fuel-air ratio,  $FA_6$ , of the particle. The efficiency,  $\eta$ , is assumed to be a function of the fuel-air ratio and the stability parameter,  $\psi = V_6/NP_6 T_1^{1/2}$ . The fuel-air ratio of the particle was set a time  $t_d/V_6$  earlier when the particle crossed the spraybar, where  $t_d/V_6$  is the time required to drift from Station (4) to (6).

$$\begin{aligned} T_1 &= \text{fcn}(FA_6) \\ \eta &= \text{fcn}(FA_6, \psi) \\ FA_6(t) &= FA_4(t - t_d/V_6) \end{aligned} \quad (17)$$

Because of the large pressure drop in the fuel spraybar injector, changes in fuel flow in response to augmentor pressure at the spraybar are small compared to changes in airflow. Consequently, fuel flow can be considered constant, and the fuel-air ratio is determined by changes in airflow only.

$$FA_6 = \frac{\text{constant}}{W_6} \quad (18)$$

For small perturbations, with the station locations fixed and the time delays taken as constants, equations (14) through (16), written in terms of the Laplace transform of each normalized variable, reduce to:

$$q'_6 = W'_6 \left[ \frac{FA_6}{T_1} \frac{\partial T_1}{\partial FA_6} + \frac{FA_6}{\eta} \frac{\partial \eta}{\partial FA_6} \right] W'_6 e^{\frac{-t_d S}{V_6}} + \frac{\bar{\psi}}{\eta} \frac{\partial \eta}{\partial \psi} \psi' \quad (19)$$

$$q'_7 = q'_6 e^{\frac{-t_d S}{V_6}} \quad (20)$$

$$q'(x,S) = q'_7 e^{\frac{-xS}{V_6}} \quad (21)$$



These equations model combustion as though it behaves in a quasi-steady-state manner. The volumetric heat release rate at any location in the combustion zone will reach the steady-state value corresponding to instantaneous conditions at the flameholder and at the spraybar after a series of delays. The delays are the time required to purge the old combustion gases and refill with new combustion gases traveling at throughflow velocity.

Equation (19) computes the value of heat release rate,  $q'_s$ , which will occur in the combustion zone in response to changes in airflows,  $W'_s$  and  $W'_f$  and in stability parameter,  $\psi$ . This heat is not released until after a drift delay from the flameholders to Station (7), as defined by equation (20). The heat is then released and distributed throughout the combustion zone as defined by equation (21).

Airflows and the stability parameter are directly computed from velocities, pressures, and densities obtained from the system acoustic equations.

$$\begin{aligned} W'_f &= V'_f + \rho'_f & \psi &= V'_s - P'_s - 1.7T'_s \\ W'_s &= V'_s + \rho'_s & T'_s &= P'_s - \rho'_s \end{aligned} \quad (22)$$

Efficiency and ideal temperature rise can rapidly follow changes in mainstream fuel-air ratio. Efficiency is thought to be only able to slowly adjust to changes in stability parameter. Stability parameter has been shown (Reference 3) to be related to the heat balance between combustion heat release and heat losses in a flameholder wake. The wake is a volume which must be purged of old combustion products and refilled with new combustion products before a change in mainstream conditions can affect the wake. The flameholder metal also acts as a heat reservoir to stabilize wake temperature. These effects slow the response of wake temperature to changes in mainstream conditions. While the steady-state value of stability parameter has been shown to affect flame stabilization behind a flameholder, there are thought to be significant dynamics which may prevent efficiency from tracking changes in stability parameter at rumble frequencies. The effect of the wake dynamics would be to reduce the influence of the last term in equation (19).

Since there was no method currently available for modeling the dynamics of the flameholder wake, it was decided to assume they were sufficiently slow so the influence of stability parameter on efficiency (last term in equation (19)) could be neglected in the frequency range of interest. This assumption is valid only if the dynamics have the effect of a lag greater than about 20 milliseconds.

The modeling of transient fuel-air ratio just described is applicable if the fuel completely vaporizes within a very short distance after being injected. The resulting vapor would then be able to follow rapid changes in air velocity. The fuel-air ratio of a particle would then be set by airflow at the spraybar. If the injected fuel persists as large liquid droplets, which cannot be as easily accelerated by rapid changes in air velocity, a steady stream of fuel would occur at the flameholder. Fuel-air ratio of a particle would then be set by airflow at the flameholder. The first method introduces the drift delay,  $l_s/V_s$ , in equation (19). The second method eliminates the delay. Better tracking of test data was obtained by eliminating the delay. The true process involves both the rapid acceleration to air velocity of the portion of fuel which vaporizes and the more sluggish response of liquid droplets. This is an area identified as requiring a more thorough investigation to be able to account for the vaporization characteristics of the fuel and the injection process.

Equation (21) is used to evaluate the integrals in equations (7) and complete the description of the combustion zone.

$$\begin{aligned}\theta_1 &= q_i' \left( \frac{\bar{q}}{P} \right) (\gamma-1) \frac{M}{S} \left[ e^{\frac{-tS}{C(1+M)}} - e^{\frac{-tS}{CM}} \right] \\ \theta_2 &= q_i' \left( \frac{\bar{q}}{P} \right) (\gamma-1) \frac{M}{S} \left[ 1 - e^{\frac{-tS}{CM(1-M)}} \right] \\ \theta_3 &= q_i' \left( \frac{\bar{q}}{P} \right) (\gamma-1) \frac{t}{CM} e^{\frac{-tS}{CM}}\end{aligned}\quad (23)$$

Mean steady-state values of temperature and velocity in the combustion zone are selected so that overall sonic travel time and throughflow drift time through the zone will be correct. With the gradients in the combustion zone defined by equation (13), the mean temperature and mean velocity in the zone are:

$$T_s = T_4 \left[ \frac{T_s/T_4 - 1}{2(\sqrt{T_s/T_4} - 1)} \right]^2, \quad V_s = V_4 \frac{(T_s/T_4 - 1)}{\ln(T_s/T_4)} \quad (24)$$

Where  $T_4$ ,  $T_s$ ,  $V_4$  refer to steady-state temperatures and velocity in sections (4) and (6) of Figure 1.

Equation (19) requires that the terms

$$\frac{FA}{T_1} \frac{\partial T_1}{\partial FA} \quad (25)$$

and

$$\frac{FA}{\eta} \frac{\partial \eta}{\partial FA} \quad (26)$$

be defined. The first term is defined by the steady-state operating point on the ideal temperature rise curve, Figure 4. The second term is defined by the steady-state operating point on the efficiency curve, Figure 3.

This completes the system combustion equation development. These equations describe the response of combustion heat release throughout the combustion zone to disturbances in velocity and density at the spraybars and flameholders. A complete list of the equations is given in Appendix B. In the list,  $q_i'$  has been renamed  $q'_{in}$  where it appears in equation (20) and  $q'_{out}$  where it appears in equation (19). The reason for this change is discussed in the following section, "Solution Technique."



### (5) Solution Technique

The equations in Appendix B are the Laplace transformed versions of the time-dependent equations describing the augmentor. By setting  $q'_{in} = q'_{out}$ , which is the actual case, these equations would form a set of homogeneous equations whose determinant is the characteristic function (CF) of the system. If some small arbitrary disturbance were to be introduced into the system, and then removed, the set of equations could be solved for the time response of the system. The time response would contain terms of the form:

$$e^{rt} \sin \omega t$$

where  $r$  and  $\omega$  are the real and imaginary parts of a zero of the characteristic function. If  $r$  is positive, the time response is an oscillation of circular frequency  $\omega$  with a growing amplitude, indicating an unstable system. If  $r$  is negative, the oscillation dies out with time, and the system returns to its original state.

To solve for the time solution would require the identification of every zero of the CF, which is an involved process. An alternate technique, and the one adopted for the rumble model, is to simply determine whether there are any zero's of the CF with a positive real part without actually solving for the zero's. To do this, the following ratio, called the "open loop transfer function":

$$\frac{q'_{out}}{q'_{in}} = \frac{N(S)}{D(S)}$$

is formed from the set of system equations in Appendix B, using Cramer's rule. Then since  $q'_{in} = q'_{out}$ , it follows that:

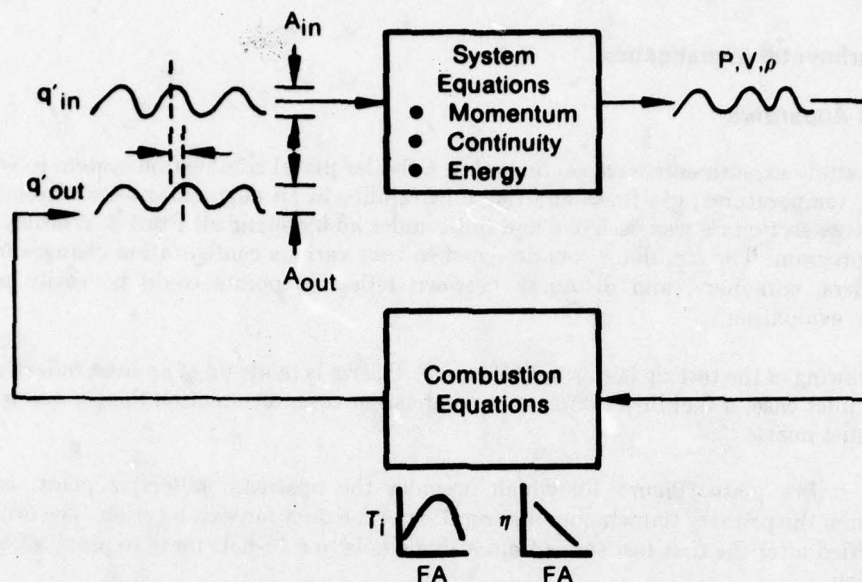
$$\frac{q'_{out}}{q'_{in}} = \frac{N(S)}{D(S)} = 1 + \frac{CF(S)}{D(S)} \quad (27)$$

At a zero of  $CF(S)$ , the open loop transfer function  $q'_{out}/q'_{in}$  will become one. If a zero of  $CF(S)$  is encircled, while avoiding encirclement of a zero of  $D(S)$ , a polar plot of the open loop transfer function will encircle the point one. By encircling the entire right half of the "S" plane, and watching for encirclements of one by  $q'_{out}/q'_{in}$ , it is determined whether there are any zero's of  $CF(S)$  with a positive real part. In practice, an amplitude and phase plot is used rather than a polar plot. As a by-product of the technique, the frequency response of every variable in the system to a sinusoidal variation in combustion heat release,  $q'_{in}$ , is obtained, which is useful in examining the model.

A physical interpretation of the solution technique can be gained by reference to Figure 7. A sinusoidal disturbance oscillation in combustion heat release,  $q'_{in}$ , produces an oscillation in pressure, velocity, and density throughout the augmentor, which, in turn, produces an oscillation in combustion heat release,  $q'_{out}$ . If the "feedback" heat release is in phase with the disturbance, and has greater amplitude, the system will be unstable.

A typical open loop transfer function is plotted in Figure 8 which indicates an instability at 56 Hz.

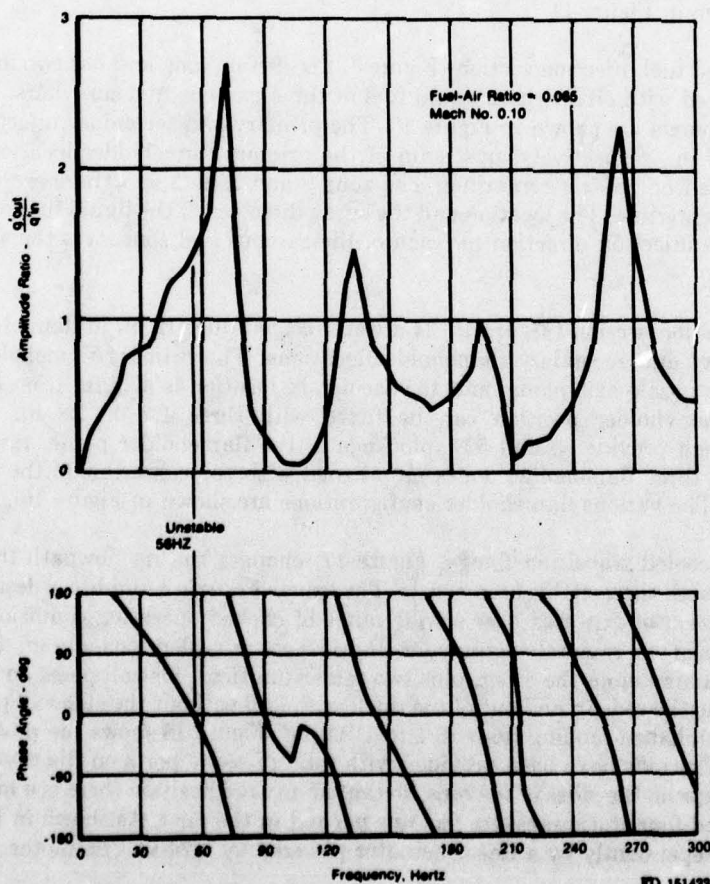




- Unstable if at Some Frequency:  $A_{out} \geq A_{in}$  and  $\phi = 0$

Figure 7. Condition for Rumble

FD 144859



FD 151433

Figure 8. Open Loop Transfer Function Baseline Configuration

### **c. Experimental Investigation**

#### **(1) Test Apparatus**

The study experiments were conducted in a (boiler plate) combustion system in which the pressures, temperatures, gas flows and flame instability in an augmentor were simulated. The circular cross-section rig was designed and built under an independent Pratt & Whitney Aircraft research program. The simulator was designed so that various configuration changes including flameholders, spraybars, and distances between reflective points could be easily made for diagnostic evaluation.

A drawing of the test rig is shown in Figure 9. The rig is made up of an inlet reflective orifice plate, an inlet case, a fuel injection case, a combustion case, a transition flange, and a variable area exhaust nozzle.

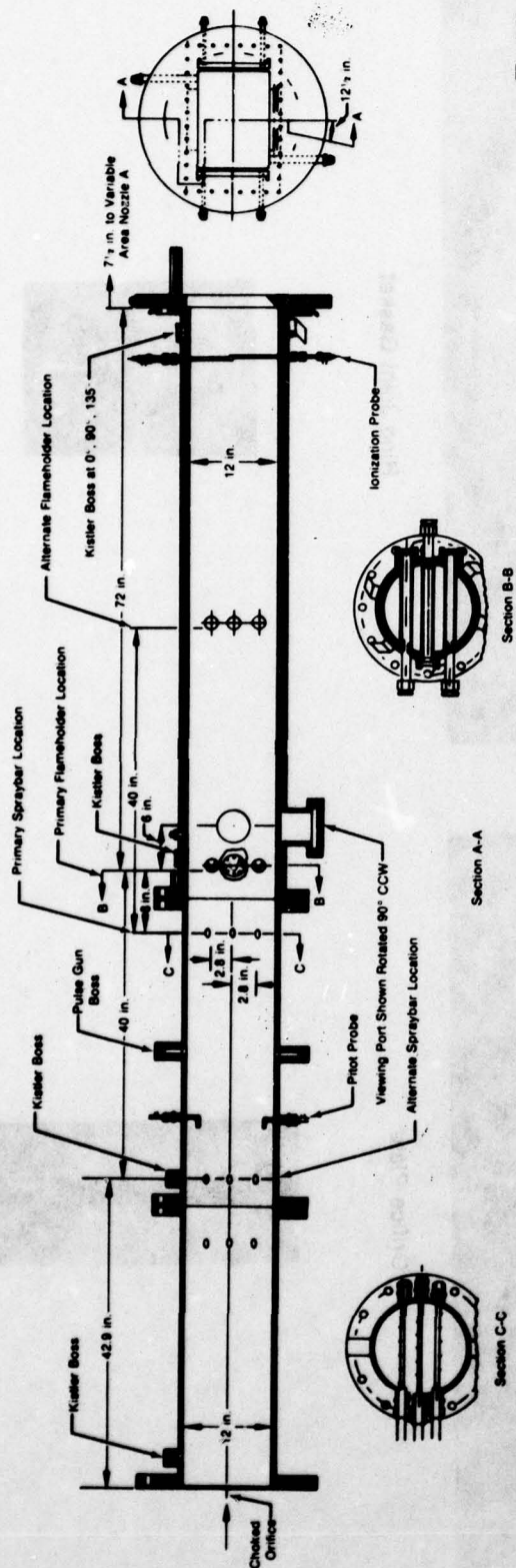
The orifice plate (Figure 10) which provides the upstream reflective point, is located 82.9 in. from the primary flameholder and represents the duct fan exit location. The orifice plate was modified after the first test series from a single hole to a 16-hole plate to provide better flow distribution.

The inlet case is 39.9 in. long with a 12 in. diameter. Its primary function is to permit a fan duct simulation length variation by inserting the orifice/reflective plate at its inlet or its exit. The inlet case is shown in Figure 11.

The uncooled fuel injection section (Figure 12) is 39.4 in. long and has two injection planes which can be fitted with either three liquid fuel or three gaseous fuel spraybars. Typical liquid and gaseous spraybars are shown in Figure 13. The primary and secondary injection planes are located 8 and 40 in., respectively, upstream of the primary flameholder location. The zone 1 spraybar is located on the rig centerline. The zone 2 and zone 3 spraybars are located 2.8 in. outboard of the centerline. The location and the spray direction of the liquid fuel zones are shown in Figure 14. The injection direction for each of the gaseous fuel zones was the same as for the liquid fuel zones.

The combustion section (Figure 15) is a water-cooled duct 12 in. in diameter and 76.6 in. long with primary and secondary flameholder locations. The primary flameholder location is 79.5 in. from the nozzle exit plane, and the secondary location is 47.5 in. from the nozzle exit plane. Either flameholder position can be fitted with three 1.2 or 1.8 in. wide V-gutter flameholders which provide 35 and 52% blockage at the flameholder plane, respectively. The centerline of the three flameholder zones are aligned with the centerline of the respective fuel spraybar zones. The various flameholder configurations are shown in Figure 16.

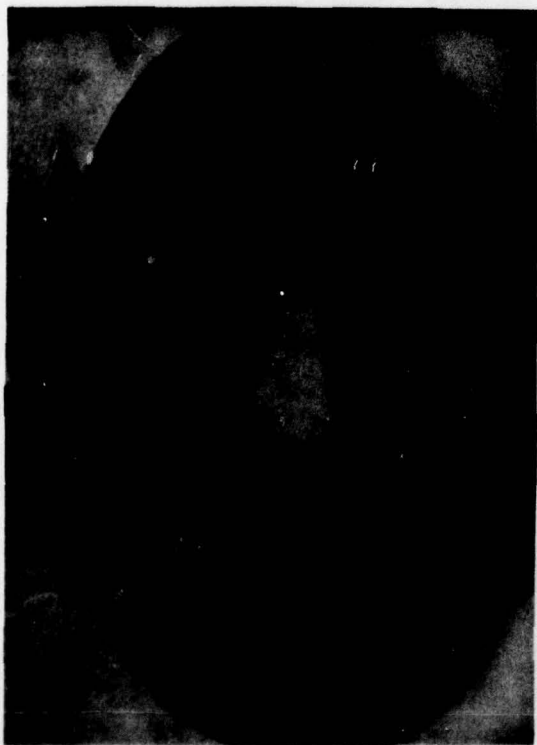
The water-cooled transition flange, Figure 17, changes the rig flowpath from circular to rectangular to match the variable area nozzle. The exhaust nozzle assembly is designed to permit continuous variation of exit area over a wide range of choked operating conditions. The nozzle assembly consists of two remotely actuated cylindrical water-cooled rods, 4½ in. diameter on one end and 1¾ in. diameter on the other, plus two semicylindrical sidewall plugs and two flat plate sidewalls. Moving the rods in and out of the duct, with and without the sidewall plugs, results in a geometric area change ranging from 16.1 to 112.9 in<sup>2</sup>. Figure 18 shows the possible geometric area extremes. The rods have been provided with total pressure ports on the upstream side and static pressure taps on the sides of the rods, so that at any rod position there is a minimum of five total pressure and four static pressure pickups per rod in the duct. As shown in Figure 19, each rod is driven independently by a linear actuator powered by a 24-volt dc motor.



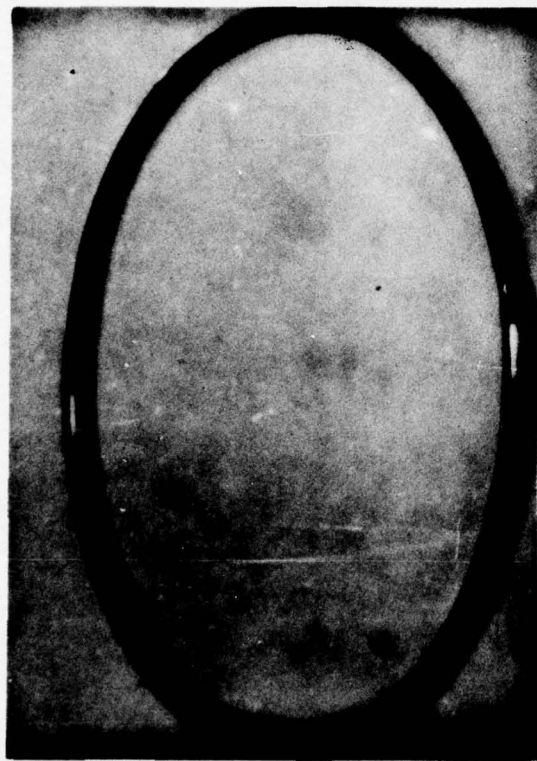
FD 146485

Figure 9. System Instability Study Test Rig

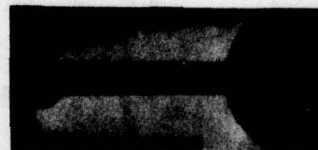




Orifice Plate



Ring Joint Gasket



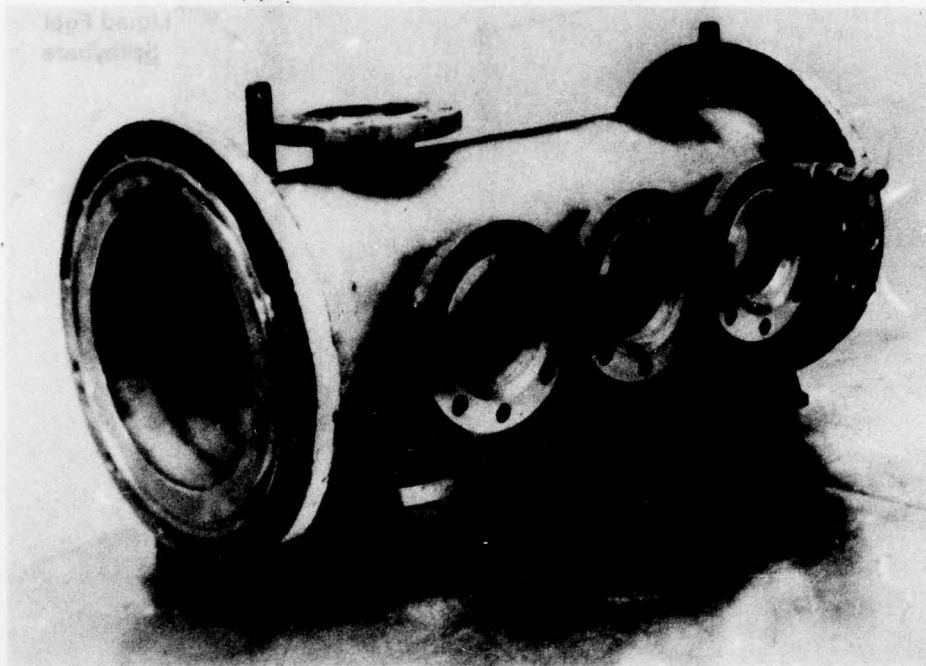
Target Probe



Flameholder Blank-Off

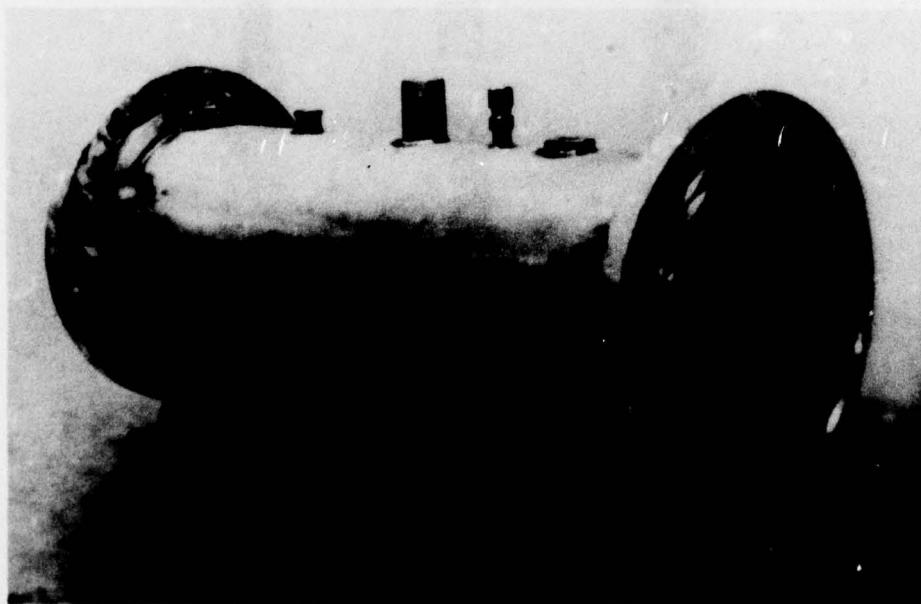
FD 140114

Figure 10. Rig Hardware



*Figure 11. Inlet Case*

FD 140128

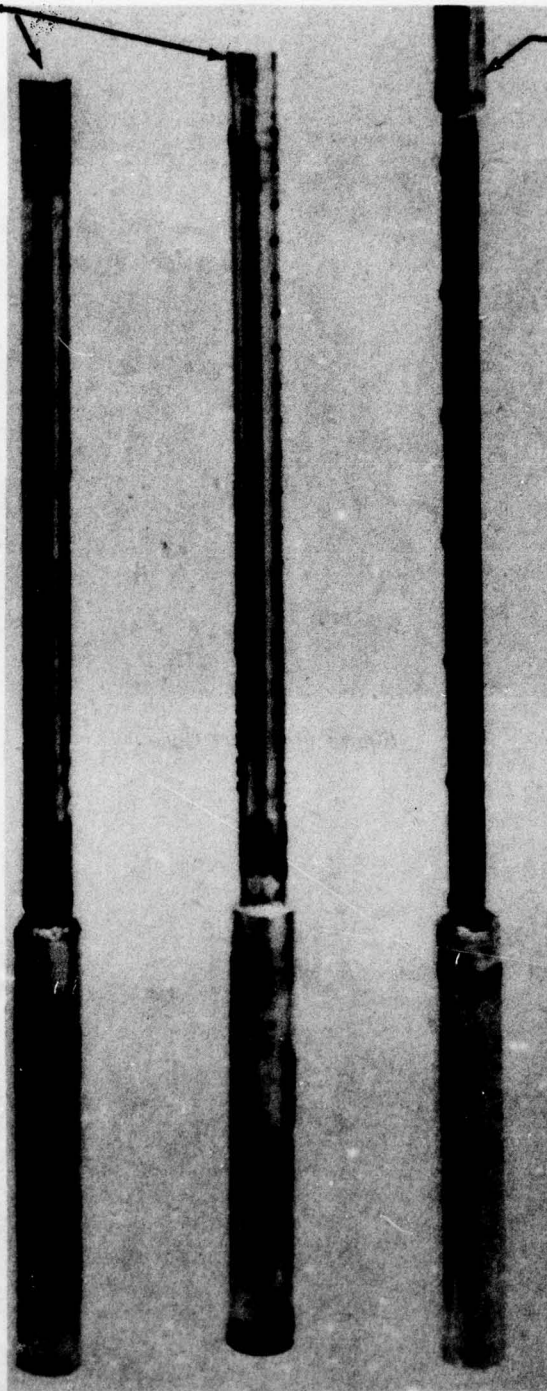


*Figure 12. Fuel Injection Case*

FD 140130

Gaseous Fuel  
Spraybars

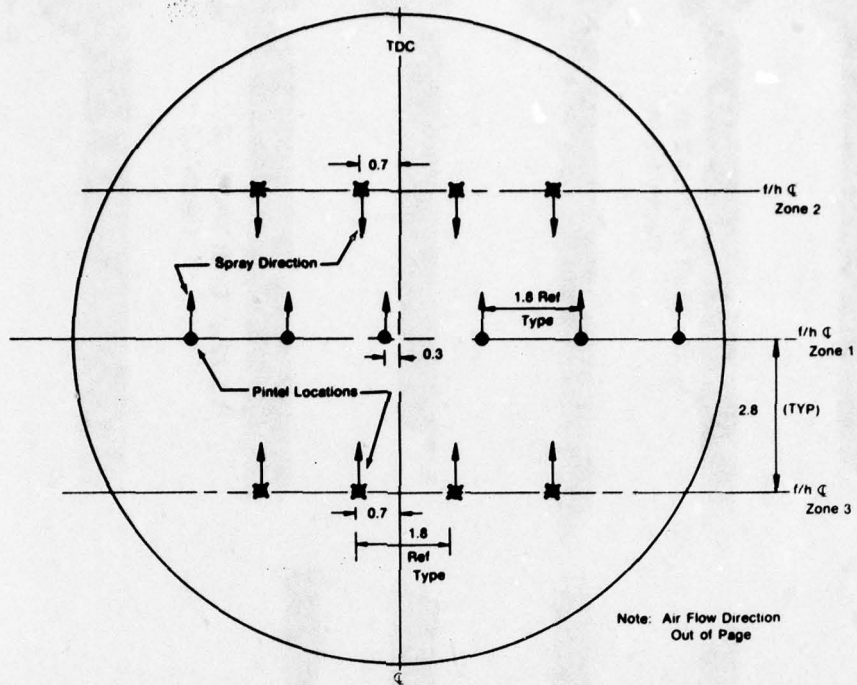
Liquid Fuel  
Spraybars



*Figure 13. Fuel Spraybars*

FD 140117





FD 140054

Figure 14. Spray Direction and Pintel Location With Liquid Fuel Injectors

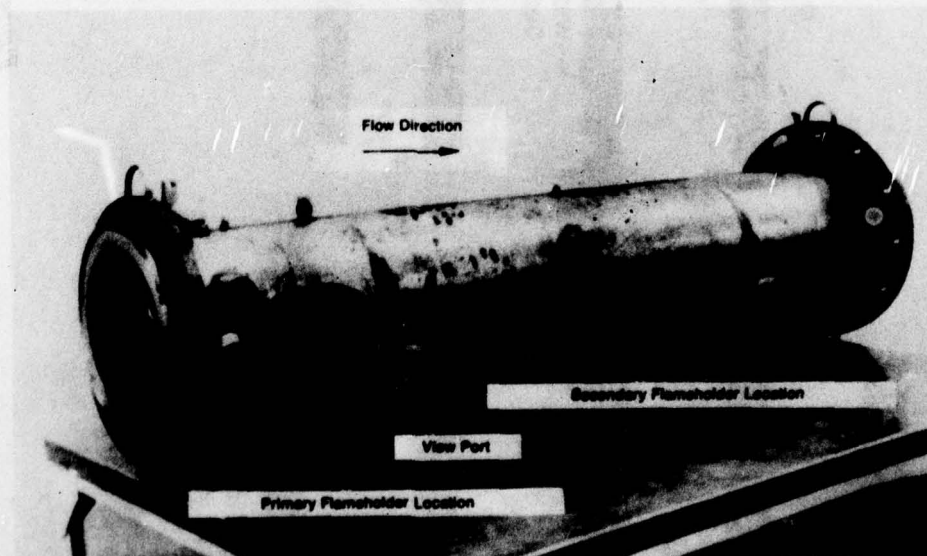
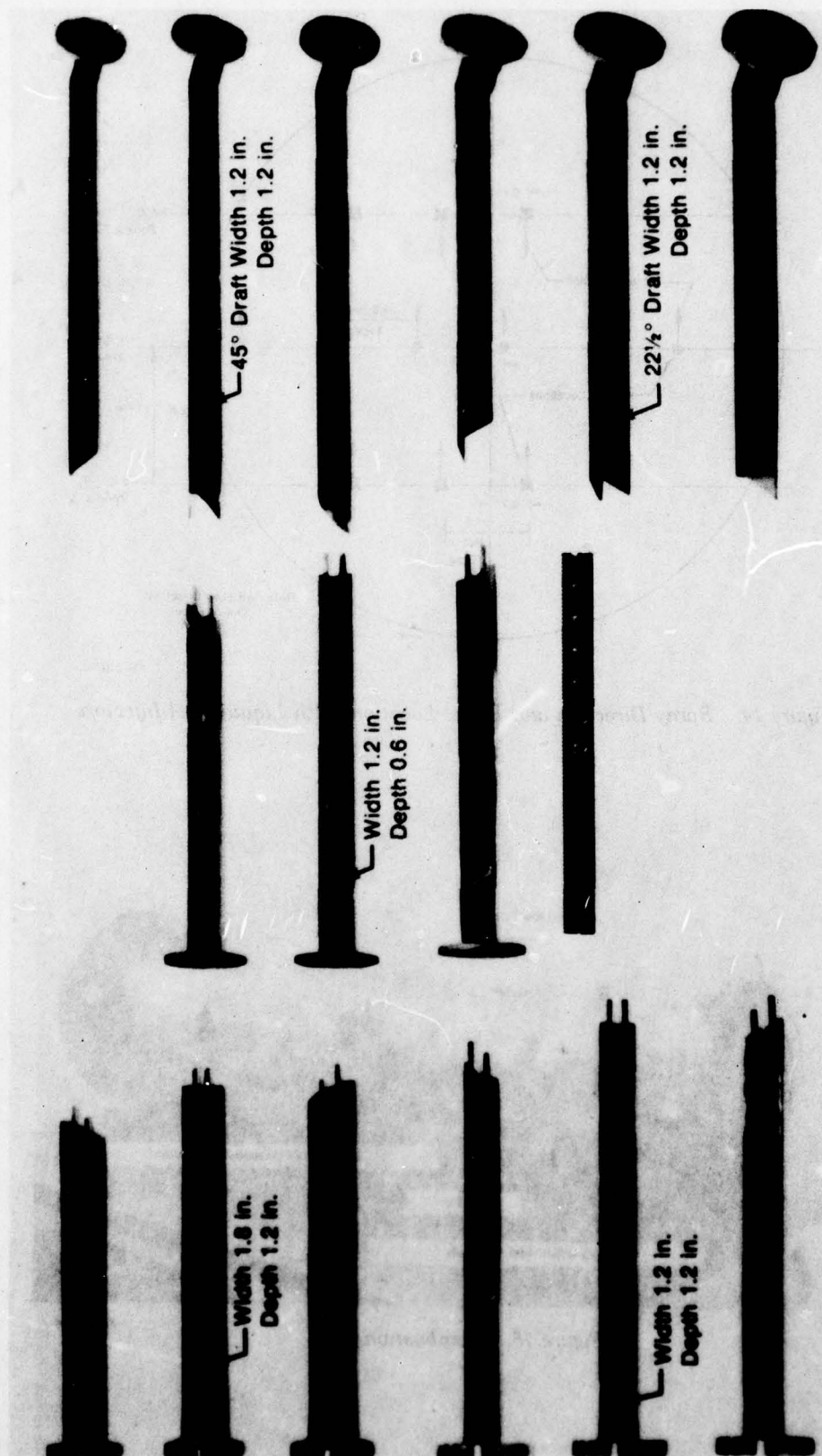


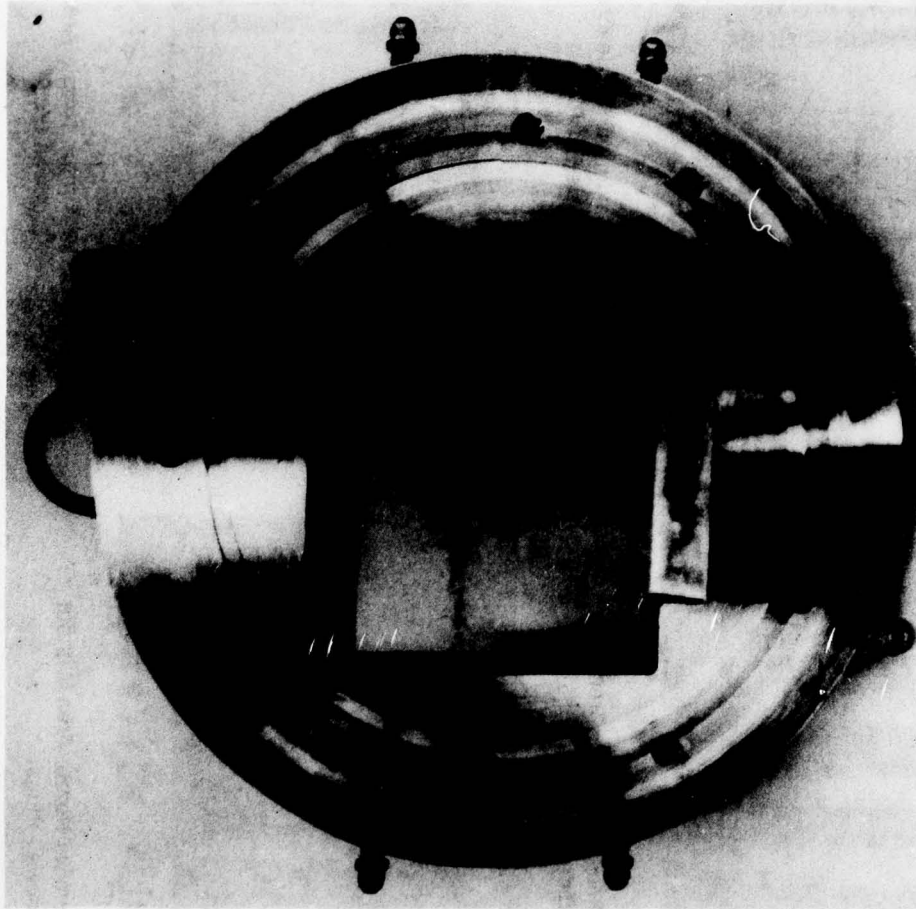
Figure 15. Combustion Case

FD 140116



FD 14015

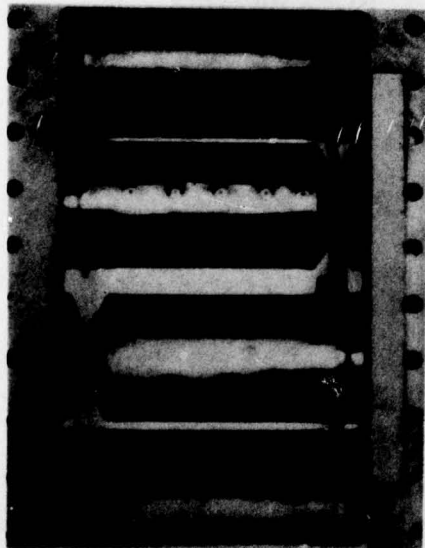
Figure 16. Flame Holders



FD 140129

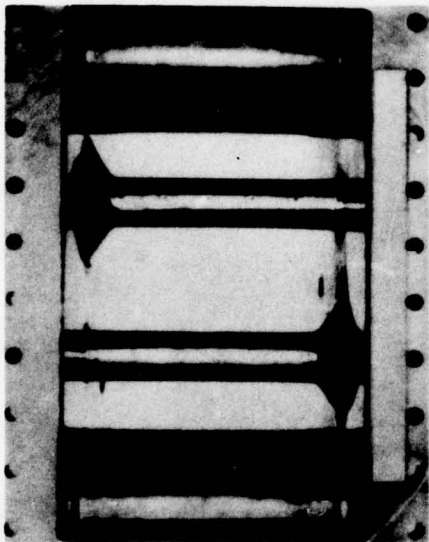
*Figure 17. Transition Flange*





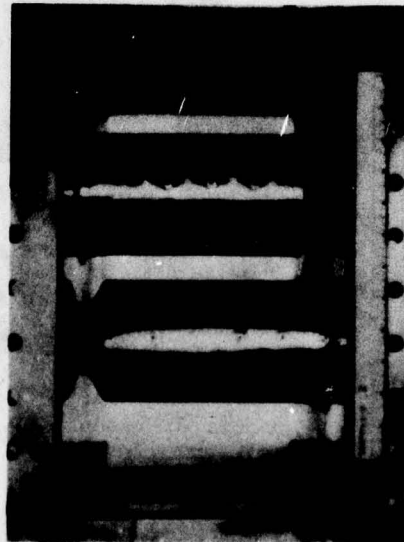
FE 89376

a. Minimum Nozzle Area With  
Sidewall Plugs



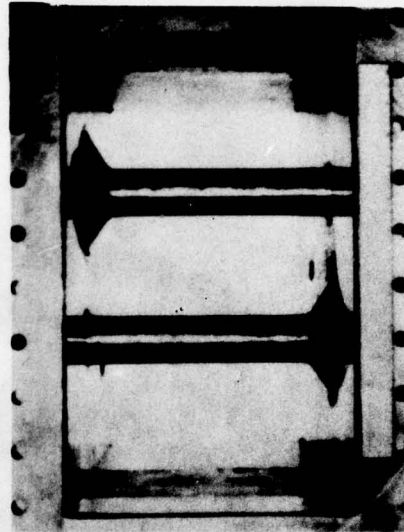
FE 89376

b. Maximum Nozzle Area With  
Sidewall Plugs



FE 89376

c. Minimum Nozzle Area Without  
Sidewall Plugs

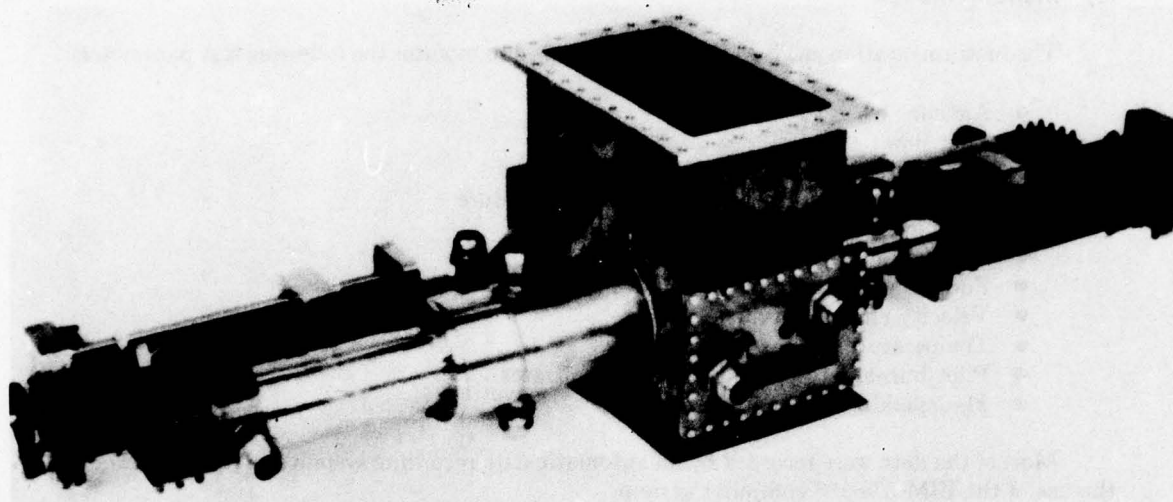


FE 89377

d. Maximum Nozzle Area Without  
Sidewall Plugs

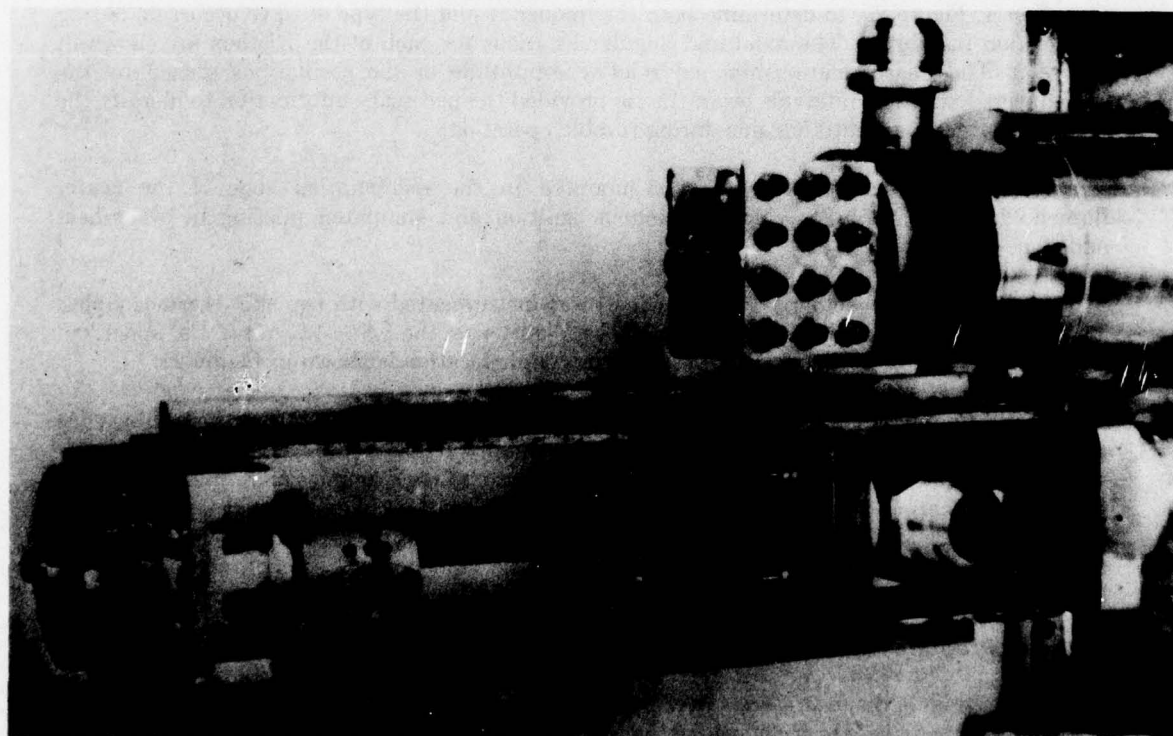
FD 14018

Figure 18. Geometric Nozzle Area Extremes



**a. Variable Area Nozzle Actuator Assembly**

FE 89373



**b. Nozzle Actuator Assembly**

FE 89381

**Figure 19. Nozzle Actuator Assembly**

PD 140113

## **(2) Instrumentation**

The instrumentation as given in Table 1 was used to monitor the following test parameters:

- Airflow
- Fuel flow
- Rig inlet total pressure and temperature
- Combustor inlet total pressure and temperature
- Combustor exit total pressure
- Combustor pressure oscillations
- Fuel temperature, flowrate, and pressure
- Velocity changes in duct
- Temperature changes in combustor
- Pilot burner oxygen and acetylene flowrates
- Flameholder skin temperature.

Most of the data were recorded by an automatic data recording system and reduced through the use of the IBM 370-168 computer system.

The special test items unique to this program are discussed in the following paragraphs.

The combustor was instrumented with six high-response Kistler Model 606A pressure transducers, Figure 20, to determine both the frequency and the type of wave occurring during combustion instability. The axial and angular locations for each of the Kistlers are shown in Figure 9. The phase relationship and relative amplitude of the oscillations sensed by the transducers located at intervals down the rig provided the necessary information to identify the wave pattern and amplitude gains during rumble operation.

An oxy-acetylene pilot torch was mounted in the recirculation zone of the center flameholder. This torch provided continuous ignition and simulated piloting by wake-heat addition.

The center flameholder position, zone 1, was instrumented with two skin thermocouples. They were attached to the upstream side of the V-gutter on the  $1.8 \times 1.2$ ,  $1.2 \times 1.2$ , and  $1.2 \times 0.6$  flameholder configurations. A typical thermocouple location is shown in Figure 21.

Two 4-in. diameter vycor glass viewing ports were located 180 deg apart at the trailing edge of the primary flameholder so that high-speed color motion pictures could be made during steady-state and rumble operation to provide comparative data on flow dynamics and combustion. Two air-cooled ionization probes (see the rig layout, Figure 9) are used to determine gas temperature increase or decrease. The temperature changes are correlated with velocity change detected by a strain gage attached to a target probe upstream of the flameholders. The correlation between local temperature and velocity changes provide additional data on the rumble mechanism.

## **(3) Test Program**

Seven series of diagnostic tests were originally planned. The purpose of these tests, as shown in Figure 22, was to isolate or determine the mechanism(s) of rumble. Test Series I was designed to determine the rumble characteristics of the test rig and served as a baseline for the program. The balance of the test program was planned to be spent investigating the effects of (1) fuel vaporization, (2) duct length, (3) turbulent level upstream of the flameholders, (4) fuel injection system stiffness, (5) heat addition on the recirculation zone, and (6) combustion efficiency oscillations on the augmentor system stability. After completion of the first test series, the test program was modified. The revised test program, as shown in Figure 23, was a composite program



combining the test requirements of both the Lo-Frequency Augmentor Instability study and the companion Flameholder Combustion Instability contract (F33615-76-C-2023) into a single test program to cost-effectively gather the most data. The test matrix was not significantly changed from the original program, i.e., most of the original items to be investigated were still included.

TABLE 1. LO-FREQUENCY AUGMENTOR INSTABILITY STUDY RIG INSTRUMENTATION DESCRIPTION

<i>Item</i>	<i>Location</i>	<i>Sensor</i>	<i>Indication</i>
1. Orifice-Pressure	Upstream of Test Rig	Two Total Pressure Probes  Two Static Pressure Taps (upstream)  Two Static Pressure Taps (downstream)	Two 150-psi Gages for Control Room Monitoring  Automatic Data Recording System
2. Orifice-Temperature	Upstream of Test Rig	Two Total Temperature Probes	Direct Reading Potentiometer for Control Room Monitoring. Automatic Data Recording.
3. Inlet Total Pressure	Fuel Injection Case	Two Total Pressure Probes	Automatic Data Recording System
4. Inlet Static Pressure	Fuel Injection Case	One Static Pressure Probe  Two Wall Static Pressure Taps	Automatic Data Recording System
5. Inlet Total Temperature	Fuel Injection Case	Chromel-Alumel Thermocouples (two locations)	Direct Reading Potentiometer for Control Room Monitoring. Automatic Data Recording.
6. Combustor Exit— Total Pressure	Exhaust Nozzle Plane	Eight Total Pressure Ports Located in Water-Cooled Exhaust Nozzle Rods (four in each rod)	Two 50-psi Gages for Control Room Monitoring. Automatic Data Recording.
Combustor Exit— Static Pressure	Combustor Case	Four Wall Static Pressure Taps	Automatic Data Recording System
7. Combustor Pressure Oscillations	Inlet Case, Fuel Injection Section and Combustor Section	Six High Response Dynamic Pressure Sensors	Oscillograph for Control Room Monitoring. FM tape recorded.
8. Fuel Flowrate	Fuel Supply Line (each zone)	Turbine Flowmeter	Electronic Counter for Control Room Monitoring. Automatic Data Recording.
9. Fuel Temperature	(1) Fuel Line Near Flowmeter (2) Fuel Line Near Test Sector	Thermocouple	Direct-Reading Potentiometer for Control Room Monitoring. Automatic Data Recording.
10. Fuel Pressure	Fuel Line Near Test Rig (each zone)	Pressure Transducer	Two 500-psi Gages for Control Room Monitoring. Automatic Data Recording.
11. Velocity Changes	Fuel Injection Case — 7 in. Upstream of Primary Fuel Injection Plane	Strain Gage — Target Probe	Oscillograph for Control Room Monitoring. FM tape recorded.
12. Temperature Changes	Combustor Case — 14 and 69 in. From Nozzle Exit Plane	One Ionization Probe	Oscillograph for Control Room Monitoring. FM tape recorded.

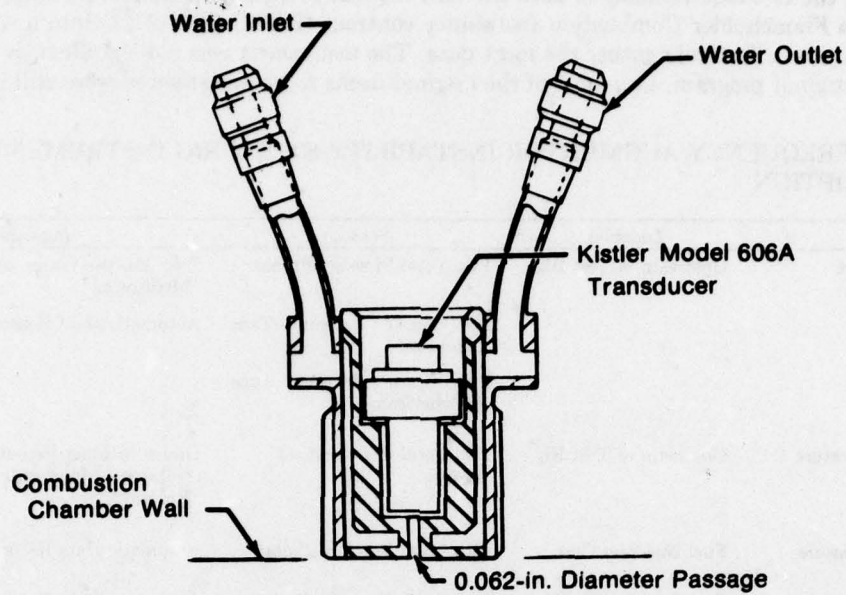
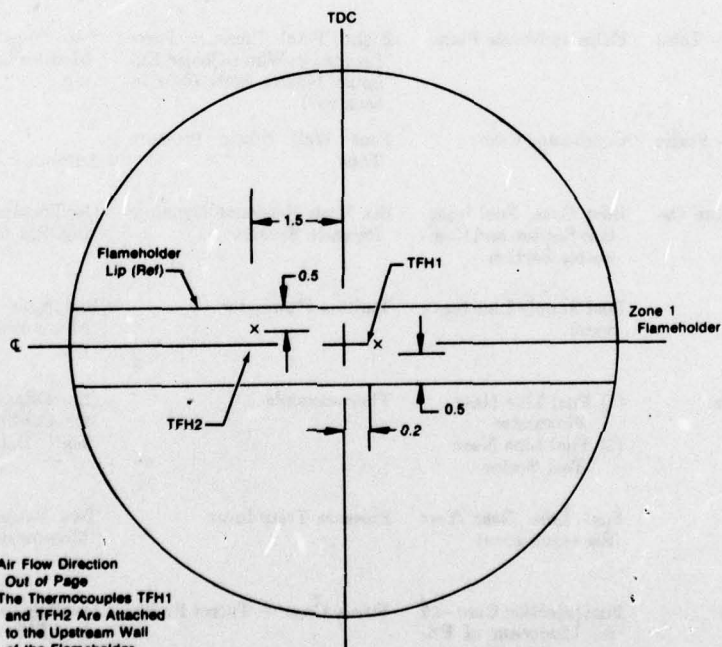


Figure 20. Kistler Model 606A Installed in Water Cooled Adapter

FD 65612A



- Note: 1. Air Flow Direction  
Out of Page
2. The Thermocouples TFH1  
and TFH2 Are Attached  
to the Upstream Wall  
of the Flameholder

FD 140055

Figure 21. Flameholder Skin Thermocouple Locations

Series	Test Cond No.	Flameholders			Fuel Type	Orifice to Nozzle Distance in.	Spraybar to Flameholder Distance in.	Flameholder to Nozzle Distance in.	Test Conditions				Test Purpose
		Number	Width in.	Blockage %					Inlet Pressure psia	Inlet Temp °F	Inlet Mach No	Fuel/Air Ratio	
I	1	3	1.2	35	JP-4	163	9	78	6.5	200	0.12-0.25	0.045-0.15	Map System Low Frequency Stability Characteristics of the Experimental Apparatus. High Speed Motion Pictures Will Be Filmed During "Rumble"
	2	3	1.2	35	JP-4	163	9	78	10	400	0.12-0.25	0.045-0.15	
	3	3	1.2	35	JP-4	123	9	78	30	1300	0.12-0.25	0.045-0.15	
	4	3	1.8	52	JP-4	163	9	78	6.5	200	0.12-0.25	0.045-0.15	
	5	3	1.8	52	JP-4	163	9	78	10	400	0.12-0.25	0.045-0.15	
	6	3	1.8	52	JP-4	123	9	78	30	1300	0.12-0.25	0.045-0.15	
II	7	3	(1)	(1)	JP-4	163	42	78	(2)	(2)	(2)	(2)	Determine the Effect of Fuel Vaporization on System Stability
	8	3	(1)	(1)	JP-4	163	42	78	(2)	(2)	(2)	(2)	
	9	3	(1)	(1)	CH <sub>4</sub>	163	42	78	(2)	(2)	(2)	(2)	
	10	3	(1)	(1)	CH <sub>4</sub>	163	42	78	(2)	(2)	(2)	(2)	
III	11	3	(1)	(1)	JP-4	123	9	78	(2)	(2)	(2)	(2)	Determine the Effect of System Length on System Stability
	12	3	(1)	(1)	JP-4	123	9	78	(2)	(2)	(2)	(2)	
IV	13	3	(1)	(1)	JP-4	123	9	78	(2)	(2)	(2)	(2)	Determine the Effect of Turbulence at the Flameholders and Spraybars on System Stability (3)
	14	3	(1)	(1)	JP-4	163	9	78	(2)	(2)	(2)	(2)	
	15	3	(1)	(1)	JP-4	163	9	78	(2)	(2)	(2)	(2)	
	16	3	(1)	(1)	JP-4	163	9	78	(2)	(2)	(2)	(2)	
V	17	3	(1)	(1)	JP-4	163	9	78	(2)	(2)	(2)	(2)	Determine the Effect of Injection Point ΔP on System Stability (4)
	18	3	(1)	(1)	JP-4	163	9	78	(2)	(2)	(2)	(2)	
VI	19	3	(1)	(1)	JP-4	163	42	41	(2)	(2)	(2)	(2)	Determine the Effect of Combustion Efficiency Oscillations on System Stability
	20	3	(1)	(1)	JP-4	163	42	41	(2)	(2)	(2)	(2)	
VII	21	3	(1)	(1)	JP-4	163	9	78	(2)	(2)	(2)	(2)	Determine the Effect of Flameholder Recirculation Wake Energy on System Stability (5)
	22	3	(1)	(1)	JP-4	163	9	78	(2)	(2)	(2)	(2)	

Notes:

- (1) Geometry of Test Conditions 7 through 22 Will Be Based on the Stability Limits Determined in Test Conditions 1 through 6.
- (2) Exact Test Conditions Will Depend on Stability Limits Determined During Test Conditions 1 through 6.
- (3) Two Different Screens Will Be Tested. Both Screens Will Be 123 inches from the Nozzle.
- (4) Two Different Spraybar JP's at the Same Flowrate Will Be Tested.
- (5) Energy Will Be Added by Use of an Oxy-Acetylene Burner at the Flameholder.

Figure 22. Lo-Frequency Augmentor Instability Investigation Test Matrix



Test Point	Flameholder Configuration	Fuel Type	Special Test Instrumentation	Test Condition	Test Purpose
1	1.8X1.2 50% Blockage	JP4	None	Repeat Baseline at 200° and 400°F Inlet Temperature at 10 psi and 0.1, 0.15 Mach Number	Repeat Series I Baseline Tests to Checkout System
2	Same as 1	JP4	Iso-Kinetic Probe Wake FA Probe Flameholder T/C's	Test Matrix, Torch Flowrate Variation at 200° and 400°F Inlet	Characterization of Approach and Wake Fuel-Air Ratio as a Function of Velocity Pressure, Temperature and Flameholder Geometry
3	1.2X1.2 35% Blockage	JP4	Wake FA Probe Flameholder T/C's	Same as 2	Same as 2
4	1.2X0.6 35% Blockage	JP4	Same as 3	Same as 3	Same as 2
5	1.2X1.2 35% Blockage 22½° Draft	JP4	None	Same as 1	Evaluate the Effect of Flameholder Drafting on Rumble and Combustion Efficiency
*6	1.2X1.2 35% Blockage 45° Draft	JP4	None	Same as 5	Same as 5
7	1.8X1.2 50% Blockage	JP4	Flameholder T/C's Two Turbulence Screens	Same as 1	Evaluate the Effect of Turbulence
8	Same as 2	CH4	Flameholder T/C's	Same as 1	Evaluation of Gaseous Fuel on Efficiency and Stability Limits
9	Same as 2	JP4	Flameholder T/C's	Relocate Fuel Injectors	Evaluate the Effect of Increased Fuel Injector to Flameholder Distance
10	Same as 2	JP4	Flameholder T/C's	Relocate Flameholders	Evaluate the Effect of Reduced Augmentor Length
11	Same as 3	JP4	Flameholder T/C's	Relocate Flameholders to Nominal Position, 1300°F Inlet Condition	Simulate Core Stream Effects. Evaluate the Effect of Augmentor Length - Shorten Cold Duct
*Did Not Test at This Point					

FD 146492

Figure 23. Lo-Frequency Augmentor Model and Flameholder Model Rig Tests

The only item deleted was the effect of fuel injection system stiffness because (1) a consensus of the investigators believed its impact on the program was minimal and (2) more test time could be allocated to the other suspected mechanisms. Most of the test program changes were reflected in the test operating conditions. In the original test matrix, bands of pressures, temperatures, duct Mach numbers and fuel-air ratios were given. The Series I test results, however, specifically defined the test conditions of interest within the capabilities of the system. The resultant test conditions are shown in Table 2. The revised program was approved by the Air Force project engineer.

TABLE 2. REVISED TEST CONDITIONS

Test No.	Inlet Pressure (psia)	Inlet Temperature (°F)	Equivalence Ratio $\phi$	Duct Mach Number
A	10	200 *	0.5, 1.0, 1.5	0.088
B	10	200	0.5, 1.0, 1.5	0.155
C	10	400 *	0.5, 1.0, 1.5	0.088
D	10	400	0.5, 1.0, 1.5	0.155
E	15	400 *	0.5, 1.0, 1.5	0.088
F	15	400	0.5, 1.0, 1.5	0.155
G	15	400	0.5, 1.0, 1.5	0.238

\* Run 2 or 3 torch flowrate variations at the completion of the isokinetic and wake FA data acquisition.

#### (4) Experimental Program Problems

##### (a) Series I Testing

The primary purpose of the Series I testing was to determine the rumble characteristics of the test rig, which would serve as a baseline for the Series II test program. A secondary purpose of the Series I testing was to evaluate the test rig hardware and instrumentation, which for the most part had not undergone previous testing.

The overall test rig condition after Series I testing was very good. No major damage was incurred. The target probes, ionization probes, and a total pressure probe, however, were damaged during the course of the testing. The damaged probes were repaired with slight modifications incorporated to improve durability. The upstream orifice, which had been installed to provide a known reflective location, was sending a jet of airflow throughout the burner system at the high airflow rates (10 to 13 lbm/sec). This jet was apparently not attached to any wall surface for the entire length of the burner system. To remedy the problem, the orifice plate was reworked by plugging the large single hole and remachining to include 16 smaller holes to maintain the same total open area. Since combustion efficiency could not be determined from the data with an unchoked nozzle, the sidewall plugs discussed earlier (Figure 18) were installed in the nozzle before Series II testing to ensure that choked flow could be maintained and combustion efficiency determined over the full range of operating conditions.

##### (b) Series II Testing

Some minor problems were also encountered during the Series II testing. The test facility ejector system was not operating at its specified efficiency and would have required major repairs to correct the deficiencies. Since combustion efficiency measurements were desired, choked flow at the exhaust nozzle was required. To maintain choked flow the lowest rig pressure was limited to approximately 14 psia and the rig duct Mach number to 0.12 compared to a planned rig pressure of 10 psia and duct Mach number of 0.155. It was determined that these revised conditions would provide the required input for the model, and the test program was modified accordingly.



Upon completion of the test program it was determined that the target probe, which had been modified at the conclusion of the Series I testing, was often vibrating at frequencies between 200 and 600 Hz when the airflow dynamic pressure measurements were 55 Hz. It was also determined that the ionization probes were occasionally grounded due to dampness that resulted in a 60 Hz, high gain signal. Because the test program had been completed when these two discrepancies were determined and the elimination of these two pieces of instrumentation would have only a minor impact on the model input, the data was disregarded. It was felt that disregarding all data would be more prudent than to draw conclusions from data that may or may not be correct.

The final problem area of the Series II testing involved the zone 3 spraybar. After the completion of the testing with the turbulence screens it was determined that the spraybar had been partially plugged with Teflon tape that had been used to seal the fuel system fittings. The tape was removed and the spraybar recalibrated prior to resuming the test program, but the data from the previous test sequence involving zone 3 full flow was disregarded. This problem also had a minor impact on the model input.

#### **(5) Data Analysis**

During rumble, pressure amplitudes were recorded as a function of time. Typical amplitudes prior to blowout are shown in Figure 24. It is apparent in this figure that there may be more than one frequency present and that the amplitude of the higher frequency component varies with time.

These frequency and amplitude shifts make it difficult to determine the phase and amplitude relationships between the various Kistler probes. To overcome this problem, all the pressure amplitude data recorded on magnetic tape in the Series II testing was electronically processed in transfer function form. A transfer function is expressed as the amplitude ratio and phase difference between two pressures as a function of frequency. The flameholder Kistler probe was selected as the base for comparison.

Figure 25 shows a typical transfer function. The data used to define this figure was averaged over a 16-sec time interval. For the example data point, rumble occurs in two distinct frequency bands  $\approx 10$  Hz wide, centered at 45 and 60 Hz. Any amplitudes which were less than 5% of the average pressure amplitude were deleted. Transfer function results are summarized in Appendix A.

#### **(6) Experimental Results**

##### **(a) Series I Tests**

Experimental rig tests were conducted in two phases. The first test phase was designed to map the test rig's rumble characteristics and to determine the test rig's structural integrity.

Approximately 100 different combinations of inlet pressure, temperature, airflow, fuel-air ratio, choked and unchoked nozzles were investigated in the first test phase for two different flameholder blockages. Fuel distribution and exhaust nozzle conditions were found to have a significant effect on rumble amplitudes and blowout characteristics.

Fuel distribution is shown in Figure 26 to effect both rumble amplitude and blowout fuel-air ratio. The lowest pressure amplitudes and the widest blowout limits are obtained with uniform fuel distribution. It should also be noted that fuel distribution only affects stability at high fuel-air ratios. This is significant because rumble in turbofan engines occurs at high fuel-air ratios and serves to ensure confidence that data from the test rig is representative of engine data.



The only item deleted was the effect of fuel injection system stiffness because (1) a consensus of the investigators believed its impact on the program was minimal and (2) more test time could be allocated to the other suspected mechanisms. Most of the test program changes were reflected in the test operating conditions. In the original test matrix, bands of pressures, temperatures, duct Mach numbers and fuel-air ratios were given. The Series I test results, however, specifically defined the test conditions of interest within the capabilities of the system. The resultant test conditions are shown in Table 2. The revised program was approved by the Air Force project engineer.

TABLE 2. REVISED TEST CONDITIONS

Test No.	Inlet Pressure (psia)	Inlet Temperature (°F)	Equivalence Ratio $\phi$	Duct Mach Number
A	10	200 *	0.5, 1.0, 1.5	0.088
B	10	200	0.5, 1.0, 1.5	0.155
C	10	400 *	0.5, 1.0, 1.5	0.088
D	10	400	0.5, 1.0, 1.5	0.155
E	15	400 *	0.5, 1.0, 1.5	0.088
F	15	400	0.5, 1.0, 1.5	0.155
G	15	400	0.5, 1.0, 1.5	0.238

\* Run 2 or 3 torch flowrate variations at the completion of the isokinetic and wake FA data acquisition.

#### (4) Experimental Program Problems

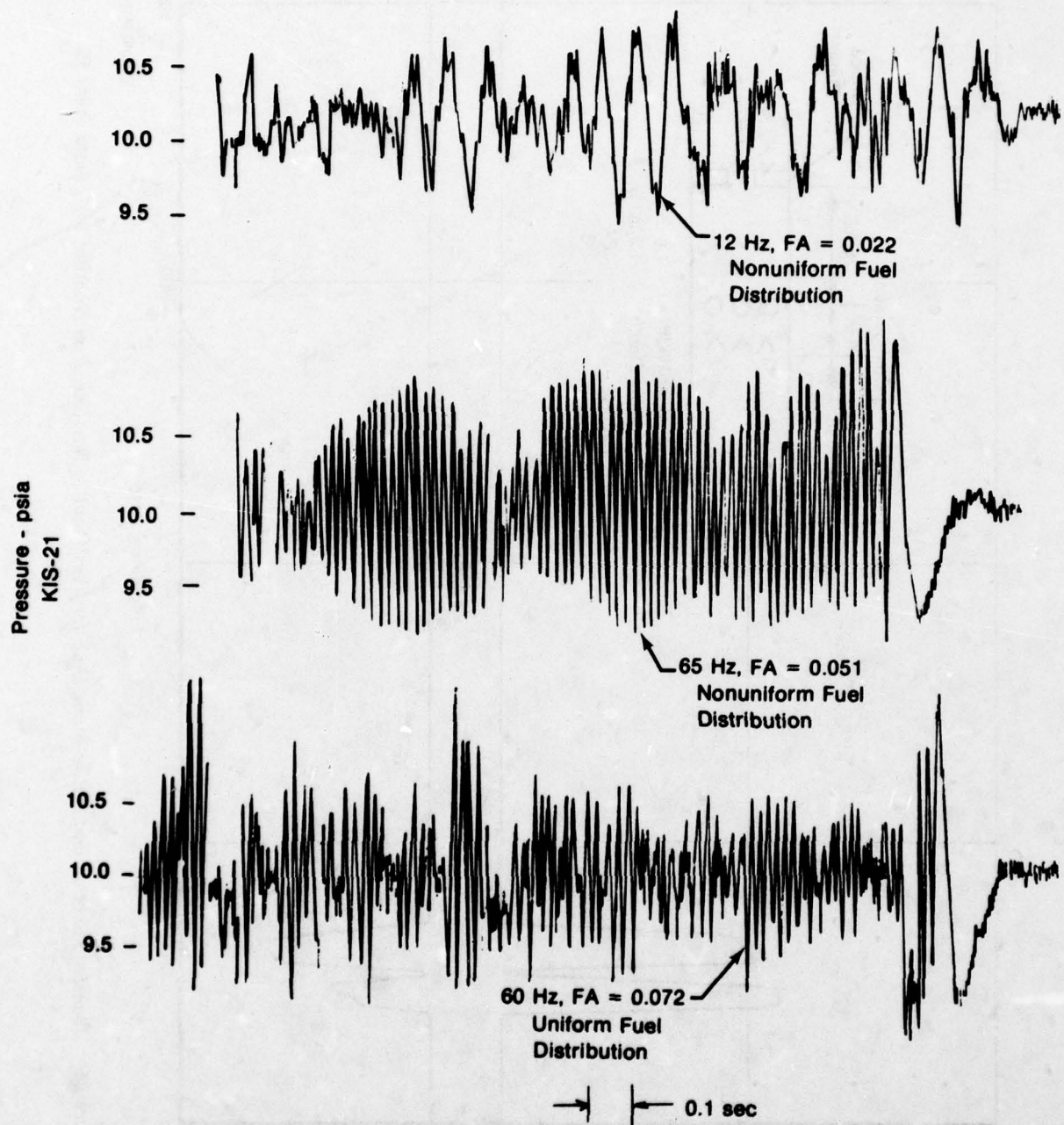
##### (a) Series I Testing

The primary purpose of the Series I testing was to determine the rumble characteristics of the test rig, which would serve as a baseline for the Series II test program. A secondary purpose of the Series I testing was to evaluate the test rig hardware and instrumentation, which for the most part had not undergone previous testing.

The overall test rig condition after Series I testing was very good. No major damage was incurred. The target probes, ionization probes, and a total pressure probe, however, were damaged during the course of the testing. The damaged probes were repaired with slight modifications incorporated to improve durability. The upstream orifice, which had been installed to provide a known reflective location, was sending a jet of airflow throughout the burner system at the high airflow rates (10 to 13 lbm/sec). This jet was apparently not attached to any wall surface for the entire length of the burner system. To remedy the problem, the orifice plate was reworked by plugging the large single hole and remachining to include 16 smaller holes to maintain the same total open area. Since combustion efficiency could not be determined from the data with an unchoked nozzle, the sidewall plugs discussed earlier (Figure 18) were installed in the nozzle before Series II testing to ensure that choked flow could be maintained and combustion efficiency determined over the full range of operating conditions.

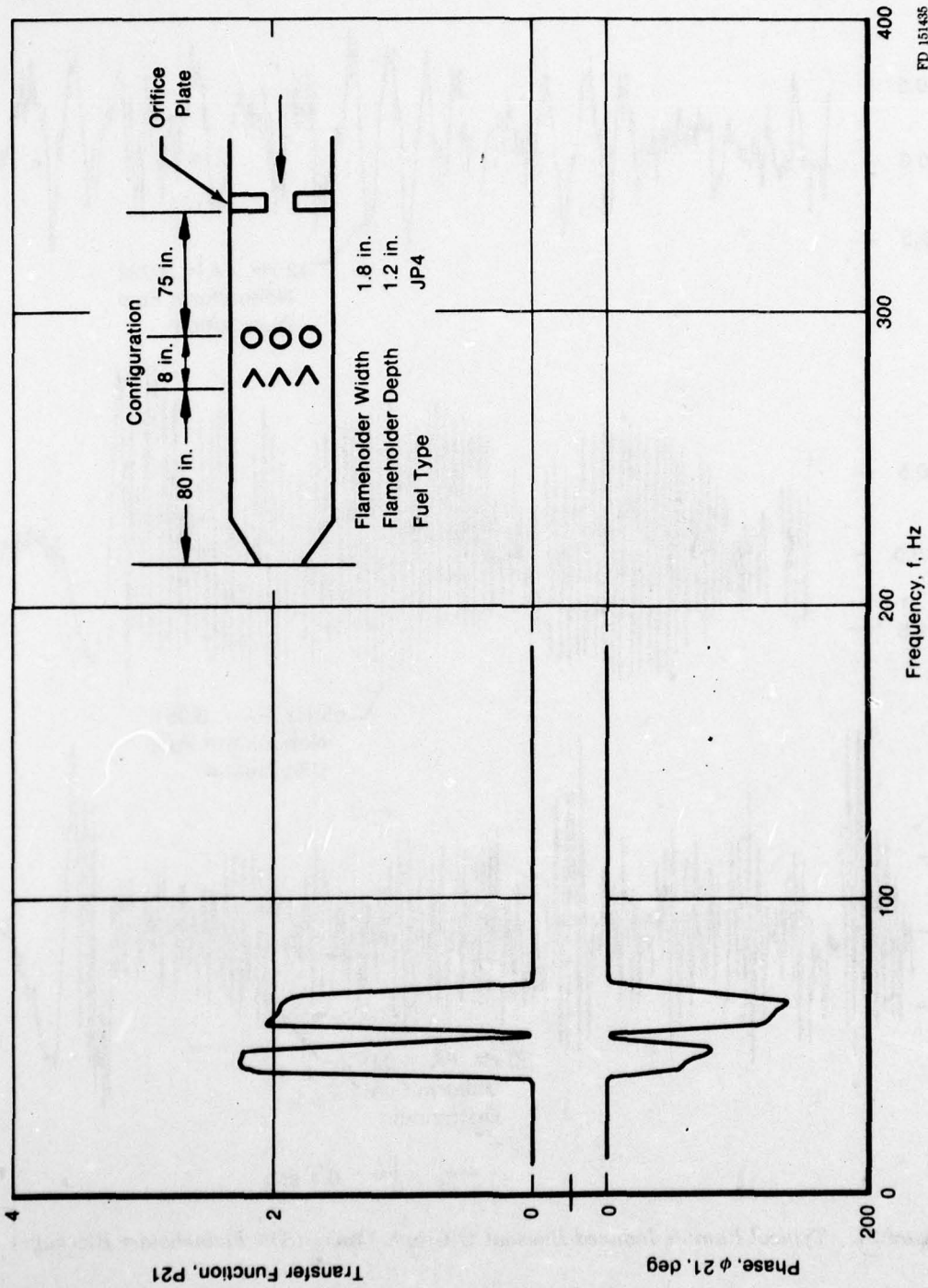
##### (b) Series II Testing

Some minor problems were also encountered during the Series II testing. The test facility ejector system was not operating at its specified efficiency and would have required major repairs to correct the deficiencies. Since combustion efficiency measurements were desired, choked flow at the exhaust nozzle was required. To maintain choked flow the lowest rig pressure was limited to approximately 14 psia and the rig duct Mach number to 0.12 compared to a planned rig pressure of 10 psia and duct Mach number of 0.155. It was determined that these revised conditions would provide the required input for the model, and the test program was modified accordingly.



FD 151434

Figure 24. Typical Rumble Induced Blowout O-Graph Traces (50% Flameholder Blockage)



FD 151435

Figure 25. Transfer Function and Phase Angle Data for Test Point 1, Baseline, Run Number 7.01, Data Point 22



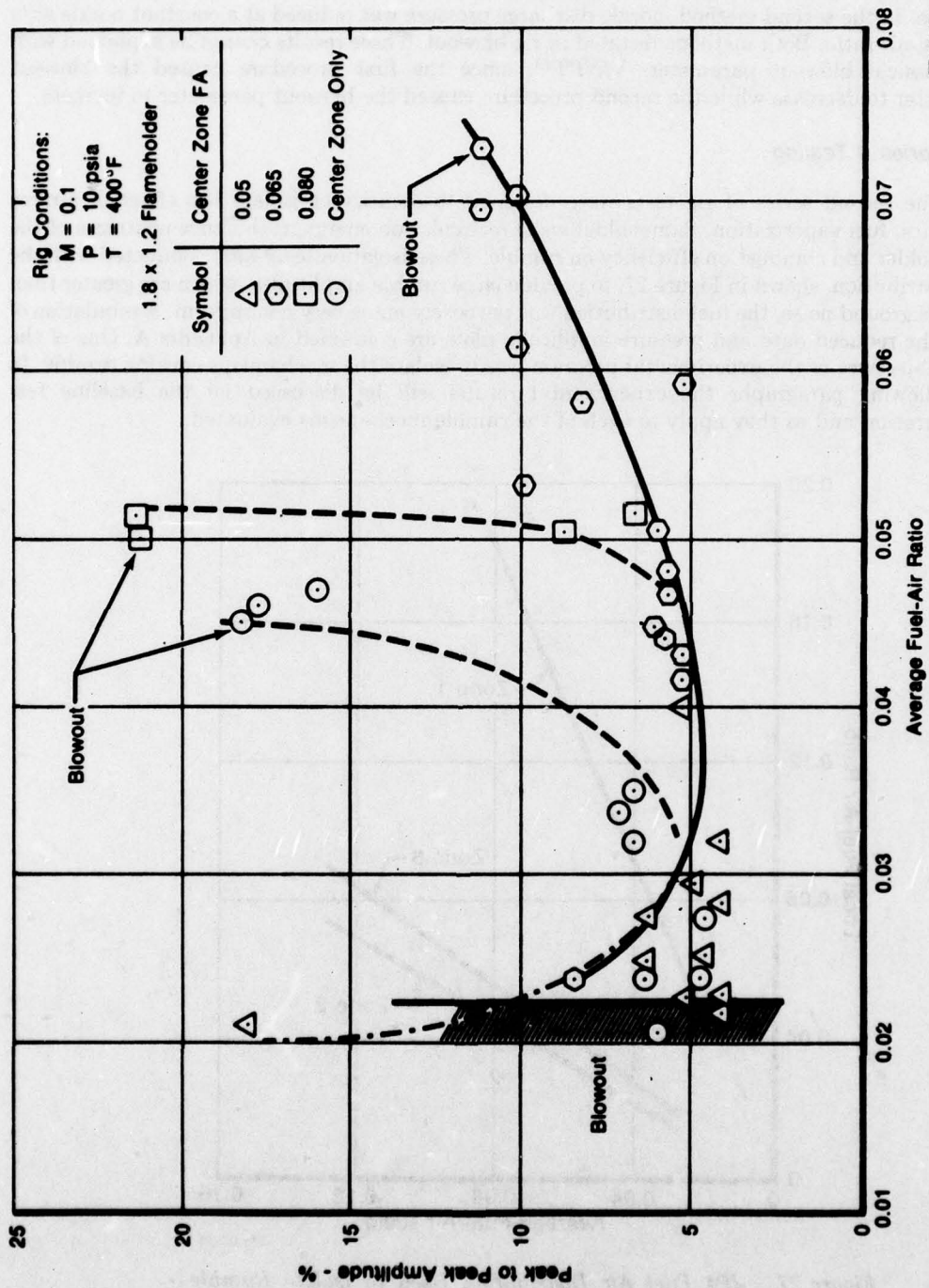


Figure 26. Fuel Distribution Affects Combustion Stability

The effect of nozzle conditions on stability was evaluated by two distinct methods. For both methods, combustion was initiated with an unchoked nozzle and then the nozzle was choked. In the first method, the nozzle area was closed holding a constant fuel-air ratio and nozzle discharge pressure. In the second method, nozzle discharge pressure was reduced at a constant nozzle area and fuel-air ratio. Both methods resulted in rig blowout. These results cannot be explained with the classical blowout parameter,  $V/NPT^{1/2}$ , since the first procedure caused the blowout parameter to decrease while the second procedure caused the blowout parameter to increase.

**(b) Series II Testing**

The second series of rig tests were designed to identify or isolate the effect of airflow dynamics, fuel vaporization, flameholder wake recirculation energy, turbulence upstream of the flameholder and combustion efficiency on rumble. These isolation tests were conducted with the fuel distribution, shown in Figure 27, to provide large rumble amplitudes, which are greater than the background noise, the fuel distribution was purposely made very nonuniform. A tabulation of all of the reduced data and pressure amplitude plots are contained in Appendix A. One of the basic objectives of the experimental program was to isolate the mechanisms causing rumble. In the following paragraphs the experimental results will be discussed for the baseline test configuration and as they apply to each of the rumble mechanisms evaluated.

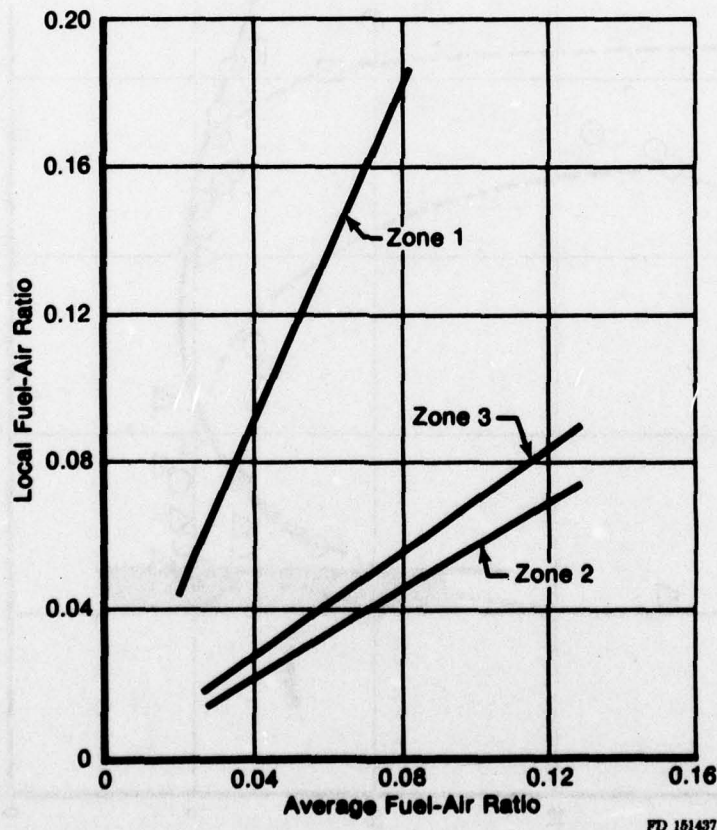


Figure 27. JP4 Fuel Air Distribution Used to Isolate Rumble Mechanisms

### 1. Baseline Test Rig Configuration

The baseline rig configuration used to isolate the rumble mechanisms is as follows:

- Choked inlet orifice to flameholder distance — 83 in.
- Spraybar to flameholder distance — 8 in.
- Flameholder to nozzle distance — 80 in.

The instability pressure amplitudes recorded during the baseline configuration testing are shown in Figure 28 to be primarily a function of fuel-air ratio and to a lesser extent a function of the blowout parameter. The trends depicted in this figure are representative of most of the configurations tested. The baseline rumble frequencies encountered ranged between 50 and 70 Hz.

### 2. Airflow Dynamics

The system airflow dynamics are dependent on pressure waves which are reflected between an upstream and downstream boundary which in turn cause a change in the combustion process. This change in combustion process generates pressure waves which can sustain an oscillation. The oscillations may be initiated by any disturbance and can continue to grow in amplitude until augmentor blowout or engine stall occurs. In an engine system the choked exhaust nozzle provides the downstream reflecting surface while the upstream surface may be either the flameholder or possibly the fan.

In the test rig the possibility of airflow dynamics being a rumble contributor was investigated by changing the location of the upstream reflecting surface of the combustion system. This provided data for different duct lengths and was accomplished by removing a section of ducting between the upstream choked orifice and the fuel spraybars. The theory behind this test sequence was if the frequency of rumble increased in proportion to the decreased duct length, then system stability is affected by airflow dynamics. The results of the testing as shown in Figure 29 indicate that the rumble amplitude was significantly reduced with a shorter duct. An examination of the test data as shown in Appendix A, shows that frequencies of  $\approx 80$  Hz were observed with the shorter duct compared to  $\approx 60$  Hz with the baseline configuration. Since the resulting frequency,  $f$ , is inversely proportional to the duct lengths, i.e.,

$$f_{\text{short}} = f_{\text{long}} \times \frac{L_{\text{long}}}{L_{\text{short}}} = 60 \text{ Hz} \times \frac{83_{\text{in}} + 83_{\text{in}}}{43_{\text{in}} + 83_{\text{in}}} = 79 \text{ Hz}$$

It is concluded that airflow dynamics are indeed a contributor to sustaining rumble and must be considered a rumble mechanism.

### 3. Fuel Vaporization

As described in the report (Reference 1) on the companion contract, F33615-76-C-2023, poor fuel vaporization has the effect of increasing the flameholder wake mixture ratio above the freestream value. Consequently, it is possible to have a stoichiometric mixture in the flameholder wake and a leaner condition in the freestream. Under these conditions, further increases in fuel flow creates an overly rich flameholder wake, reducing wake efficiency. This decrease in wake efficiency lowers the overall combustion efficiency. With a stiff fuel system, any change in airflow will change the fuel distribution of the wake and freestream affecting combustion efficiency. This coupling between airflow dynamics and the combustion process can result in an instability.



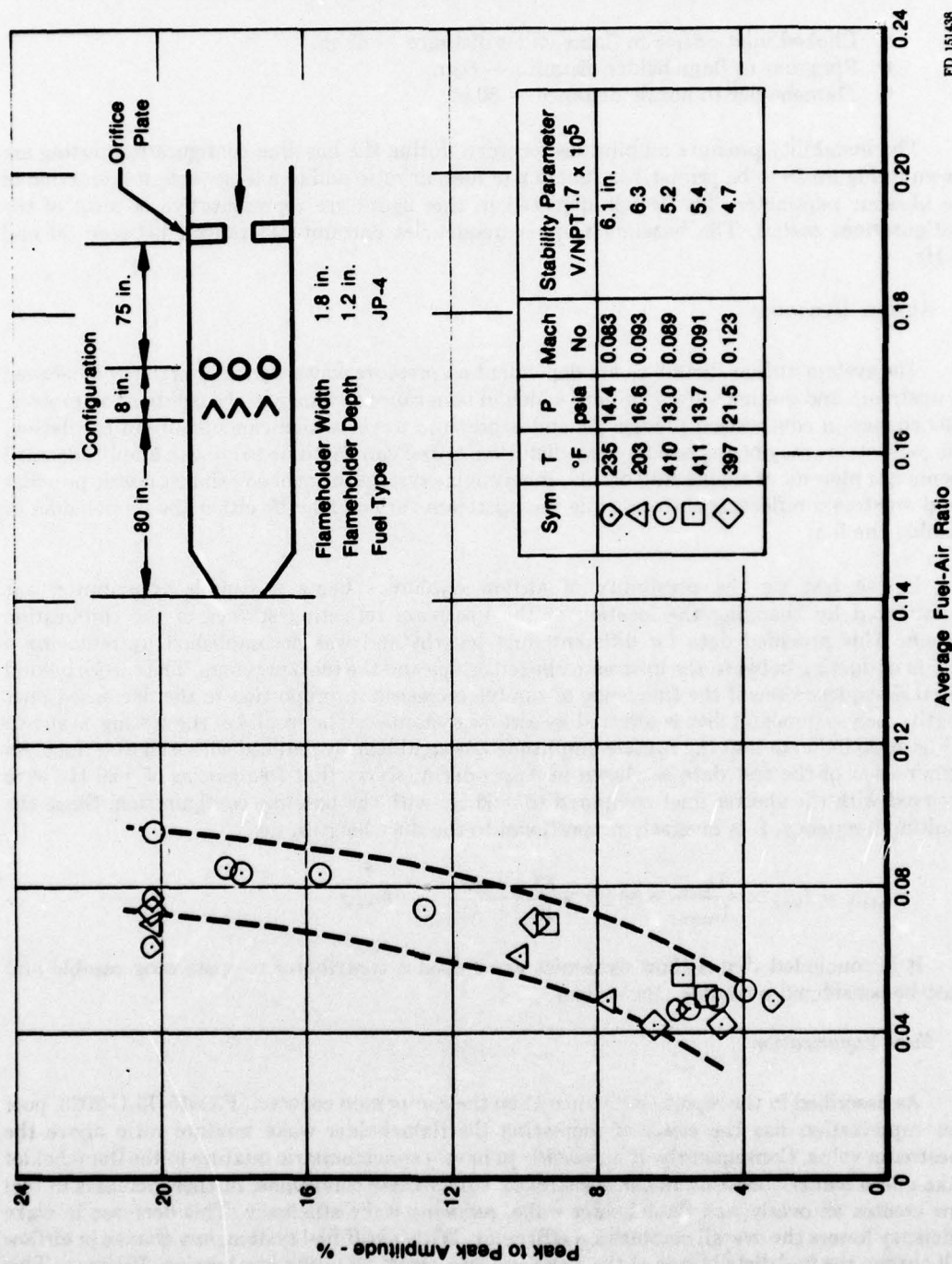
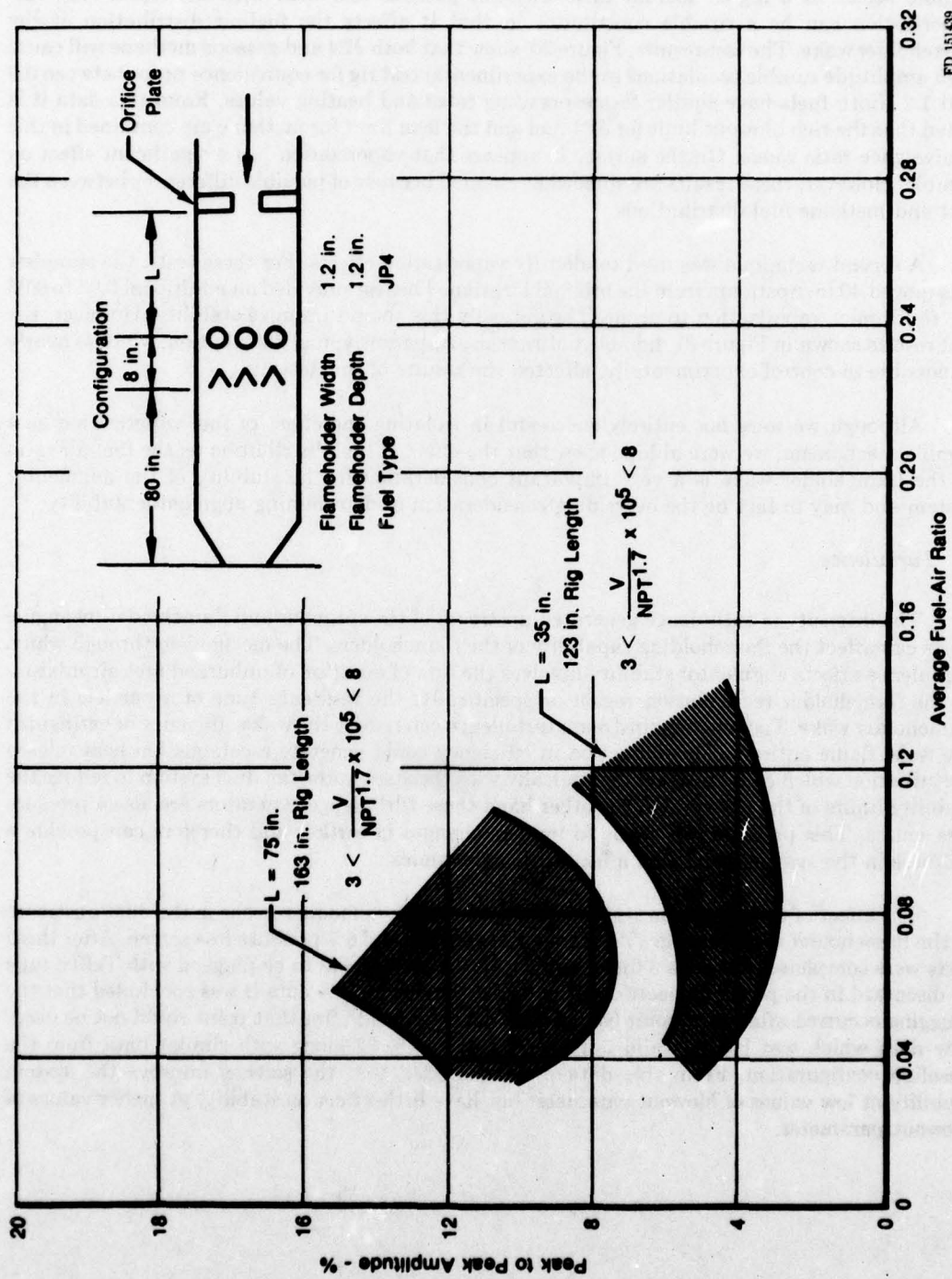


Figure 28. Rumble Amplitude Correlated With Fuel-Air Ratio and Stability Parameter, Test Point 1

FD 151/438



FD 151439

Figure 29. The Effect of Cold Duct Length on Stability. A Comparison of Test Point 11 and Test Point 3.

This mechanism was evaluated experimentally by testing with gaseous fuel having nearly the same heating value and flamespreading rate as liquid fuel and by comparing the results. If rumble occurs at a higher fuel-air ratio with the gaseous fuel than with the liquid fuel, fuel vaporization can be a rumble contributor in that it affects the fuel-air distribution at the flameholder wake. The test results, Figure 30, show that both JP4 and gaseous methane will cause high amplitude rumble oscillations in the experimental test rig for equivalence ratios between 0.9 and 1.2. Both fuels have similar flamespreading rates and heating values. From this data it is noted that the rich blowout limit for JP4 fuel and the lean limit for methane are contained in this equivalence ratio range. On the surface it appears that vaporization has a significant effect on rumble. However, these results are somewhat clouded because of possible differences between the JP4 and methane fuel distributions.

A second technique was used to identify vaporization effects. For these tests, the spraybar was moved 40 in. upstream from the original location. The test provided an additional 0.02 to 0.05 sec for droplet vaporization to occur. Theoretically this should improve stability. However, the test results shown in Figure 31 did not confirm this. Apparently, fuel distribution, which is nearly impossible to control experimentally, effected the results of this testing.

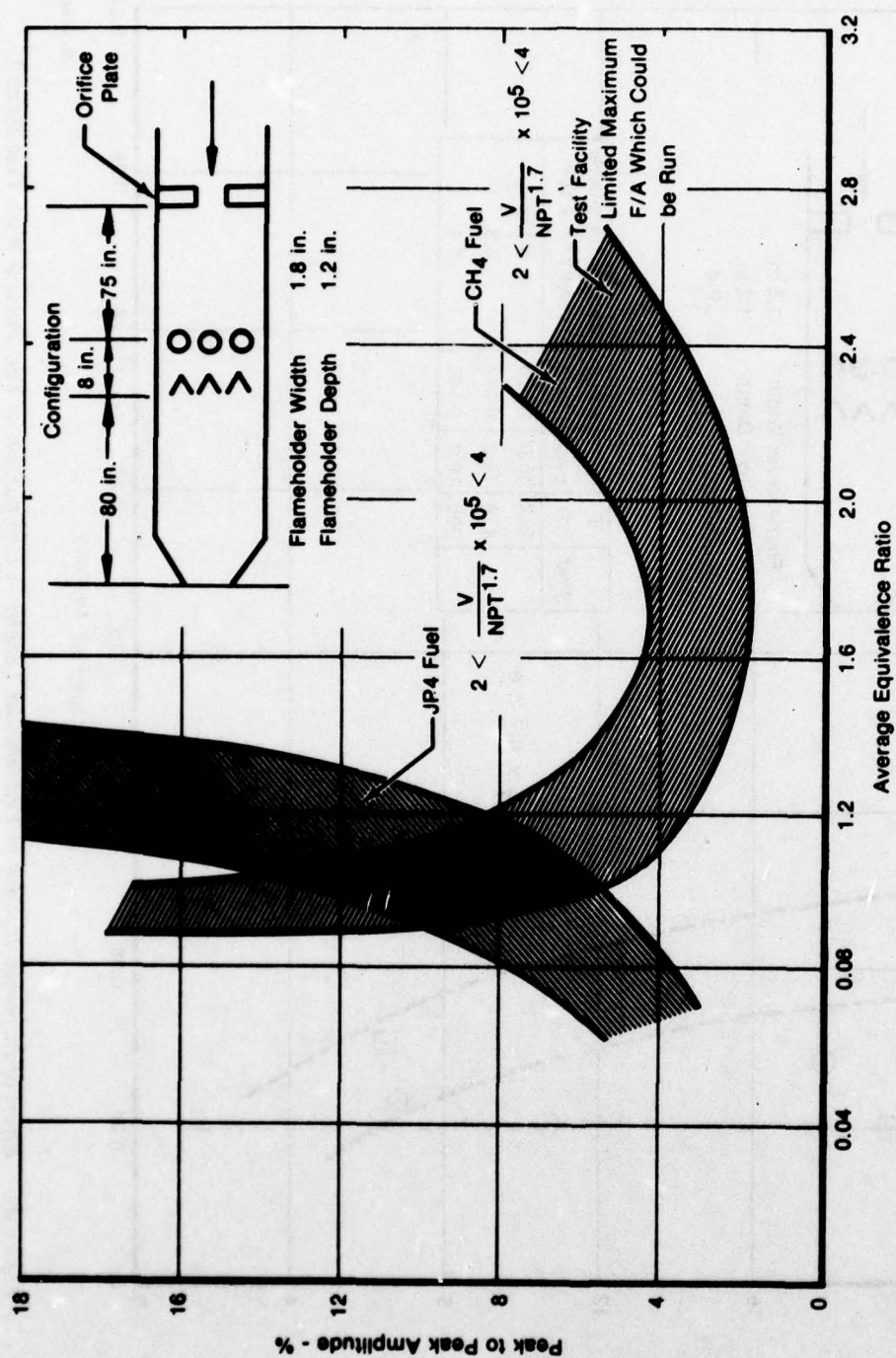
Although we were not entirely successful in isolating the effect of fuel vaporization as a rumble mechanism, we were able to show that the effect of fuel distribution on the fuel-air ratio in the flameholder wake is a very important consideration in the stability of the augmentor system and may in fact be the overriding consideration in determining augmentor stability.

#### 4. Turbulence

The intensity of turbulence generated upstream of the spraybar and flameholder by engine parts can affect the flameholding capability of the flameholders. The mechanism through which turbulence affects augmentor stability involves the rate of addition of unburned fuel-air mixture to the flameholder recirculation region or specifically, the residence time of a particle in the flameholder wake. Too much mainstream turbulence can reduce the wake efficiency or extinguish the wake flame entirely. This reduction in efficiency could generate a combustion heat release perturbation which could interact dynamically with the augmentor-fan duct system to reduce the stability limits of the system. On the other hand these turbulence generators are also a pressure loss source. This pressure loss tends to impede changes in airflow and therefore can provide a stiffness in the system which can affect airflow dynamics.

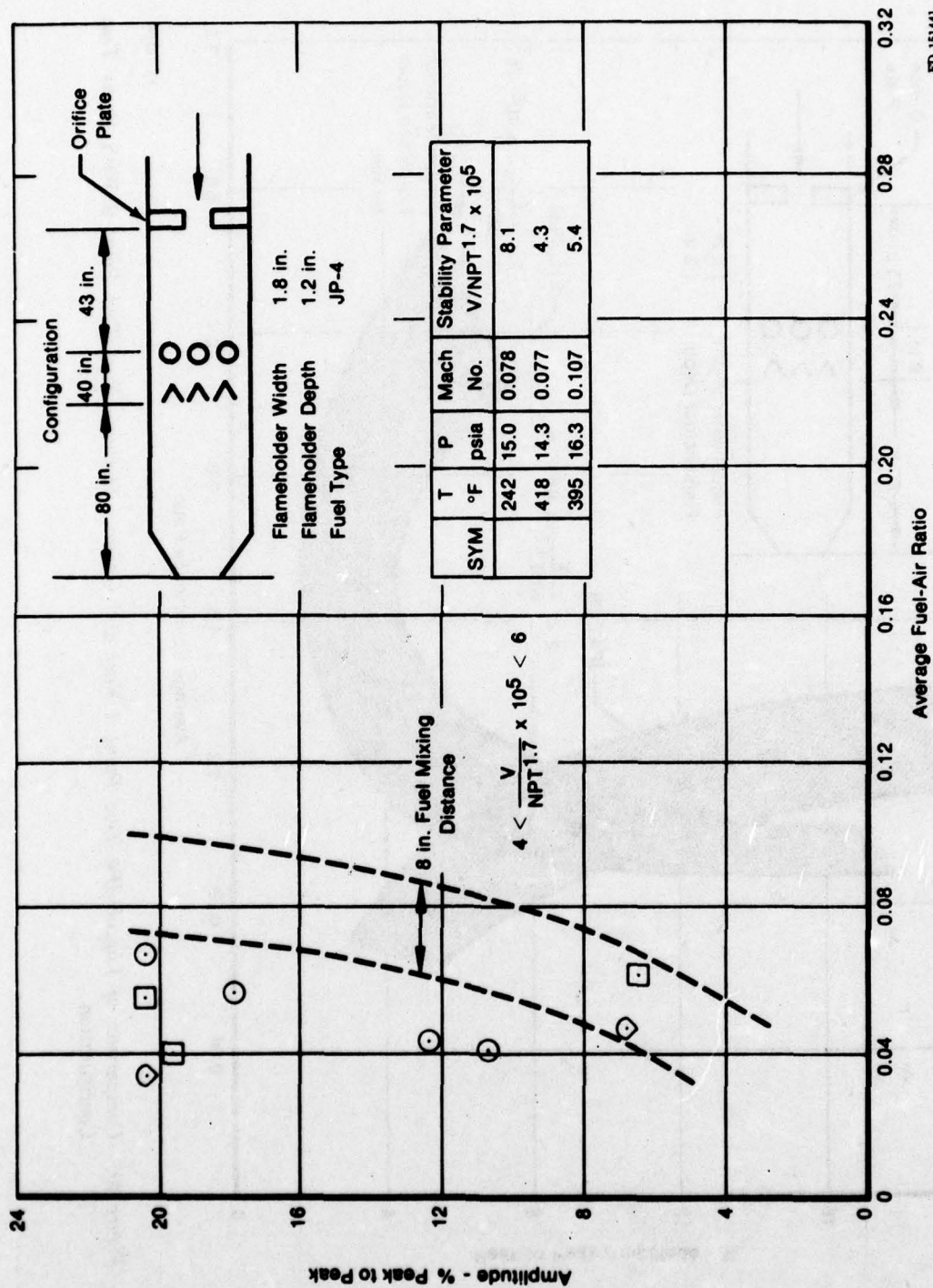
The effect of turbulence on stability was evaluated by placing screens in the duct upstream of the flameholder and spraybar. Tests were run with a 2 and 5% pressure loss screen. After these tests were completed, the zone 3 fuel spraybar pintles were found to be plugged with Teflon tape as discussed in the problems section of the report. Reviewing the data it was concluded that the plugging occurred after data point 58 and that data recorded after that point could not be used. The data which was judged valid is presented in Figure 32 along with similar data from the baseline configuration. From this data it is concluded that the screens improve the system stability at low values of blowout parameter but have little effect on stability at higher values of blowout parameter.





FD 151440

Figure 30. Comparison of Liquid JP4 Test Point 1 Fuel and Gaseous Methane Fuel Test Point 2 With Same Test Configuration



FD 15141

Figure 31. Effect of Increased Injector to Flameholder Length. A Comparison of Test Point 9 With Test Point 1.

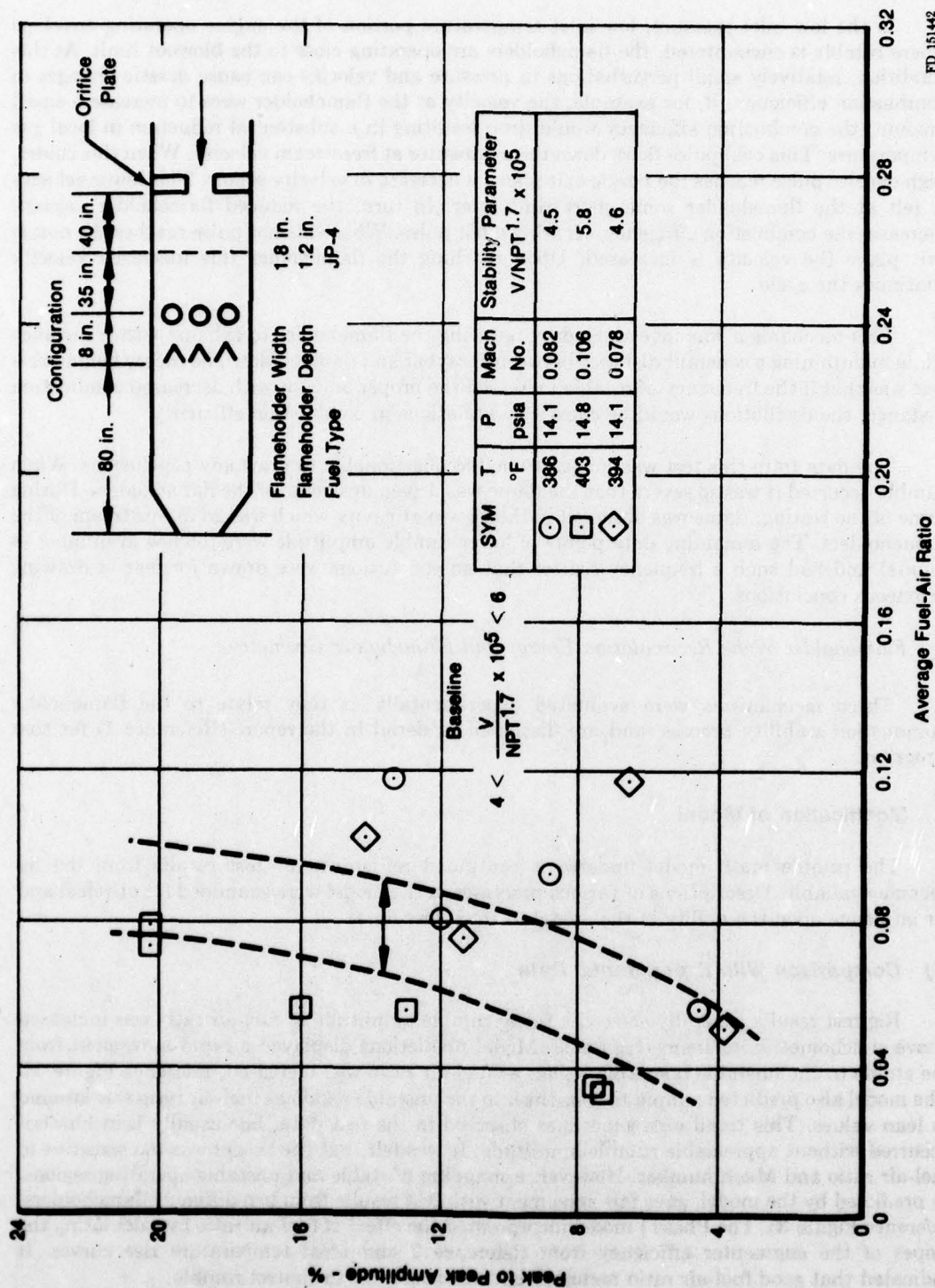


Figure 32. Effect of Turbulence Screen on Stability. A Comparison of Test Point 7 With Test Point 1.



## 5. Combustion Efficiency Oscillations

In the low inlet pressure, low inlet temperature portion of the engine operating envelope where rumble is encountered, the flameholders are operating close to the blowout limit. At this condition, relatively small perturbations in pressure and velocity can cause drastic changes in combustion efficiency. If, for example, the velocity at the flameholder were to increase a small amount, the combustion efficiency would drop resulting in a substantial reduction in local gas temperature. This cold pulse flows down the augmentor at freestream velocity. When this colder, high density pulse reaches the nozzle exit plane, a decrease in velocity occurs. This lower velocity is felt at the flameholder some short time later. In turn, the reduced flameholder velocity increases the combustion efficiency, creating a hot pulse. When this hot pulse reaches the nozzle exit plane the velocity is increased. Upon reaching the flameholder this increased velocity continues the cycle.

This mechanism was investigated by reducing the flameholder to exhaust nozzle distance while maintaining a constant distance between spraybar and flameholder. The theory behind this test was that if the frequency of rumble increased the proper amount with decreased combustion distance, the oscillations would be caused by variations in combustion efficiency.

The data from this test was judged to be too questionable to draw any conclusions. When rumble occurred it was so severe that the flame was driven upstream of the flameholders. During some of the testing, flame was observed in the view port cavity which was 26 in. upstream of the flameholders. The remaining data points of lower rumble amplitude were too few in number (4 points) and had such a frequency scatter that no conclusions were drawn for fear of drawing erroneous conclusions.

## 6. Flameholder Wake Recirculation Energy and Flameholder Geometry

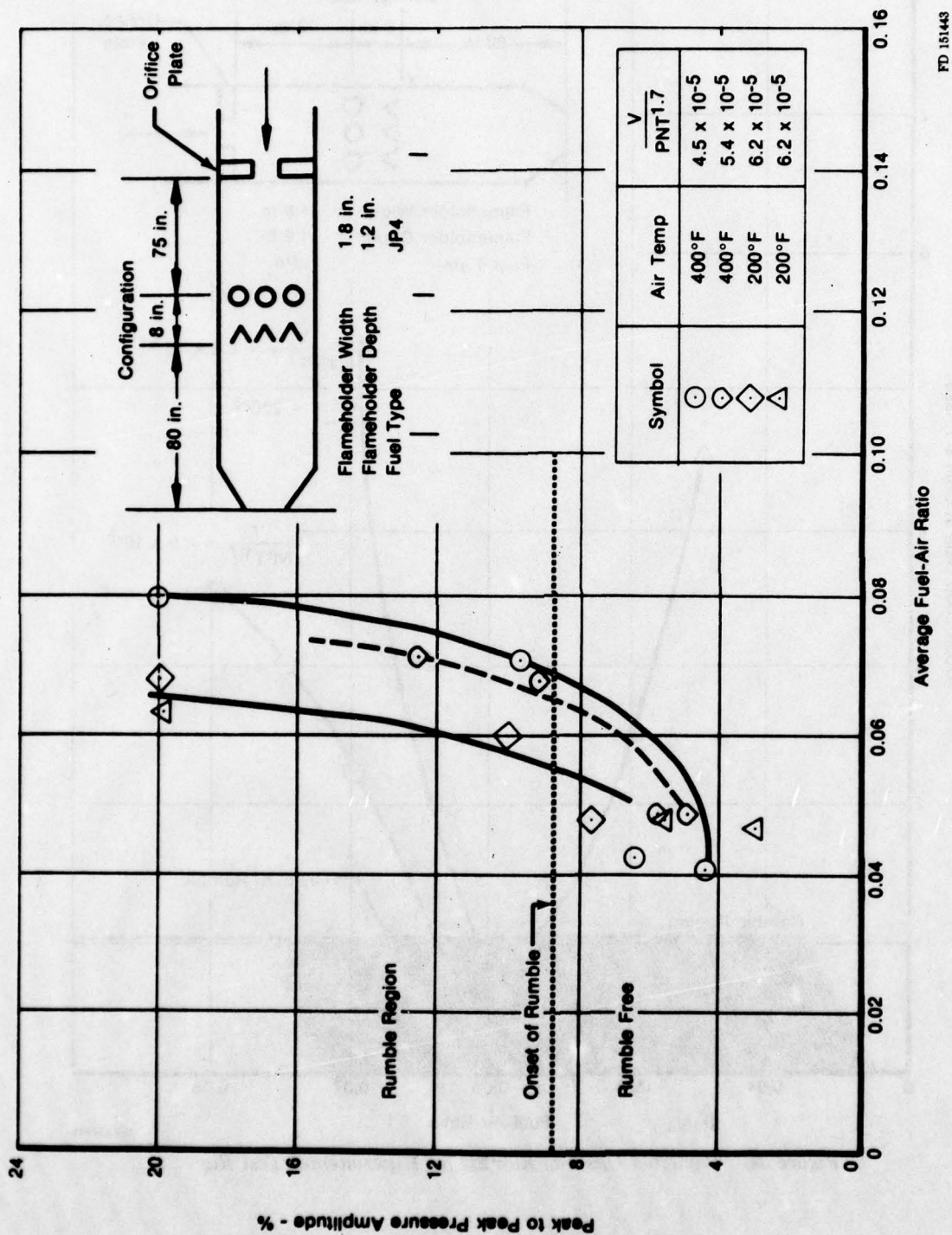
These mechanisms were evaluated experimentally as they relate to the flameholder combustion stability process, and are discussed in detail in the report (Reference 1) for that program.

### **d. Modification of Model**

The rumble math model underwent continued refinement as test results from the rig became available. Descriptions of various processes in the model were examined for physical and for influence upon the ability of the model to track test data.

#### **(1) Comparison With Experimental Data**

Rig test results generally showed a rising rumble amplitude as fuel-air ratio was increased above stoichiometric, reference Figure 33. Model predictions displayed a rapid movement from the stable to the unstable operating region as fuel-air ratio was increased, reference Figure 34. The model also predicted a rapid movement into the unstable region as fuel-air ratio was lowered to lean values. This trend was sometimes observed in the test data, but usually lean blowout occurred without appreciable rumble amplitude. It was felt that the model was too sensitive to fuel-air ratio and Mach number. However, a mapping of stable and unstable operating regions, as predicted by the model, gave fair agreement with test results from two different flameholders, reference Figure 35. The Phase I model incorporated the effect of fuel-air ratio by calculating the slopes of the augmentor efficiency from Reference 2 and ideal temperature rise curves. It indicated that good fuel-air ratio management was necessary to control rumble.



FD 151443

Figure 33. Rumble Amplitude Correlates With Blowout Parameter and Fuel-Air Ratio

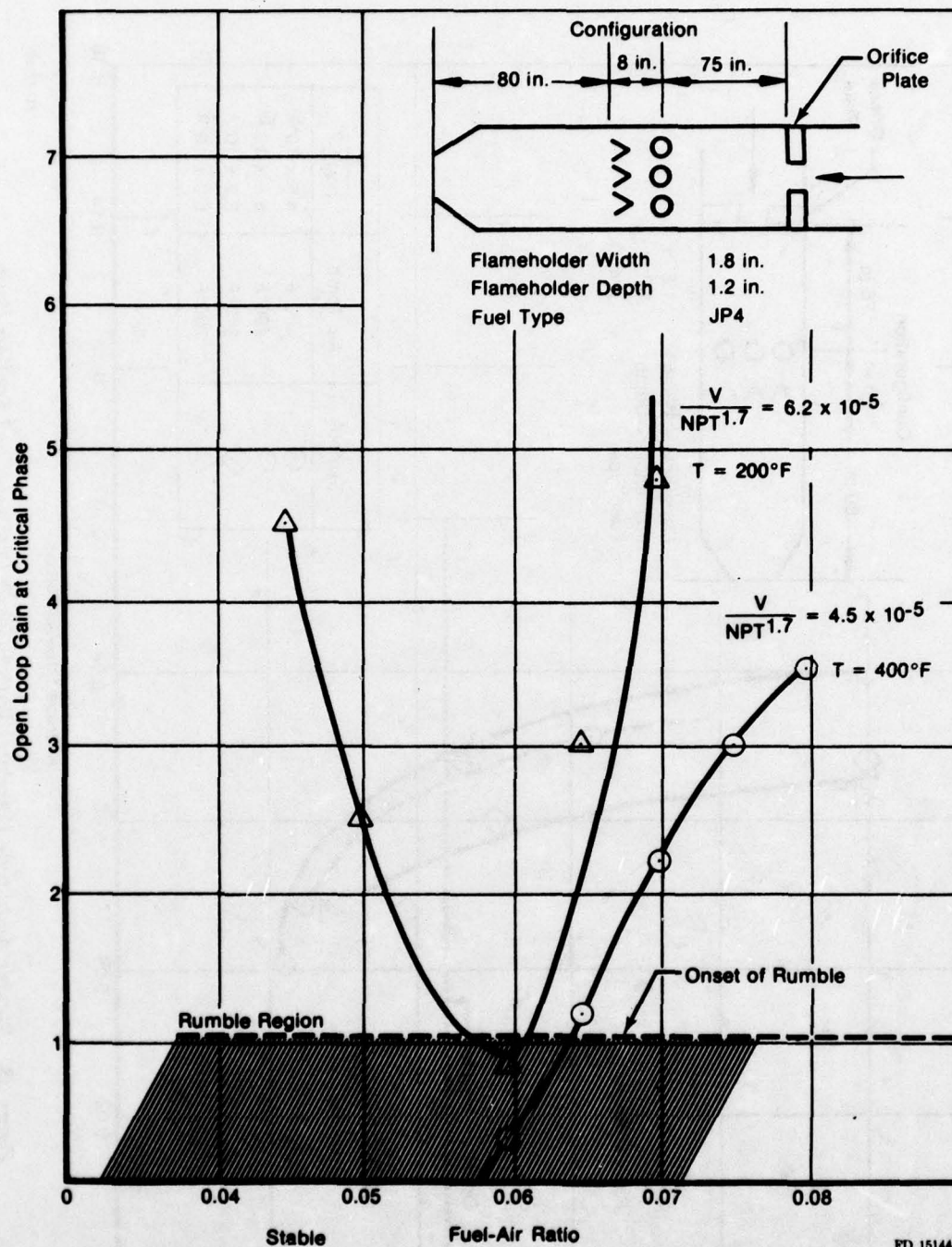


Figure 34. Predicted Onset of Rumble for Experimental Test Rig

FD 151444



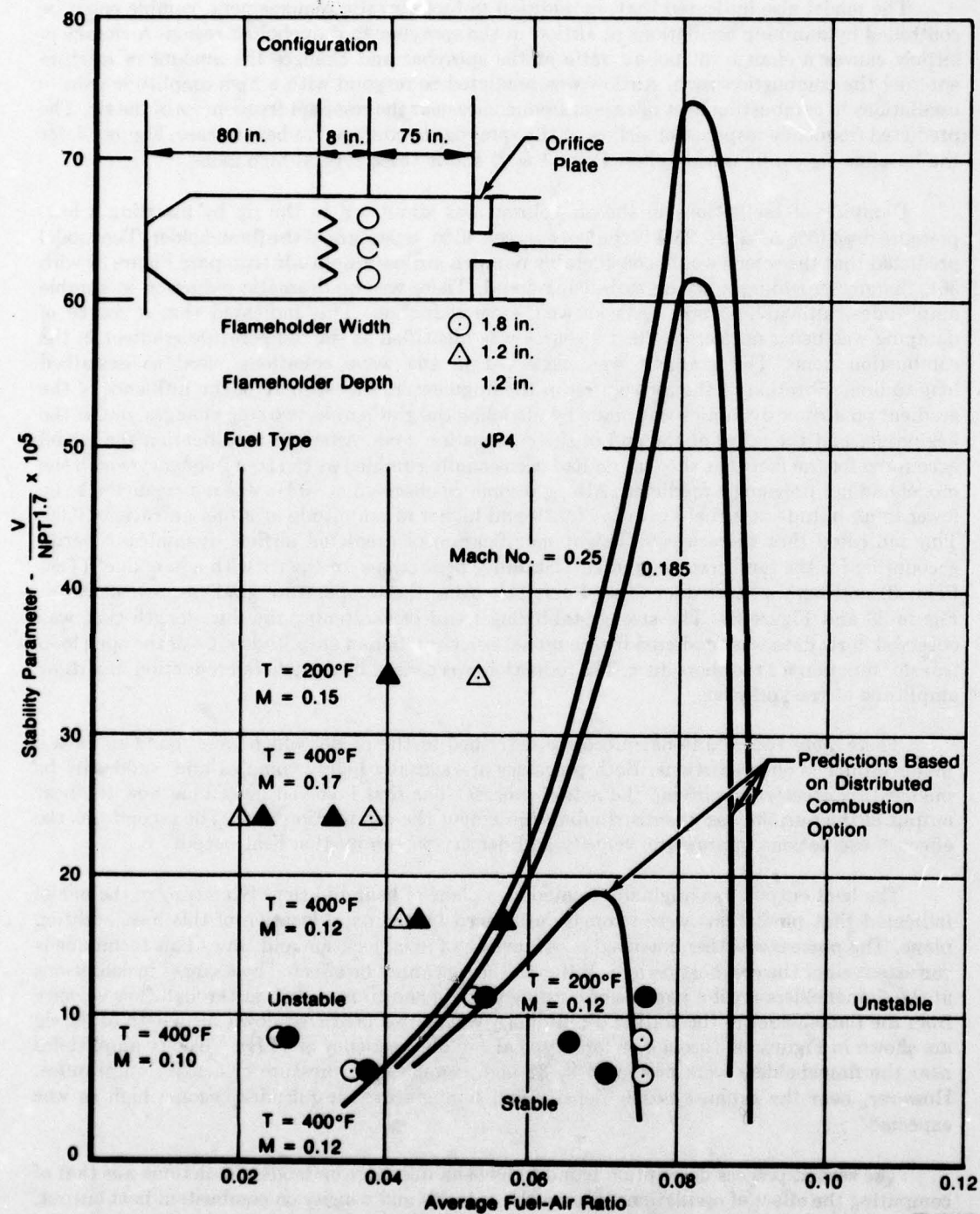


Figure 35. Comparison of Model Prediction With Rig Data

The model also indicated that, in addition to fuel-air ratio management, rumble could be controlled by damping oscillations in airflow in the spraybar-to-flameholder region. A change in airflow causes a change in fuel-air ratio at the spraybar and changes the amount of mixture entering the combustion zone. Airflow was predicted to respond with a high amplitude gain to oscillations in combustion heat release at frequencies near the resonant frequencies of the rig. The predicted frequency response of airflow at the spraybar to combustion heat release, Figure 36, for the baseline rig configuration (Test Point 1 & 2) shows these typical high gains.

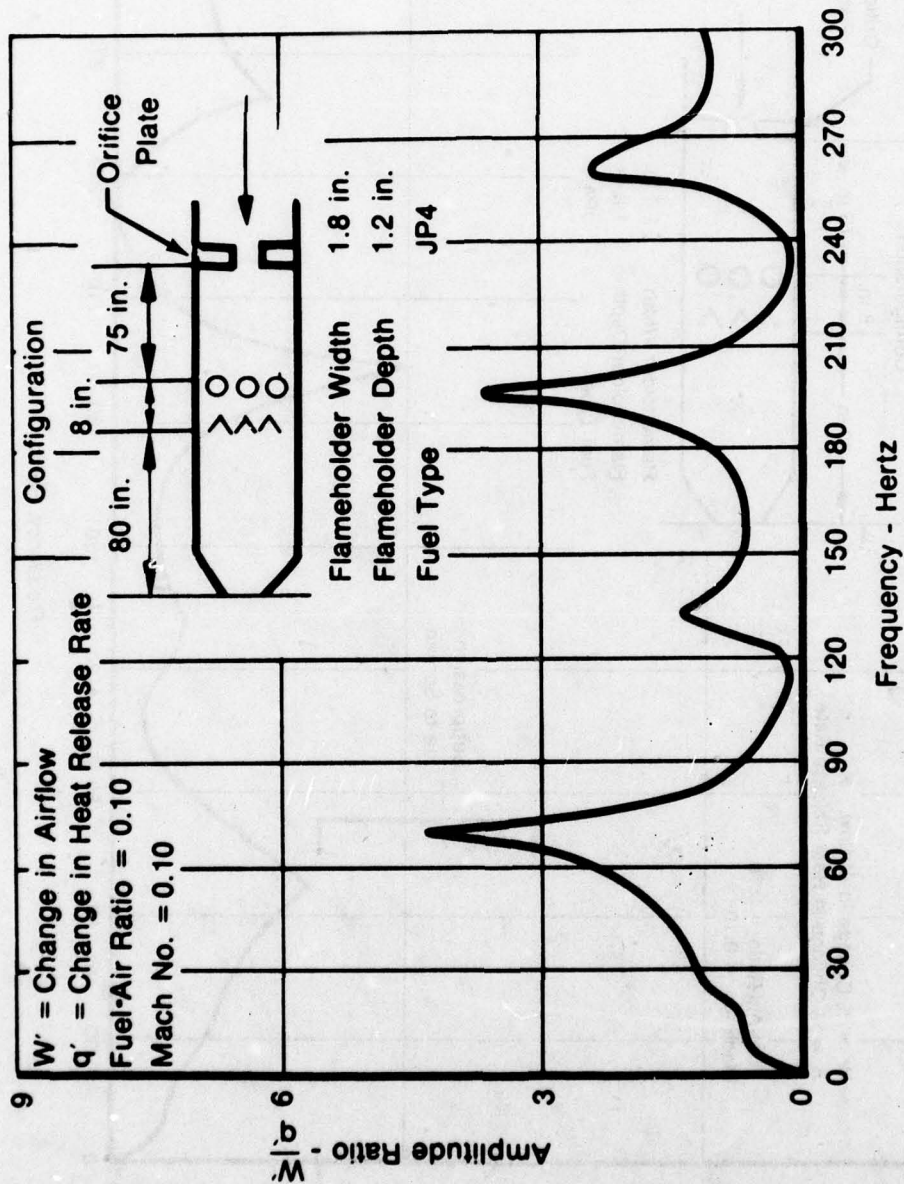
Damping of oscillations in the air column was simulated in the rig by inserting a low-pressure drop (5%  $\Delta P/P$  at .2M) turbulence screen 40 in. upstream of the flameholder. The model predicted that the screen would considerably dampen airflow amplitude (compare Figure 37 with 36), thereby providing a strong stabilizing trend. There was no dramatic reduction in rumble amplitudes, although several tests showed some reduction. This indicated that a source of damping was being neglected. Such a source was identified as the temperature gradient in the combustion zone. The gradient was neglected in the wave equations, used to describe longitudinal vibration of the air column in the augmentor. An estimate of the influence of the gradient on airflow dynamics was made by modeling the gradient as two step changes, one at the beginning, and the other at the end of the combustion zone. After the modification the model accounted for the fact that the test rig had occasionally rumbled at 25 Hz, a frequency which the model had not previously predicted. Also, a resonance observed at 70 Hz was not predicted to be lower in amplitude at a fuel-air ratio of 0.10 and higher in amplitude at a fuel-air ratio of 0.06. This indicated that there was sufficient modification of predicted airflow dynamics to verify accounting for the temperature gradient. Stability predictions for the rig with a long duct (Test Point 3) and with a short duct (Test Point 11), using the temperature gradient, are shown in Figure 38 and Figure 39. The strong stabilizing trend of shortening the duct length that was observed in rig data was predicted by the model as a reduction in amplitude ratio of the open-loop transfer function for the short duct. The reduction was caused by a predicted reduction in airflow amplitude at the spraybar.

There were two additional processes described in the model which were found to have a major influence on predictions. Both processes are actually highly complex and could only be modeled by greatly simplifying the actual process. The first involved describing how the heat output of the burning gas was distributed throughout the combustion zone. The second was the effect of oscillations in pressure, velocity and density on combustion heat output.

The heat output was originally treated as a plane of heat addition. Exercising of the model indicated that predictions were strongly influenced by the axial location of this heat addition plane. The process was then modeled as a function of axial location and time. This technique is consistent since the combustion at a station in the rig cannot be affected by changes in conditions at the flameholders until a particle of burning gas has had time to drift at through-flow velocity from the flameholder to the station. Preliminary waveforms predicted down the length of the rig are shown in Figures 40 through 43 for a typical rumble frequency of 53 Hz. Velocity amplitudes near the flameholders were predicted to be high compared to pressure or density amplitudes. However, near the exhaust nozzle density and temperature, amplitudes become high as was expected.

The second process description found to have an influence on model predictions was that of computing the effect of oscillations in pressure, velocity and density on combustion heat output. The simplest description available was incorporated. This description assumes that augmentor efficiency and ideal temperature rise transiently obey steady-state curves. In deciding whether this description could account for various spraybar and flameholder designs, it was realized that there were dynamics in this region which the model did not recognize.

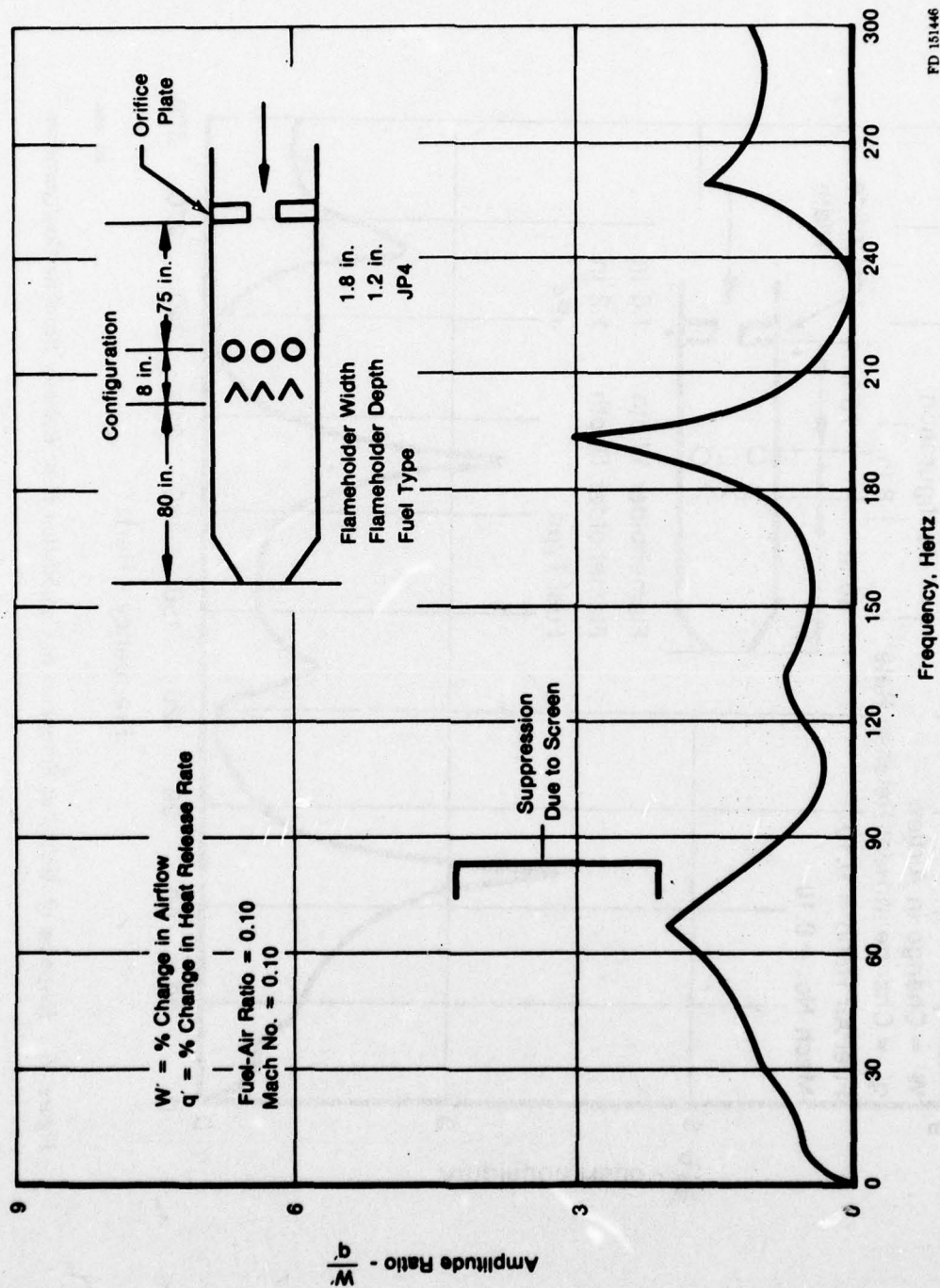




FD 144858

Figure 36. Response of Airflow at Spraybars to Combustion Heat Release: Baseline Configuration





FD 151446

Figure 37. Response of Airflow at Spraybars to Combustion Heat Release, Screen 40 Inches Upstream of Flameholders

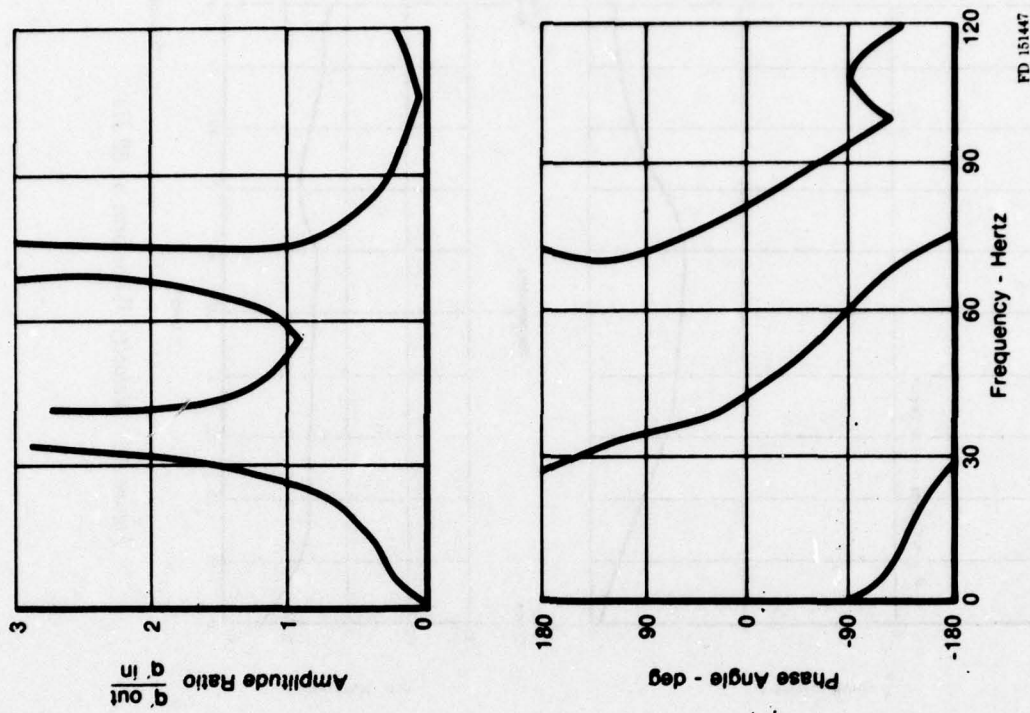


Figure 38. Open Loop Transfer Function Long Duct (Run 11.01) (Test Point 3)

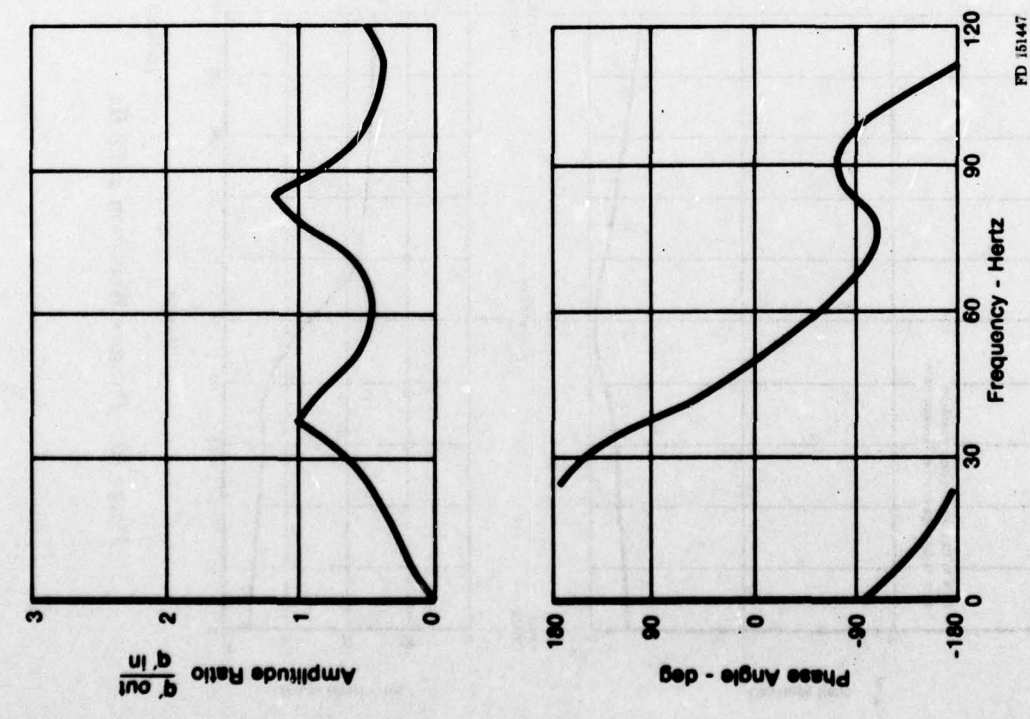


Figure 39. Open Loop Transfer Function Short Duct (Run 14.01) (Test Point 11)

FD 151447

FD 151447

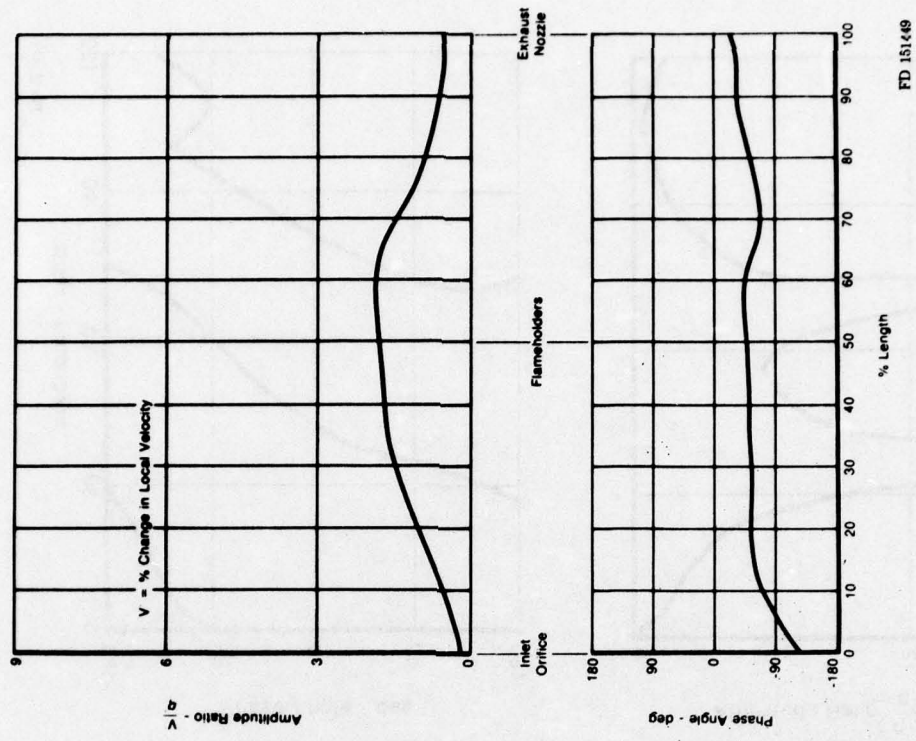


Figure 40. Pressure Waveform at 52 Hz

FD 151448

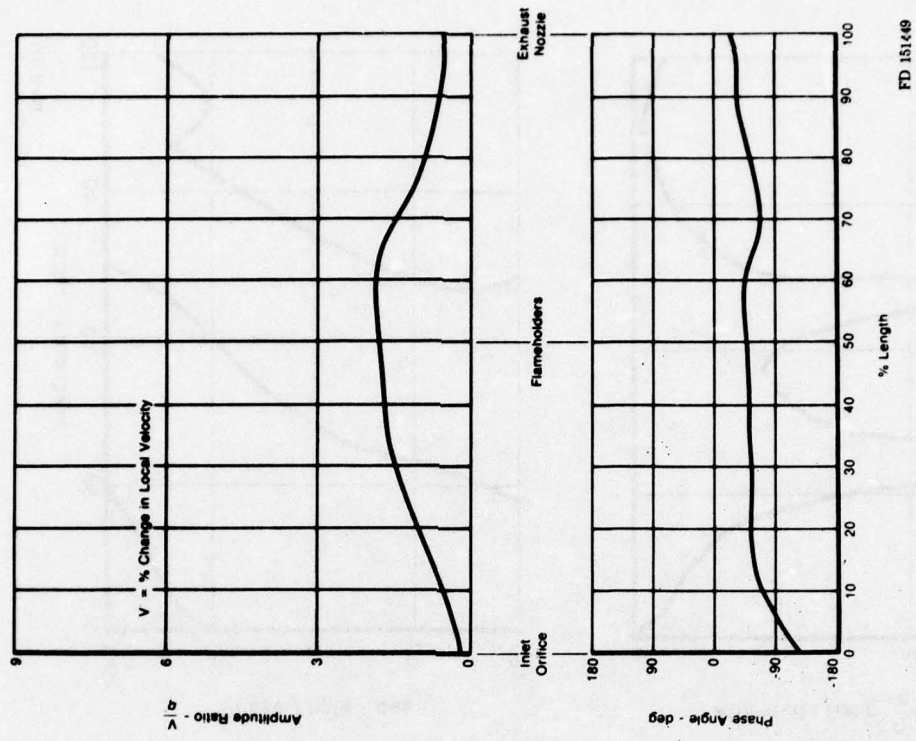
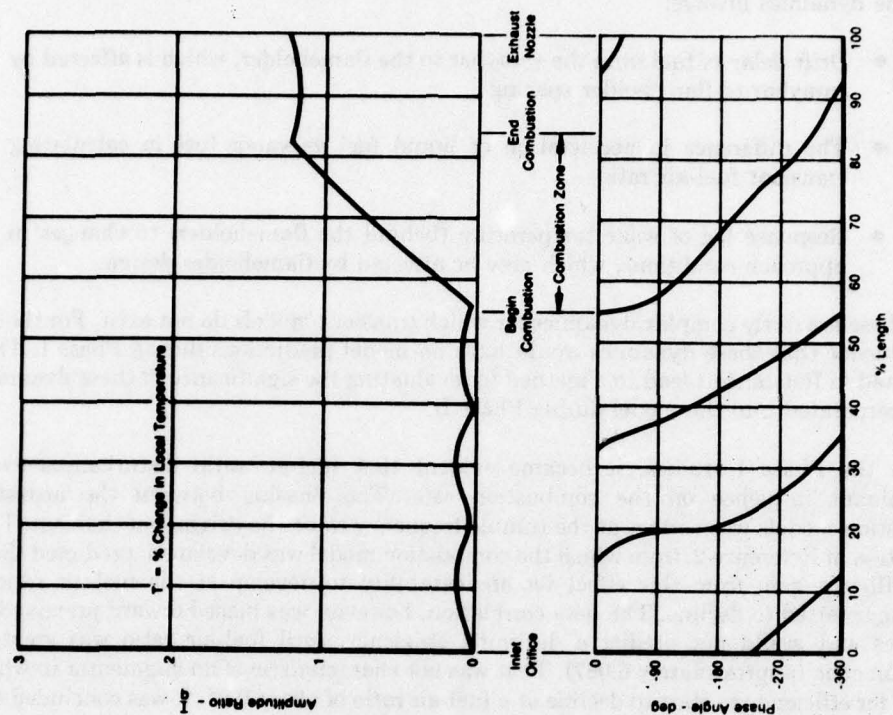


Figure 41. Velocity Waveform at 52 Hz

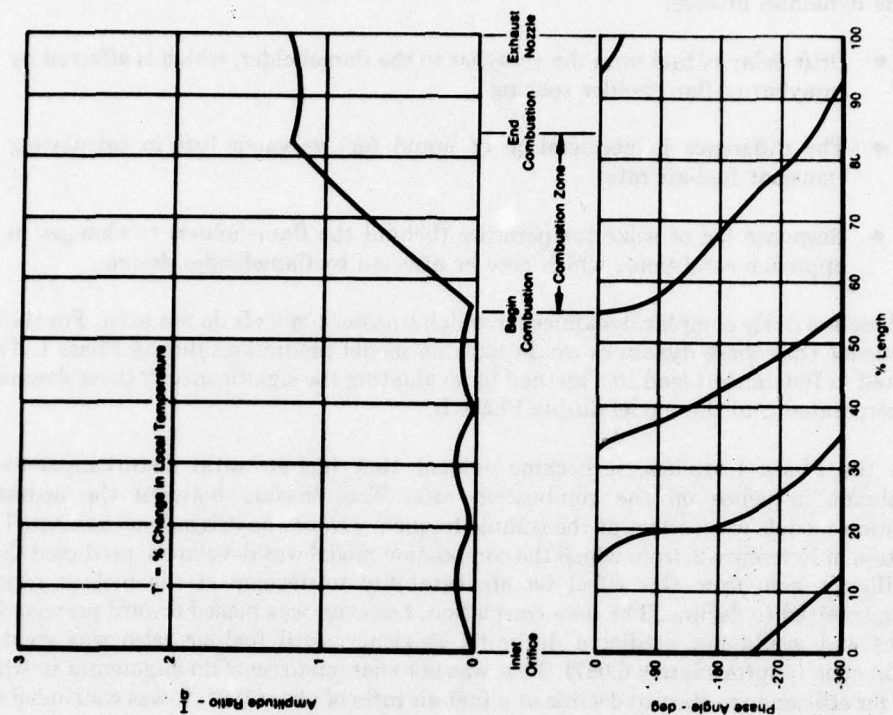
FD 151449





FD 151450

Figure 42. Density Waveform at 52 Hz



FD 146451

Figure 43. Temperature Waveform at 52 Hz

The dynamics involve:

- Drift delay of fuel from the spraybar to the flameholder, which is affected by spraybar-to-flameholder spacing
- The difference in acceleration of liquid fuel vs vapor fuel in calculating transient fuel-air ratio
- Response lag of wake temperature (behind the flameholder) to changes in approach conditions, which may be affected by flameholder design.

These are fairly complex dynamics for which transient models do not exist. For that reason the influence that these dynamics would have on model predictions during Phase I. The work completed in Reference 1 lead to a method for evaluating the significance of these dynamics and was incorporated into the model during Phase II.

In the Phase I studies, it became evident that fuel-air ratio disturbances exerted a predominant influence on the combustion rate. The phasing between the acoustic and combustion models was correct at the rumble frequency to be the driving mechanism. The beta correlation in Reference 2, from which the combustion model was developed, predicted that there was sufficient gain from this effect for an instability to develop at the fuel-air ratio where efficiency started to decline. The beta correlation, however, was biased toward premixed gas-air mixtures and would not predict a declining efficiency until fuel-air ratio was greater than stoichiometric (approximately 0.067). That was not characteristic of an augmentor in which it is typical for efficiency to start to decline at a fuel-air ratio of about 0.04. It was concluded that the "beta" correlation was inaccurate and needed to be replaced.

## **2. PHASE II — MODEL REFINEMENT AND EXTENSION**

### **a. Background**

In Phase II, an analytical effort was conducted in which the rumble model developed in Phase I for a V-gutter augmentor rig was adapted to a self-contained computer program and extended to account for a turbofan engine geometry and for the different combustion characteristics of the fan and core streams. The combustion characteristics were refined by an independent augmentor combustion model developed under the Flameholder Combustion Instability Study contract (Reference 1).

The rumble model was used to make stability predictions for the Full-Scale Engine Research (FSER) program turbofan engine with a conventional augmentor operating subsonically at high altitude. Additional predictions were made for the FSER operating conditions in which flameholder geometry, duct pressure loss and flameholder wake temperature were varied. Several configurations were chosen to be tested. The augmentor hardware was designed and fabricated during this phase to provide these configurations to substantiate the model during Phase III.

The rumble model was extended to include the system characteristics of the newer "Vorbix" and "Full-Swirl" Augmentor concepts.

### **b. Fully Computerize Model**

At the end of Phase I, the model was composed of a series of analyses which required intermediate engineering interpretation and input. During this task the model formulation was refined and adapted to a self-contained computer program with a readily usable input — output format (Reference 4).



### **(1) Modeling Approach**

Rumble has long been associated with the relatively low frequency longitudinal, or axial, modes of vibration of the air column in the augmentor, thus the model was formulated to take only the longitudinal dimension into account. Accordingly, each station in the model was considered to represent a plane over which the value of any parameter (such as velocity, pressure or density) could be considered as uniform at any instant in time.

The equations developed for describing rumble can be classified into two types. First, there are the momentum, continuity and energy equations, together with the boundary conditions, which describe how each parameter at any station in the augmentor responds to a disturbance in combustion heat release. These are referred to as the acoustic equations. Secondly, there are the combustion equations which describe how combustion heat release responds to variations in the system parameters such as velocity, pressure and density. Together, the acoustic equations and the combustion equations describe the rumble mechanism, by which a perturbation in combustion causes a disturbance in velocity, pressure and density throughout the augmentor which in turn causes an additional disturbance in combustion. A description of the equations, boundary conditions and assumptions is presented in the Appendix D.

Since the purpose of the program was to develop an understanding of the rumble mechanism and demonstrate the onset of rumble could be predicted, thereby defining the boundary between stable and unstable operating regions, it was necessary only to model the augmentor for the first few increments of time before the oscillation had built up into an appreciable amplitude. This allowed use of a small perturbation technique which led to linear equations and mathematical simplification. Linear equations can describe the system for small oscillation amplitudes and can predict whether the system initially at rest would begin to oscillate. Because the nonlinearities associated with large amplitude oscillations (which eventually stop the amplitude from growing) were ignored, the linear equations do not allow a prediction of the final limit-cycle amplitude.

### **(2) Model Description**

The rumble model was designed for simple input-output and requires no intermediate engineering interpretation, Figure 44. The input requires engine geometry and pressures, temperatures and Mach numbers, obtained from engine steady-state cycle tables. The user may select to input augmentor fuel-air ratio and empirical combustion data or he may exercise the flameholder combustion model which calculates and supplies the required augmentor combustion data to the rumble model. No calculation nor dynamic information is required. The user may select either tabular and plotted output or only plotted output, as shown in Figure 45. From the plot the user identifies the frequencies at which the phase is zero. He then checks the gain at each of the identified frequencies. If the gain is one or greater, the program has predicted that rumble will occur. If the gain is less than one the program has predicted that the operating point is stable. For example, Figure 45 indicates rumble at 60 and at 140 Hz. The user can then change geometry or operating point inputs and repeat the process to determine the effects of the change. This form of output was chosen because it facilitated development of the model, yielded a compact, easy to interpret answer, and made better use of computer time than a time-domain solution.

To model rumble required a transient description of the longitudinal dynamics of the augmentor system. To computerize the formulation, the mathematical description was simplified by restricting the range of validity of the equations to small perturbations about a mean steady-state operating point. This allowed linearization of the equations to a form which correctly described small-scale transients, but in which the nonlinear terms which are important in large-scale transients could be omitted. The resultant linearized model accurately described the initial



period of time when rumble oscillations began to grow and are valid to the point where the rumble amplitude reached values at which the nonlinear terms became important. This was sufficient to determine whether an engine, if placed at a specific operating point, would spontaneously rumble.

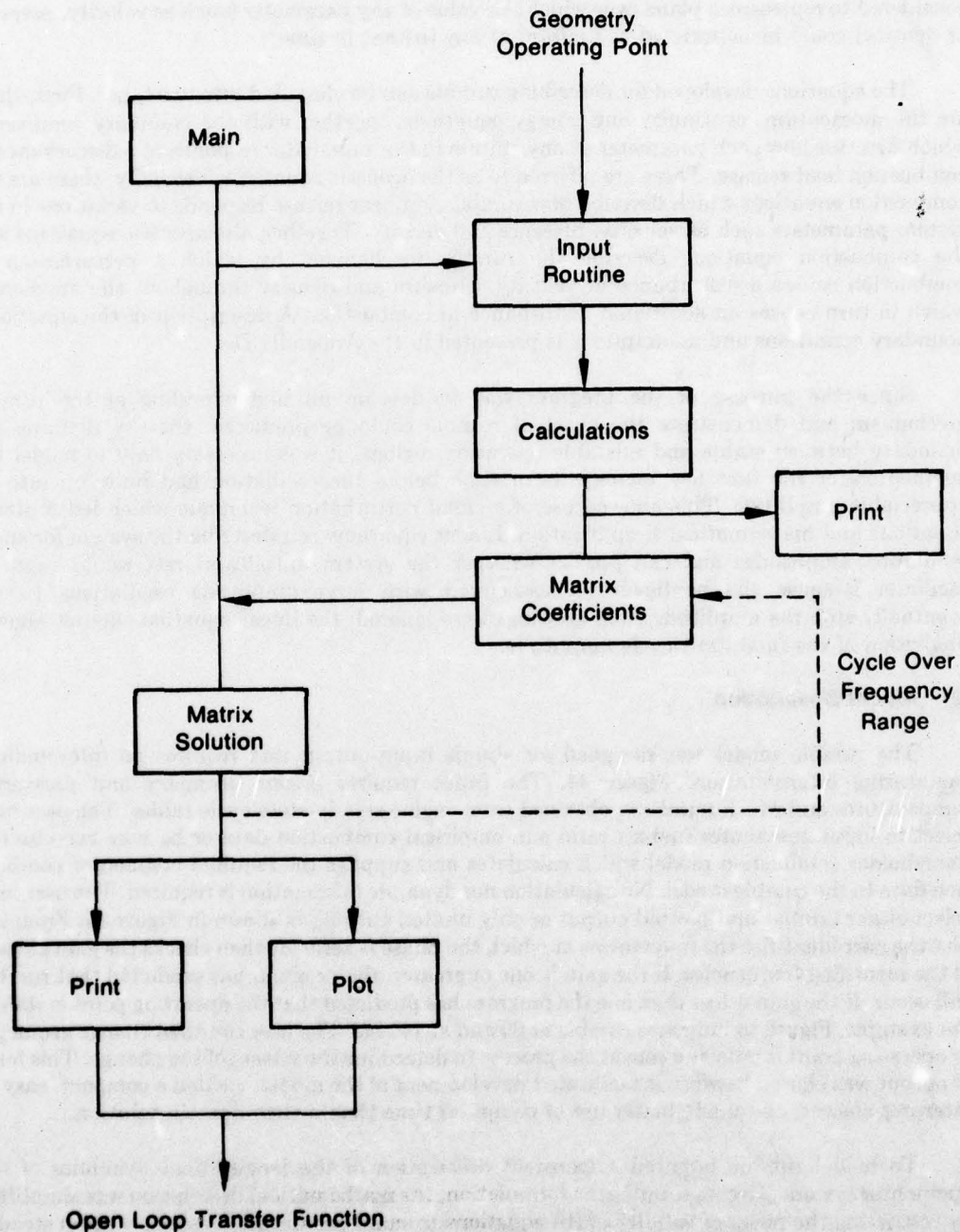
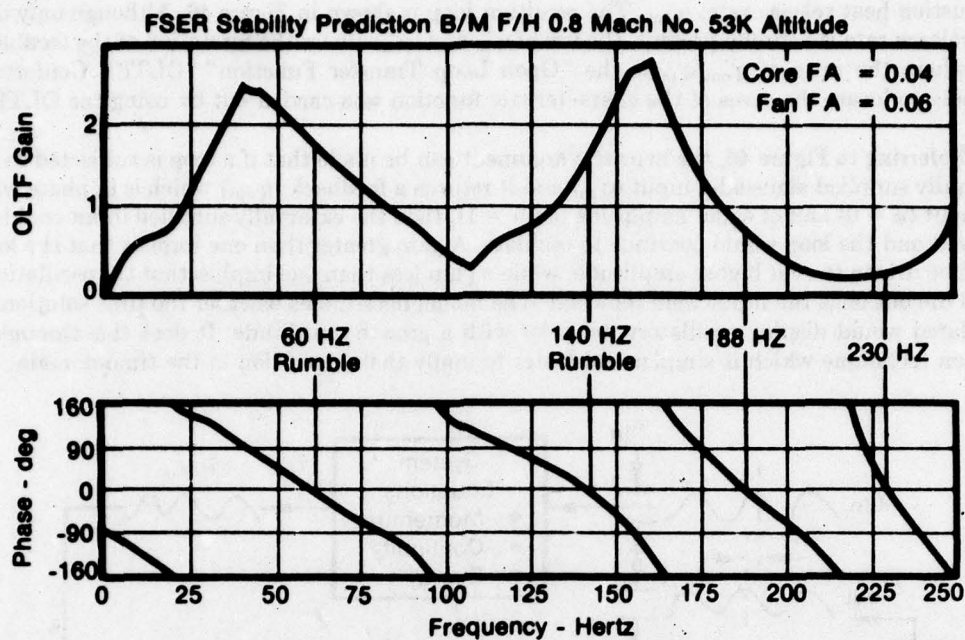


Figure 44. Rumble Model Flow Chart

FD 148452



FD 146463

Figure 45. Open Loop Transfer Function at 53,000 Feet Altitude and 0.8 Mach Number

The model could be made to yield solutions in the time-domain by programming the equations on an analog computer. The output is a time trace of any selected parameter (e.g., augmentor pressure). At a stable operating point the trace is a straight line, whereas at an unstable operating point the trace shows a sinusoidal oscillation with an increasing amplitude. The amplitude would grow without bound for as long as the solution continues, because of the omission of the nonlinear terms.

The same information was more easily obtained by a nontime-domain solution technique. Such a technique was chosen for the rumble model. Commonly called the Nyquist criterion, it is based upon the fact that the allowable forms of the time-domain solution are known. This technique allows use of a matrix program which can quickly solve large numbers of simultaneous equations.

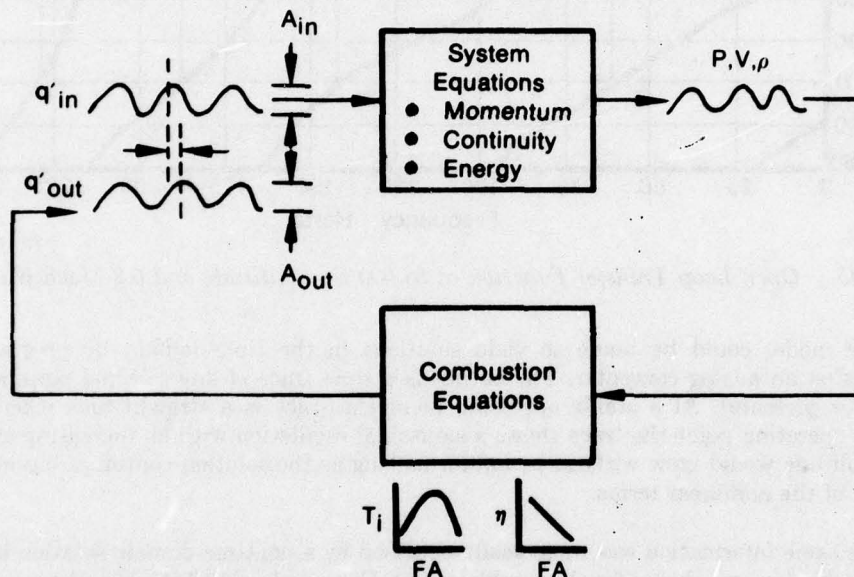
The Nyquist criterion is a procedure which makes use of the Laplace transform and conformal mapping to determine whether the transient solution would show unstable behavior. To apply the criterion, the time-domain equations are transformed into the Laplace "S" domain. The result is a square homogeneous matrix. The determinant of the matrix coefficients is a function of "S," called the characteristic function, and contains all of the information needed to determine whether the system being described is stable or unstable. If all zeros of the characteristic function have negative real parts, the system is stable; if any zeros have positive real parts, the system is unstable. Although the Nyquist criterion is complex, its application is straight-forward.

To accomplish the conformal mapping needed to determine stability, the equations which describe the system were written to describe a "feedback loop." The feedback loop was formed for the rumble model by considering that the overall combustion rate,  $q'_{in}$ , was an input to the acoustic equations. This yielded pressure, velocity, and density at each station throughout the engine. The output was fed back through the combustion equations to form a "feedback"



combustion heat release rate,  $q'_{out}$ . The resultant loop is shown in Figure 46. Although only one heat release rate is actually present, the use of  $q'_{in}$  and  $q'_{out}$  allows the formation of the feedback loop where the ratio of  $q'_{out}/q'_{in}$  is the "Open Loop Transfer Function" (OLTF). Conformal mapping to locate the zeros of the characteristic function was carried out by using the OLTF.

Referring to Figure 46, the heuristic argument can be made that if a loop is subjected to an externally supplied sinusoidal input ( $q'_{in}$ ) and it returns a feedback ( $q'_{out}$ ) which is in phase with the input ( $\phi = 0$ ) and of equal amplitude (gain = 1), then the externally supplied input could be removed and the loop would continue to oscillate. A gain greater than one implies that the loop would be driven to ever higher amplitude, while a gain less than one implies that the oscillations would die out once the input were removed. The model determines whether the time solution, if calculated would display oscillatory behavior with a growth amplitude. It does this through a solution technique which is simpler and faster to apply than a solution in the time-domain.



- Unstable if at Some Frequency:  $A_{out} \geq A_{in}$  and  $\phi = 0$

Figure 46. Condition for Rumble

FD 144859

### c. FSER Engine Stability Predictions

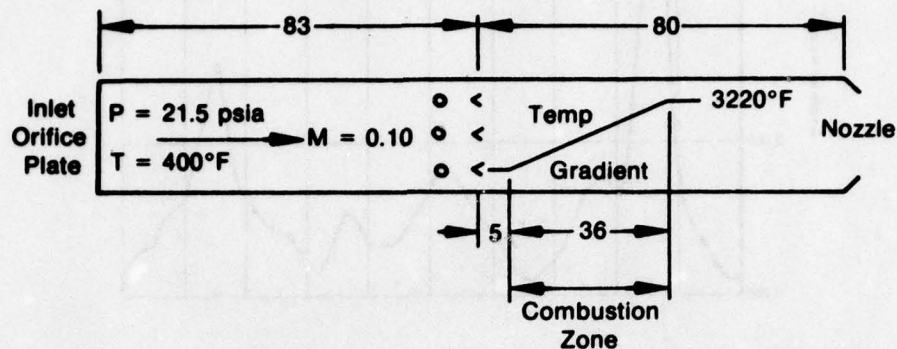
Task 1a was an analytical effort during which the rumble model developed in Phase I for a single stream V-gutter (boiler plate) combustion system was extended to account for a turbofan engine geometry and for the different combustion characteristics of the fan and core streams. Rumble predictions were made for the FSER engine with a B/M augmentor and for several proposed changes to the B/M augmentor which were expected to alter the occurrence of rumble.

#### (1) Extending the Model to Account for Turbofan Engine

Development of the wave equations to describe the longitudinal acoustics of the various sections of the single stream (boiler plate) combustion system was presented in Section II-1, Model Development. In that presentation it was assumed that terms associated with the axial pressure, velocity, and temperature gradients through the combustion zone could be neglected. The development has since been extended to account for the gradients. The effect of the gradient

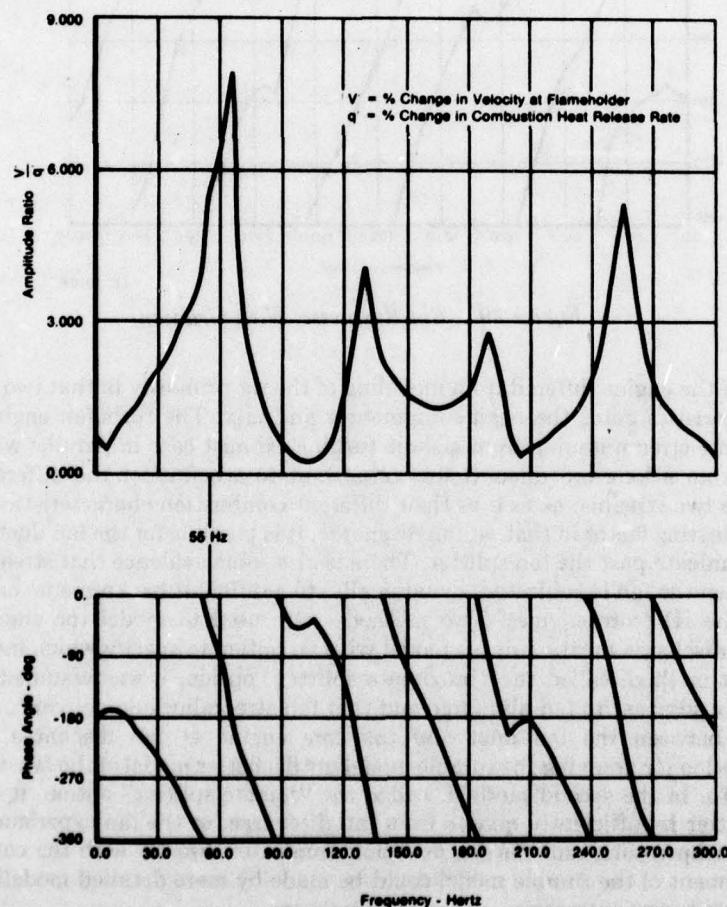


terms was examined for the augmentor rig, Figure 47, by calculating the response of air velocity at the flameholders to a combustion rate disturbance. When the gradient terms were neglected, a 55 Hz first resonance was predicted as shown in Figure 48. When the gradient terms were accounted for, a 40 Hz resonance was predicted as shown in Figure 49. This difference was sufficient reason to include the gradient terms in the wave equations.



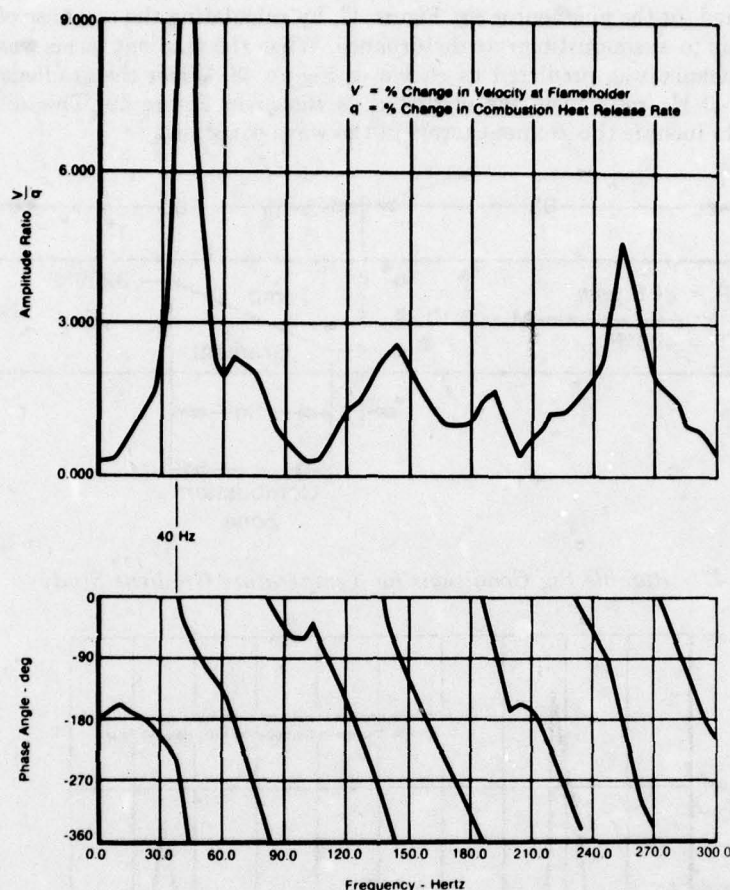
FD 146452

Figure 47. Rumble Rig Conditions for Temperature Gradient Study



FD 146455

Figure 48. Rig Response Without Gradient



FD 146456

Figure 49. Rig Response With Gradient

Modeling of the engine differed from modeling of the rig primarily in that two streams with different characteristics enter the engine augmentor and mix. The turbofan engine has a hot, partly vitiated core stream issuing from a short turbine exhaust case in parallel with a cold fan stream issuing from a long fan duct. It was important to account for the different upstream geometries of the two streams, as well as their different combustion characteristics. The engine also has a complicating factor in that, at fan discharge, it is possible for the fan duct and the core engine to communicate past the fan splitter. There is also some evidence that streamlines in the fan may shift when the fan is subjected, dynamically, to a different backpressure on the OD (fan duct) than on the ID (core engine). Two methods were used to model the engine boundary condition at fan discharge for the rumble model with an option to specify which method is to be used. In the first method, called the "proximate splitter" option, it was assumed that the fan splitter is directly adjacent to fan discharge and that fan streamlines do not shift, so there is no communication between the fan duct and the core engine at fan discharge. This is the recommended option for applying the rumble model until a better model of the fan discharge area becomes available. In the second method, called the "remote splitter" option, it was assumed that the fan splitter is sufficiently remote from fan discharge, so the fan experiences a radially uniform static backpressure, and the fan duct communicates directly with the compressor. An additional refinement of the rumble model could be made by more detailed modeling of the fan duct, fan and core engine interaction at the fan discharge.



The extension from the experimental rig to an engine was made to the model by applying the basic equations to the different geometry. A schematic of the rumble model as applied to a turbofan engine with a conventional V-gutter flameholder augmentor is shown in Figure 50. In this schematic, station (1) represents fan discharge on the fan duct side of the fan splitter; fan duct pressure drop is taken at station (2); the fan stream discharges into the augmentor at the mixing plane, station (3); the core stream exits the turbine at station (2H) and discharges into the augmentor at the mixing plane, station (3H). At the mixing plane the fan and core streams have a common static pressure but different velocities and temperatures. Accordingly, the fan stream combustion heat release rate was computed from instantaneous properties at station (3), while the core stream heat release rate was computed from properties at station (3H). Steps in the combustion process for a stream are depicted in Figure 51. Development of the equations to describe these steps for a single stream was presented in Section II-1, Model Development. It was found that the potential volumetric heat release rate of a stream, for example, the fan stream (subscript "C"), as it is being ignited by the flameholder wake can be expressed as:

$$q_c = \left[ 1 - \left( \frac{FA}{T_i} \frac{\partial T_i}{\partial FA} + \frac{FA}{\eta} \frac{\partial \eta}{\partial FA} \right)_c e^{-\tau_{DC}s} \right] W'_{sc} \quad (28)$$

Similarly, for the core stream (subscript "H"):

$$q'_H = \left[ 1 - \left( \frac{FA}{T_i} \frac{\partial T_i}{\partial FA} + \frac{FA}{\eta} \frac{\partial \eta}{\partial FA} \right)_H e^{-\tau_{DH}s} \right] W'_{sH} \quad (29)$$

These equations are written in terms of the Laplace transform of the normalized variables. They reflect that the combustion heat release rate in a stream will respond to changes in the amount of fuel and air mixture being ignited, to changes in the potential chemical energy in a pound of mixture (reflected in the ideal temperature rise), and to changes in the efficiency of the process as affected by fuel-air ratio. The major effect, and the one believed to be predominant in rumble, is the change in efficiency with fuel-air ratio causing large disturbances in the combustion heat release rate in response to small disturbances in air flow.

The fan and core stream heat release rates, from equations (28) and (29), were added to form the overall heat release rate of the augmentor (subscript "t"):

$$q'_t = \left[ \frac{Q_c}{Q_c + Q_H} \right] q'_c + \left[ \frac{Q_H}{Q_c + Q_H} \right] q'_H \quad (30)$$

$Q_c$  and  $Q_H$  are the steady-state heat release rates (watts or Btu/s) in the fan and core streams, respectively. The effect that an airflow disturbance in a stream has on overall augmentor heat release rate then depends upon the size of the airflow disturbance, the sensitivity of combustion in the stream to the disturbance (primarily the sensitivity of efficiency to fuel-air ratio), and the percentage of overall heat release rate contributed by the stream. The long fan duct allows high airflow disturbances, particularly at low frequency. At high fuel-air ratio, fan stream efficiency became very sensitive to fuel-air ratio. The fan stream contributed about half of the augmentor heat release rate. These considerations pointed to high fuel-air ratio in the fan stream as the most probable conditions leading to low-frequency rumble.

Downstream of the flameholders, the model is unchanged from that developed for the rig. The fan and core streams are assumed to mix and come to a common temperature and velocity at station (4). The overall heat release of the two streams, from equation (30), is assumed to begin at station (5), which can be coincident with station (4), and to end at station (10), which can be coincident with station (11). Intermediate stations between (5) and (10) are used to account for the axial temperature and velocity gradients through the combustion zone. Combustion products exited through an exhaust nozzle at station (11).



## (2) Turbofan (FSER) Engine Stability Predictions

To verify the model, five basic types of tests were planned for the FSER tests. They were:

1. Map rumble characteristics of the B/M augmentor for model evaluation
2. Add a screen in the fan duct for additional damping
3. Add heat to the fan stream flameholder wake
4. Add a mixer to increase air temperature of the fan stream
5. Tailor fuel sprayings to obtain a more uniform fuel-air ratio.

Test (1) was used to evaluate the accuracy of the model in predicting the fuel-air ratio and altitude at which rumble occurs. In test (2), an attempt was made to delay the onset of rumble by damping airflow oscillations in the fan duct. Because of the pressure drop penalty involved, this was not considered a viable engine modification to eliminate rumble. The test was made with a simple hardware change, which provided the opportunity to verify model predictions concerning engine changes other than modification of augmentor combustion characteristics. The remaining three tests were structured to change rumble characteristics by modifying the efficiency vs fuel-air ratio characteristic of the augmentor. The model has identified the declining efficiency vs fuel-air ratio characteristic as the primary cause of rumble. This efficiency decline was almost always encountered at fuel-air ratio greater than about 0.04. If a sufficiently large portion of the total augmentor heat release rate (e.g., the fan stream) reached an operating point at which it becomes highly sensitive to fuel-air ratio, rumble should occur. Increasing the temperature of the flameholder wake, increasing the temperature of the fan stream, or creating a uniform fuel-air ratio were identified analytically as possible ways to "flatten" the augmentor efficiency curve and thereby reduce the tendency toward rumble.

Rumble predictions were made for tests (1) through (4). Predictions for test (5) were generated after an airflow mapping tests of the augmentor which determined the nonuniformity of the fuel-air ratio distribution using the B/M sprayings. The predictions for the first four tests were generated for the FSER engine operating at 0.8 Mach number at altitudes from 40,000 to 55,000 feet.

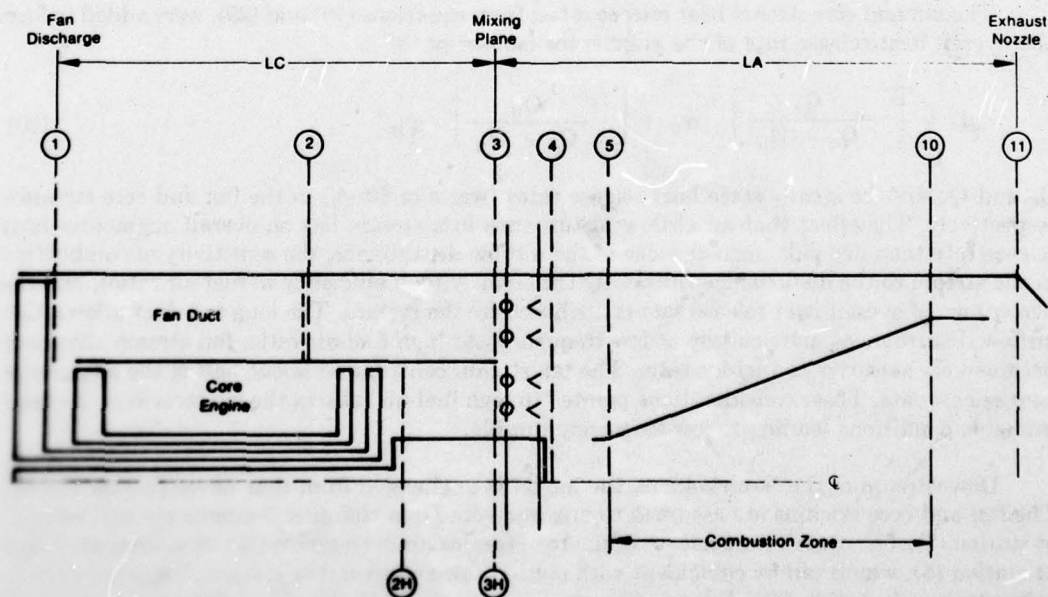
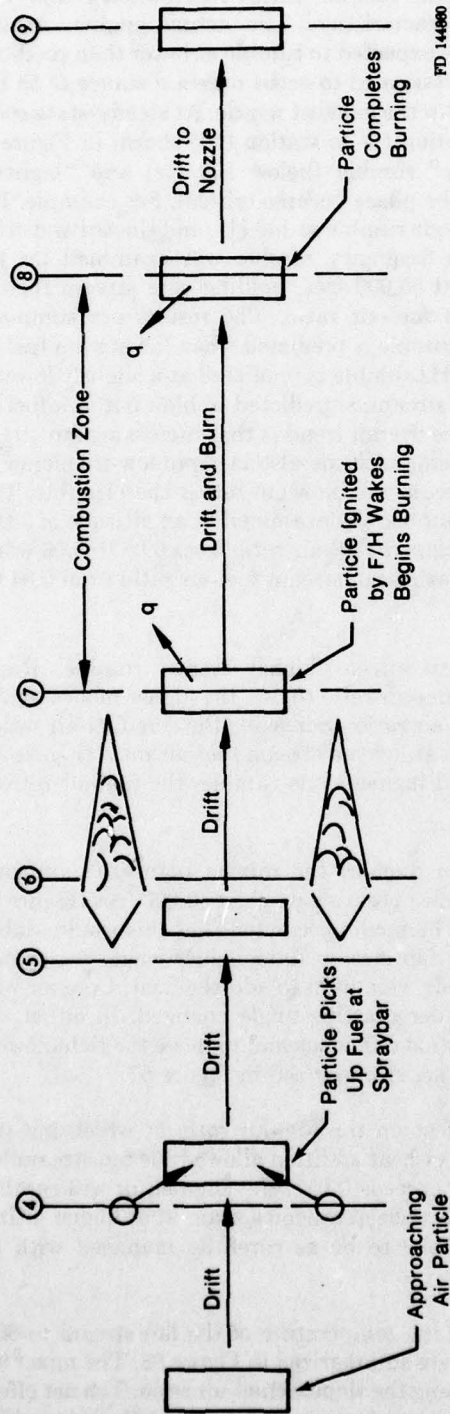


Figure 50. V-Gutter Rumble Model Schematic

FD 146457



FD 144860

Figure 51. Steps in Augmentor Combustion Process



The rumble model required transient definition of the combustion rates in the fan and core streams. This was done by means of equations based upon the efficiency vs fuel-air ratio predictions contained in Reference 1 and which are presented in Appendix C. The efficiency predictions were based upon assumed uniform fuel-air ratio distributions, and therefore, represented the best possible efficiency characteristics. The actual engine, exhibiting a nonuniform fuel-air ratio distribution, would be expected to rumble at lower than predicted fuel-air ratios. For all predictions, combustion was assumed to occur over a distance of 55 in. in the area from just downstream of the flameholders to the exhaust nozzle. At steady-state conditions, this creates a linear temperature rise from station (5) to station (10) shown in Figure 50. The predictions are classified into "low-frequency" rumble (below 100 Hz) and "higher mode" rumble, identified by the frequency at which the phase became critical. For example, Figure 45 shows "low-frequency" rumble at 60 Hz, 2nd mode rumble at 140 Hz, and the 3rd and 4th modes, at 188 and 230 Hz respectively, stable. Low-frequency rumble was examined for the B/M flameholder at altitudes of 40,000, 53,000, and 55,000 feet, holding core stream fuel-air ratio constant at 0.04 and varying the fan stream fuel-air ratio. The results are summarized in Figure 52. At an altitude of 40,000 feet, 60 Hz rumble is predicted when fan stream fuel-air ratio reaches 0.064. At an altitude of 53,000 feet, 60 Hz rumble is predicted at a slightly lower fuel-air ratio of 0.057. At an altitude of 55,000, the fan stream is predicted to blow out at a fuel-air ratio just below that required to produce rumble. The overall trend is that increasing fan stream fuel-air ratio leads to low-frequency rumble. Increasing altitude also leads to low-frequency rumble, until an altitude is reached at which the fan stream will blow out rather than rumble. The effect of core stream fuel-air ratio on low-frequency rumble was examined at an altitude of 53,000 feet. Results are summarized in Figure 53. Increasing core fuel-air ratio from 0.04 to 0.06 would have no effect on low-frequency rumble onset. Increasing fan stream fuel-air ratio from 0.04 to 0.057, however, would cause rumble.

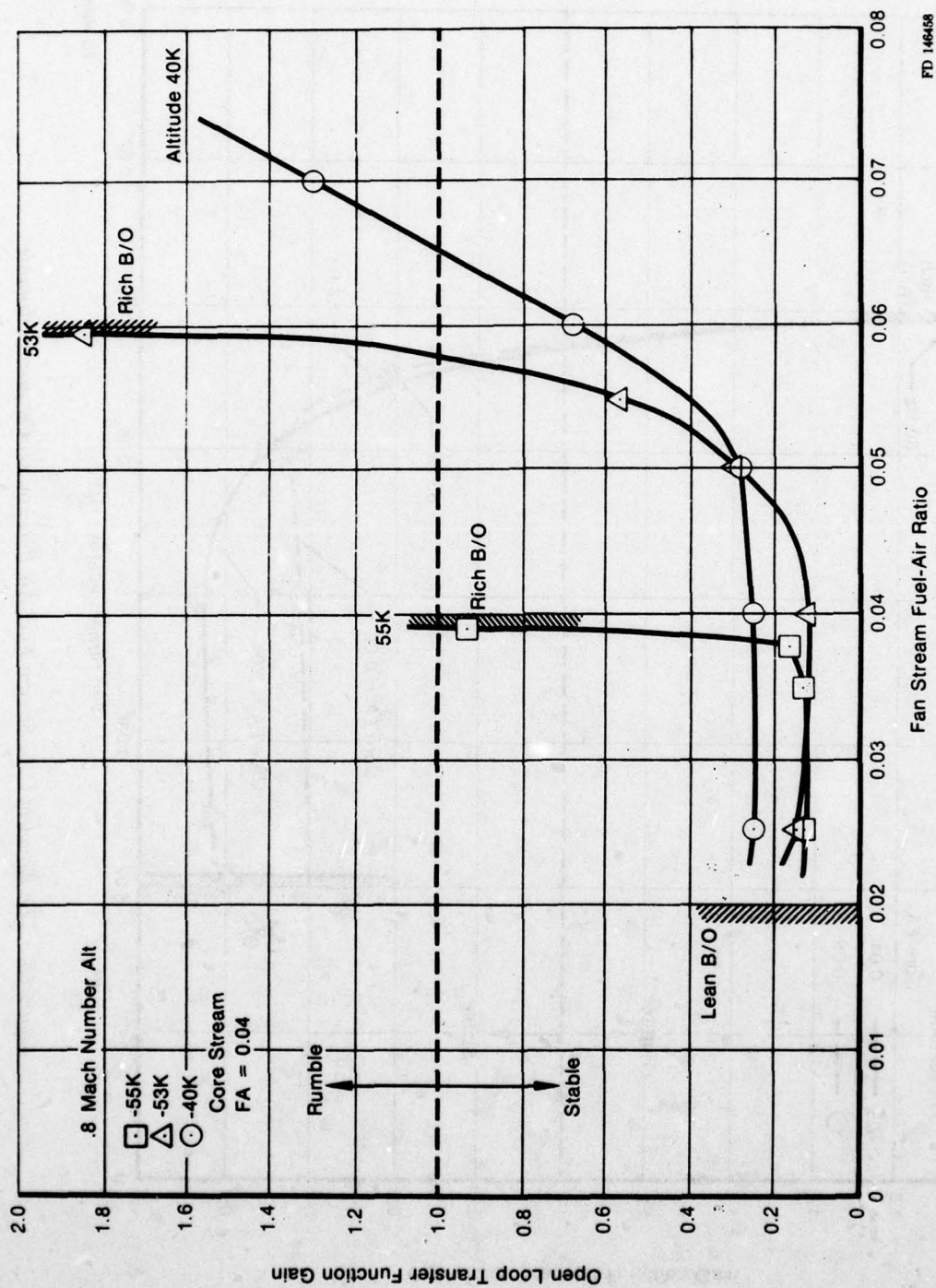
Core stream fuel-air ratio was found to affect "higher mode" rumble. Results are summarized in Figures 54 and 55. At low core fuel-air ratio (0.04), the higher modes tended to be stable (Figure 54), except at very high fan fuel-air ratio. Increasing the core fuel-air ratio to 0.06 drove the 2nd mode (140-165 Hz) unstable even at low fan stream fuel-air ratio (Figure 55). This indicated that to avoid both low-frequency and higher mode rumble, the fuel-air ratio in both streams must be properly managed.

The effect of adding a screen in the fan duct at the mixing plane to dampen airflow oscillations was examined at a predicted unstable operating point at 40,000 feet (Figure 56). The test added a screen with a 6% pressure drop. The model predicted that this would stabilize the augmentor. The effect of heat addition to the fan stream flameholder wake was examined at altitudes of 45,000 and 55,000 feet. Two methods were used to add the heat. Core air was piped directly to the flameholder, and the flameholder drafting angle changed. In either case, the predicted effect was to raise fan stream combustion efficiency and to move the rich blowout limit to a higher fuel-air ratio. Stability predictions are summarized in Figure 57.

At 45,000 feet, heat addition had no effect on the fuel-air ratio at which low-frequency rumble would first be encountered. At 55,000 feet heat addition allowed the fan stream to remain lit to higher fuel-air ratio. If the fuel-air ratio exceeds 0.057, the augmentor will rumble before blowing out. The major effect of heat addition is to keep the fan stream lit at higher altitudes. To avoid rumble, the fuel-air ratio would still have to be as carefully managed with the B/M flameholder.

The effect of adding a mixer to increase the temperature of the fan stream to 800°F was evaluated at an altitude of 45,000 feet. Results are summarized in Figure 58. The mixer increased fan stream combustion efficiency while steepening the slope vs fuel-air ratio. The net effect would be to cause low-frequency rumble at a slightly lower fuel-air than without the mixer. The major effect of the mixer would be to keep the fan stream lit at higher altitudes because of heat addition to the flameholder.





FD 146458

Figure 52. The Effect of Fan Stream Fuel-Air Ratio and Altitude on Rumble

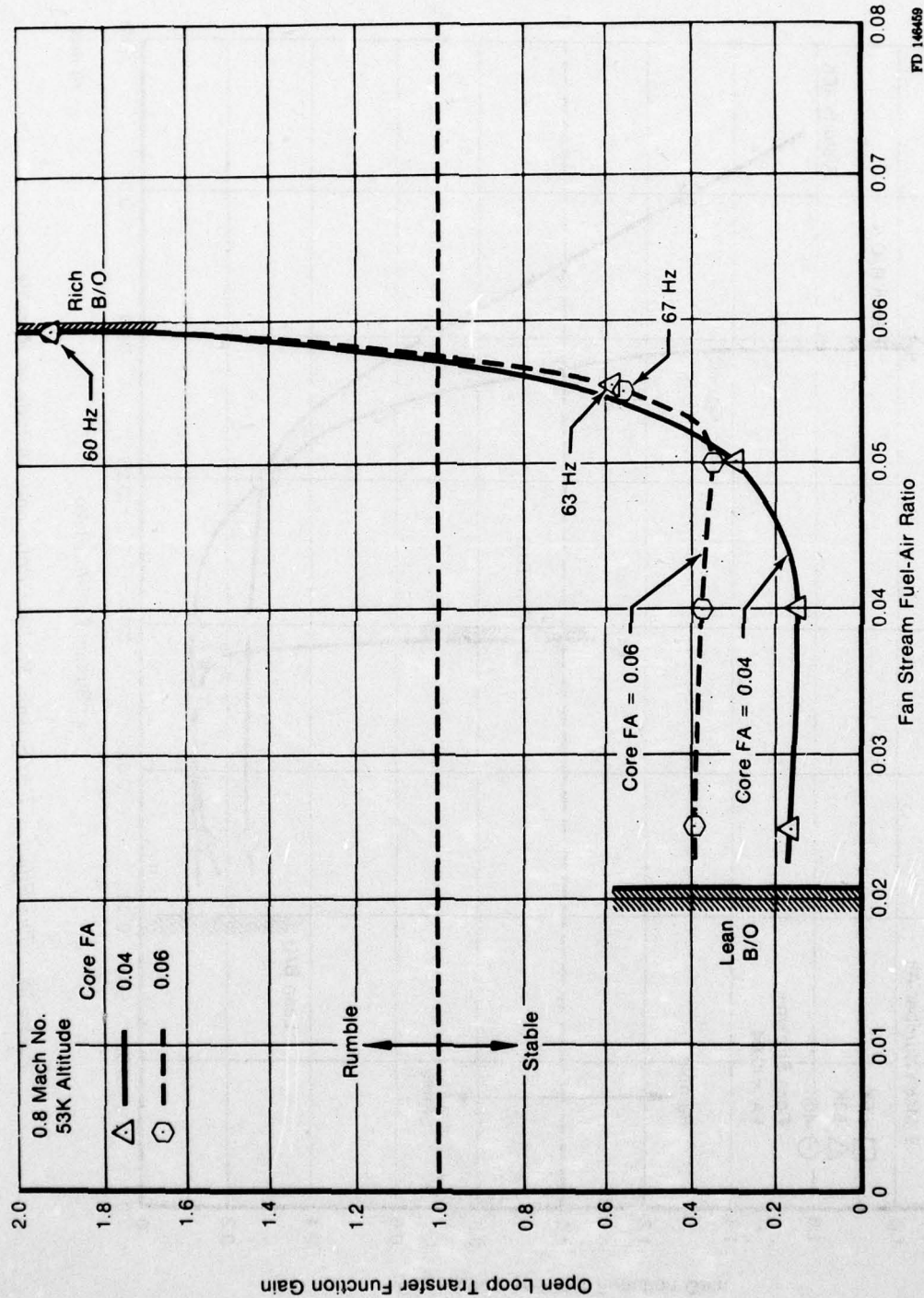
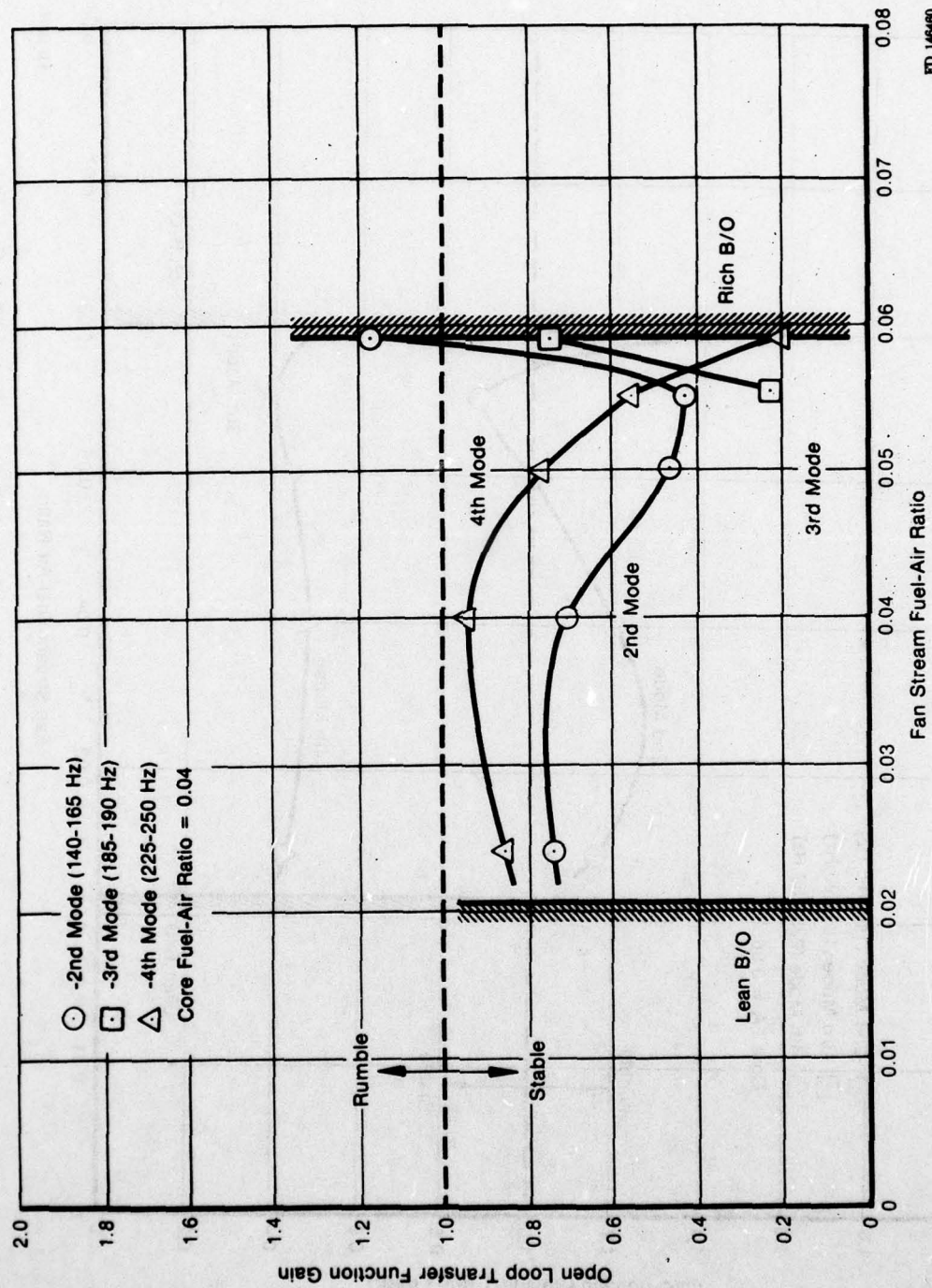


Figure 53. The Effect of Core Stream Fuel-Air Ratio on Lo-Frequency Rumble



FD 146480

Figure 54. The Effect of Low Core Stream Fuel-Air Ratio on Higher Mode Stability



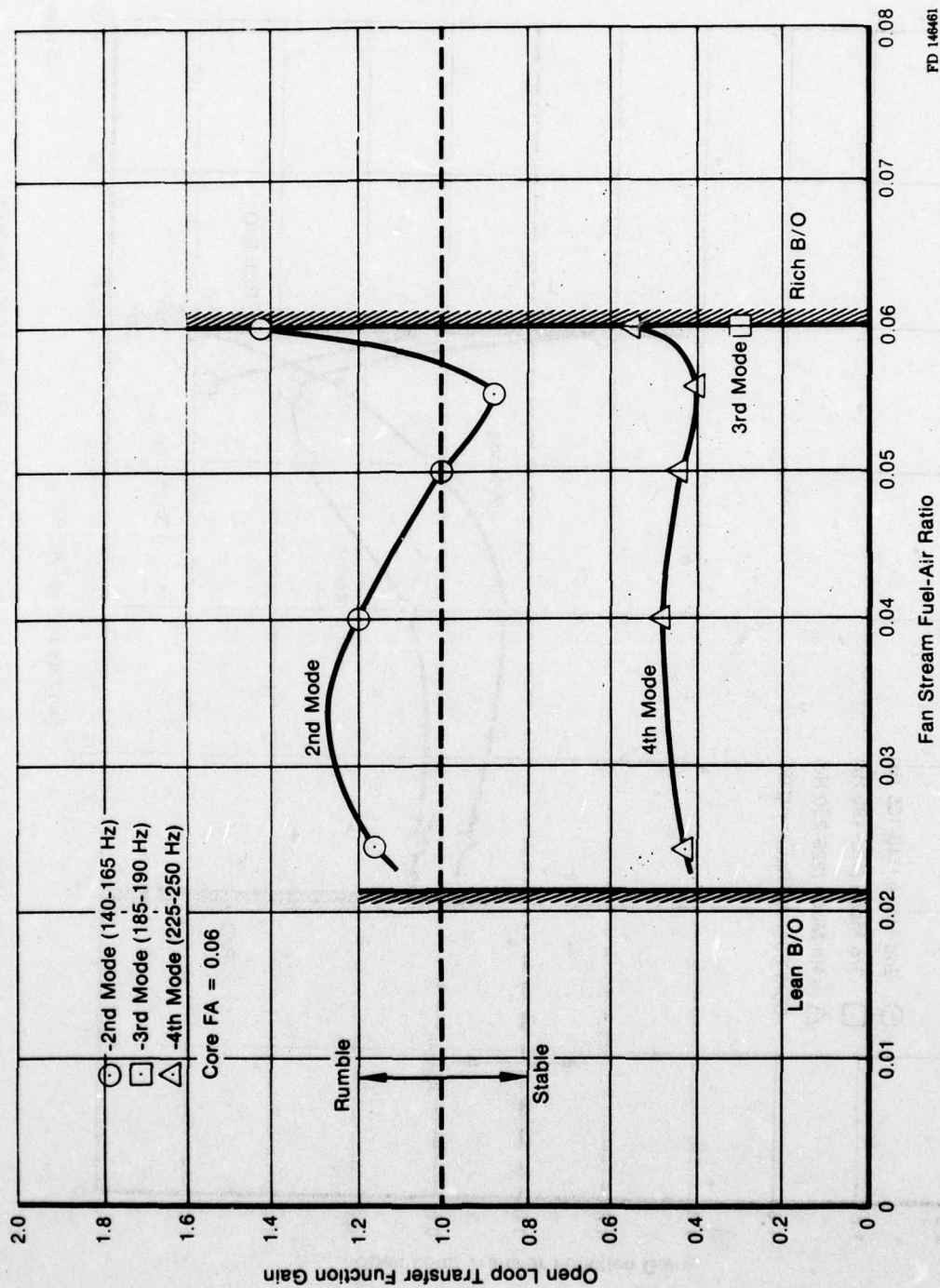
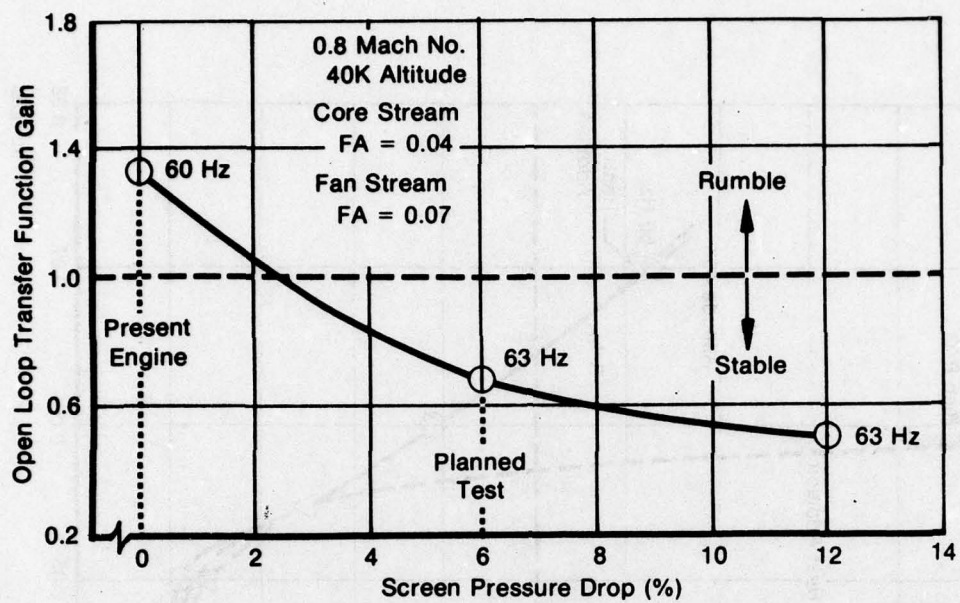
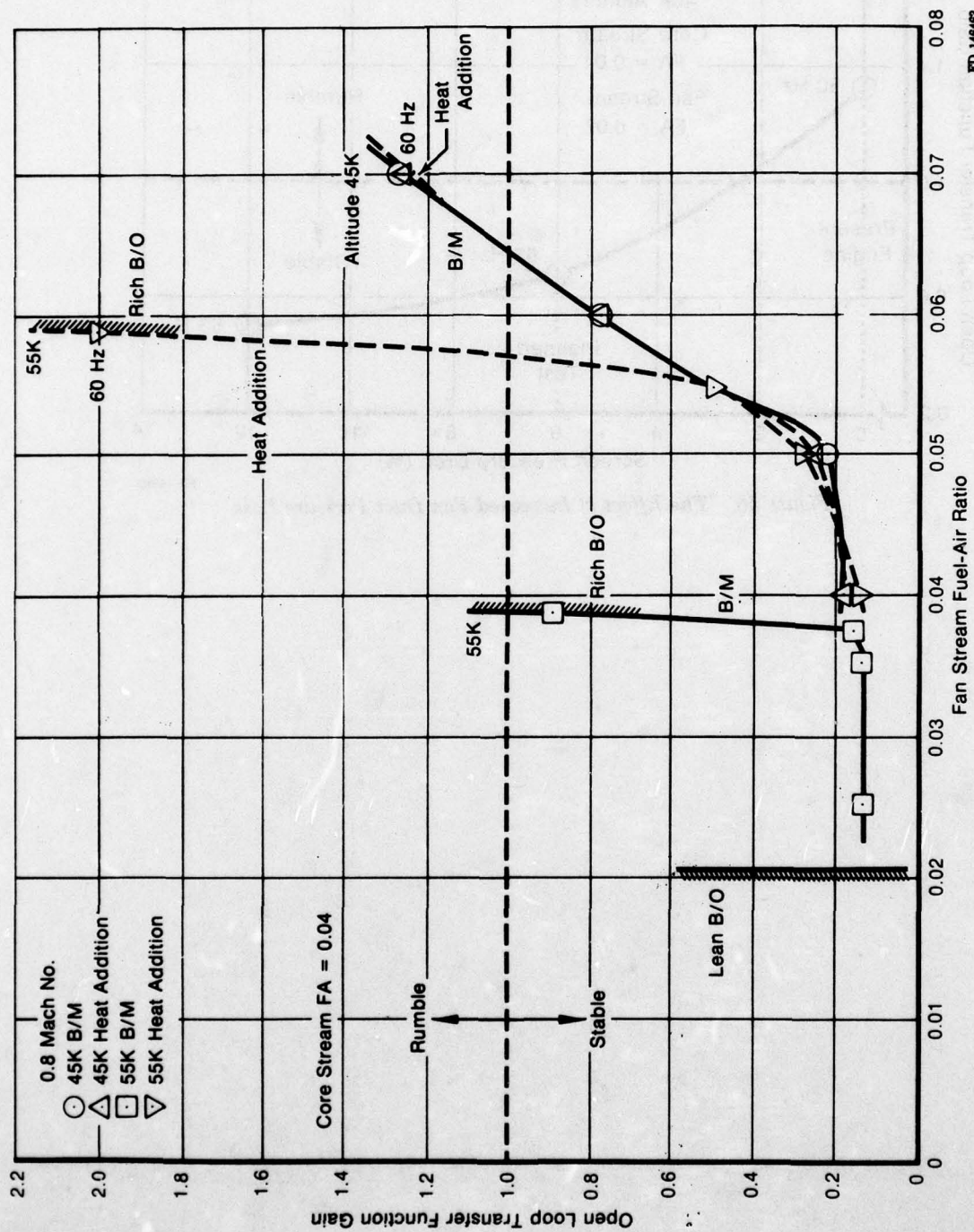


Figure 55. The Effect of High Core Stream Fuel-Air Ratio on Higher Mode Stability



FD 146462

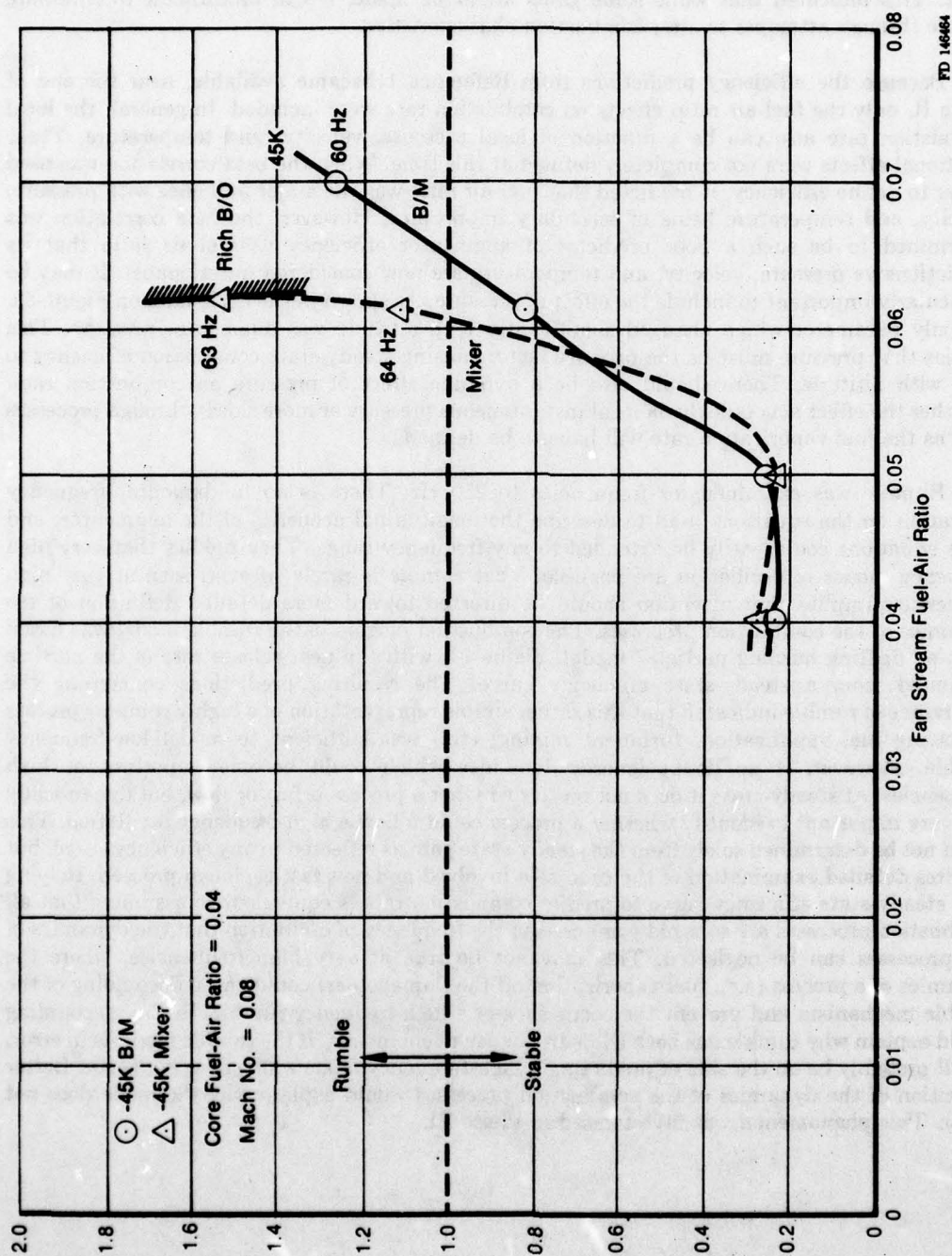
Figure 56. The Effect of Increased Fan Duct Pressure Loss



FD 146483

Figure 57. The Effect of Heat Addition to Fan Stream on Rumble





FD 146464

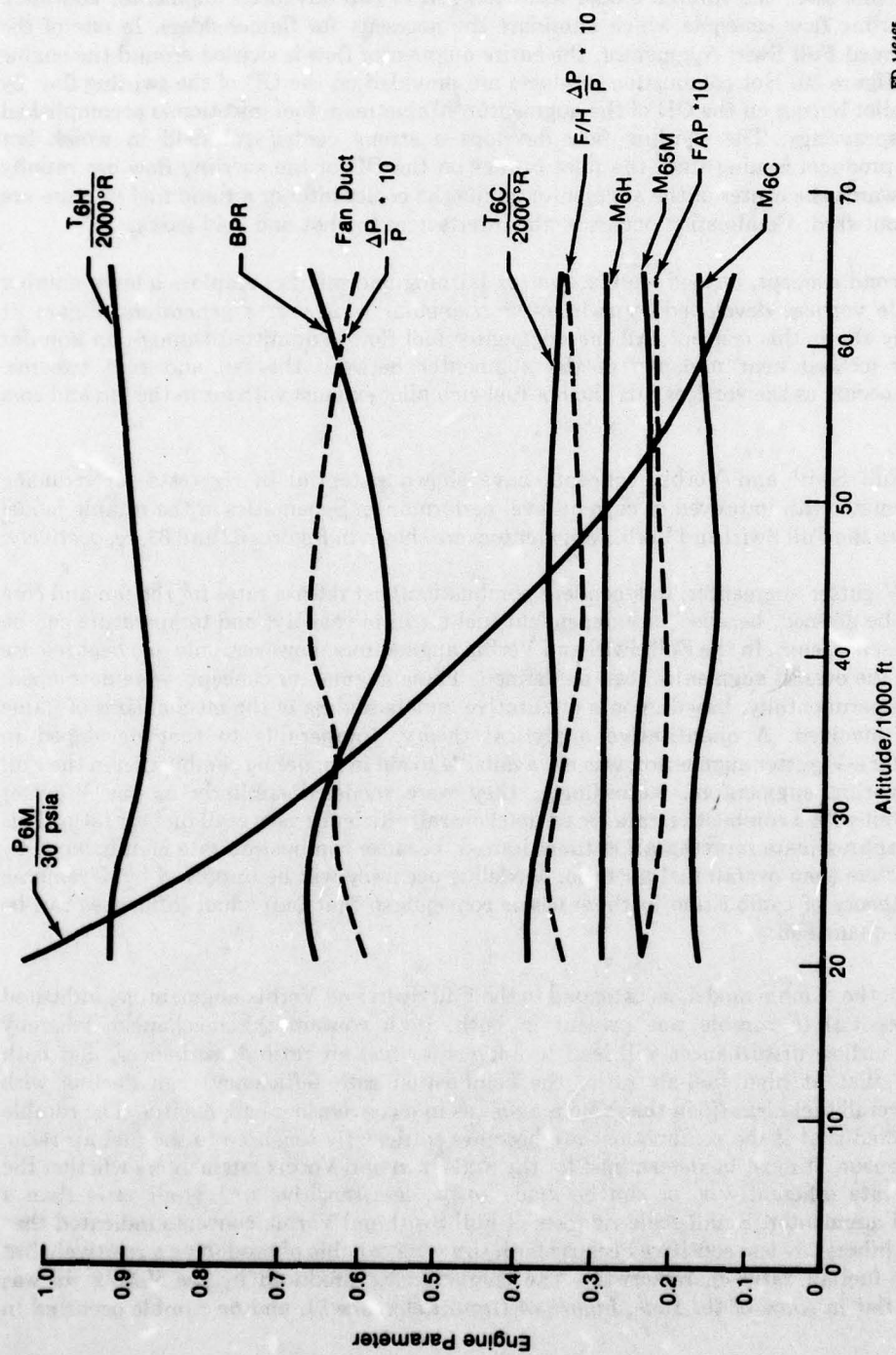
Figure 58. The Effect of Mixer on Stability

The tests to alter the occurrence of rumble were predicted to be unable to clearly eliminate rumble. Tests (2) and (3) showed some promise that the onset of rumble, or of blowout, could be delayed to a slightly higher altitude or fuel-air ratio. Test (4) was predicted to have an adverse effect. This indicated that while some gains might be made, it will be difficult to eliminate rumble through attempts to alter combustion characteristics.

Because the efficiency predictions from Reference 1 became available, near the end of Phase II, only the fuel-air ratio effects on combustion rate were included. In general, the local combustion rate also can be a function of local pressure, velocity, and temperature. These additional effects were not completely defined at this time. When the beta correlation was used earlier to define efficiency, it predicted that fuel-air ratio was the major influence with pressure, velocity, and temperature being of secondary importance. However, the beta correlation was determined to be such a poor predictor of augmentor efficiency vs fuel-air ratio that its predictions vs pressure, velocity, and temperature are now considered questionable. It may be particularly important to include the effect of pressure. As shown in the cycle data on Figure 59, the only parameter which changed significantly with altitude was augmentor pressure. This implies that pressure must be the primary factor causing steady-state combustion efficiency to vary with altitude. There should also be a dynamic effect of pressure on combustion rate. Whether the effect acts quickly on local instantaneous pressure or more slowly through processes such as the fuel vaporization rate will have to be defined.

Rumble was examined for frequencies to 250 Hz. There is no fundamental frequency limitation on the equations used to describe the longitudinal acoustics of the augmentor, and these equations could easily be extended to any frequency range. They predict that very high frequency modes of oscillation are possible. That rumble is rarely, if ever, seen at very high frequencies implies that attention should be directed toward more detailed definition of the dynamics of the combustion processes. The combustion portion of the rumble model was based upon a "drifting burning particle" model, Figure 51, with the heat release rate of the particle computed from a steady-state efficiency curve. The resulting predictions concerning the occurrence of rumble indicated that this rather simple representation of a highly complex process (involving fuel vaporization, turbulent mixing, etc.) was sufficient to model low-frequency rumble. However, it no doubt ignores dynamics which could become important at high frequencies. At steady-state it does not matter whether a process is fast or slow, but dynamically it is very important to identify whether a process could follow a high-frequency oscillation. This could not be determined solely from the steady-state gain as reflected in any efficiency curve, but requires detailed examination of the processes involved and how fast each can proceed. Relying on a steady-state efficiency curve to predict combustion rate is equivalent to assuming that all combustion processes are so rapid compared to the frequency of oscillation that the dynamics of the processes can be neglected. This may not be true at very high frequencies, where the dynamics of a process (e.g., fuel vaporization off the flameholder) could cause decoupling of the rumble mechanism and prevent the occurrence of a high-frequency rumble. Such a decoupling would explain why rumble has been a low-frequency phenomenon. If the rumble model is in error, it will probably be on the side of predicting a high-frequency mode which does not occur. Better definition of the dynamics of the combustion processes would explain why the mode does not occur. This phenomenon was investigated in Phase III.





FD 146466

Figure 59. A Comparison of Engine Parameters at Various Flight Altitudes



#### **d. Extend Model to Other Types of Augmentors**

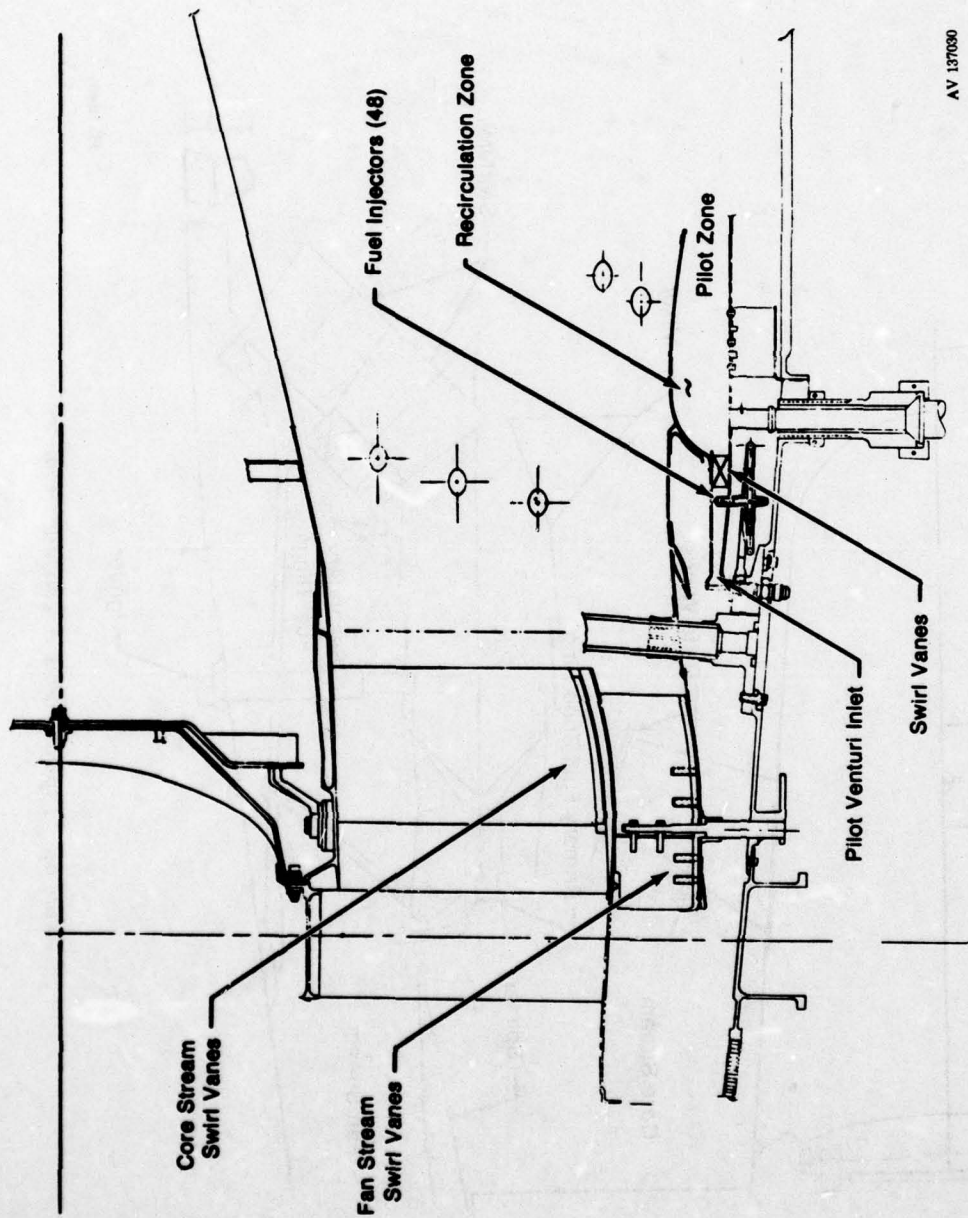
During this task, the rumble model was extended to two advanced augmentor concepts. Both are swirling flow concepts which eliminate the necessity for flameholders. In one of the concepts, termed Full Swirl Augmentor, the entire augmentor flow is swirled around the engine center line, Figure 60. Hot combustion products are provided on the OD of the swirling flow by an annular pilot burner on the OD of the augmentor. Mainstream fuel injection is accomplished by several sprayings. The swirling flow develops a strong centrifugal field in which hot combustion products issuing from the pilot burner on the OD of the swirling flow are rapidly displaced towards the center of the augmentor, while the cooler interior air and fuel mixture are centrifuged outward. Combustion occurs at the interface of the hot and cold gases.

The second concept, termed Vorbix, (vortex burning and mixing) employs a large number of small-scale vortices developed by swirlers or triangular wing vortex generators. Figure 61 schematically shows this concept. All the augmentor fuel flow is admitted through an annular pilot burner located near midspan of the augmentor between the fan and core streams. Combustion occurs as the vortices mix the hot fuel-rich pilot exhaust with air in the fan and core streams.

Both Full Swirl and Vorbix concepts have shown potential in rig tests for reducing augmentor length with improved or current level performance. Schematics of the rumble model as extended to the Full Swirl and Vorbix augmentors are shown in Figures 62 and 63, respectively.

In the V-gutter augmentor, independent combustion heat release rates for the fan and core streams can be defined, because an independent fuel-air ratio velocity, and temperature can be assigned to each stream. In the Full Swirl and Vorbix augmentors, however, only one heat release rate, that of the overall augmentor, can be defined. These augmentor concepts were developed, essentially experimentally, based upon a qualitative understanding of the mechanisms of flame propagation involved. A quantitative analytical theory, comparable to that developed in Reference 1 for a V-gutter augmentor, was not available to aid in modeling combustion in the Full Swirl and Vorbix augmentors. Accordingly, they were modeled similarly as the V-gutter augmentor, but with a combustion rate based upon overall efficiency vs overall fuel-air ratio. This was a more approximate representation than desired, because combustion rate is influenced by more parameters than overall fuel-air ratio. Modeling accuracy will be improved by developing further the theory of combustion in these newer concepts so that individual influences can be isolated and quantified.

Even so, the rumble model, as extended to the Full Swirl and Vorbix augmentors, indicated that the potential to rumble was present in both. Both contain the mechanism whereby longitudinal airflow disturbances will lead to augmentor fuel-air ratio disturbances, and both have shown that at high fuel-air ratio, the combustion rate (efficiency) can decline with increasing overall fuel-air ratio in the same manner as in a conventional augmentor. The rumble model predicted that if the combustion rate becomes sufficiently sensitive to the fuel-air ratio, rumble will ensue. It must be determined for the Full Swirl and Vorbix augmentors whether the combustion rate inherently is, or can be made to be, less sensitive to fuel-air ratio than a conventional augmentor. Small-scale rig tests of Full Swirl and Vorbix concepts indicated that they may be inherently less sensitive because both rigs were capable of producing a relatively flat efficiency vs fuel-air ratio characteristic. The characteristic produced by the Vorbix rig was particularly flat in some of the runs, Figure 64 (from Reference 5), and no rumble occurred in testing.



AV 137030

Figure 60. Typical Swirl Augmentor Geometry

AD-A065 144

PRATT AND WHITNEY AIRCRAFT GROUP WEST PALM BEACH FL 6--ETC F/6 21/5  
LO-FREQUENCY AUGMENTOR INSTABILITY STUDY.(U)

DEC 78 P L RUSSELL, G BRANT

F33615-76-C-2024

UNCLASSIFIED

PWA-FR-10397

AFAPL-TR-78-82

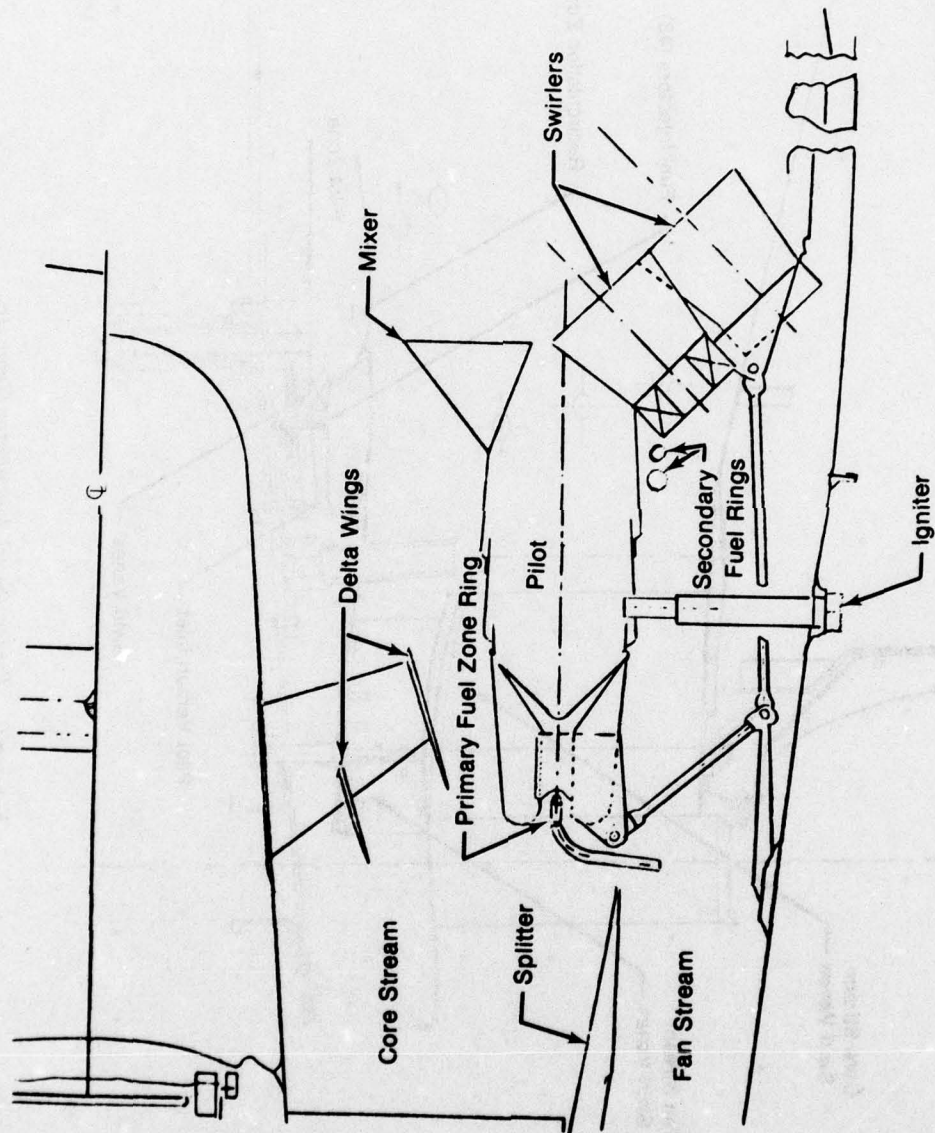
NL

2 of 3

AD  
A065144

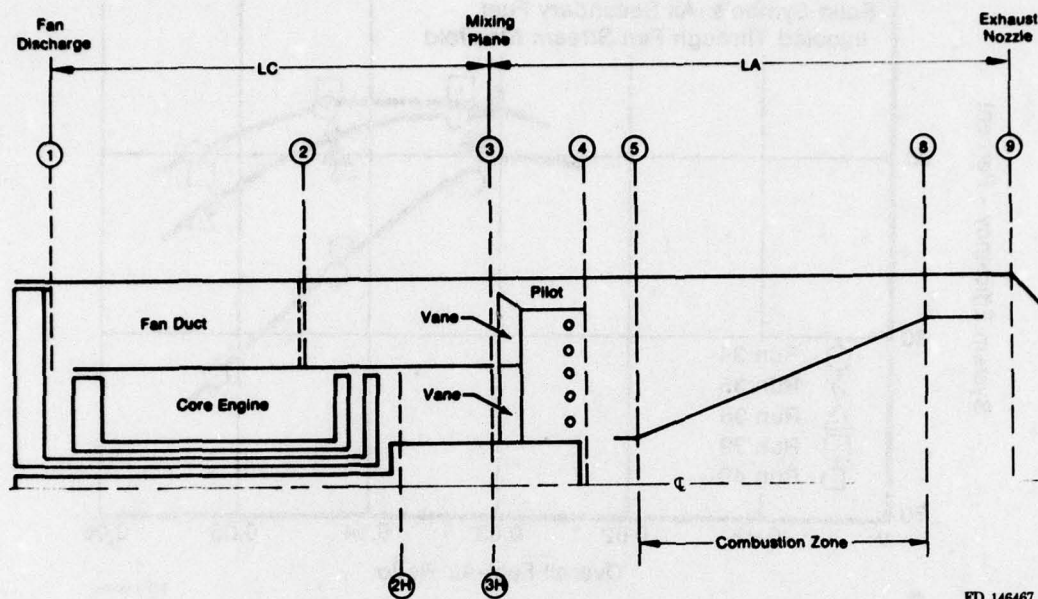






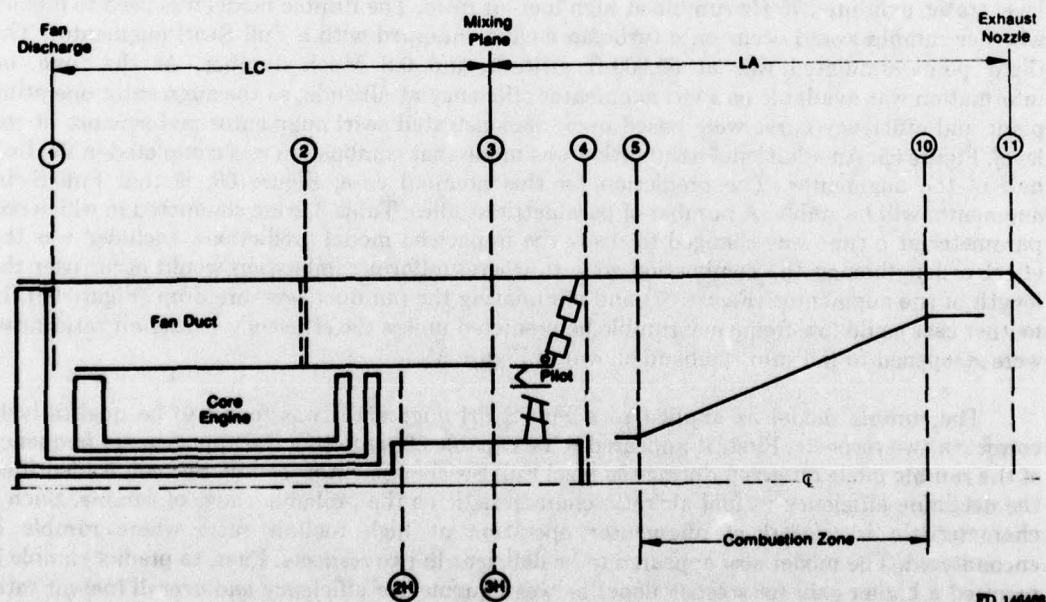
FD 146466

Figure 61. Typical Vorbix Augmentor Geometry



FD 146467

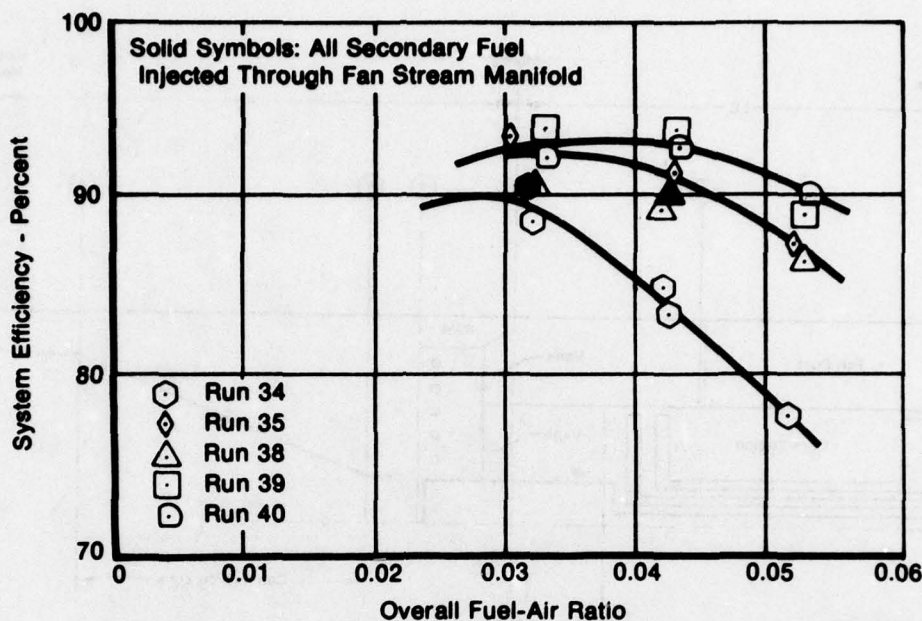
Figure 62. Full Swirl Augmentor Model Schematic



FD 146468

Figure 63. Vorbix Rumble Model Schematic





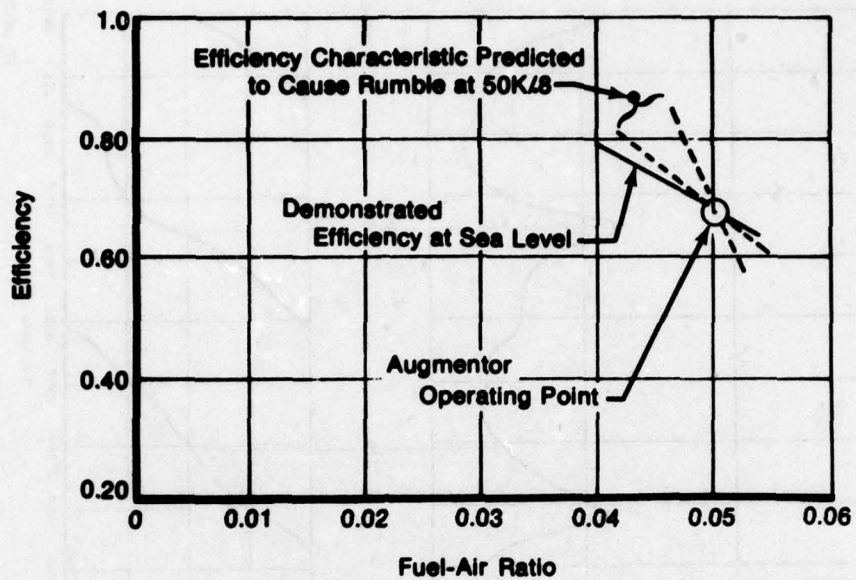
FD 146469

Figure 64. System Efficiency Characteristics for the Configuration With Swirlers Removed (Run 34) and for the Vorbix II Augmentor Configurations (Run 35, 38-40)

The Full Swirl rig experienced 90 to 100 Hz rumble, which was eliminated by properly zoning the fuel (Reference 6). In addition, the Full Swirl augmentor, when run on an engine at sea level static, exhibited 75 Hz rumble at high fuel-air ratio. The rumble model was used to predict whether rumble would occur on a turbofan engine equipped with a Full Swirl augmentor. The flight point simulated was at 50,000-ft altitude and 0.8 Mach number. At the time, no information was available on swirl augmentor efficiency at altitude, so the augmentor operating point and efficiency curve were based upon demonstrated swirl augmentor performance at sea level, Figure 65. An additional assumption was made that combustion was completed in the first half of the augmentor. The prediction for this nominal case, Figure 66, is that Full Swirl augmentor will be stable. A number of parametric studies, Table 3, were conducted in which one parameter at a time was changed to study the impact on model predictions. Included was the effect of lengthening the combustion zone to where uniform combustion would occur over the length of the augmentor (Figure 67) and eliminating the fan duct pressure drop (Figure 68). In neither case could low-frequency rumble be predicted unless the efficiency vs fuel-air ratio curve were steepened to fall into the band shown in Figure 65.

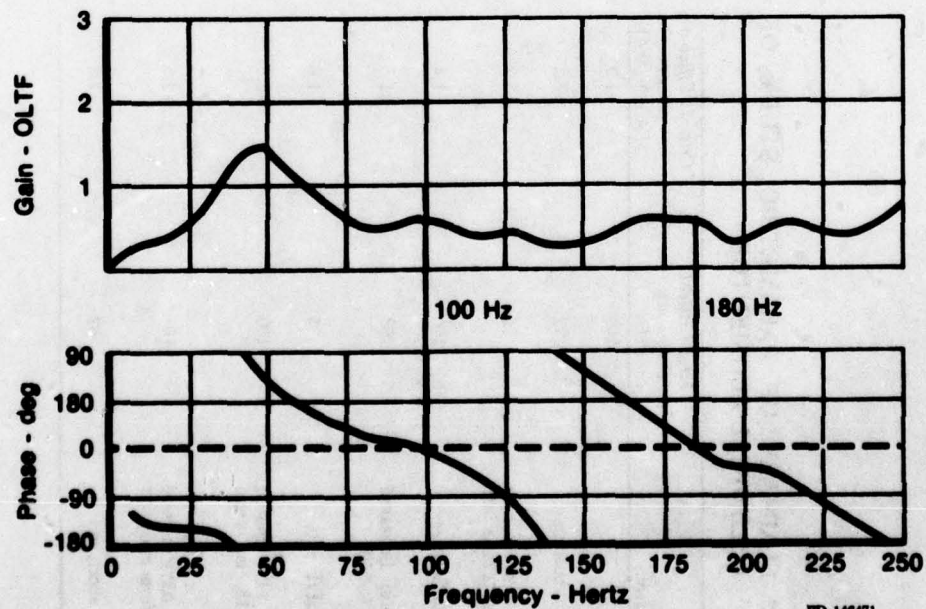
The rumble model as applied to a Full Swirl augmentor was found to be qualitatively correct in two respects. First, it appeared to be capable of predicting the approximate frequency of the rumble mode observed during sea level Full Swirl augmentor testing. Second, it identified the declining efficiency vs fuel-air ratio characteristic as the probable cause of rumble. Such a characteristic is typical of augmentor operation at high fuel-air ratio where rumble is encountered. The model also appeared to be deficient in two respects. First, to predict rumble it required a higher gain (or steeper slope) between augmentor efficiency and overall fuel-air ratio than the Full Swirl augmentor has demonstrated. Second, it did not show a decided preference for the first mode, but often predicted that a higher frequency mode was more likely to occur. It is expected that a more detailed treatment of the Full Swirl augmentor combustion process will overcome these deficiencies.





FD 146470

Figure 65. Full Swirl Augmentor Efficiency Characteristic at High Fuel-Air Ratio

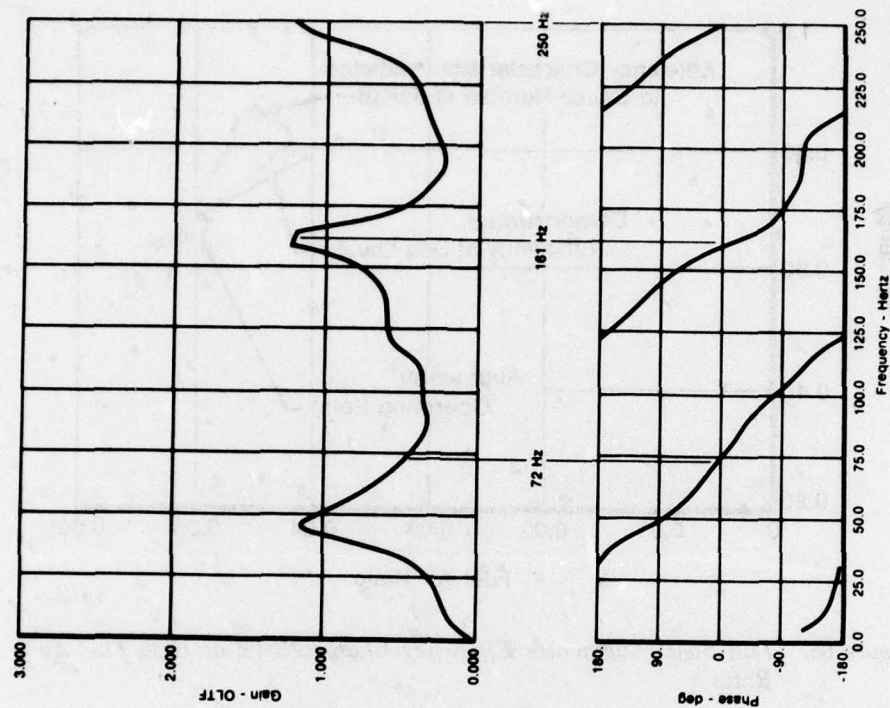


FD 146471

Figure 66. Open Loop Transfer Function and Phase as a Function of Frequency for the Full Swirl Nominal Case

TABLE 3. SUMMARY OF PARAMETRIC STUDY OF  
FULL SWIRL AUGMENTOR

Case	First Critical Frequency (Hz)	Critical Efficiency Slope (FA/η <sub>av</sub> /aFA)
Nominal	100	-1.9
Uniform combustion	72	-2.2
Mixed Mach number re- duced from 0.24 to 0.16	75	-1.2
Remote Fan Splitter	100	-1.4
Bypass ratio increased from 0.63 to 0.78	98	-1.8
Fan duct ΔP/P = 0	75	-1.6
Fan duct ΔP/P moved forward 18 in. from midpoint	100	-3.0
Fan duct ΔP/P moved aft 18 in. from midpoint	107	-2.5
Fan duct shortened by 12 in.	92	-1.3



FD 146472

Figure 67. Full Swirl With Uniform Combustion

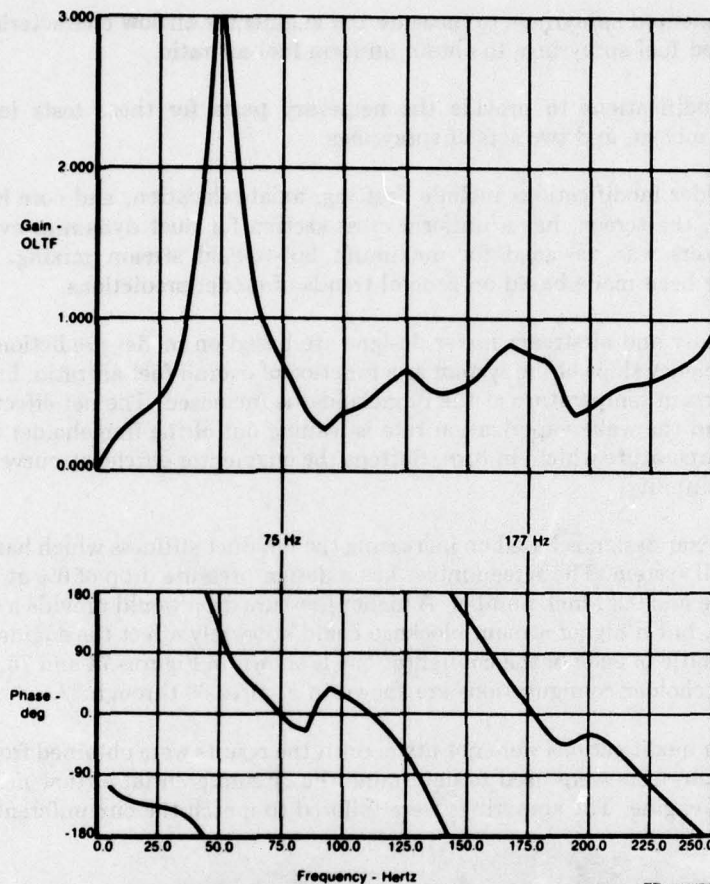


Figure 68. Full Swirl With Fan Duct  $\Delta P/P = 0$

There was little information available on which to base rumble predictions for a turbofan engine equipped with a Vorbix augmentor. The Vorbix has been run only as a small-scale rig. If a Vorbix augmentor, scaled to full engine size, displayed the same declining efficiency vs fuel-air ratio characteristic found on the Full Swirl augmentor, the predictions would duplicate those for the swirl augmentor. If a full-scale Vorbix augmentor were to maintain the flat efficiency characteristic found on the Vorbix rig, Figure 64, then it would be predicted to be stable. Without a prediction of combustion efficiency for a Vorbix augmentor at altitude, a definite prediction on the occurrence of rumble cannot be made.

#### e. Design and Fabrication of Engine Hardware Modifications

The objective of these tasks was to design and provide modifications to F100 augmentor hardware obtained from the F100 component improvement program that were used for the FSER model verification test program during Phase III.

The configurations required for the FSER test program were:

1. A B/M augmentor
2. A screen for additional fan duct dampening
3. Flameholders that add heat to the fan stream flameholder wake
4. A mixer for the fan duct exit plane to raise fan stream temperature



5. Instrumented sprayings to measure the augmentor airflow characteristics
6. Tailored fuel sprayings to obtain uniform fuel-air ratio.

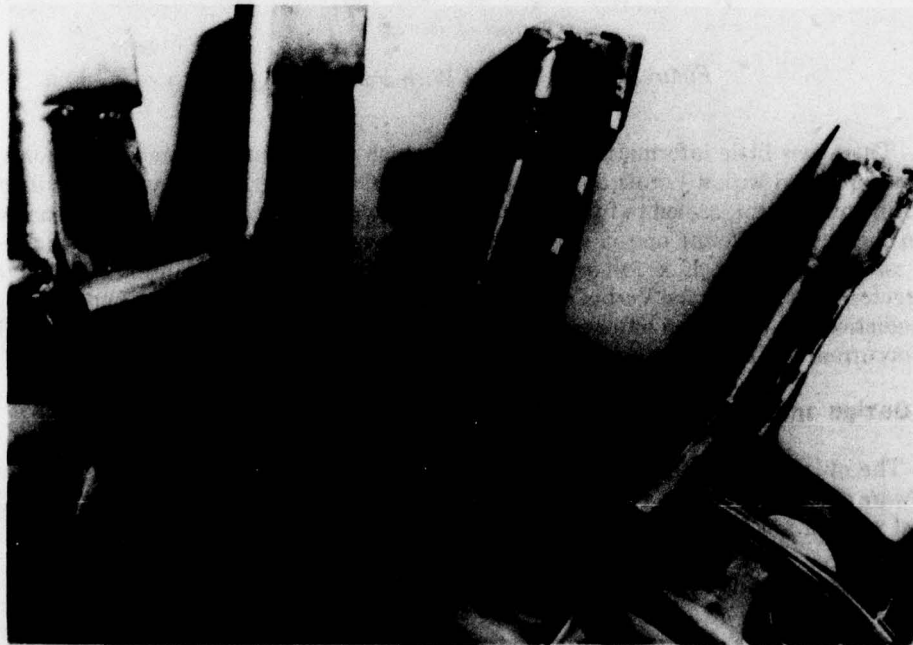
Hardware modifications to provide the necessary parts for these tests included three flameholders, two mixers, and two sets of sprayings.

The flameholder modifications include drafting, axial relocation, and core heat addition. One set of mixers, the screen, has a uniform cross section for duct dynamics evaluation; the second set of mixers was designed for maximum hot-to-cold stream mixing. Each of the modifications have been made based on general trends of model predictions.

The flameholder and airstream mixer designs are based on model predictions affected by changes in the efficiency slope of the system as a function of overall fuel-air ratio. In each of these designs, the fan stream temperature at the flameholder is increased. The net effect on the wake kinetic reaction and the wake vaporization rate is leaning out of the flameholder wake, and an increased wake temperature which, in turn, flattens the augmentor efficiency curve and provides improved system stability.

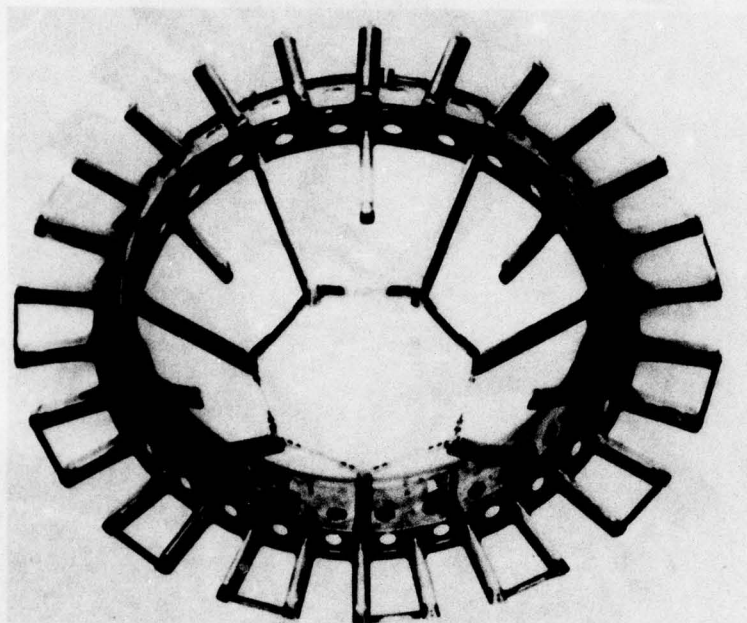
The screen mixer design is based on increasing the fan duct stiffness which has a stabilizing effect on the overall system. The screen mixer has a design pressure drop of 6% at a flight point of 40,000-ft altitude and 0.8 Mach number. A higher pressure drop would provide a stiffer system and more stability, but a higher stream blockage could adversely affect the engine match point operation. A schematic of each of the configurations is shown in Figures 74 and 75. Photographs of the various flameholder configurations are shown in Figures 69 through 73.

The spraying modifications were not made until the results were obtained from the airflow mapping tests. These tests were used to determine the circumferential airflow nonuniformities that existed in the engine. The sprayings were tailored to match the circumferential airflow.



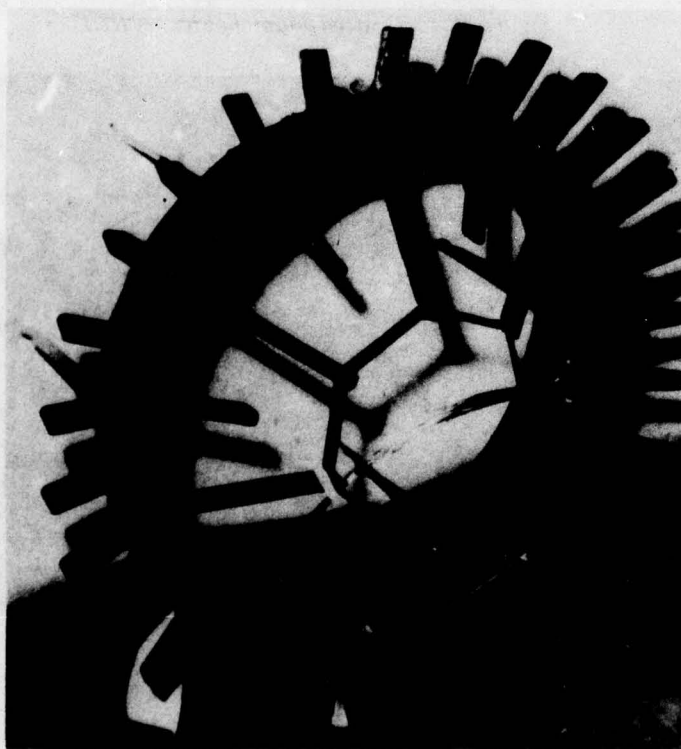
FC 61033

*Figure 69. Core Heat to Fan Stream Flameholder Close-up — HB1*



PC 61029

*Figure 70. B/M Flameholder*



PC 61030

*Figure 71. Extended Mount Flameholder*

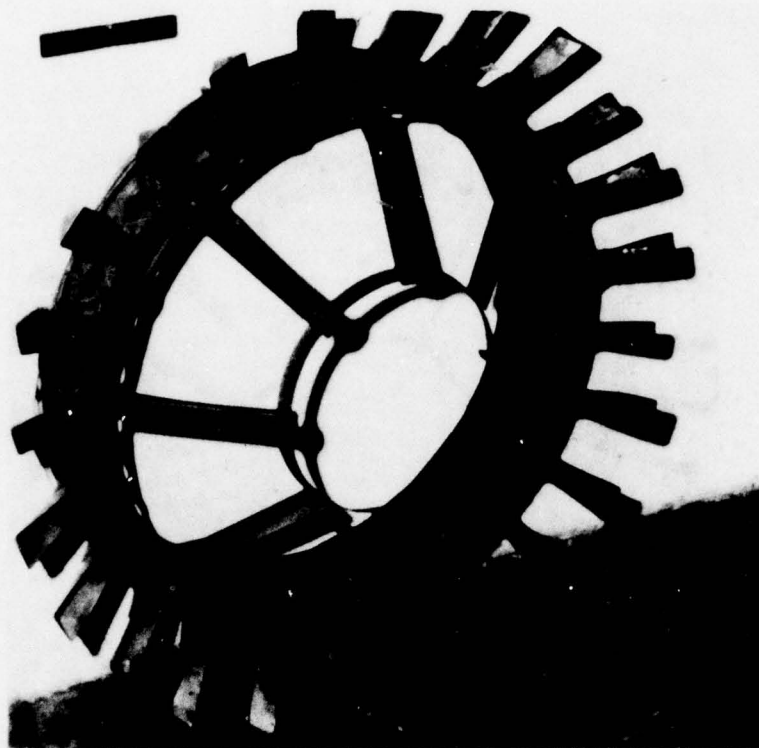


Figure 72. Drafted Flameholder — RE1

FC 61031

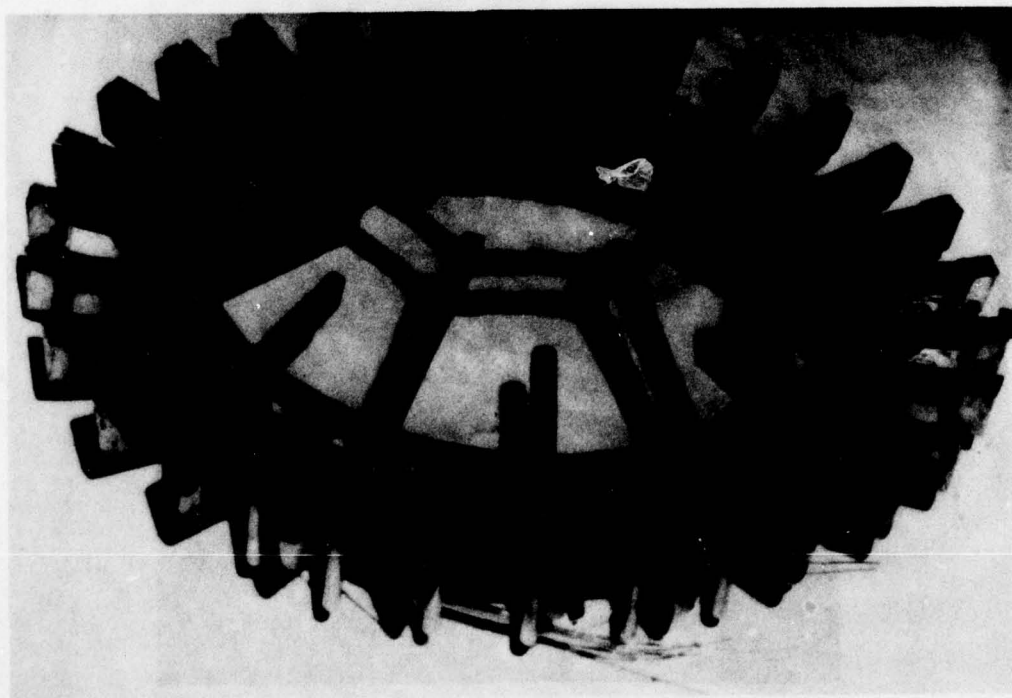
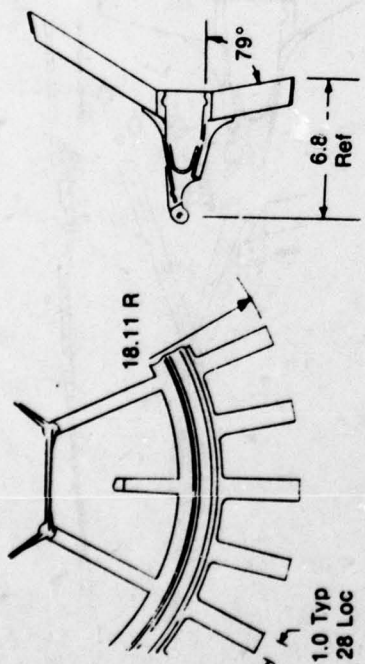
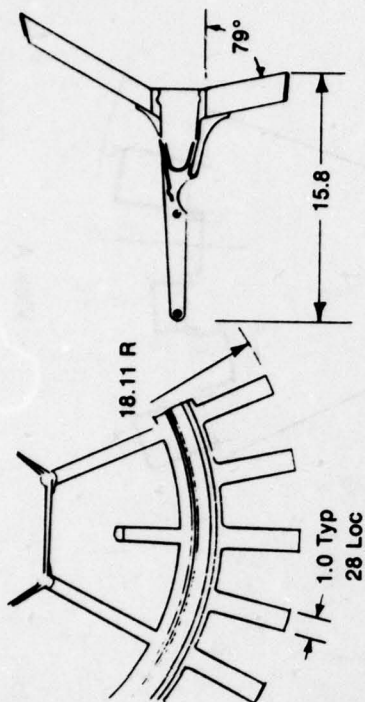


Figure 73. Core Heat to Fan Stream Flameholder — HB1

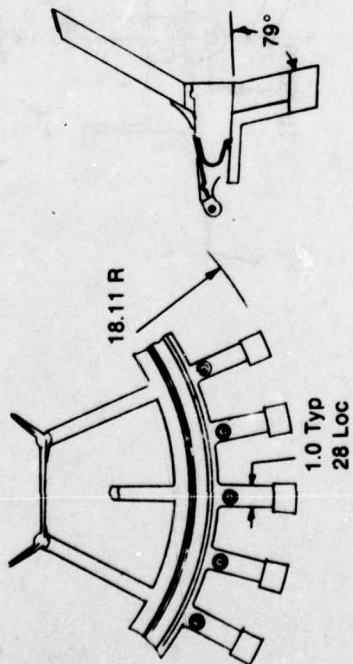
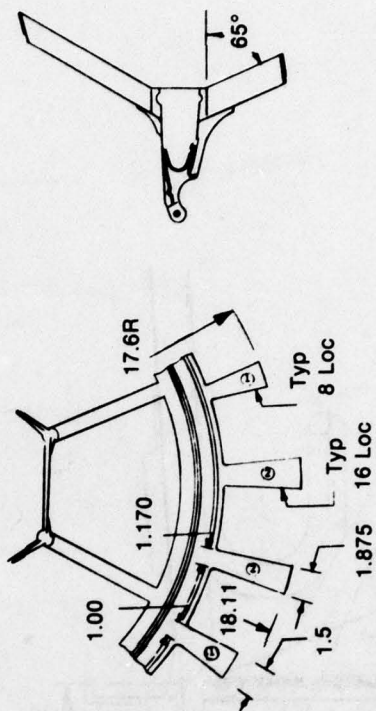
FC 61032





Extended Mount F/H Configuration

B/M F/H Configuration

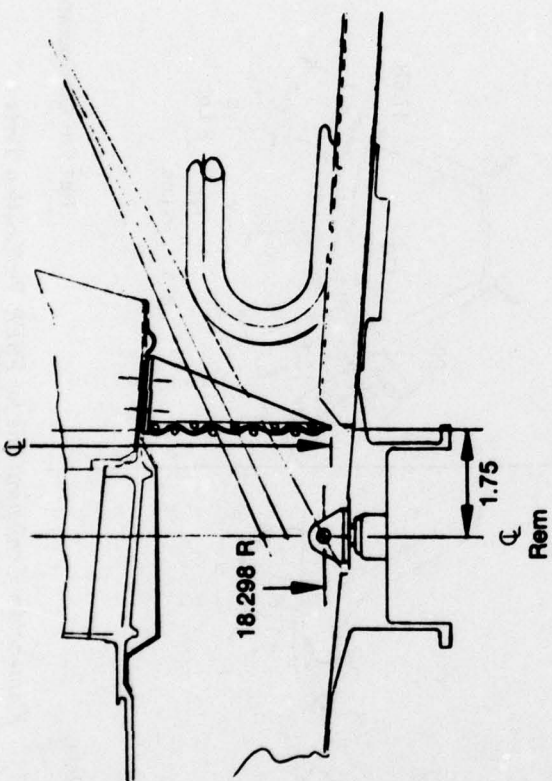


Re1 F/H Configuration

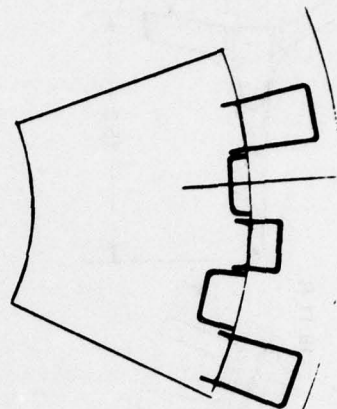
HB1 F/H Configuration

Figure 74 Flameholder Configurations for FSER Verification Tests

18.55 From Eng

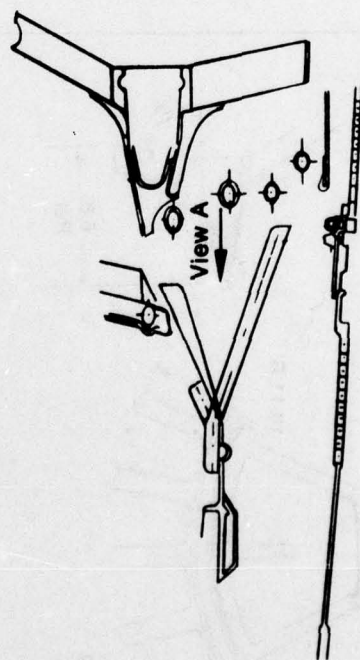


Mixer No. 2 - Screen



View A

FD 146475



Mixer No. 1

Figure 75. Mixer Configurations for FSER Verification Tests

### **3. PHASE III — MODEL DEMONSTRATION**

#### **a. Background**

During Phase III, concurrent experimental and analytical studies were conducted. The Full Scale Engine Research (FSER) experimental test program was conducted at NASA Lewis Research Center to evaluate the engine hardware modifications described in Section II.2.e. The experimental program included tests to (1) map the rumble characteristics of the B/M configuration, (2) map the airflow characteristics of the spraybar planes for each configuration, (3) evaluate the effect of fan duct damping, (4) evaluate the effect of heat addition to the fan stream flameholder wake, (5) evaluate the effect of a finger mixer to raise the temperature of the fan stream, and (6) evaluate the effect of more uniform fuel-air distribution. The test envelope encompassed the upper left hand corner instability region ( $M = 0.6$  to  $1.0$ ,  $Alt = 30$  to  $50K$  ft).

As part of the analytical studies the augmentor rumble model was combined with the flameholder combustion model (Reference 1) and a User's Manual (Reference 7) was published for the combined model. The combined augmentor rumble/flameholder combustion model was then exercised at conditions duplicating selected FSER test points. The results of the FSER test program and combined model predictions were used to establish development and test criteria for determining system low-frequency stability in future engine development programs. Recommendations are made as to how analytical predictions and limited experimental data are to be interpreted in identifying rumble driving mechanisms and how these mechanisms respond to practical design changes.

#### **b. Investigate Design Improvements**

Parametric studies to determine the effect of augmentor design on engine stability were made earlier in the program to provide test configurations for the FSER tests. The results show that to operate stably at high augmentation, which requires high fuel-air ratio, the augmentor design parameters should be chosen to eliminate or minimize the decrease in augmentor combustion rate with increasing fuel-air ratio. This was the primary influence on rumble so far identified by the model. The design parameters include all effects which influence the efficiency curve, i.e., flameholder apex angle flameholder width, drafting, wake temperature, etc. The fan stream efficiency is predicted to be far more sensitive to fuel-air ratio than the core stream, thus particular emphasis should be given to those design parameters which influence fan stream efficiency.

Another important consideration is that the fuel-air ratio in a stream should be as uniformly distributed as possible. Any portion of an augmentor stream which has a fuel-air ratio above average will become sensitive first. If this portion of the stream is sufficiently large, rumble can occur at relatively low average fuel-air ratio. A uniform distribution will allow operation to higher fuel-air ratio and altitude with higher augmentation before rumble is encountered.

A third result of the parameters study shows that additional damping of airflow oscillations is predicted to retard the occurrence of rumble. This can be accomplished by increasing the pressure drop in the fan duct or across the flameholders or by some type of acoustical dampening to change the fan duct impedance.



### **c. Investigate Design Improvements on FSER Engine**

#### **(1) Test Apparatus**

The engine used for the FSER investigation to verify the rumble model at the NASA Lewis Research Center high altitude facility was a two-spool turbofan engine. The compressor system overall pressure ratio was 24 to 1, the fan pressure ratio was 3 to 1, with a fan bypass ratio of 0.7 at sea level static and intermediate throttle position. A splitter ring divides the core and fan airflow at the exit of the fan 3rd-stage rotor. The annular fan duct airflow combines with the turbine core flow in the afterburner diffuser. The combined flow discharges through a variable area exhaust nozzle.

#### **(2) Instrumentation**

The instrumentation as listed in Table 4 was used to monitor the following test parameters:

- Airflow
- Fuel flow
- Inlet total pressure and temperature
- Fan discharge total pressure and temperature
- Fan discharge static pressure and dynamic static pressure
- Compressor exit total pressure and temperature
- Compressor exit dynamic static pressure
- Augmentor liner static pressures and surface temperatures
- Exhaust nozzle convergent seal total and static pressures
- Exhaust nozzle convergent seal temperatures
- Exhaust nozzle convergent flap temperatures
- Exhaust nozzle divergent seal temperatures
- Exhaust nozzle divergent flap static pressures
- Exhaust nozzle external surface static pressures
- Compressor inlet variable vane angle
- Rear compressor variable vane angle
- Combustor static pressure
- Fan turbine inlet total temperature
- Fan duct dynamic static pressure
- Fan duct exit and turbine exit mixed total pressure
- Flameholder temperatures
- Augmentor liner dynamic static pressure
- Engine thrust
- Engine performance parameters.

The engine thrust bed preload forces were measured separately with 10,000 lb strain-gage type load cells. The load cells were independently calibrated. The thrust measuring system error was  $\pm 0.08\%$  full scale.

The engine fuel flow was measured by two turbine type flow meters mounted in series. The engine fuel temperature was measured at the upstream flowmeter inlet. The afterburner zone fuel flows were individually measured with turbine flowmeters. All turbine flowmeters were individually calibrated and accurate to  $\pm 0.6\%$  full scale.

Pressures were recorded on individual transducers and on scanivalves which were operated by the facility computer. The differential type scanivalve transducers were calibrated while in use and had system accuracy of  $\pm 0.26\%$  full scale. The individual differential type transducer accuracy was  $\pm 0.6\%$  full scale.

**TABLE 4. LO-FREQUENCY AUGMENTOR INSTABILITY STUDY FSER  
INSTRUMENTATION DESCRIPTION**

<i>Item</i>	<i>Location</i>	<i>Sensors</i>
1. Inlet Plenum Total Temperature	Test Section Inlet Plenum	17 Total Temperature Probes
2. Inlet Plenum Total Pressure	Test Section Inlet Plenum	4 Total Pressure Probes
3. Inlet Labyrinth Seal Static Pressure	Test Section Inlet Labyrinth Seal	8 Static Pressure Probes
4. Airflow Measuring Station Total and Static Pressure	Inlet Duct Upstream of Engine Inlet	4 Total Pressure Rakes (8 Probes Each) 4 Wall Static Pressure Probes
5. Airflow Measuring Station Total Temperature	Inlet Duct Upstream Engine Inlet	2 Total Temperature Probes
6. Fan Duct Exit Total Pressure and Temperature	Fan Duct Exit (Sta. 2.5)	2 Total Pressure Rakes (5 Probes Each) 2 Total Temperature Rakes (5 Probes Each)
7. Low Compressor Exit Total Pressure and Temperature	Low Compressor Exit (Sta. 2.5)	2 Total Pressure Rakes (5 Probes Each) 2 Total Temperature Rakes (5 Probes Each)
8. Fan Duct Exit Static Pressure and Dynamic Static Pressure	Fan Duct Exit (Sta. 2.5)	2 Static Pressure Probes 2 Dynamic Static Pressure Probes
9. Low Compressor Exit Static Pressure	Low Compressor Exit (Sta. 2.5)	2 Static Pressure Probes
10. High Compressor Exit Total Pressure and Temperature	High Compressor Exit (Sta. 3)	3 Total Pressure Rakes (5 Probes Each) 3 Total Temperature Rakes (5 Probes Each)
11. High Compressor Exit Dynamic Static Pressure	High Compressor Exit (Sta. 3)	2 Dynamic Static Pressure Probes
12. Augmentor Liner Static Pressure	5 Stations Along Augmentor Liner	4 Static Pressure Probes at 5 Augmentor Liner Stations
13. Augmentor Liner Total Temperature	5 Stations Along Augmentor Liner	2 Total Temperature Probes at 5 Augmentor Liner Stations
14. Convergent Seal Total & Static Pressure	Exhaust Nozzle Convergent Seals (F & K)	2 Total Pressure Probes on F & K Seals 1 Static Pressure Probe on F & K Seals
15. Convergent Seal Total Temperature	Exhaust Nozzle Convergent Seals (F & K)	2 Total Temperature Probes on F & K Seals



TABLE 4. LO-FREQUENCY AUGMENTOR INSTABILITY STUDY FSER  
INSTRUMENTATION DESCRIPTION (Continued)

<i>Item</i>	<i>Location</i>	<i>Sensors</i>
16. Convergent Flap Temperature	Exhaust Nozzle Convergent Flaps	15 Thermocouples
17. Convergent Seal Temperature	Exhaust Nozzle Convergent Seals	15 Thermocouples
18. Divergent Seal Temperature	Exhaust Nozzle Divergent Seals	15 Thermocouples
19. Divergent Flap Static Pressure	Exhaust Nozzle Divergent Flaps	5 Static Pressure Probes on Outside 3 Static Pressure Probes on Backside on F & K Flaps
20. Divergent Flap Temperature	Exhaust Nozzle Divergent Flaps (F & K)	3 Surface Temperature Probes on Backside of F & K Flaps
21. Divergent Seal Static Pressure	Exhaust Nozzle Divergent Seals (F & K)	5 Static Pressure Probes on F & K Seals
22. Divergent Seal Temperature	Exhaust Nozzle Divergent Seals (F & K)	2 Surface Temperature Probes on F & K Seals
23. Exhaust Nozzle External Surface Static Pressure	Exhaust Nozzle External Surface	3 Surface Static Pressure Probes at Each of 3 Radial Locations
24. Combustor Static Pressure	Combustor Chamber	1 Static Pressure Probe
25. Fan Turbine Inlet Total Temperature	Fan Turbine Inlet (Sta. 4.5)	7 Thermocouples
26. Fan Duct Dynamic Static Pressure	Fan Duct	1 Dynamic Static Pressure Probe at Each of 2 Axial Fan Duct Locations
27. Mixing Plane Total Pressure	Fan Duct Exit and Turbine Exit Mixing Plane (Sta. 6)	10 Total Pressure Probes (5 Each at Fan Duct Exit and Turbine Exit)
28. Augmentor Liner Dynamic Static	Augmentor Liner (2 Axial Positions)	2 Dynamic Static Pressure Sensors (1 at Each Axial Location)
29. Augmentor Liner Temperature	Augmentor Liner (3 Axial Positions)	2 Thermocouples at Each of 3 Axial Positions
30. Flameholder Surface Temperature	Flameholder	12 Surface Temperature Probes on Each of B/M, RE1 and HB1 Flameholders 8 Surface Temperature Probes on Extended Mount Flameholder



Three ring rakes with total pressure and temperature probes replaced the three outermost fuel spraying locations for several tests to map the airflow characteristics at the spraybar planes for various augmentor configurations.

Dynamic static pressure transducers were used to monitor pressure oscillations in the fan duct and at two locations on the augmentor.

More detailed explanation of sensor locations described in Table 4 is provided in Appendix F.

### **(3) Test Program**

The test program, described in Table 5 was designed to (a) provide stability baseline data, (b) provide an airflow map for fuel flow tailoring and (c) provide stability data for several augmentor configurations at low Mach number (0.6 to 1.0) and high altitude operation (30 to 50K ft). The augmentor configurations tested were:

- B/M flameholder
- B/M flameholder with tailored sprayings
- B/M flameholder with airflow map instrumentation
- Heat addition — HB1 (flameholder with core heat ducted to fan stream)
- Heat addition — HB1 with tailored sprayings
- Heat addition — RE1 (drafted flameholder)
- Heat addition — RE1 with tailored sprayings
- Heat addition — RE1 and finger mixers (to increase fan stream temperature)
- RE1 and finger mixer with airflow map instrumentation
- B/M with 6% pressure drop screen at fan duct exit.

### **(4) Experimental Program Problems**

Several problems were encountered before and during the testing that affected the overall program. The FSER engine was released to our program approximately two months after the intended start date due to delays in previous programs. When delivered the engine required rework. The augmentor duct and several nozzle flaps were damaged during the final swirl augmentor test. A new augmentor duct was available but required rework. Two Kistler dynamic pressure bosses and two instrumentation routing bosses were installed on the duct through the stress skin. A second program was scheduled to be "piggybacked" with model verification testing; it required a strain gage instrumented fan. After replacing the augmentor duct and installing the new fan package the engine shakedown tests were initiated. An oil leak was detected around the sliding seal of the instrumentation lead slip ring. This problem resulted in several days of delay until the proper pressure bleed into the seal was determined. The No.1 bearing was subsequently removed to determine if any damage had resulted from the loss of oil. Problems with an engine control speed sensor further delayed testing. These delays added up to the point where the program had to be compressed in time to test all the configurations of interest.

During the baseline testing it was determined that the augmentor pressure was not constant from day to day. A variation in steady-state operating pressure of up to 1.85 psia was observed for a Mach number = 1.0 and an altitude of 45K ft testing. Similar variations were observed for other operating points tested. After the rumble limits were determined, a desired augmentor static pressure was identified for each operational point, for example the 1/45K point pressure was 9.5 psia. All of the configuration tests were then attempted at the identified pressure by varying the simulated altitude from the nominal value.

TABLE 5. FSER TEST PROGRAM RUN LOG

Data Point	Configuration	M	PS6	FAAB	FAH	FAC	Comments
124	B/M	1.0	10.6	.0361	—	—	
143	B/M	.8	13.08	.037	.0315	.0465	
149	B/M	.6	9.5	.039	.0379	.0396	
150	B/M	.6	9.45	.044	.0413	.0463	
158	B/M	1.0	10.9	—	—	—	
159	B/M	1.0	11.05	.042	.0376	.0472	
160	B/M	1.0	11.28	.046	.0406	.0537	
161	B/M	1.0	11.76	.049	.0422	.0599	
162	B/M	.80	12.57	—	—	—	
163	B/M	.81	13.13	.042	.0352	.0535	
164	B/M	.80	13.29	.047	.0389	.0612	
165	B/M	.80	13.16	.049	.0409	.064	
166	B/M	.82	10.75	.039	.0316	.0502	
167	B/M	.82	10.66	.040	.0331	.0535	
168	B/M	.80	10.62	.043	.0352	.0551	
169	B/M	.81	10.53	.045	.0376	.0583	
170	B/M	.81	10.62	.048	.0404	.0621	
171	B/M	.8	10.62	.0495	.0411	.0645	
172	B/M	.6	13.2	—	—	—	
173	B/M	.62	13.76	.044	.0383	.0503	
174	B/M	.61	13.52	.048	.0417	.0547	
175	B/M	.6	13.57	.050	.0436	.0592	
176	B/M	.63	10.92	.041	.0346	.0496	
177	B/M	.63	10.85	.046	.0398	.0563	
178	B/M	.63	10.85	.049	.042	.058	
179	B/M	.57	8.52	.046	.0387	.0573	
180	B/M	.57	8.52	.048	.0412	.0598	
181	B/M	.62	7.8	.040	.0359	.0486	
192	B/M	1.0	9.11	.0106	.0176	—	
193	B/M	1.0	9.42	.0214	.0183	.0242	
194	B/M	1.0	9.66	.036	.0443	.0253	
195	B/M	1.0	9.78	.046	.045	.0464	Rumble
196	B/M	1.0	10.37	.046	.0446	.0467	
197	B/M	1.0	10.23	.044	.0448	.0427	
198	B/M	1.0	10.64	.046	.0495	.0411	Rumble
199	B/M	1.0	10.58	.044	.0476	.0398	
200	B/M	1.0	10.58	.041	.0424	.0391	
201	B/M	.82	12.3	.003	—	—	
202	B/M	.82	12.1	.041	.0425	.0392	
203	B/M	.80	12.2	.044	.0424	.0445	
204	B/M	.81	12.34	.046	.0424	.0502	
205	B/M	.81	12.56	.048	.0428	.0557	
206	B/M	.80	12.77	.053	.0428	.0678	
207	B/M	.81	13.13	.053	.0422	.0709	
208	B/M	.81	13.00	.0485	.0506	.0433	
209	B/M	.81	12.91	.055	.0618	.0423	
210	B/M	.81	12.86	.057	.0634	.0425	
211	B/M	.85	8.56	.044	.0472	.0376	Rumble
212	B/M	.81	8.69	.042	.0474	.0341	Rumble
213	B/M	.83	8.38	.045	.0532	.0326	Rumble
223	B/M	1.0	9.78	—	—	—	
224	B/M	1.0	10.05	.041	.0375	.0447	
225	B/M	1.0	10.53	.040	.0422	.0343	
226	B/M	1.0	10.76	.045	.0399	.0517	
227	B/M	1.0	10.89	.050	.0438	.0564	
228	B/M	1.0	11.04	.052	.0456	.0588	
229	B/M	.80	12.39	—	—	—	
230	B/M	.80	12.44	.048	.0405	.0573	
231	B/M	.79	12.57	.050	.0418	.0609	
232	B/M	.79	12.79	.053	.0441	.0657	
233	B/M	.82	8.83	.044	.0405	.0471	
234	B/M	.80	8.44	.049	.0465	.0513	
235	B/M	.79	8.63	.052	.0484	.0550	
236	B/M	.80	13.45	—	—	—	
237	B/M	.59	13.46	.043	.0393	.0454	
238	B/M	.59	13.54	.062	.0388	.0544	
239	B/M	.58	13.51	.044	—	—	
240	B/M	.57	13.41	.050	.0396	.0693	
241	B/M	.61	13.89	.048	.0412	.0583	
251	B/M	1.0	9.40	—	—	—	



TABLE 5. FSER TEST PROGRAM RUN LOG (Continued)

Data Point	Configuration	M	PS6	FAAB	FAH	FAC	Comments
252	B/M	1.0	9.42	.0461	.0452	.0449	Rumble
253	B/M	.82	11.53	—	—	—	
254	B/M	.80	11.18	.0422	.0381	.0456	
255	B/M	.80	11.45	.0473	.0416	.0536	
256	B/M	.80	11.31	.0522	.0468	.0679	
257	B/M	.79	11.55	.0439	.0421	.0436	
258	B/M	.80	11.59	.0456	.0427	.0479	
259	B/M	.80	11.63	.0475	.0419	.0533	
260	B/M	.81	11.68	.0484	.0521	.0400	
261	B/M	.80	6.6	—	—	—	
262	B/M	.80	6.6	—	—	—	
268	B/M	.61	8.88	.033	.0397	.0204	
269	B/M	.60	8.89	.043	.0407	.0428	
270	B/M	.61	8.85	.043	.0404	.0429	
271	B/M	.58	8.87	.048	.0444	.0490	
375	RE1 & Mixer	1.0	10.05	.043	.037	.051	
376	RE1 & Mixer	1.0	9.56	.0497	.043	.059	
377	RE1 & Mixer	.99	9.33	.049	.051	.043	
378	RE1 & Mixer	.99	9.47	.053	.052	.052	
379	RE1 & Mixer	.96	9.19	.053	.052	.052	
381	RE1 & Mixer	.97	7.3	.051	.050	.049	
382	RE1 & Mixer	.98	7.0	—	—	—	B/O
383	RE1 & Mixer	.83	9.23	.047	.045	.047	
384	RE1 & Mixer	.80	8.87	.043	.044	.038	
385	RE1 & Mixer	.79	8.84	.050	.057	.036	
386	RE1 & Mixer	.79	9.12	.048	.053	.039	
387	RE1 & Mixer	.79	8.83	.047	.049	.044	
388	RE1 & Mixer	.82	8.20	.050	.050	.048	
389	RE1 & Mixer	.79	7.21	—	—	—	
390	RE1 & Mixer	.59	8.74	.046	.038	.055	B/O
391	RE1 & Mixer	.59	8.8	.048	.038	.063	
392	RE1 & Mixer	.59	8.6	.050	.054	.041	
393	RE1 & Mixer	.60	8.5	.051	.055	.043	
394	RE1 & Mixer	.59	8.6	.046	.043	.044	
395	RE1 & Mixer	.60	6.7	—	—	—	B/O B/O
411	RE1	1.0	9.6	—	—	—	
412	RE1	1.0	9.84	.041	.038	.044	
413	RE1	1.0	10.04	.047	.042	.051	
414	RE1	1.0	9.74	.049	.053	.041	
415	RE1	.98	9.72	.053	.053	.051	
417	RE1	.98	9.05	.055	.056	.052	
418	RE1	1.0	8.2	.051	.052	.048	
419	RE1	1.0	11.56	.033	.045	.014	
420	RE1	.83	8.8	.041	.045	.033	
421	RE1	.82	9.037	.043	.046	.037	
422	RE1	.82	8.95	.051	.047	.053	
423	RE1	.82	8.22	.054	.054	.053	
424	RE1	.63	9.12	.0405	.036	.046	
425	RE1	.63	8.91	.044	.038	.049	
426	RE1	.57	9.02	.0432	.055	.033	
427	RE1	.59	9.175	.0354	.032	.038	
428	RE1	.59	8.95	.042	.042	.039	
429	RE1	.59	8.92	.042	.044	.037	
420	RE1	.04	8.41	—	—	—	
442	B/M with Screen	.99	9.46	.0429	.0389	.0470	
443	B/M with Screen	1.00	9.63	.0478	.0429	.0536	
444	B/M with Screen	.99	9.71	.0531	.047	.059	
445	B/M with Screen	.99	9.65	.0548	.048	.063	
446	B/M with Screen	.99	9.44	.0479	.051	.041	
447	B/M with Screen	1.01	9.58	.0525	.057	.044	
448	B/M with Screen	.98	9.74	.0504	.044	.057	
449	B/M with Screen	1.01	8.61	.055	.050	.061	
450	B/M with Screen	.78	8.32	.045	.043	.046	
451	B/M with Screen	.78	8.65	.048	.046	.048	
452	B/M with Screen	.79	8.46	.050	.048	.051	
453	B/M with Screen	.78	8.53	.053	.049	.057	



TABLE 5. FSER TEST PROGRAM RUN LOG (Continued)

Data Point	Configuration	M	PS6	FAAB	FAH	FAC	Comments
454	B/M with Screen	.79	8.68	.053	.048	.060	
455	B/M with Screen	.80	8.75	.052	.045	.058	
456	B/M with Screen	.78	8.34	.049	.044	.054	
457	B/M with Screen	.80	7.9	.050	.047	.053	
458	B/M with Screen	.60	8.84	.043	.037	.052	
459	B/M with Screen	.58	8.72	.047	.041	.054	
460	B/M with Screen	.58	8.48	.052	.044	.061	
461	B/M with Screen	.59	8.52	.053	.046	.060	
462	B/M with Screen	.61	8.57	.047	.0366	.0508	
463	B/M with Screen	.61	8.46	.049	.054	.0376	
464	B/M with Screen	.61	8.69	.049	.0543	.0372	
465	B/M with Screen	.60	8.61	.050	.0545	.0390	
466	B/M with Screen	.60	8.42	.051	.0419	.0555	
467	B/M with Screen	.60	8.53	.041	.0399	.0410	
468	B/M with Screen	.60	8.66	.046	.0423	.0488	
469	B/M with Screen	.60	8.74	.050	.0458	.0540	
482	HB1	1.03	9.68	.044	.042	.045	
483	HB1	1.04	9.72	.050	.057	.037	Rumble
484	HB1	.99	9.70	.046	.040	.053	Rumble
485	HB1	.78	8.55	.042	.048	.033	
486	HB1	.80	9.10	.047	.043	.050	
487	HB1	.78	8.61	.050	.045	.055	Rumble
488	HB1	.78	8.61	.046	.043	.050	Rumble
489	HB1	.79	8.64	.044	.041	.047	
490	HB1	.80	8.60	.047	.040	.055	Rumble
491	HB1	.83	6.16	—	—	—	
492	HB1	.61	8.71	.048	.044	.052	Rumble
493	HB1	.62	8.76	.044	.038	.051	
494	HB1	.60	8.61	.049	.043	.054	Rumble
495	HB1	.58	8.52	.043	.049	.032	
496	HB1	.58	8.39	—	—	—	
497	HB1	.58	8.54	.046	.044	.046	
498	HB1	.58	8.44	.048	.047	.047	
499	HB1	.57	8.16	—	—	—	
500	HB1	1.04	9.33	.006	.008	—	
501	HB1	1.02	9.40	.011	.017	—	
502	HB1	1.00	9.28	.020	.017	.024	
503	HB1	.99	8.35	.036	.045	.022	
504	HB1	1.02	8.65	.048	.044	.049	Rumble
505	HB1	.98	8.87	.045	.040	.050	Rumble
506	HB1	.99	8.91	.044	.040	.046	Rumble
507	HB1	.99	8.81	—	—	—	
529	B/M with Tailored S/R	.99	9.61	.039	.042	.033	
530	B/M with Tailored S/R	1.01	9.59	.040	.041	.035	
531	B/M with Tailored S/R	1.01	9.49	.040	.042	.036	
532	B/M with Tailored S/R	1.01	9.88	.045	.041	.048	Rumble
533	B/M with Tailored S/R	1.01	9.91	.045	.041	.050	Rumble
534	B/M with Tailored S/R	1.03	9.65	.049	.052	.041	Rumble
535	B/M with Tailored S/R	1.03	9.86	.049	.051	.043	Rumble then B/O
536	B/M with Tailored S/R	1.02	9.79	.044	.036	.053	
537	B/M with Tailored S/R	1.01	9.45	.044	.037	.051	
538	B/M with Tailored S/R	1.01	9.36	.048	.044	.050	Rumble
539	B/M with Tailored S/R	.82	8.39	.042	.044	.036	
540	B/M with Tailored S/R	.79	9.01	.044	.037	.052	
556	HB1 with Tailored S/R	1.03	9.50	—	—	—	
557	HB1 with Tailored S/R	1.00	9.49	.041	.036	.046	
558	HB1 with Tailored S/R	.99	9.47	—	—	—	Rumble then B/O
559	HB1 with Tailored S/R	.98	9.37	.043	.036	.052	Rumble
560	HB1 with Tailored S/R	1.02	9.62	.041	.036	.048	
561	HB1 with Tailored S/R	.99	9.54	.047	.045	.047	
562	HB1 with Tailored S/R	.99	9.24	.046	.040	.053	
563	HB1 with Tailored S/R	1.00	9.17	.046	.041	.053	
564	HB1 with Tailored S/R	1.00	9.28	.043	.041	.047	Rumble
565	HB1 with Tailored S/R	.99	9.12	.046	.040	.054	Rumble
566	HB1 with Tailored S/R	.98	8.95	.047	.042	.053	
567	HB1 with Tailored S/R	1.0	8.50	.048	.044	.052	Rumble
568	HB1 with Tailored S/R	.98	8.09	—	—	—	
569	HB1 with Tailored S/R	.77	8.67	.041	.042	.036	

TABLE 5. FSER TEST PROGRAM RUN LOG (Continued)

Data Point	Configuration	M	PS6	FAAB	FAH	FAC	Comments
570	HB1 with Tailored S/R	.79	8.43	.045	.040	.051	
571	HB1 with Tailored S/R	.78	8.62	.045	.039	.051	Rumble
572	HB1 with Tailored S/R	.79	8.42	.041	.036	.047	
573	HB1 with Tailored S/R	.79	8.49	.043	.036	.053	
574	HB1 with Tailored S/R	.80	8.70	.045	.035	.061	Rumble
575	HB1 with Tailored S/R	.80	8.61	.045	.035	.059	Rumble
576	HB1 with Tailored S/R	.79	8.54	.043	.036	.053	
577	HB1 with Tailored S/R	.77	7.53	.047	.041	.052	B/O After Point Taken
578	HB1 with Tailored S/R	.79	6.70	—	—	—	
579	HB1 with Tailored S/R	.59	8.24	.047	.041	.055	
580	HB1 with Tailored S/R	.60	8.13	—	—	—	
581	HB1 with Tailored S/R	.61	7.95	.047	.048	.043	B/O After Point Taken
582	HB1 with Tailored S/R	.60	7.89	—	—	—	
583	HB1 with Tailored S/R	.60	7.97	.048	.045	.049	Rumble
584	HB1 with Tailored S/R	.60	8.50	.040	.040	.036	
585	HB1 with Tailored S/R	.60	8.09	.041	.042	.038	
586	HB1 with Tailored S/R	.61	7.73	—	—	—	
602	RE1 with Tailored S/R	1.10	6.50	—	—	—	
603	RE1 with Tailored S/R	.99	9.46	.043	.036	.052	
604	RE1 with Tailored S/R	1.03	9.39	.042	.036	.052	
605	RE1 with Tailored S/R	1.02	9.39	.044	.036	.055	
606	RE1 with Tailored S/R	1.01	9.36	—	—	—	
607	RE1 with Tailored S/R	1.00	9.38	.048	.041	.057	
608	RE1 with Tailored S/R	.99	9.29	.050	.042	.063	
609	RE1 with Tailored S/R	1.00	9.52	.050	.043	.059	
610	RE1 with Tailored S/R	1.0	9.48	.043	.034	.056	
611	RE1 with Tailored S/R	1.0	9.55	.044	.034	.061	
612	RE1 with Tailored S/R	.99	9.36	.045	.034	.062	
613	RE1 with Tailored S/R	1.0	9.47	.047	.039	.059	
614	RE1 with Tailored S/R	1.01	9.64	.050	.050	.046	
615	RE1 with Tailored S/R	1.0	9.56	.049	.051	.044	
616	RE1 with Tailored S/R	.99	9.42	.048	.040	.057	
617	RE1 with Tailored S/R	.78	9.16	.047	.042	.056	
618	RE1 with Tailored S/R	.76	9.21	.051	.036	.095	
619	RE1 with Tailored S/R	.83	8.85	.041	.034	.052	
620	RE1 with Tailored S/R	.81	8.92	.043	.036	.054	
621	RE1 with Tailored S/R	.80	8.84	.044	.035	.058	
622	RE1 with Tailored S/R	.79	8.86	.045	.035	.060	
623	RE1 with Tailored S/R	.83	6.67	—	—	—	
624	RE1 with Tailored S/R	.61	8.93	.046	.036	.065	
625	RE1 with Tailored S/R	.60	9.26	.046	.034	.072	
626	RE1 with Tailored S/R	.59	9.38	.047	.036	.073	
627	RE1 with Tailored S/R	.60	8.86	.049	.037	.075	
628	RE1 with Tailored S/R	.60	8.19	.042	.044	.036	
629	RE1 with Tailored S/R	.60	8.19	.041	.044	.035	
630	RE1 with Tailored S/R	.59	8.07	.042	.036	.050	
631	RE1 with Tailored S/R	.59	7.98	.044	.038	.051	
632	RE1 with Tailored S/R	.58	8.11	.048	.042	.057	
633	RE1 with Tailored S/R	.61	9.43	.037	.030	.047	
634	RE1 with Tailored S/R	.59	9.31	.037	.031	.047	
635	RE1 with Tailored S/R	.60	9.14	—	—	—	
636	RE1 with Tailored S/R	.58	9.40	.044	.039	.054	

During the configuration tests an igniter problem prevented operation with the extended mount flameholder. The special igniter fabricated for this configuration functioned well for several check out augmentor lights but stopped functioning when the test series began. Checks, both visual and electrical, did not detect the source of the problem. Several auto-ignition attempts at augmentor pressures up to 20 psia were unsuccessful. Unfortunately the compressed schedule did not provide time to trouble shoot the ignition system and this configuration was not further tested.



## **(5) Data Analysis**

During rumble, pressure amplitudes were recorded as a function of time. Four dynamic static pressure probes were used, two Kulite probes in the fan duct and two Kistler probes in the augmentor. The Kistler probe (AK1) which was 4.25 in. downstream of the "K" flange (augmentor/turbine case joint) was used to determine rumble during the FSER tests. This Kistler probe was located at the downstream edge of the flameholder behind the augmentor cooling liner. Rumble was determined by peak-to-peak pressure amplitudes greater than 1.5 psi at this probe location. The peak-to-peak pressure amplitudes at the other three dynamic pressure locations were normally less than those encountered at the AK1 position.

## **(6) Experimental Results**

Several airflow map tests were conducted with an instrumented aft fan duct package to determine the local airflow distribution in the augmentor. These tests were made to provide information to tailor the fuel flow to match the airflow, and thus to provide a more uniform fuel-air.

The results of the airflow mapping of the B/M augmentor configuration are shown in Figure 76. The data are presented as local airflow per unit area divided by the average airflow of the measurement ports. The local measurements were made with Keel head total pressure and total temperature cups. There are 60 cup locations on each of the sprayings 2 and 5 and 56 locations on spraying 3.

Static pressures were measured at eight locations on spraying 3. A sketch showing the relative locations of the sprayings is presented in Figure 77. In the calculations for the local airflow per unit area incompressible flow is assumed. Thus the equation is

$$\frac{W}{A} = \frac{\sqrt{2g_c P_s (P_t - P_s)}}{RT_t}$$

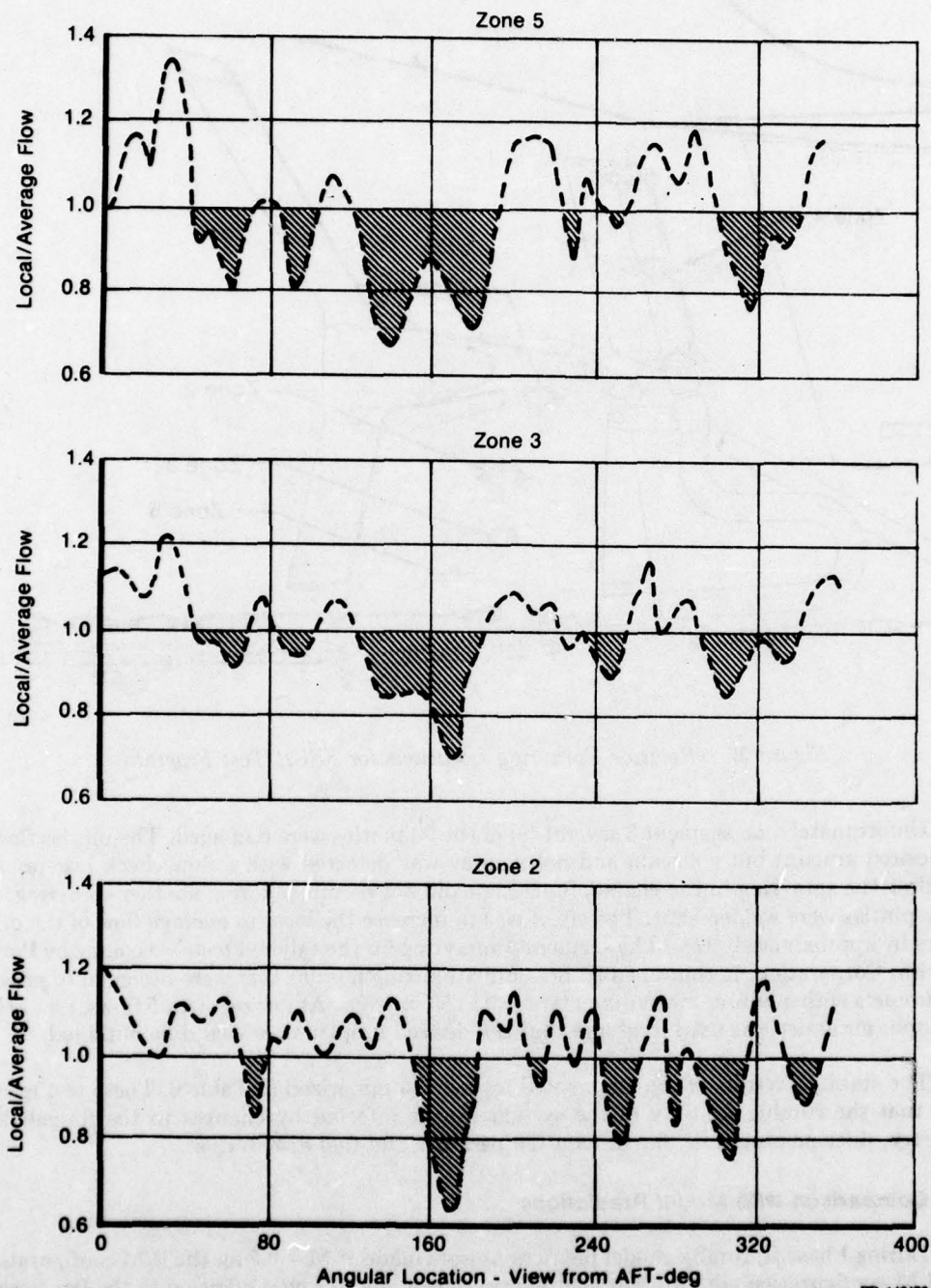
where:

- $\frac{W}{A}$  - local airflow/unit area
- $g_c$  - gravitational constant
- $P_s$  - static pressure
- $P_t$  - total pressure
- $T_t$  - total temperature
- $R$  - gas constant.

The incompressible flow assumption results in less than 0.5% error for the pressure, temperatures and Mach numbers experienced in the augmentor.

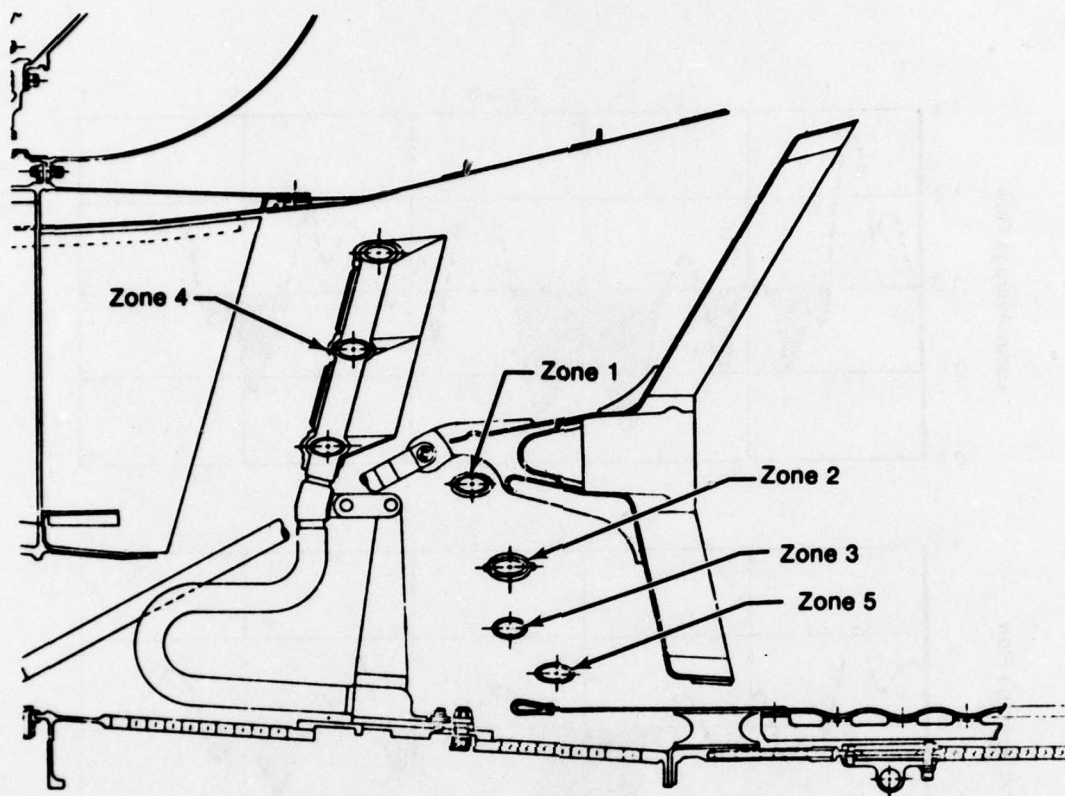
As shown in Figure 76, the B/M configuration exhibits a low airflow region in the fan stream (Zones 3 and 5) from 120 to 190 deg. If uniform fuel flow is assumed, a local rich fuel-air in excess of 1.4 times an intended average fuel-air would exist. For the tailored fuel tests this region of excess fuel was reduced by decreasing the fuel flow of pintles in that area. Other areas of excess fuel-air were also modified to provide a more uniform fuel-air. The sprayings were tailored and the local fuel flow per pindle measured on a flow bench.





PD 146476

**Figure 76. Local to Average Airflow Distribution for Engine P026 With B/M Augmentor**



FD 146477

Figure 77. Relative Spraying Locations for FSER Test Program

Unfortunately, on segment 3 several (9) of the 90 pintles were damaged. The pintles flowed the desired amount but a stream and not a spray was detected with a flow check just prior to installing the spraying in the engine. Since time did not permit tailoring another spraying, the faulty pintles were welded shut. The effect was to increase the local to average flow of the other pintles by approximately 12%. The segment 5 spraying for the tailored tests was made by Parker Hannifin Corporation. It contained 90 pressure atomizing nozzles that were designed to provide fuel droplets with a Sauter mean diameter of 40 to 50 microns. At low segment 5 flows, i.e., below 1500 pph, air assist was used to assure that the desired droplet sizes would be obtained.

The stability results of the augmented tests are summarized in Table 6. These test results show that the rumble stability of the system can be affected by changes in the flameholder geometry, duct pressure loss, fan stream temperature and fuel distribution.

#### (7) Comparison with Model Predictions

During Phase II, rumble model predictions were made at  $M = 0.8$  for the B/M configuration, the B/M configuration with a 6% pressure drop screen, and for heat addition to the fan stream. These predictions and the FSER test results are presented in Table 7. The predictions were based on F100 Design Tables and uniform fuel-air distribution in the augmentor fan or core streams. Due to the engine operational behavior and facility variations at set points, the tests could not be conducted for the exact conditions at which the predictions had been made. In addition, the air distribution discussed earlier (Figure 76) indicates a nonuniform fuel-air distribution existed.

Figures 78 and 79 show the fuel-air distribution for the B/M spraying configuration. Large areas are well above the average fuel-air ratio. For example, 55% of Zone 5 is more than 30% above the average fuel-air ratio. Figures 80 and 81 present the fuel-air distribution for the tailored spraying configuration. Although there is some improvement over the B/M distribution, there are still substantial fuel rich areas. For example, 20% of Zone 5 is still more than 10% above average. The fuel-air distribution results are summarized in Table 8. Thus, consideration should be given to the test trends observed and not to the point-to-point comparison with the predictions.

The trends observed indicate that heat addition to the fan stream results in augmentor operation at higher fuel-air ratios and altitudes. Also, tailored sprayings (i.e., more uniform fuel-air distribution) results in augmentor operation at higher overall fuel-air ratios. From the results, further studies into improved fuel-air management and heat addition to the fan stream are warranted. The 6% pressure drop screen eliminated rumble as predicted, thus substantiating the model. It is, however, not considered a viable solution because of the performance penalty.

For all the FSER test predictions, the combustion input was from early predictions of the flameholder combustion model. The effects of pressure, temperature and velocity on the combustion process were not included at that time. Only the effects of fuel-air ratio variations were considered. Since that time, the effects of pressure, temperature and velocity have been included in the flameholder combustion model and the subsequent slopes of efficiency vs these three parameters are used by the rumble model in addition to the slope of efficiency vs fuel-air ratio.

TABLE 6. SUMMARY OF FSER TEST RESULTS

Configuration	M = 0.6	M = 0.8	M = 1.0
B/M	Rumble at 42K with FAAB = 0.042 B/O at 43K with FAAB = 0.042	Rumble at 45K with FAAB = 0.045 B/O at 46K with FAAB = 0.045	Rumble at 44K with FAAB = 0.046 B/O at 45K with FAAB = 0.046
B/M with Tailored Sprayings	NO DATA	Rumble at 34K with FAAB = 0.046 B/O at 46K with FAAB = 0.046	Rumble at 44K with FAAB = 0.049 B/O at 45K+ with FAAB = 0.049
Heat Addition — HB1 (core heat ducted to fan stream)	Rumble at 42K with FAAB = 0.049 B/O at 42K with FAAB = 0.049	Rumble at 44K with FAAB = 0.06 B/O at 49K with FAAB = 0.065	Rumble at 45K with FAAB = 0.050 B/O at 47K with FAAB = 0.048
Heat Addition — HB1 with Tailored Sprayings	Rumble at 42K with FAAB = 0.048 B/O at 43K with FAAB = 0.047	Rumble at 42K with FAAB = 0.045 B/O at 47K with FAAB = 0.047	Rumble at 45K with FAAB = 0.048 B/O at 46K with FAAB = 0.049
Heat Addition — RE1 (drafted flameholder)	No Rumble to 43K with FAAB = 0.044 B/O at 43K with FAAB = 0.046	No Rumble to 45K with FAAB = 0.064 No B/O encountered at 46K up to FAAB = 0.064 (Aug Eff 25%)	No Rumble to 47K with FAAB = 0.055 Verge of B/O at 48K with FAAB = 0.051
Heat Addition — RE1 with Tailored Sprayings	No Rumble to 42K with FAAB = 0.049 B/O at 43K with FAAB = 0.049	No Rumble to 45K with FAAB = 0.047 B/O at 46K with FAAB = 0.046	No Rumble to 44K with FAAB = 0.050 Verge of B/O at 44K with FAAB = 0.050
Heat Addition — RE1 and Finger Mixers	No Rumble to 44K with FAAB = 0.051 B/O at 46.5K with FAAB = 0.050	No Rumble to 47K with FAAB = 0.060 B/O at 47K with FAAB = 0.062	No Rumble to 45K with FAAB = 0.053 B/O at 49.5K with FAAB = 0.051
B/M with 6% Pressure Drop Screen at Fan Duct Exit	No Rumble to 44K with FAAB = 0.063 B/O at 44.5K with FAAB = 0.060	Stable at 45K with FAAB = 0.063 B/O at 47K with FAAB = 0.062	No Rumble to 47K with FAAB = 0.065 Verge of B/O at 47+K FAAB = 0.065

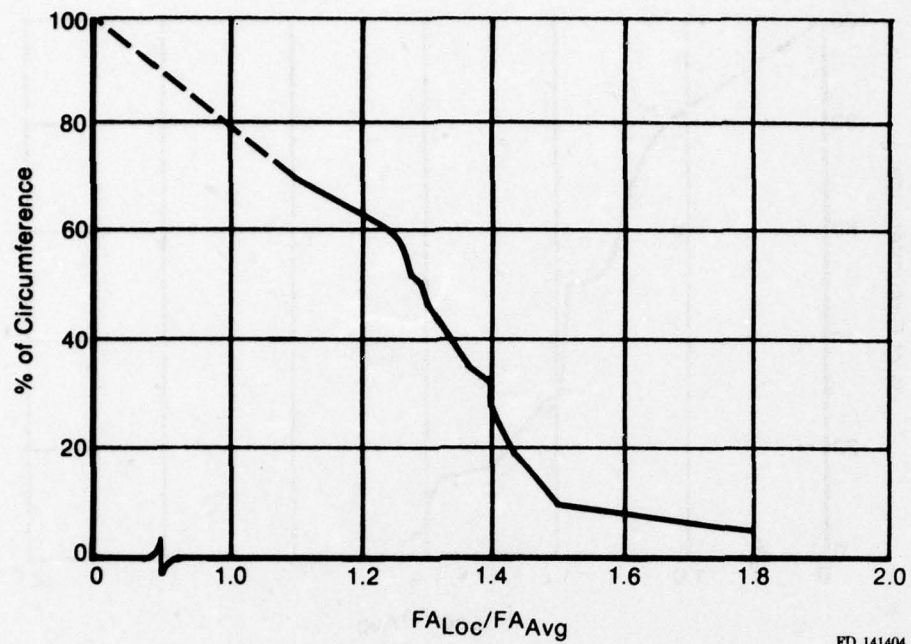


**TABLE 7. SUMMARY OF PHASE II MODEL PREDICTIONS AND FSER TEST RESULTS**

**Mach Number = 0.8**

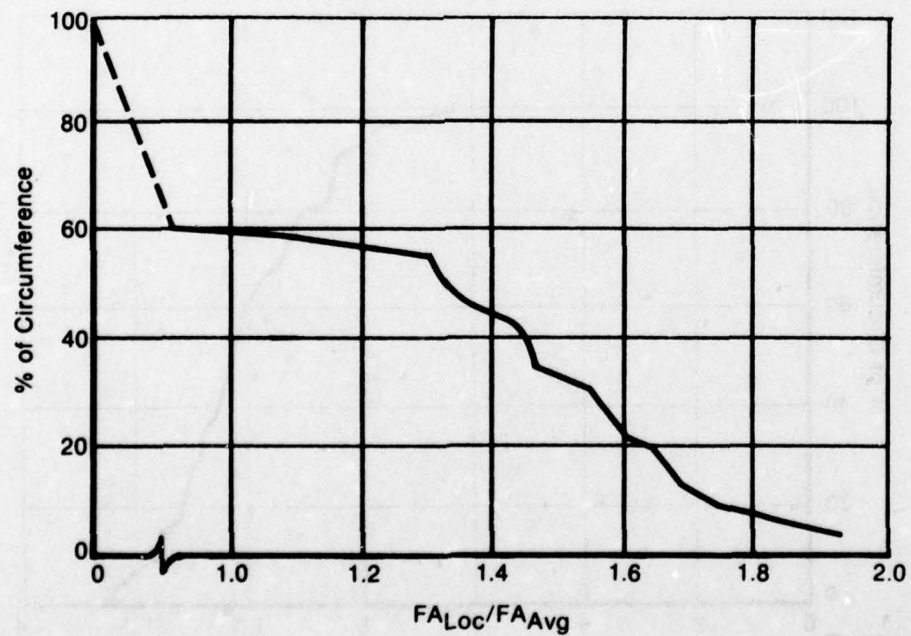
<i>Configuration</i>	<i>Phase II Predictions*</i>	<i>FSER Test Results</i>
B/M	Rumble at 0.8/45K with FAC = 0.064 B/O at 0.8/55K with FAC = 0.037	Rumble at 0.8/45K with FAC = 0.037 B/O at 0.8/46K with FAC = 0.037
B/M with Tailored Sprayrings	Rumble at 0.8/45K with FAC = 0.064 B/O at 0.8/55K with FAC = 0.037	Rumble at 0.8/45K with FAC = 0.040 B/O at 0.8/46K with FAC = 0.040
Heat Addition — HB1 (Core heat ducted to fan stream)	Rumble at 0.8/45K with FAC = 0.064 B/O at 0.8/55K with FAC = 0.055	Rumble at 0.8/45K with FAC = 0.050 B/O at 0.8/49K with FAC = 0.059
Heat Addition — HB1 with Tailored Sprayrings	Rumble at 0.8/45K with FAC = 0.064 B/O at 0.8/55K with FAC = 0.055	Rumble at 0.8/45K with FAC = 0.052 B/O at 0.8/47K with FAC = 0.053
Heat Addition — RE1 (drafted flameholder)	Rumble at 0.8/55K with FAC = 0.064 B/O at 0.8/55K with FAC = 0.055	No Rumble encountered at 0.8/45K up to FAC = 0.054  No B/O encountered at 0.8/46K up to FAC = 0.057 (Aug Eff 25%)
Heat Addition — RE1 with Tailored Sprayrings	Rumble at 0.8/45K with FAC = 0.064 B/O at 0.8/55K with FAC = 0.055	No rumble encountered at 0.8/45K up to FAC = 0.060  B/O at 0.8/46K with FAC = 0.060
Heat Addition — RE1 and Finger Mixers	Rumble at 0.8/45K with FAC = 0.064 B/O at 0.8/55K with FAC = 0.055	No rumble encountered at 0.8/45K up to FAC = 0.048  B/O at 0.8/47K with FAC = 0.048
B/M with 6% Pressure Drop Screen at Fan Duct Exit	Stable at 0.8/40K with FAC = 0.70 B/O at 0.8/55K with FAC = 0.037	Stable at 0.8/45K with FAC = 0.060 B/O at 0.8/47K with FAC = 0.057

\* Phase II predictions were based on F100 Design Tables and assumed uniform fuel-air distribution. In fact, fuel-air distribution varied by as much as 40% (maximum-to-minimum) resulting in rumble at lower overall fuel-air ratios and blowout at lower altitudes.



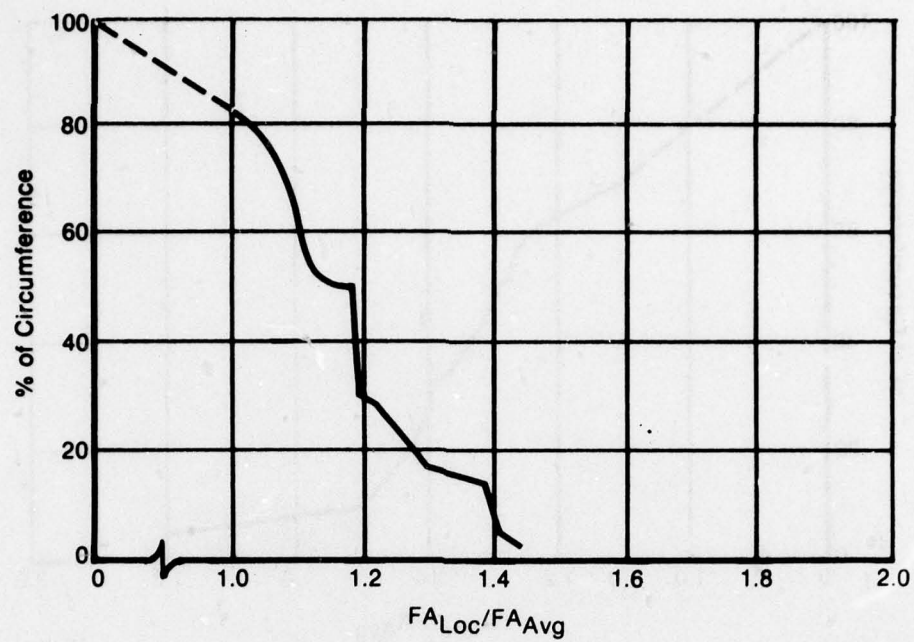
FD 141404

Figure 78. Zone 3 Untailored B/M Fuel-Air Map



FD 141405

Figure 79. Zone 5 Untailored B/M Fuel-Air Map



FD 141406

Figure 80. Zone 3 Tailored B/M Fuel-Air Map



FD 141407

Figure 81. Zone 5 Tailored B/M Fuel-Air Map



TABLE 8. SUMMARY OF FUEL-AIR DISTRIBUTION FOR B/M AND TAILORED SPRAYRINGS

Local FA/Avg FA	Fan Stream			
	Zone V		Zone III	
	B/M	Tailored	B/M	Tailored
	Percent Greater Than Local FA/Avg FA			
1.0	60.0	61.0	83.0	83.0
1.05	60.0	33.0	79.0	79.0
1.10	59.0	20.0	75.0	64.0
1.15	58.0	10.0	74.0	52.0
1.20	57.0	6.0	72.0	32.0
1.25	56.0	3.0	66.0	25.0
1.30	55.0	0.0	50.0	16.0
1.35	47.0		40.0	15.0
1.40	45.0		33.0	8.0
1.45	36.0		19.0	3.0
1.50	33.0		9.0	0
1.55	30.0		7.0	
1.60	22.0		6.0	
1.65	19.0		5.0	
1.70	13.0		4.0	
1.75	11.0		3.0	
1.80	7.0		2.0	
1.85	6.0		0.0	
1.90	4.0			
1.95	0.0			

The combined augmentor rumble/flameholder combustion model was first exercised at six (6) specific operating points for the B/M configuration where the FSER test indicated rumble. The test results and combined model predictions are summarized in Table 9 (row 1 vs row 2). For three of the test points, the combined model predicted rumble at higher frequencies than indicated by test. For the three remaining test points, the combined model predicted stable operation. Review of the combined model predictions indicated an inaccuracy in the flameholder combustion model solution technique resulting in incorrect combustion parameters (slopes of efficiency vs fuel-air ratio, pressure, velocity and temperature) being used by the rumble model.

As a further check, the flameholder combustion model was exercised over a range in fuel-air ratio, pressure, velocity and temperature. The results are presented in Figures 82 and 83. Fan stream efficiency predictions (ETAC) vary by as much as 7% with only slight variations in pressure, velocity, temperature and fuel-air ratio. These variations are not observed in the core stream efficiency predictions (ETAH). Preliminary analysis indicates that the numeric accuracy of the fan stream calculations in the flameholder combustion model is insufficient, resulting in large errors in the slopes of efficiency vs fuel-air ratio, pressure, velocity and temperature. The core calculations, which are much simpler, do not suffer from this numeric accuracy problem. A means of resolving this deficiency of the fan stream calculations in the flameholder combustion model is required, but was beyond the scope of this program.

In order to use the flameholder combustion model predictions but alleviate the numeric accuracy problems, the flameholder combustion model was exercised over a range in fuel-air ratio, pressure, velocity and temperature for each of the six FSER test cases. The results were plotted, and hand-calculated slopes were generated from lines faired through the output. These hand-calculated slopes were then input to the rumble model. In all cases, the rumble model predicted stable operation (Table 9, row 1 vs row 3) at the specific data fuel-air ratio in the fan. The falloff in fan stream efficiency with increasing fan stream fuel-air ratio is the prime driver identified for rumble; the flameholder combustion model predicts this trend. However, it predicts the falloff in efficiency at a higher fuel-air ratio than observed in the tests. Since the fuel-air

distribution is very nonuniform, the fuel rich areas can lead to rumble at lower overall fuel-air ratio than if the fuel distribution were uniform. The rumble model uses only one slope of efficiency vs fuel-air ratio; therefore, it treats the fuel-air distribution as if it were uniform. The normalized slope of fan stream efficiency with fuel-air ratio (ZEFC) was increased in the rumble model input until rumble was predicted. These results are summarized in Table 9 (row 1 vs row 4). The rumble predictions with the hand-calculated slopes and increased ZEFC (row 4) are in good agreement with the test results for the 1st mode (57- to 60-Hz rumble); however, the rumble model still predicts a second mode around 130 Hz which was not observed during the tests.

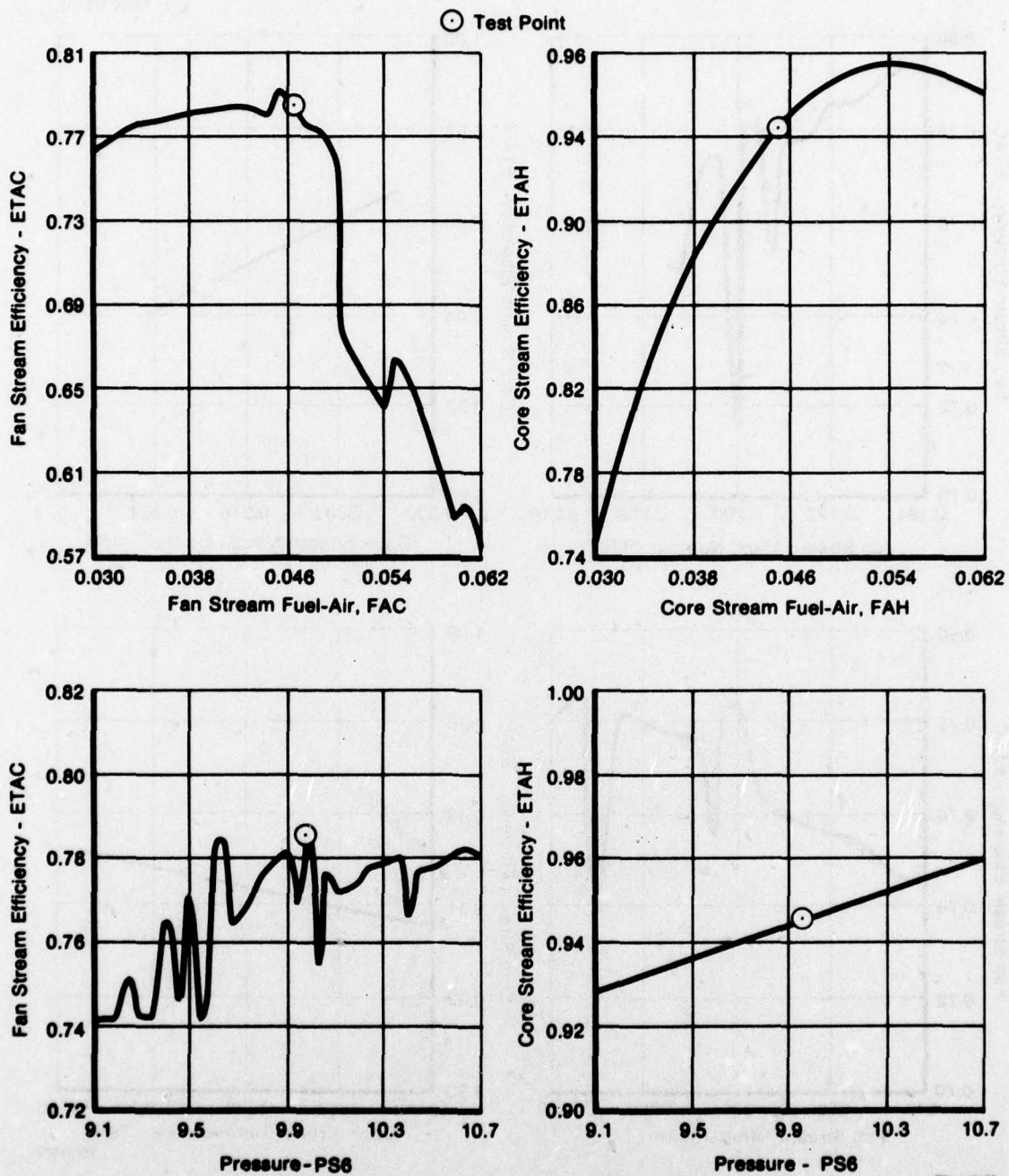
One possible explanation for the rumble model predicting the second rumble mode and the slightly higher than observed first mode is there is a lag in the heat release rate ( $q'_{out}$ ) that is not accounted for in the rumble model. This is not an unreasonable concept, but further investigation into the physics of the process (liquid fuel particle dynamics in the spraybar/flameholder area) will be required. The rumble model was modified to incorporate a lag on the  $q'_{out}$  term and run with several sample values ranging from 0.001 to 0.008 sec. A lag of 0.003 sec input to the  $q'_{out}$  term in the rumble model caused the predictions to agree very well with test results (Table 9, row 1 vs row 5). The predicted first mode frequency was reduced to the frequency observed during the FSER tests, and the second mode was eliminated.

A sample of the rumble model output is presented in Figures 84 and 86. Figure 84 presents the combined augmentor rumble/flameholder combustion model output for FSER data point 195. The model predicts rumble at 68 Hz, 143 Hz and 225 Hz (Table 9, row 2). Figure 85 presents the rumble model output for the same test point using hand-calculated Z's and predicts rumble at 60 Hz and 132 Hz (Table 9, row 4). Finally, Figure 86 presents the rumble model output with a 0.003 sec lag on the  $q'_{out}$  term. The predicted 52-Hz rumble and no second mode rumble are in agreement with the test results (Table 9, row 5).

TABLE 9. MODEL PREDICTIONS VS FSER TEST RESULTS

Data Point	B/M Configuration					
	195	198	211	212	213	252
M/Alt	1.0/44.2K	1.0/45.4K	0.85/45.0K	0.81/44.5K	0.83/45.0K	1.0/44.9K
(1) Rumble Frequency Indicated by FSER Test	52 Hz	55 Hz	45 Hz	47 Hz	45 Hz	52 Hz
(2) Rumble Frequency Indicated by Combined Model	68 Hz 143 Hz 225 Hz	100 Hz 170 Hz	Stable	Stable	100 Hz 165 Hz 242 Hz	Stable
(3) Rumble Frequency Indicated by Rumble Model with Hand-Calculated Combustion Parameters	Stable	Stable	Stable	Stable	Stable	Stable
(4) Rumble Frequency Indicated by Rumble Model with Hand-Calculated Combustion Parameters and ZEFC Increased	60 Hz 132 Hz Actual FAC=0.046 Reqd FAC=0.050	60 Hz 132 Hz	57 Hz 127 Hz Actual FAC=0.038 Reqd FAC=0.047	57 Hz 127 Hz	57 Hz 126 Hz	58 Hz 128 Hz
(5) Rumble Frequency Indicated by Rumble Model with 0.003 Lag on $q'_{out}$ Term	52 Hz	51 Hz	48 Hz	48 Hz	48 Hz	50 Hz





FD 146478

Figure 82. Flameholder Combustion Model Predictions Data Point 195



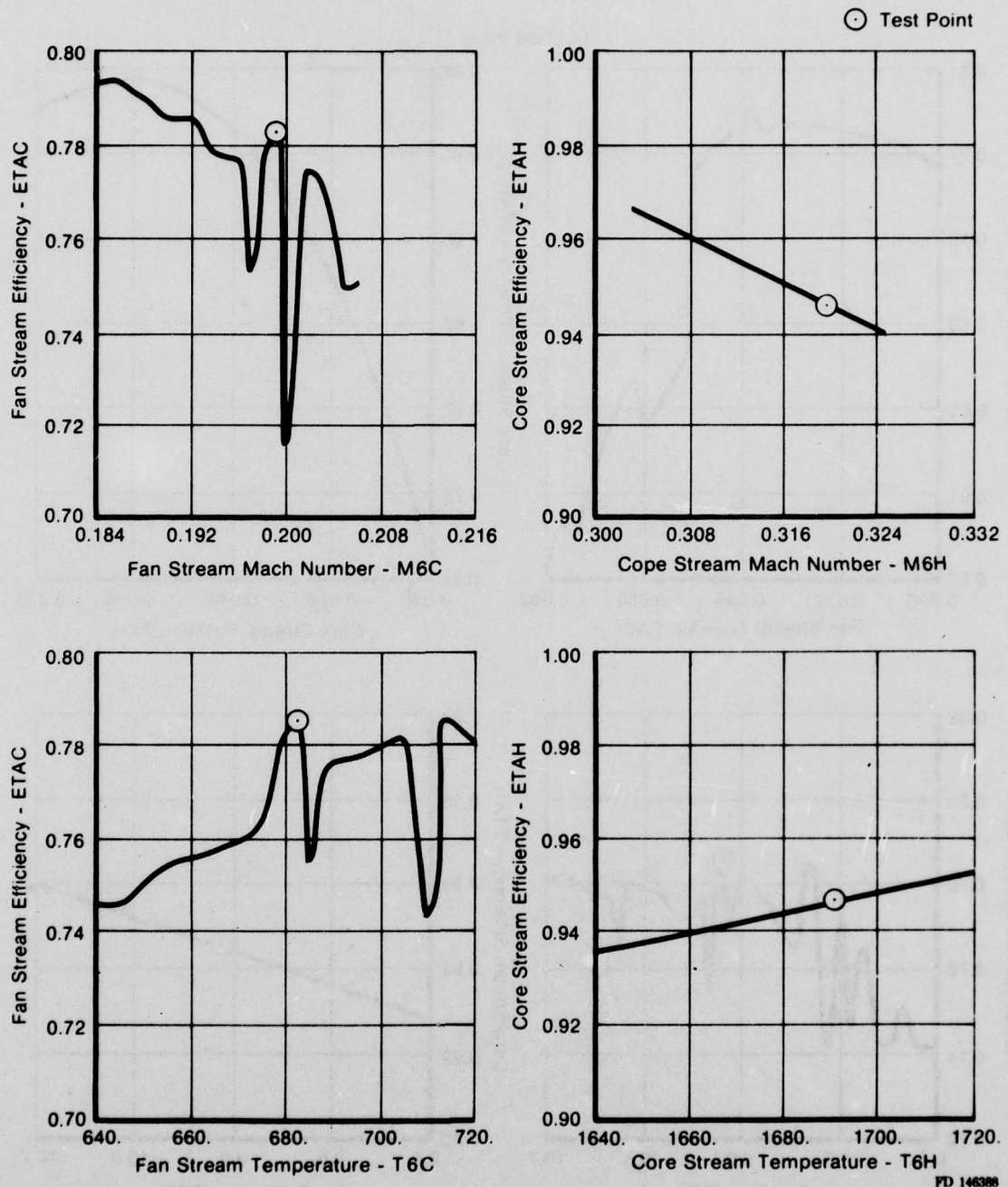
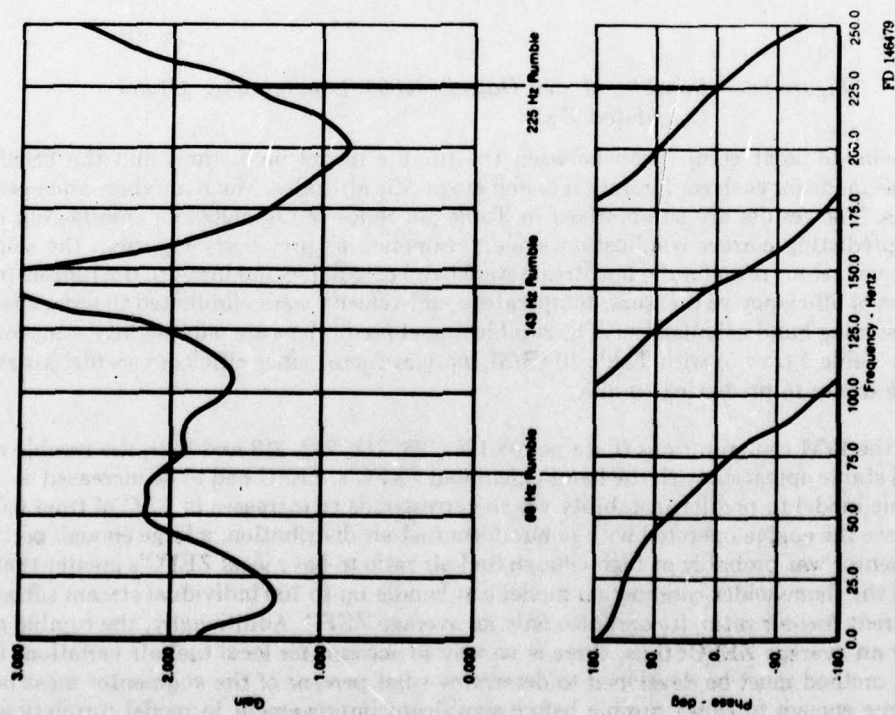
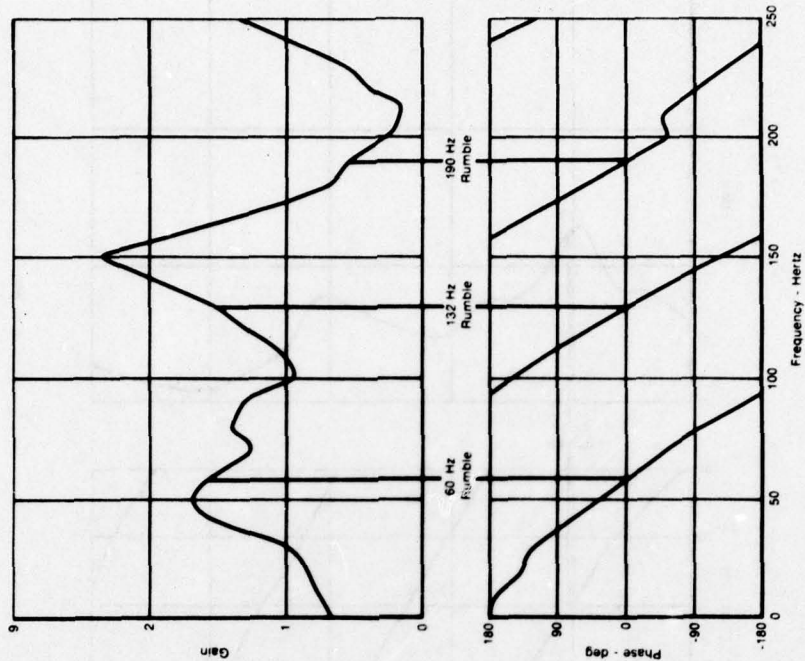


Figure 83. Flameholder Combustion Model Predictions Data Point 195



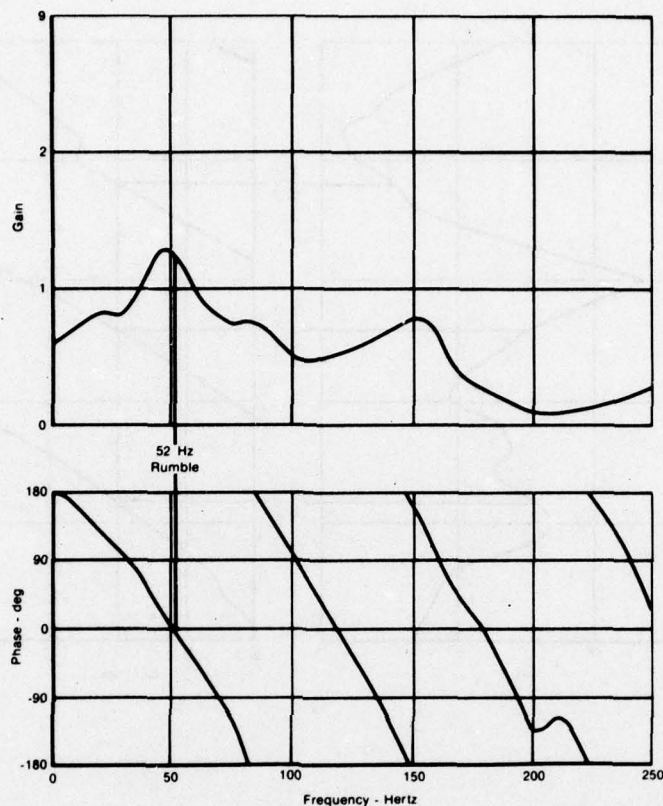
FD 146479

Figure 84. Combined Augmentor Rumble/Flam:holder Combustion Model Output



FD 141409

Figure 85. Rumble Model Output (Hand Calculated Z's)



FD 141410

Figure 86. Rumble Model Output 0.003 Lag on  $q'_{out}$  (Hand Calculated Z's)

A point-to-point comparison between the rumble model predictions and the FSER test results was made for each configuration tested at specific altitudes, Mach numbers and operating conditions. The results are summarized in Table 10. Since the flameholder combustion model was not predicting correct combustion slope parameters as previously reported, the slopes of efficiency vs fuel-air ratio for the fan stream were hand calculated and input to the rumble model. The slopes of efficiency vs pressure, temperature and velocity were eliminated to reduce tedious time-consuming hand calculations. The rumble model predictions are only slightly compromised (compare Table 9 (row 5) with Table 10 (B/M configuration)) since efficiency vs fuel-air ratio is the prime driver in predicting rumble.

For the B/M configurations (data points 195, 198, 211, 212, 213 and 252), the rumble model predicted stable operation with the hand-calculated ZEFC's. ZEFC had to be increased to  $-4$  for the rumble model to predict instability which corresponds to increases in FAC of from 0.004 to 0.015. Since the engine operated with nonuniform fuel-air distribution, a large enough portion of the augmentor was probably at high enough fuel-air ratio to have local ZEFC's greater than  $-4$ . Although the flameholder combustion model can handle up to 100 individual stream tubes each at a different fuel-air ratio, it computes only an average ZEFC. Additionally, the rumble model uses only an average ZEFC; thus, there is no way to account for local fuel-air variations in the model. A method must be developed to determine what percent of the augmentor must be at a ZEFC large enough to cause rumble before significant improvement in model correlation with test results will occur.



TABLE 10

<sup>a</sup>Using ZEFEC and ZEPH only. 0.003 lag on  $q'_{out}$  assumed uniform fuel-air distribution

<sup>a</sup>Using ZEFEC and ZEPH only. 0.003 lag on  $q'_{out}$  assumed uniform fuel-air distribution

109

For the B/M configuration with a 6% pressure drop screen at the fan duct exit (data points 458, 457, 449), the rumble model predicted stable operation for ZEFC's greater than -4. Since the flameholder combustion model failed for all fan stream fuel-air ratios (FAC) greater than 0.048, it was impossible to determine what FAC this corresponded to for ZEFC's greater than -4. The FSER engine with this configuration did not rumble at any of the points tested. This included tests with FAC up to 0.061 and augmentor fuel-air ratio up to 0.055.

For the HB1 configuration, the rumble model (using hand-calculated ZEFC's) predicted rumble for two data points (494 and 567). For the remaining points (487, 484, 504, 583, and 571) FAC had to be increased by 0.0001 to 0.005 in order to calculate ZEFC's = -4, which resulted in the rumble model predicting rumble. Thus, for the HB1 configuration, the flameholder combustion model predictions and rumble model predictions were in good agreement with the FSER test results.

The FSER engine with the RE1 flameholder did not rumble at any point tested with either the B/M sprayings, B/M sprayings and finger mixers, or tailored sprayings. The rumble model (using hand-calculated ZEFC's) predicted stable operation for all the data points checked. The model indicates that in order to get ZEFC's large enough to predict rumble (ZEFC = -5) the fan stream fuel-air ratio (FAC) would have to be increased well beyond 0.063, which is from 0.004 to 0.026 greater than the test points checked. Again, the model predictions are in good agreement with FSER test results.

The flameholder model could not be used to predict the high fuel air combustion characteristics for the B/M and screen configuration. Thus to verify the rumble model it was necessary to obtain these characteristics from the test data. The overall augmentor efficiency vs the overall augmentor fuel-air ratio were plotted for the M = 1.0 and 45K ft altitude points. A curve fit was used to determine the shape of the line through the data. The normalized efficiency slopes were calculated at each point of interest by using:

$$ZEF = \frac{\Delta\eta}{\Delta FA} \times \frac{FA}{\eta}$$

where:

$$\frac{\Delta\eta}{\Delta FA} = \text{slope of the efficiency vs overall fuel-air ratio at point of interest}$$

$$FA = \text{overall fuel-air ratio at points of interest}$$

$$\eta = \text{overall efficiency at point of interest.}$$

The normalized augmentor efficiency slope (ZEF) was -3.3 for an overall fuel-air ratio of 0.055. The model was exercised at this point and for several other fuel-air ratio points. For this analysis, the calculated values of ZEF were assumed to be the same for both core and fan streams. The results indicate stable operation would be expected up to air FAAB of 0.060 for a ZEF of -5.14.

As a further check of the system model the combustion characteristics of the B/M, HB1, and RE1 were obtained from the test data for several operating points. The rumble model was exercised at several test points for each configuration and for higher fuel-air ratios assuming other augmentor parameters constant.

The results are summarized in Table 11. These results verify that the system model can be used to predict augmentor stability if the combustion characteristics are known.



TABLE 11. STABILITY SUMMARY AT 1/45K FSER TEST TO MODEL PREDICTION\*

Configuration	/	Data Point	Test Results		Model Results		$\Delta$
			Stability	FA	Stability	FA	
B/M	/	198	R	0.046	R	0.042	0.003
B/M-Screen	/	449	S	0.055	S	0.055	0.005
					R	0.060	
Ducted	/	504	R	0.048	R	0.045	0.003
Drafted	/	417	S	0.055	R	0.051	0.004

\* Model input ( $Z$ 's,  $\eta$ , FA) was determined from FSER overall efficiency vs overall fuel-air ratio test data.

#### e. Establish Development and Test Criteria

##### (1) Combined Augmentor Rumble/Flameholder Combustion Model

During Phase III the augmentor rumble model was combined with the flameholder combustion model. The combined model can be operated in any one of 5 combinations; (1) rumble model operating with a V-gutter flameholder augmentor simulation and combustion data directly from the flameholder combustion model, (2) rumble model operating with a V-gutter flameholder augmentor simulation and empirical combustion data, (3) rumble model operating with a Vorbix augmentor simulation and empirical combustion data, (4) rumble model operating with a Swirl augmentor simulation and empirical combustion data or (5) flameholder combustion model only. A schematic of the combined model is presented in Figure 87.

##### (a) Combined Model Input

Input to the combined model includes program options, engine and augmentor geometry, pressures, temperatures, Mach numbers and combustion parameters. The input list and the parameters required for each of the five model combinations described above are presented in Figure 88. A description of the input parameters is presented in Table 12.

##### (b) Combined Model Output

The combined model output consists of (a) rumble model output, (b) flameholder combustion model output or (c) both outputs. The rumble model output consists of Open Loop Transfer Function (OLTF) plots and tabular output. The OLTF plots allow quick determination of engine/augmentor operating point stability or instability and at what frequency the instability occurs. The rumble model tabular output is presented in Table 13. The flameholder combustion model output consists of tabular output described in Table 14.

##### (c) Program Description

A detailed description of the rumble model was presented in Section II-2, and development of the rumble model equation is presented in Appendix D. A detailed description of the flameholder combustion model and the flameholder combustion model equations are presented in Appendix E.



## (2) Design Criteria

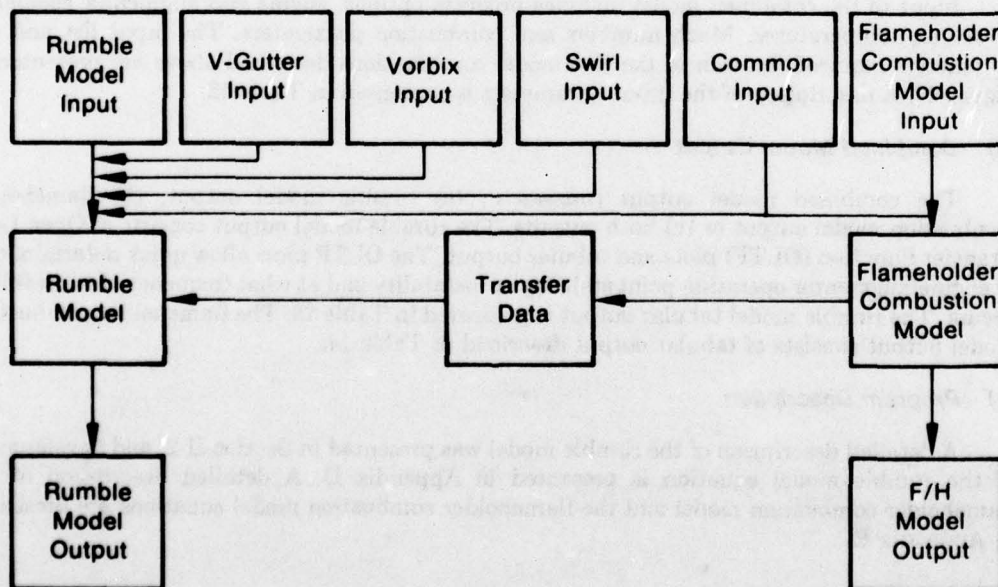
The most important consideration in providing rumble free operation in the upper left hand corner is the slope of the efficiency vs fuel-air ratio curve. The Phase II analytical studies have identified a negative slope to be the driving mechanism for rumble. The Phase III verification FSER program results supported this premise.

The stability criterion for UHLC steady state operation should be chosen such that the system is stable at the lowest augmentor pressure in the flight envelope. Rumble was identified in Phase I as system airflow dynamics coupled with the combustion process. Thus, to provide stable operation, the designer must either eliminate the combustion driving potential or provide sufficient system stiffness to prevent coupling.

The system stiffness, i.e. impedance properly located in the duct, will retard airflow oscillations. This can be accomplished by increasing the pressure drop near the fan duct exit or across the flameholders. The impedance could be mechanical blockage or a reflective acoustic device. The second type of impedance was not evaluated in this program, but basic acoustic principles indicate potential. A second method of decoupling the system from the combustion process would be to change the length of the system, i.e. change the length of the fan duct.

If the system cannot tolerate the lengths or losses required to decouple the process, then the designer must carefully select the flameholder or combustion stabilizing system to reduce the declining efficiency. Results from the combustion model show that the declining efficiency can be reduced by any design action or concept variation which reduces the dependence of flame speed on fuel air ratio, pressure, temperature and velocity. The following will, in general, reduce the tendency to rumble:

- Wake heat addition
- Increased turbulence level
- Uniform fuel air distribution



PD 141408

Figure 87. Combined Model Schematic

Input List	Rumble Model				F/H Comb. Model V-Gutter
	V-Gutter		Vorbix	Swirl	
	F/H Model Combustion Data	Empirical Combustion Data	Empirical Combustion Data	Empirical Combustion Data	
ALPHAC (100)	ALPHAC (100)				ALPHAC (100)
ALPHAH (100)	ALPHAH (100)				ALPHAH (100)
BPR	BPR	BPR	BPR	BPR	BPR
DPCS				DPCS	
DPD	DPD	DPD	DPD	DPD	
DPH	DPH	DPH	DPH		
DPHS				DPHS	
DPS	DPS	DPS	DPS	DPS	
EPSC	EPSC				EPSC
EPSH	EPSH				EPSH
ETA			ETA	ETA	
ETAC		ETAC			
ETAH		ETAH			
FA			FA	FA	
FAC		FAC			
FAC (100)	FAC (100)				FAC (100)
FAH		FAH			
FAH (100)	FAH (100)				FAH (100)
FAV	FAV	FAV	FAV	FAV	FAV
FHWC (100)	FHWC (100)				FHWC (100)
FHWH (100)	FHWH (100)				FHWH (100)
JFUEL	JFUEL	JFUEL	JFUEL	JFUEL	JFUEL
LA	LA	LA	LA	LA	
LB		LB	LB	LB	
LC	LC	LC	LC	LC	
LH	LH	LH	LH	LH	
LI		LI	LI	LI	
LK		LK	LK	LK	
LSC		LSC			
LSC (100)	LSC (100)				LSC (100)
LSH		LSH			
LSH (100)	LSH (100)				LSH (100)
L2	L2	L2	L2	L2	
M6C	M6C	M6C	M6C	M6C	M6C
M6H	M6H	M6H	M6H	M6H	M6H
M6R	M6R	M6R	M6R	M6R	
NAUGOP	NAUGOP	NAUGOP	NAUGOP	NAUGOP	
NCOMOP	NCOMOP	NCOMOP	NCOMOP	NCOMOP	
NFSOP	NFSOP	NFSOP	NFSOP	NFSOP	
NPRNTF	NPRNTF				NPRNTF
NPRNTR	NPRNTR	NPRNTR	NPRNTR	NPRNTR	
NSC (100)	NSC (100)				NSC (100)
NSH (100)	NSH (100)				NSH (100)
NTC	NTC				NTC
NTH	NTH				NTH
PFSR (100)	PFSR (100)				PFSR (100)
PRNOZ	PRNOZ	PRNOZ	PRNOZ	PRNOZ	
PS6	PS6	PS6	PS6	PS6	PS6
TAUC (100)	TAUC (100)				TAUC (100)
TAUH (100)	TAUH (100)				TAUH (100)
TCORE	TCORE	TCORE	TCORE	TCORE	
TEXT (100)	TEXT (100)				TEXT (100)
TFSR (100)	TFSR (100)				TFSR (100)
T3H	T3H				T3H
T6C		T6C	T6C	T6C	
T6C (100)	T6C (100)				T6C (100)
T6H		T6H	T6H	T6H	
T6H (100)	T6H (100)				T6H (100)
WCOOL	WCOOL				WCOOL
WEST (100)	WEST (100)				WEST (100)
ZEF			ZEF	ZEF	
ZEFC		ZEFC			
ZEFC		ZEFC			
ZEFP			ZEFP	ZEFP	
ZEP			ZEP	ZEP	
ZEPC		ZEPC			
ZEPH		ZEPH			
ZETC		ZETC			
ZETH		ZETH			
ZEVC		Z3VC			
ZEVH		ZEVH			
XLC (100)	XLC (100)				XLC (100)
XLH (100)	XLH (100)				XLH (100)

FD 151083

Figure 88. Input List for Five Model Combinations

TABLE 12. COMBINED MODEL INPUT PARAMETER DESCRIPTION

<i>Parameter Name</i>	<i>Description</i>
ALPHAC (100)	Fan Stream Flameholder Apex Angle, Deg.
ALPHAH (100)	Core Stream Flameholder Apex Angle, Deg.
BPR	Bypass ratio, fan duct airflow/core airflow, dimensionless.
DPCS	Fan side vane pressure loss ( $\Delta P/P$ ) from mixing plane to ignition plane (STA 3 to STA 4), dimensionless (Swirl augmentor only).
DPD	Fan duct pressure loss ( $\Delta P/P$ ) allocated to STA 2, dimensionless. Allocate remainder to STA 3; see DPS.
DPH	Pressure loss ( $\Delta P/P$ ) from mixing plane to ignition plane (STA 3 to STA 4), dimensionless. For V-gutter augmentor this accounts for spraybar and flameholder pressure loss. For Vorbix augmentor this accounts for Vortex generator and pilot pressure loss (core and fan combined).
DPHS	Core side vane pressure loss ( $\Delta P/P$ ) from mixing plane to ignition plane (STA 3H to STA 4), dimensionless (Swirl augmentor only).
DPS	Fan duct pressure loss ( $\Delta P/P$ ) allocated to STA 3, dimensionless. Allocate remainder to STA 2; see DPD.
EPSC	Fan stream turbulence factor, dimensionless.
EPSH	Core stream turbulence factor, dimensionless.
ETA	Augmentor overall combustion efficiency, actual temperature rise/ideal temperature rise, dimensionless.
ETAC	Augmentor fan stream combustion efficiency, actual temperature rise/ideal temperature rise, dimensionless.
ETAH	Augmentor core stream combustion efficiency, actual temperature rise/ideal temperature rise, dimensionless.
FA	Augmentor overall fuel-air ratio, dimensionless. Defined as augmentor total fuel flow/fan stream airflow (STA 3) plus core stream airflow (STA 3H) plus primary engine fuel flow (STA 3H).
FAC	Augmentor fan stream fuel-air ratio, dimensionless. Defined as augmentor fan stream fuel flow/fan stream airflow (STA 3).
FAC (100)	Augmentor/fuel-air ratio for each individual fan stream flow tube, dimensionless.
FAH	Augmentor core stream fuel-air ratio, dimensionless. Defined as augmentor core stream fuel flow/core stream airflow (STA 3H) plus primary engine fuel flow (STA 3H).
FAH (100)	Augmentor fuel-air ratio for each individual core stream flow tube, dimensionless.
FAV	Vitiated fuel-air ratio of core stream at entry to augmentor (STA 3H), dimensionless. Defined as primary engine fuel flow (STA 3H)/core stream airflow (STA 3H).
FHWC (100)	Individual flameholder widths in fan stream, in.
FHWH (100)	Individual flameholder widths in core stream, in.
LA	Length of augmentor, mixing plane to nozzle (STA 3 to STA 11), in.
LB	Distance from ignition plane to nozzle (STA 4 to STA 11), in.
LC	Length of fan duct, fan discharge to mixing plane (STA 1 to STA 3), in.
LH	Distance from turbine discharge to mixing plane (STA 2H to STA 3H), in.
LI	Distance from ignition plane to beginning of combustion zone (STA 4 to STA 5), in.
LK	Distance from ignition plane to end of combustion zone (STA 4 to STA 10), in.



TABLE 12. COMBINED MODEL INPUT PARAMETER DESCRIPTION (Continued)

<i>Parameter Name</i>	<i>Description</i>
LSC	Distance from spraybar to flameholder in fan stream, in.
LSC (100)	Distance from spraybar to flameholder for each individual stream tube in the fan stream, in.
LSH	Distance from spraybar to flameholder in core stream, in.
LSH (100)	Distance from spraybar to flameholder for each individual stream tube in the core stream, in.
L2	Distance from fan duct pressure loss (DPD) to mixing plane (STA 2 to STA 3), in.
M6C	Fan stream Mach number at entry to augmentor (STA 3), dimensionless. (Must be >0.)
M6H	Core stream Mach number at entry to augmentor (STA 3H), dimensionless. (Must be >0.)
M6R	Mach number of mixed augmentor stream flow prior to combustion (STA 4), dimensionless. (Must be 0.)
NSC (100)	Number of fan stream flow tubes of this type, integer.
NSH (100)	Number of core stream flow tubes of this type, integer.
NTC	Number of stream tube types in the fan flow, integer.
NTH	Number of stream tube types in the core flow, integer.
PFSR (100)	Individual spraybar fuel pressure for each fan flow tube, psia.
PRNOZ	Exhaust nozzle pressure ratio (always >1), dimensionless. If nozzle is choked any value greater than critical value required to choke nozzle (approximately 2.0) may be input. Exact value of PRNOZ is required only if nozzle is choked.
PS6	Augmentor static pressure at entry to augmentor (STA 3), psia.
TAUC (100)	Individual stream tube blockage ratio for fan stream, dimensionless.
TAUH (100)	Individual stream tube blockage ratio for core stream, dimensionless.
TCORE	Core engine time constant, mass of air in core engine volume/mass flowrate of air through the core engine, sec.
TEXT (100)	External flow temperature for individual flow tubes in the fan duct, deg R.
TFSR (100)	Spraybar fuel temperature for individual flow tubes in the fan flow, deg R.
T3H	Main burner inlet temperature, deg R.
T6C	Fan stream temperature at entry to augmentor (STA 3), deg R.
T6C (100)	Fan stream temperature at entry to augmentor (STA 3), for individual flow tubes, deg R.
T6H	Core stream temperature at entry to augmentor (STA 3H), deg R.
T6H (100)	Core stream temperature at entry to augmentor (STA 3H), for individual flow tubes, deg R.
WCOOL	Ratio of nozzle cooling air to total engine airflow, dimensionless.
WEXT (100)	External flow ratio for individual flow tubes in the fan stream, dimensionless.
XLC (100)	Distance from flameholder to nozzle for individual fan stream flow tubes, in.
XLH (100)	Distance from flameholder to nozzle for individual core stream flow tubes, in.
ZEF	Normalized slope, augmentor overall combustion efficiency vs overall fuel-air ratio, FA/ETA $\partial$ ETA/ $\partial$ FA, dimensionless.

TABLE 12. COMBINED MODEL INPUT PARAMETER DESCRIPTION (Continued)

<i>Parameter Name</i>	<i>Description</i>
ZEFC	Normalized slope, augmentor fan stream combustion efficiency vs fan stream fuel-air ratio, $FAC/ETAC \partial ETAC / \partial FAC$ , dimensionless.
ZEFH	Normalized slope, augmentor core stream combustion efficiency vs core stream fuel-air ratio, $FAH/ETAH \partial ETAH / \partial FAH$ , dimensionless.
ZEFP	Normalized slope, augmentor overall combustion efficiency vs fuel-air ratio of the pilot burner, $FAP/ETA \partial ETA / \partial FAP$ , dimensionless.
ZEP	Normalized slope, augmentor overall combustion efficiency vs pressure at ignition plane, $P/ETA \partial ETA / \partial P$ , dimensionless.
ZEPC	Normalized slope, augmentor fan stream combustion efficiency vs pressure at ignition plane, $P/ETAC \partial ETAC / \partial P$ , dimensionless.
ZEPH	Normalized slope, augmentor core stream combustion efficiency vs pressure at ignition plane, $P/ETAH \partial ETAH / \partial P$ , dimensionless.
ZETC	Normalized slope, augmentor fan stream combustion efficiency vs fan stream entry temperature $T6C/ETAC \partial ETAC / \partial T6C$ , dimensionless.
ZETH	Normalized slope, augmentor core stream combustion efficiency vs core stream entry temperature $T6H/ETAH \partial ETAH / \partial T6H$ , dimensionless.
ZEVC	Normalized slope, augmentor fan stream combustion efficiency vs fan stream entry velocity $V/ETAC \partial ETAC / \partial V$ , dimensionless.
ZEVH	Normalized slope, augmentor core stream combustion efficiency vs core stream entry velocity $V/ETAH \partial ETAH / \partial V$ , dimensionless.

TABLE 13. RUMBLE MODEL TABULAR OUTPUT

<i>Parameter(s)</i>	<i>Description</i>
NAMLIST INPUT	The "namelist" input parameters and the values input are listed for verification.
KNOZ	A parameter that relates the influence of pressure at Station 11 on velocity at Station 11, dimensionless.
FAAB	Augmentor overall fuel-air ratio, dimensionless.
ETAAB	Augmentor overall efficiency, dimensionless.
DTIAB	Augmentor overall ideal temperature rise, deg R.
DTAB	Augmentor overall actual temperature rise, deg R.
T6M	Augmentor mixed temperature before combustion (Station 3), deg R.
TKC	Augmentor mixed exhaust temperature (Station 10), deg R.
XLHV	Lower heating value for the fuel selected, Btu/lb <sub>m</sub> .

TABLE 13. RUMBLE MODEL TABULAR OUTPUT (Continued)

DTC	Fan stream temperature rise, deg R.
QCQT	Fraction of total heat release contributed to fan stream, dimensionless.
DTIC	Fan stream ideal temperature rise, deg R.
TAUDC	Fan stream drift delay from spraybar to flameholder, sec.
DTH	Core stream temperature rise, deg R.
QHQT	Fraction of total heat release contributed by core stream, dimensionless.
DTIH	Core stream ideal temperature rise, deg R.
TAUDH	Core stream drift delay from spraybar to flameholder, sec.
ZTFC	Normalized slope, augmentor fan stream ideal temperature rise vs fan stream fuel-air ratio, $FAC/DTIC \approx DTIC/\Delta FAC$ , dimensionless.
ZTFH	Normalized slope, augmentor core stream ideal temperature rise vs core stream fuel-air ratio, $FAH/DTIH \approx DTIH/\Delta FAH$ , dimensionless.
L (1-11)	Distance between model stations, in.
YL (1-11)	Station locations references to Station 1, in.
C (1-11)	Velocity of sound at each station in./sec.
CH	Velocity of sound in core stream at Station 3H, in./sec.
M (1-11)	Mach number at each station, dimensions.
MH	Mach number in core stream at Station 3H, dimensionless.
T (1-11)	Temperature at each station, deg R.
TH	Temperature in core stream at Station 3H, deg R.
PRHOT	Pressure drop through combustion zone (Station 5 - Station 10), Psia.
G (1-11)	Ratio of specific heats at each station, dimensionless.
GH	Ratio of specific heats in core stream at Station 3H, dimensionless.
TAUF (1-11)	Time delays for downstream running sonic waves between stations, sec.
TAUFH	Time delay for downstream running sonic wave between Stations 2H and 3H, sec.
TAUG (1-11)	Time delays for upstream running sonic waves between stations, sec.
TAUGH	Time delay for upstream running sonic wave between station 2H and 3H, sec.
TAUE (1-11)	Time delays for downstream running entropy waves between stations, sec.
TAUEH	Time delay for downstream running entropy wave between stations 2H and 3H, sec.
QOP (1-11)	Ratio of volumetric heat release rate at each station to pressure at each station, 1/sec.



**TABLE 14. FLAMEHOLDER COMBUSTION MODEL OUTPUT**

<i>Parameter(s)</i>	<i>Description</i>
Fan Stream	Identifies following sections as fan duct output.
Streamtube Type	Identifies for this set of input variables.
No. of This Type	The number of streamtubes with this set of input variables.
Static Pressure (PS6)	Inlet static pressure, psia.
Approach Temperature (T6C)	Inlet temperature, °R.
Approach Mach No. (M6C)	Inlet flow Mach No., dimensionless.
Input FA Ratio (FAC)	Inlet fuel-air ratio, dimensionless.
Effective FA Ratio	Effective fuel-air ratio accounting for liner cooling air-flow.
F/H Width (FWWC)	Flameholder width, in.
Blockage Ratio (TAUC)	Ratio of flameholder width to streamtube width, dimensionless.
F/H Apex Angle (ALPHAC)	V-gutter flameholder apex angle, deg.
S/R Fuel Temperature (TFSR)	Temperature of the fuel within spraying °R.
S/R Fuel Pressure (PFSR)	Pressure of the fuel within the spraying, psia.
S/R to F/H Distance (LSC)	Axial separation distance between the spraying and the flameholder, in.
F/H to Nozzle Distance (XLC)	Axial distance from the flameholder to the exhaust nozzle throat, in.
Turbulence Level (EPSC)	Ratio of RMS turbulence velocity to the approach velocity of the inlet, dimensionless.
Wake Flow Addition (WEXT)	Ratio of external wake flow to recirculated flow, dimensionless.
Flow Source Temperature (TEXT)	Temperature of above flow, °R.
Effective Inlet Temperature	Mass average of WEXT flow at TEXT and recirculated flow at T6C, °R.
Fuel Type (JFUEL)	Identifies for fuel 1 = JP-4 2 = JP-5
Mean Droplet Size	The mass median droplet size produced by the injector, microns.
Flash Vaporization	Fraction of the liquid fuel which is vaporized by injection from PFSR to PS6, dimensionless.
Beta 1	Droplet vaporization fraction.
Beta 2	Droplet collection fraction.
Beta 3	Surface vaporization fraction.

**TABLE 14. FLAMEHOLDER COMBUSTION MODEL OUTPUT (Continued)**

<i>Parameter(s)</i>	<i>Description</i>
K1	Recirculation fraction.
Wake FA	Flameholder wake vapor phase fuel-air ratio, dimensionless.
Wake Temperature	Reaction temperature in the flameholder wake, °R.
Initial Speed	Laminar flame speed at the flameholder, ft/sec.
Initial Turbulence	Turbulence intensity at the flameholder, dimensionless.
Ideal Temperature Rise R.	Ideal temperature rise for effective fuel-air ratio, °
Efficiency	Streamtube combustion efficiency; ratio of flame penetration to streamtube width, dimensionless.
Actual Temperature Rise	Efficiency times ideal temperature rise, °R.
Exit Temperature	Streamtube exit temperature without liner cooling air, °R.
Flowrate — Air	Air flowrate for this streamtube, lb <sub>m</sub> /sec.
Flowrate — Fuel	Fuel flowrate for this streamtube, lb <sub>m</sub> /sec.
Cooling Flow/Total Engine Flow (WCOOL)	Ratio of liner cooling air flowrate to total engine flowrate, dimensionless.
Chemical Combustion Efficiency	Average efficiency based on average streamtube exit temperature and average effective fuel-air ratio, dimensionless.
Thermal Combustion Efficiency	Average efficiency based on streamtube average exit temperature plus cooling air and average input fuel-air ratio, dimensionless.
Average Cooling Air Temperature	Mass averaged inlet temperature used for cooling, °R.
Average Streamline Exit Temperature	Mass average of the streamtubes without cooling air, °R.
Average Duct Exit Temperature	Mass average of streamtubes plus cooling air, °R.
Total Flowrate	Total of each streamtube type times the number of each type, lb <sub>m</sub> /sec.
Average Fuel-air Ratio	Mass average of the input fuel-air ratios.
Core Stream	Identified following sections as core stream output.
Wake Recirculation Coefficient	Same as K1 in fan duct, dimensionless.
Ideal Temperature Rise	Ideal temperature rise based on input fuel-air ratio and main burner fuel-air ratio. See Appendix B.
M/B Fuel-air Ratio	Fuel-air ratio of the vitiated air entering the core streamtubes.
M/B Inlet Temperature	Inlet temperature to the main burner, dimensionless.
Average Distance from Spraybar to F/H	Average axial distance from the spraybars to the flameholders, in.
<b>NOTE:</b> Any core stream parameters which are not listed above have the same definition as their fan stream counterpart.	



The augmentor design parameters that are available for evaluation are flameholder blockage, width, draft angle, apex angle, surface area, heat addition, fuel injection to flameholder distance and fuel injection droplet size.

If the above design study cannot sufficiently desensitize the augmentor in the UHLC or the engine cycle cannot tolerate the additional losses and/or tolerate the performance at other design points, the fuel air ratio will have to be restricted below the critical value at which rumble is encountered. This will require scheduling maximum fuel air ratio vs. the flight point.

#### **4. PHASE IV — SWIRL AUGMENTOR MODEL VERIFICATION**

##### **a. Background**

The swirl augmentor employs a novel flamespreading concept wherein the augmentor inlet flow is swirled to create a strong centrifugal field and flame is propagated by buoyant displacement of hot combustion products through the more dense inlet mixture. No flameholder is used. Figure 89 shows a cross section of a swirl augmentor on an F100 turbofan engine. Swirl vanes in the turbine exhaust and in the rear fan duct impart swirl to the augmentor inlet flow which is then fueled by a series of sprayings. A portion of the augmentor flow bypasses the fan swirl vanes and feeds the augmentor and exhaust nozzle cooling liners as well as a small annular pilot burner around the outer diameter of the augmentor. The pilot burner initiates the combustion process by exhausting hot, relatively rare, combustion products on the outer perimeter of the augmentor. The unburned fuel-air mixture inboard of the pilot burner is denser so centrifuge effects create a crossflow of hot combustion products moving towards the augmentor centerline and the denser unburned fuel-air mixture moving towards the outer diameter. This crossflow propagates combustion through the unburned fuel-air mixture which generates more hot combustion products which are likewise buoyed towards the center until the entire stream is burned. The augmentor flow is moving downstream during this process and the combination of radial flamespreading during axial flow give the appearance of a nearly conical flamefront emanating from the pilot burner. Potential advantages are:

1. Improved cruise TSFC — no flameholder and resulting pressure losses are required. Further, the relatively cool inlet vanes can be made variable to eliminate swirl losses during nonaugmented, or cruise, operation
2. Reduced augmentor length — the combustion rate is controlled by the intensity of the centrifugal field which, in turn, is controlled by the swirl imparted to the inlet flow. Length reductions of 50% appear feasible as compared to conventional flameholder systems
3. Improved performance at low augmentor pressure levels — the combustion process is controlled by buoyancy effects which are independent of pressure level.

The objective of this phase of the program was to verify the low frequency instability model for swirl augmentors.

##### **b. Approach**

The model verification program consists of sea level testing of a full-scale swirl augmentor on an F100 turbofan engine. The tests were made to determine augmentor combustion efficiency and stability characteristics with varied fuel-air ratio and internal fuel distribution. Predictions were made of the stability characteristics with the model using the measured augmentor efficiency characteristics as input. A comparison was made of the predicted and measured stability characteristics.



### **c. Results**

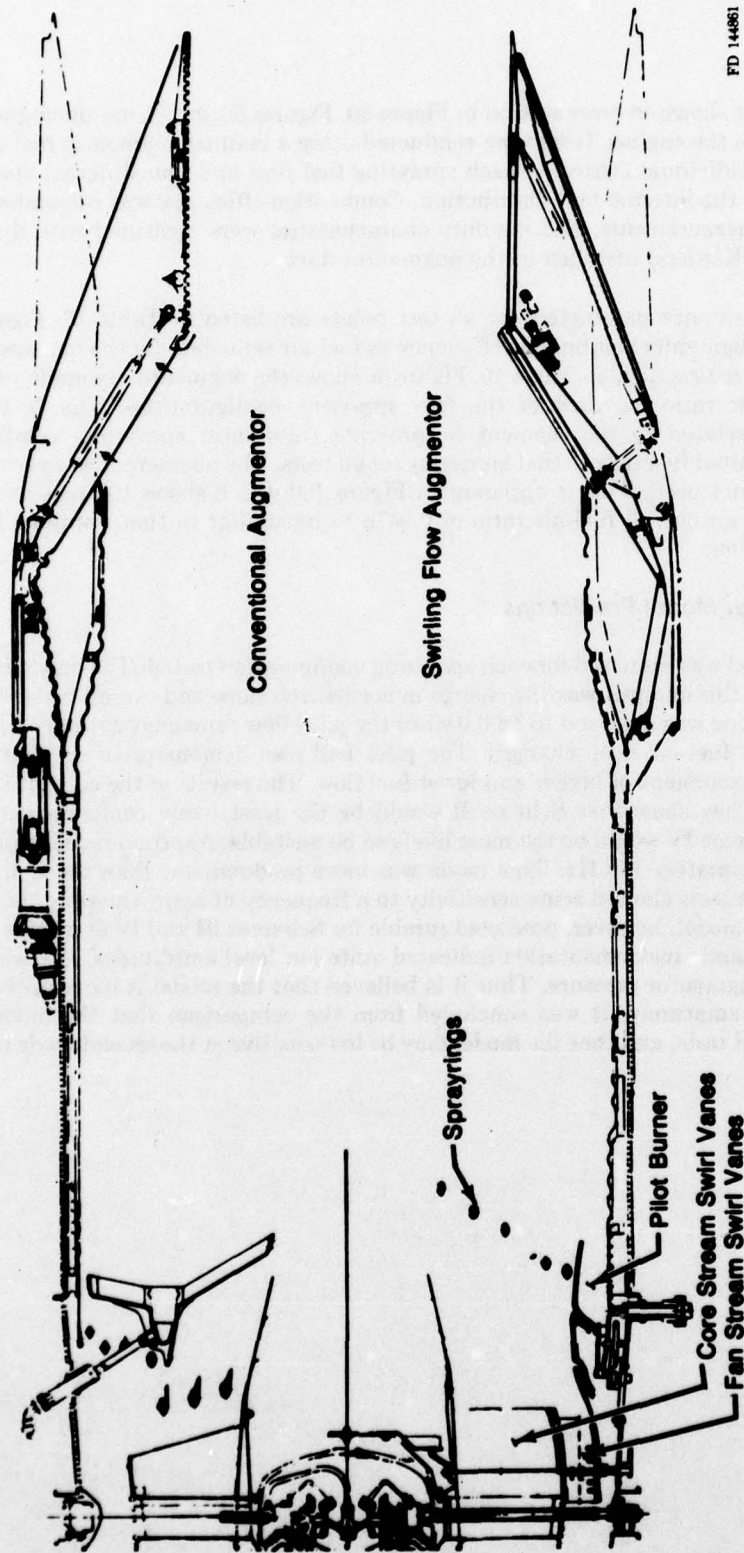
#### **(1) Experimental**

The augmentor is shown in cross section in Figure 89. Figures 90 and 91 are photographs of the actual hardware on the engine. Tests were conducted using a manual augmentor fuel control system that enabled individual control of each spraying fuel flow and four different spraying configurations to vary the internal fuel distribution. Combustion efficiency was calculated from engine performance measurements, and stability characteristics were measured with dynamic pressure transducers (Kistlers) installed in the augmentor duct.

Significant performance parameters for all test points are listed in Table 15. Figures 92 through 95 show the augmentor combustion efficiency vs fuel-air ratio data for the four spraying configurations which are described in Table 16. Figure 96 shows the augmentor dynamic pressure traces at high fuel-air ratio for each of the four spraying configurations. The  $\approx 165$  Hz instability shown is related to the segment 5 spraying (innermost spraying) combustion characteristics and limited fuel flow to that spraying for all tests. The augmentor was very stable when segment 5 was not used. This is apparent in Figure 100 which shows the pressure trace without segment 5 at an overall fuel-air ratio of 0.0476 to be similar to that obtained during nonaugmented operation.

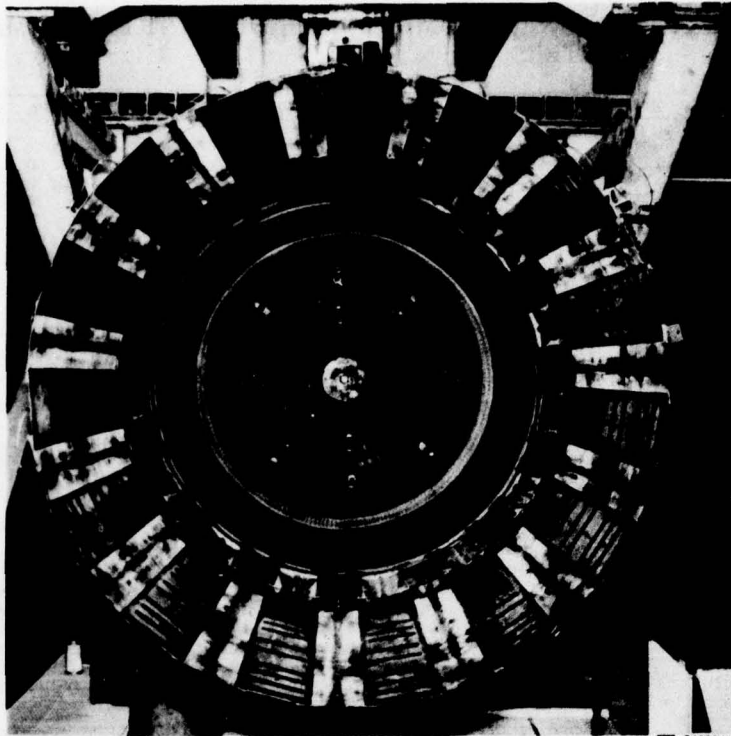
#### **(2) Comparison With Model Predictions**

The rumble model was exercised for each spraying configuration tested. The only variables input to the model for this analysis was the change in normalized slope and overall fuel-air ratio. The pilot efficiency slope was assumed to be 0.0 since the pilot flow remained virtually constant with increased overall fuel-air ratio changes. The pilot had also demonstrated no changes in efficiency for several excursions of higher and lower fuel flow. The results of the comparison are shown in Table 17. They show that Scheme II would be the least likely configuration to be unstable and that Scheme IV would be the most likely to be unstable. A second mode instability is predicted at approximately 155 Hz. This mode was more predominant than the first mode ( $\sim 65$  Hz). The engine tests showed some sensitivity to a frequency of approximately 165 Hz as discussed earlier. The model, however, predicted rumble for Schemes III and IV at a point where the amplitudes of dynamic instrumentation indicated quite low level amplitudes, i.e., less than 5% peak to peak of augmentor pressure. Thus it is believed that the model is too sensitive and predicts this mode prematurely. It was concluded from the comparison that the model was verified by the sea level tests, and that the model may be too sensitive at the second mode rumble frequency.

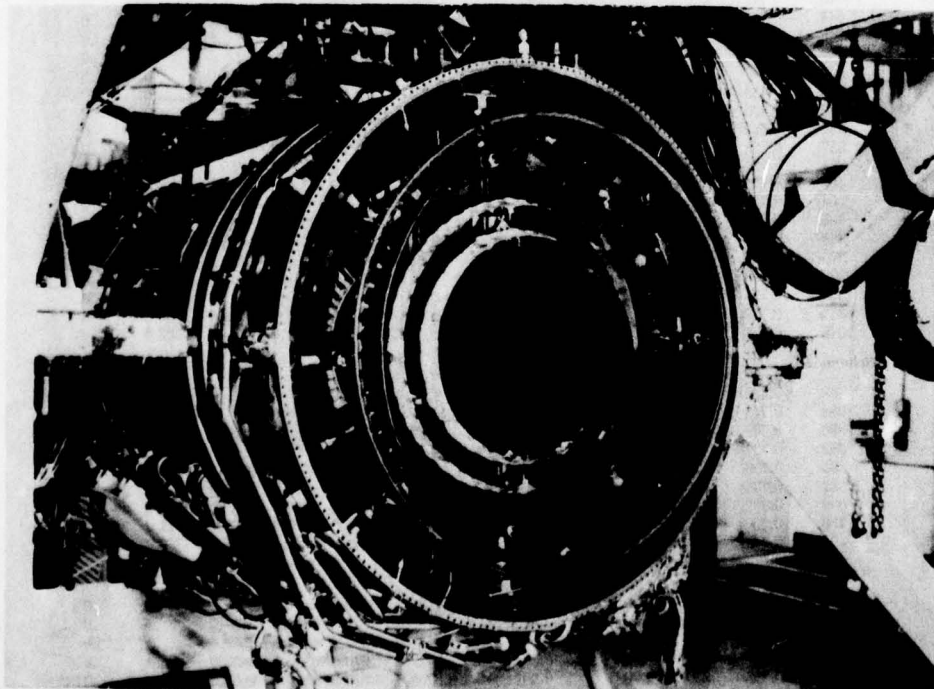


FD 144861

Figure 89. Cross Section Sketch of Swirl Augmentor Compared to Conventional Augmentor



**Figure 90.** *Swirl Augmentor With Cooling Liner Duct and Nozzle Installed*



**Figure 91.** *Swirl Augmentor Without Duct and Nozzle Installed*



TABLE 15. PO72 SWIRL AUGMENTOR SIGNIFICANT PERFORMANCE PARAMETERS

ADR No.	BPR	WGGM	FAAB	$\eta_2$	% Aug	WFPIL	WF1	WF2	WF3	WF4	WF5
<i>Scheme I</i>											
263	0.734	219.5	0.0087	90.2	16.3	2079.2	4718.3	.0	.0	.0	.0
264	0.730	218.9	0.0117	93.2	21.6	2007.2	7039.0	.0	.0	.0	.0
266	0.735	218.6	0.0146	89.8	25.3	1969.1	7495.9	.0	.0	.0	.0
268	0.765	218.6	0.0194	84.9	30.3	1992.3	10712.0	2335.5	.0	.0	.0
269	0.736	218.6	0.01646	88.3	27.4	2001.4	10750.0	.0	.0	.0	.0
271	0.758	218.9	0.0246	84.3	36.3	1988.2	10524.0	6752.0	.0	.0	.0
273	0.751	218.3	0.0296	84.8	41.2	1955.9	10632.0	6566.1	3786.1	.0	.0
276	0.738	219.2	0.0313	87.2	44.7	2046.3	9656.7	6646.6	6024.1	.0	.0
278	0.737	219.4	0.0322	89.4	46.2	1978.6	8701.2	6707.7	7698.3	.0	.0
281	0.739	219.0	0.037	90.2	51.4	2002.7	8612.7	6585.1	7618.3	4180.4	.0
283	0.741	219.1	0.0399	89.0	53.3	1972.8	8601.1	6537.6	7586.3	6202.2	.0
285	0.733	218.8	0.042	88.0	54.9	1964.5	8570.7	6610.9	7711.8	7763.7	.0
286	0.739	218.8	0.041	88.5	54.3	1924.0	7724.2	6779.0	7702.0	7730.5	.0
287	0.736	219.2	0.044	86.8	56.0	1916.3	7649.1	6727.8	7617.9	7670.9	2876.7
294	0.717	211.3	0.0126	93.2	22.5	1990.6	7510.7	.0	.0	.0	.0
295	0.722	211.1	0.0172	88.7	27.7	1958.5	7600.2	3264.1	.0	.0	.0
297	0.718	210.9	0.0216	89.2	33.9	1934.3	7590.0	6550.1	.0	.0	.0
299	0.728	210.8	0.0241	90.4	37.0	1975.6	7543.7	8556.0	1613.4	.0	.0
301	0.739	209.5	0.0244	87.6	36.8	2025.5	7593.9	8512.8	.0	.0	.0
303	0.739	211.2	0.0294	89.3	42.7	1996.4	7539.7	8596.6	3825.1	.0	.0
305	0.723	210.6	0.0348	88.5	47.7	1985.4	7687.2	8587.7	7684.9	.0	.0
307	0.734	210.6	0.0404	89.5	53.5	1993.3	7655.4	8556.3	7665.7	4348.8	.0
309	0.740	210.9	0.0447	87.9	56.4	2006.6	7638.3	8587.6	7670.4	7655.1	.0
311	0.729	210.5	0.0472	87.4	58.0	2037.5	7594.3	8521.5	7614.1	7606.8	1945.9
313	0.732	210.2	0.0461	88.9	57.9	2027.2	7685.9	8597.8	7677.4	5574.4	2867.9
315	0.733	209.9	0.0471	89.7	58.9	2013.3	7676.6	8589.8	7657.4	5579.2	3608.2
317	0.729	210.6	0.0494	86.7	58.9	2014.0	7631.4	8543.4	9559.3	5564.5	3595.2
319	0.736	209.9	0.0473	88.8	58.7	2011.9	7608.0	7540.4	7645.1	5568.2	2361.5
321	0.735	209.6	0.0488	86.7	58.7	2013.2	7628.3	9504.8	8636.9	5561.6	2364.9
322	0.734	210.1	0.0482	87.4	58.6	1720.7	7638.1	9530.6	8635.0	5567.8	2864.3
<i>Scheme II</i>											
335	0.744	210.6	0.009	0.817	16.2	1985.0	4691.0	.0	.0	.0	.0
337	0.747	209.1	0.0122	0.914	22.3	1991.0	7031.0	.0	.0	.0	.0
339	0.747	209.8	0.0126	0.935	24.2	1991.0	7567.0	.0	.0	.0	.0
341	0.743	210.1	0.0153	0.895	27.0	1995.0	9422.0	.0	2061.0	.0	.0
343	0.747	209.5	0.0198	0.896	33.2	1979.0	9442.0	3240.0	.0	.0	.0
344	0.744	209.9	0.0175	0.910	30.5	1976.0	7548.0	3367.0	.0	.0	.0
345	0.744	209.8	0.0217	0.904	35.7	1988.0	7592.0	6462.0	.0	.0	.0
347	0.743	209.6	0.0255	0.879	39.4	2011.0	7524.0	9414.0	.0	.0	.0
349	0.747	209.7	0.0306	0.866	44.8	2007.0	7582.0	9501.0	3689.0	.0	.0
350	0.745	210.6	0.0292	0.883	43.2	1998.0	7568.0	8554.0	3689.0	.0	.0
352	0.735	210.1	0.0332	0.881	47.0	1990.0	7543.0	8524.0	6648.0	.0	.0
354	0.752	210.5	0.0371	0.868	50.6	1998.0	7627.0	8518.0	9670.0	.0	.0
357	0.728	210.1	0.0373	0.876	51.3	2002.0	7620.0	8528.0	9633.0	.0	.0
361	0.726	208.7	0.045	0.846	55.5	2010.0	7652.0	8537.0	9569.0	5532.0	.0
363	0.732	208.6	0.0476	0.819	57.2	2017.0	7633.0	8513.0	9474.0	7808.0	.0
364	0.727	209.9	0.043	0.857	55.3	2035.0	7652.0	8621.0	9671.0	4044.0	.0
366	0.727	209.2	0.0466	0.855	58.0	2016.0	7579.0	8574.0	9527.0	4026.0	2342.0
368	0.727	209.5	0.0477	0.859	59.1	2015.0	7558.0	8637.0	9488.0	4020.0	3362.0
370	0.726	209.4	0.0493	0.849	59.6	2065.0	8611.0	8593.0	9523.0	4054.0	3825.0
372	0.729	209.5	0.0504	0.879	59.8	2032.0	8604.0	9479.0	9482.0	4048.0	3822.0
373	0.729	210.4	0.0474	0.897	58.5	2049.0	8613.0	8244.0	9113.0	3617.0	3769.0
375	0.729	209.9	0.0503	0.877	59.5	2048.0	9463.0	8531.0	9568.0	3968.0	3827.0
376	0.728	209.7	0.0494	0.893	60.0	2014.0	7586.0	8524.0	9474.0	5583.0	3645.0
<i>Scheme III</i>											
386	0.733	211.9	0.0152	0.915	27.1	2016.0	9416.0	1330.0	.0	.0	.0
388	0.742	212.3	0.0155	0.912	27.4	2137.0	9429.0	1043.0	.0	.0	.0
390	0.739	212.5	0.0157	0.918	27.8	2355.0	9455.0	.0	3564.0	.0	.0
392	0.737	212.2	0.0161	0.904	28.0	2523.0	9429.0	.0	.0	.0	.0
395	0.736	212.8	0.051	0.811	58.8	2529.0	9802.0	8565.0	9554.0	5489.0	2882.0
397	0.733	212.5	0.0482	0.820	57.4	2422.0	7596.0	8613.0	9635.0	5449.0	2800.0
399	0.732	212.6	0.0507	0.835	59.7	2412.0	10806.0	7730.0	7089.0	5529.0	2848.0
400	0.736	213.2	0.048	0.851	59.0	2365.0	9564.0	7475.0	8797.0	5422.0	2793.0
401	0.733	212.2	0.046	0.871	58.1	2326.0	8672.0	7266.0	8622.0	5332.0	2742.0
<i>Scheme IV</i>											
406	0.732	209.7	0.0132	0.914	24.3	2165.0	7599.0	.0	.0	.0	.0
409	0.734	209.3	0.0247	0.899	38.5	2168.0	7572.0	8629.0	.0	.0	.0
410	0.735	209.3	0.0378	0.854	50.3	2174.0	7651.0	8634.0	9693.0	.0	.0
412	0.739	209.6	0.0451	0.837	55.6	2172.0	7676.0	8576.0	9803.0	5498.0	.0
414	0.728	210.4	0.0477	0.807	58.1	2205.0	7616.0	8576.0	9662.0	7646.0	.0
416	0.737	210.0	0.0492	0.795	58.4	2273.0	7673.0	8292.0	9692.0	7653.0	.0
417	0.739	210.1	0.0475	0.817	58.6	2206.0	8610.0	9605.0	9652.0	5416.0	.0
419	0.729	210.2	0.015	0.90	26.2	2627.0	8533.0	.0	.0	.0	.0
420	0.729	210.3	0.0150	0.929	26.9	2629.0	8538.0	.0	.0	.0	.0

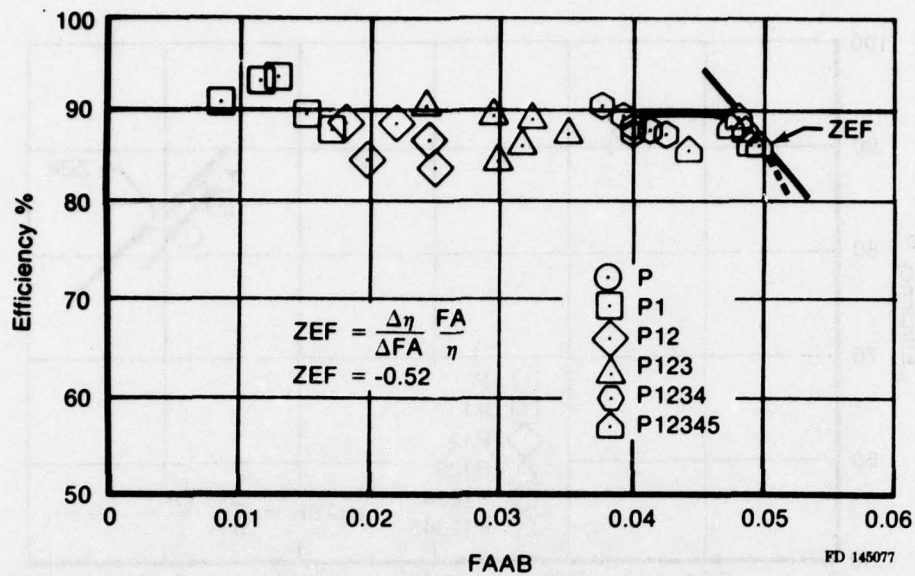


Figure 92. PO72/Swirl Augmentor Scheme No. 1

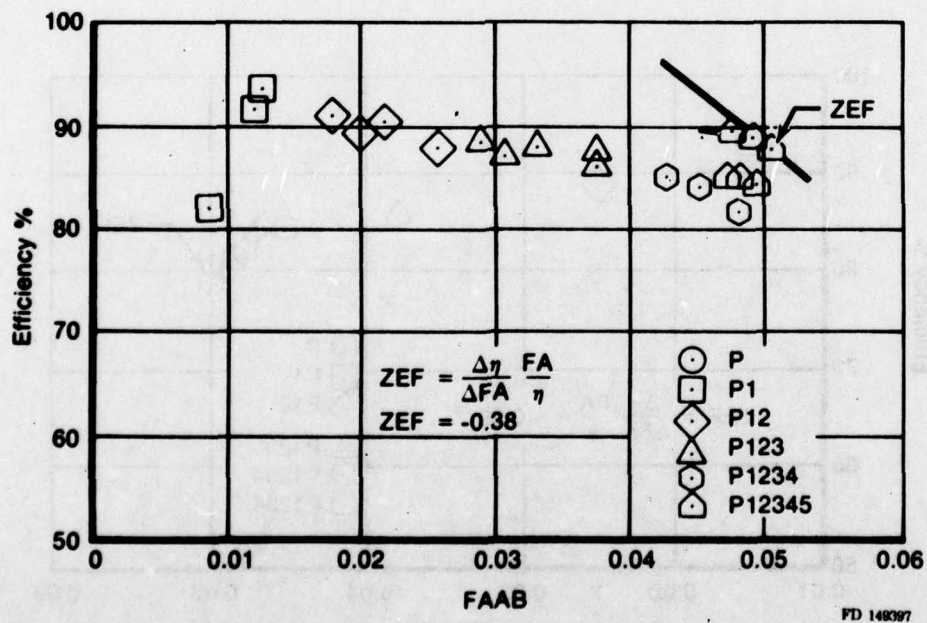


Figure 93. PO72/Swirl Augmentor Scheme No. 2

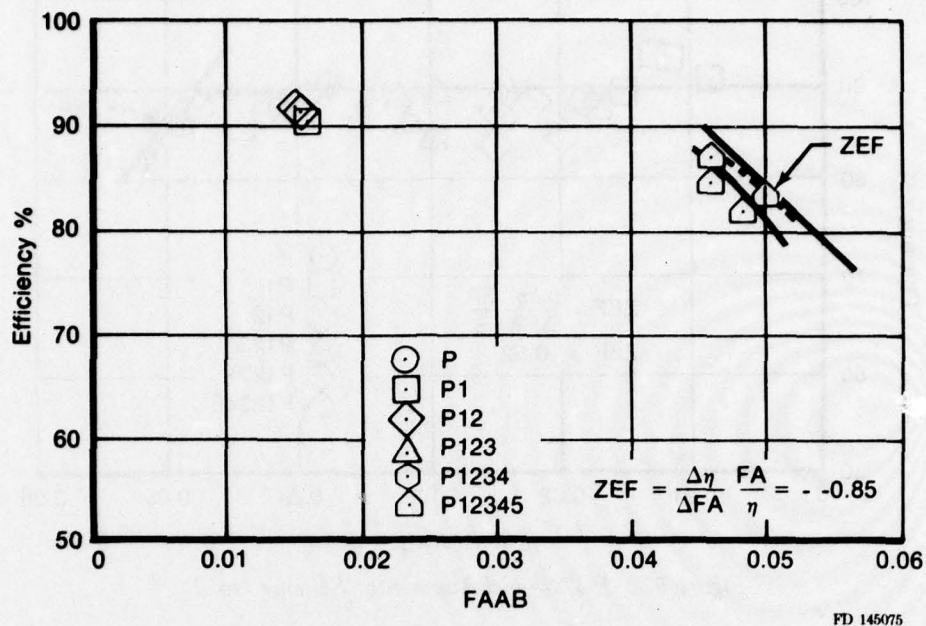


Figure 94. PO72/Swirl Augmentor Scheme No. 3

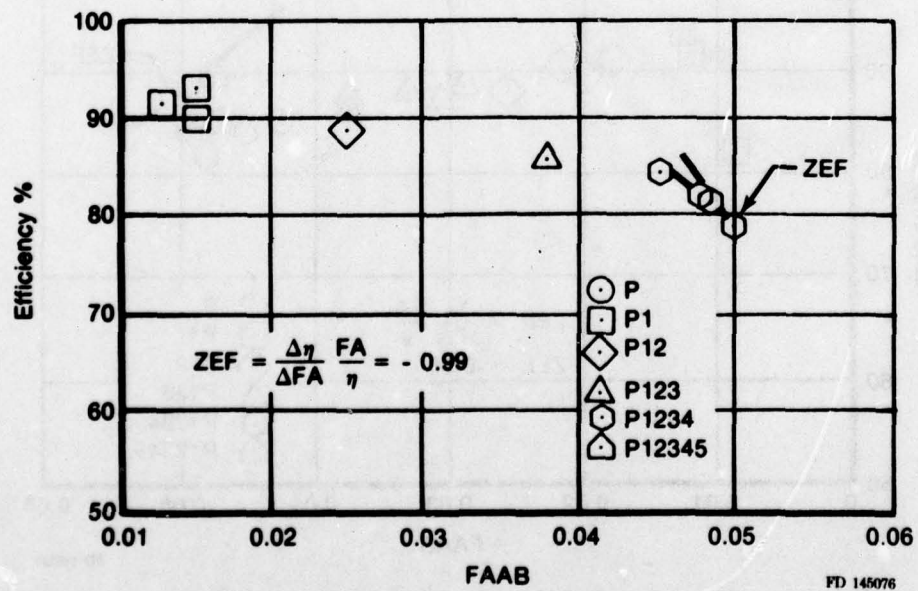
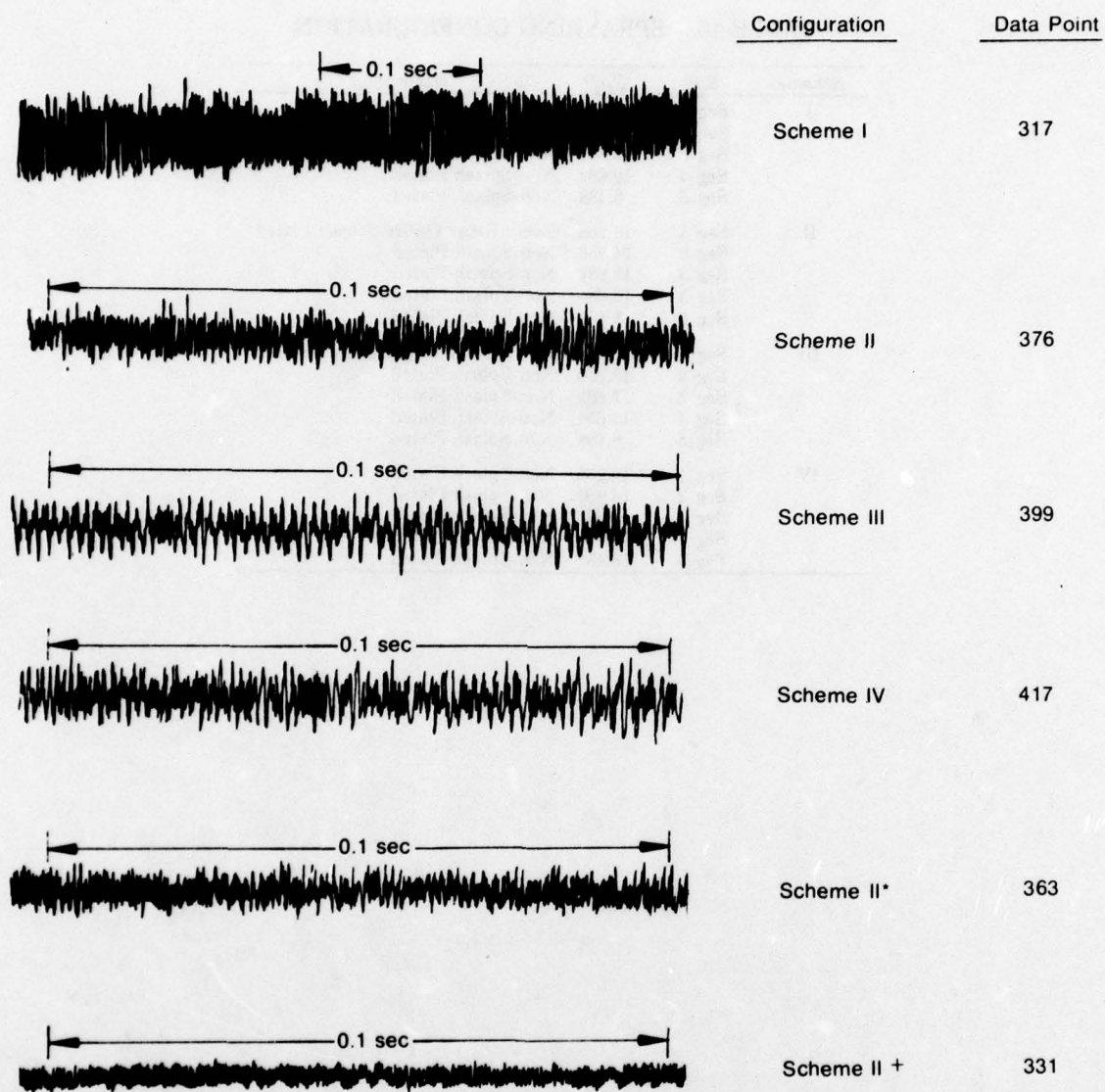


Figure 95. PO72/Swirl Augmentor Scheme No. 4



TABLE 16. SPRAYRING CONFIGURATION

<i>Scheme</i>	<i>S/R</i>	<i>RAD</i>	<i>Description</i>
I	Seg 1	16.268	Fully Splash Plated
	Seg 2	14.950	Non-Splash Plated
	Seg 3	12.881	Non-Splash Plated
	Seg 4	10.684	Non-Splash Plated
	Seg 5	8.488	Non-Splash Plated
II	Seg 1	16.268	Every Other Orifice Splash Plated
	Seg 2	14.950	Non-Splash Plated
	Seg 3	12.881	Non-Splash Plated
	Seg 4	10.684	Non-Splash Plated
	Seg 5	8.488	Non-Splash Plated
III	Seg 1	16.268	Every Other Orifice Splash Plated
	Seg 2	13.870	Non-Splash Plated
	Seg 3	12.881	Non-Splash Plated
	Seg 4	10.684	Non-Splash Plated
	Seg 5	8.488	Non-Splash Plated
IV	Seg 1	16.268	Non-Splash Plated
	Seg 2	14.950	Non-Splash Plated
	Seg 3	12.881	Non-Splash Plated
	Seg 4	10.684	Non-Splash Plated
	Seg 5	8.488	Non-Splash Plated



\*No Zone 5

+ Intermediate

FD 146480

Figure 96. Swirl Augmentor Dynamic Pressure Traces

**TABLE 17. MODEL PREDICTIONS vs SWIRL AUGMENTOR SLS RESULTS**

**A. Conditions at Test Point**

Scheme	I	II	III	IV
Data Point	317	376	399	417
FAAB	0.0494	0.0494	0.0507	0.0492
$\eta$	0.867	0.893	0.853	0.795
ZEF	-0.52	-0.38	-0.85	-0.99
Test Stability <100 Hz/amp	<0.5 psi p/p	<0.5 psi p/p	<5 psi p/p	<5 psi p/p
Test Stability >100 Hz/amp	165 Hz/1.8 Stable	165 Hz/1.3 Stable	165 Hz/2.0 Stable	165 Hz/2.25 Stable
Model Prediction <100 Hz/Q <sub>out</sub>	65 Hz/0.3 Stable	69 Hz/0.25 Stable	66 Hz/47 Unstable	65 Hz/0.45 Unstable
Model Prediction >100 Hz/Q <sub>out</sub>	155 Hz/0.85	155 Hz/0.73	155 Hz/1.1	155 Hz/1.0

**B. Conditions for Model to Predict Unstable at > 100 Hz**

Scheme	I	II	III	IV
FAAB	>0.051	>0.052	>0.050	>0.0492
$\eta$	0.84	0.855	0.835	0.795
ZEF	-0.73	-0.6	-0.85	-0.99
Frequency	155	155	155	155



## **5. RESULTS, CONCLUSIONS AND RECOMMENDATIONS**

### **a. Results**

#### **(1) V-gutter Flameholder Augmentors**

The original rumble model has gradually become more accurate as test results have been incorporated and as assumptions have been verified or disproved. As a result, the model is fairly proficient at predicting the major trends generally associated with rumble in turbofan V-gutter flameholder augmentors.

Although it will not predict accurately every observed test, the model is now capable of identifying changes which should materially affect the occurrence of rumble. One reason for the inaccuracy is that tests with augmentors have not always shown a high degree of repeatability. A second reason for the inaccuracy of the rumble model predictions is the combustion process predictions obtained from the flameholder combustion model. The flameholder combustion model has been developed to the point where it can predict V-gutter flameholder combustion efficiency as effected by fuel-air ratio, pressure, velocity and temperature variations. However, the numeric accuracy of the fan stream efficiency calculations is approximately  $\pm 3\%$  of a nominal level. This results in large errors, including sign changes, in the normalized slope calculations of efficiency vs fuel-air ratio, pressure, velocity, and temperature that are used in the rumble model.

To operate stably at high augmentation, which requires a high fuel-air ratio, the model predicts that:

1. The augmentor design parameters should be chosen to eliminate or minimize the decrease in augmentor combustion efficiency with increasing fuel-air. This decrease is typical at high fuel-air ratios and seems to grow worse at low augmentor pressure. The design parameters include all effects which influence the efficiency curve (flameholder width, surface area, drafting, etc.). Fan stream efficiency is predicted to be more sensitive to fuel-air ratio than the core stream; thus, it is particularly important that emphasis be given to design parameters which influence fan stream efficiency.
2. The fuel-air ratio in a stream should be as uniformly distributed as possible. Any portion of an augmentor stream which has a fuel-air ratio above average will become rumble sensitive first. If this portion of the stream is sufficiently large, rumble can occur at low average fuel-air ratio. A uniform distribution will allow operation to higher average fuel-air ratio, and higher augmentation, before rumble is encountered.
3. Additional system stiffness, i.e., impeding airflow oscillations is predicted to retard the occurrence of rumble. This can be accomplished by increasing the pressure drop near the fan duct exit or across the flameholders.
4. If the above items do not sufficiently desensitize the augmentor, or the engine cycle cannot tolerate the additional losses, the fuel-air ratio will have to be restricted below the critical value at which rumble is encountered. This will require scheduling maximum fuel-air ratio vs the flight point.

## **(2) Full Swirl and Vorbix Augmentors**

Rumble modeling of the Full Swirl and Vorbix augmentors is not as well developed as that of a V-gutter augmentor. Only recently has a realistic analytical steady-state combustion efficiency model for a V-gutter been developed (Reference 1). Comparable models for the Full Swirl and Vorbix augmentors are not available, and insufficient test data exist for an empirical correlation. Because of the limited information about these newer augmentor concepts, they were dynamically modeled on a less detailed level, which did not allow consideration of specific influences (such as pilot burner design).

However, from the experience gained in developing a dynamic model of a V-gutter augmentor, and from the extension of this model to the Full Swirl and Vorbix augmentors (even though the extensions were less detailed than desired), the fundamental mechanism which can lead to rumble in a conventional augmentor is also potentially present in both the Full Swirl and Vorbix concepts. If the combustion efficiency of either of these concepts becomes sufficiently sensitive to fuel-air ratio disturbances, either in the main streams or in the pilot burners, rumble can occur. Accordingly, the same considerations which will eliminate rumble in conventional V-gutter augmentors also apply to the Full Swirl and Vorbix augmentors. The only difference is the design parameters available to desensitize the combustion process in the two newer concepts are vane angles, vortex strength, pilot burner design, etc., rather than flameholder design. Whether desensitization with these parameters is inherently easier has not been firmly established. Rumble has occurred under certain operating conditions during engine testing of the Full Swirl augmentor. The Vorbix augmentor has not experienced rumble but has only been tested as a sector rig.

To make specific predictions about the rumble characteristics of the Full Swirl and Vorbix augmentors require specific predictions about the combustion process which do not currently exist for these augmentors. Further development of rumble models for the Full Swirl and Vorbix augmentors will be paced by development of these combustion models.

### **b. Conclusions**

As a result of the exploratory efforts performed under this study, the major drivers of rumble instability in turbofan augmentors have been identified. A computer program has been assembled which predicts the combustion efficiency and stability signature of a conventional turbofan augmentor and has been evaluated successfully against engine testing.

As a result of the analytical and experimental efforts of this study, the following major conclusions have been reached:

- Rumble was identified as a system problem in which the airflow dynamics couples with the combustion process.
- Experimental rig tests identified fuel distribution as a rumble contributor.
- The most significant driver of rumble is the falloff in combustion efficiency as fuel-air ratio is increased.
- The variations of augmentor efficiency caused by pressure, velocity and temperature were identified as minor rumble drivers.
- Full Scale Engine Research tests have verified that the combined rumble model predicts the stability trends correctly for a turbofan engine.



To reach the present stage in model development, whereby the model can reasonably predict the occurrence of rumble, it was necessary to make the following changes to the originally proposed model:

- Account for the axial distribution of the combustion rate. This was found to influence rumble frequency predictions.
- Account for the axial temperature and velocity gradients caused by burning. This was necessary to be able to predict the very low frequency rumble (20 to 40 Hz) observed during rig testing.
- Replace the empirical "beta" combustion efficiency correlation (Reference 2) with the combustion model developed under Reference 1. The "beta" correlation was found to be inaccurate in predicting combustion efficiency and did not account for all parameters which affect efficiency.
- Treat the combustion characteristics of the fan and core streams individually. Rumble only requires that the combustion in a large enough portion of the augmentor airstream becomes sensitive to local fuel-air ratio. Treatment of overall combustion based upon overall fuel-air ratio will not always correctly identify an unstable operating point because the same overall fuel-air ratio can be achieved with many different distributions of local fuel-air ratio.

#### **c. Recommendations**

The basic rumble model formulation, as it now exists, meets the program requirements. However, refinements or improvements can be made to enhance its accuracy as more information becomes available. The experience gained with the model before and during the FSER tests has identified areas where further refinements to the model could be made. It is not expected that these improvements will materially change model predictions concerning the causes of and solutions for rumble. Rather, they should improve model accuracy. These refinements include:

- Resolve the numeric accuracy problems associated with the flameholder combustion model and verify combustion prediction with engine test data.
- Extend the wave equations to account for different axial temperature and velocity profiles in the fan and core streams. At present, a common mixed axial profile is used, which requires that the entropy waves in each stream travel at mean mixed velocity. Actually, the entropy waves in the fan stream should travel slower than mean mixed velocity, while those in the core stream should travel faster.
- Investigate the influence on model predictions of liquid fuel particle dynamics in the spraybar and flameholder regions. Preliminary predictions have indicated that even a very small lag (0.003 sec) on the heat release term will cause rumble model predictions to more closely follow the FSER test results.
- Investigate the influence of pressure on combustion rate at the flameholders as well as further aft in the augmentor. These potential influences cannot presently be accounted for.



- Identify the axial locations of major pressure drops in the fan duct. The axial location as well as the value of fan duct pressure drop has an influence upon the dynamic response of the air column in the duct.
- Improve modeling of the fan duct and core engine interaction at fan discharge taking into account the actual proximity of the fan splitter. The fan splitter and core engine form an upstream boundary condition for the fan duct, influencing the strength and phasing of reflected waves.
- Develop combustion models for the Vorbix and Full Swirl augmentor concepts similar to the combustion model development for the V-gutter augmentor. At present, the combustion characteristics of these augmentors are known only on an overall basis and only at selected operating points where testing has been conducted.

The first five items are directed particularly toward rumble predictions. The last two affect rumble predictions also, but are related to other turbofan engine development programs and can possibly emerge from the future results of those programs.

## APPENDIX A

This appendix contains the tabulated and plotted experimental rig data. The following nomenclature is used:

T	air temperature upstream of the flameholders	°F
P	rig pressure upstream of the flameholders	psia
M	Mach number upstream of the flameholder	
$\eta$	combustion efficiency	%
TFH1, TFH2	center flameholder metal temperatures	°F
Amp	peak-to-peak pressure amplitude at flameholders	%
Freq	frequency read from o-graph	Hz

Included with this tabulation are the transfer functions for the various pressure probes. The following nomenclature is used to define the transfer functions:

$P_{21}, P_{31}, P_{43}, P_{44}$  — ratio of pressure amplitude at the subscript location to the amplitude at the flameholder.

$\phi_{21}, \phi_{31}, \phi_{43}, \phi_{44}$  — phase difference between the pressure at the subscript location and the flameholder.

$f_{21}, f_{31}, f_{43}, f_{44}$  — transfer function frequency.

TABLE 18. EXPERIMENTAL STUDY RIG DATA

TEST POINT\* 1 & 2  
TEST CONDITION Baseline  
SPE NUMBER 7.01

POINT	Rig Condition					Transfer Functions										Transfer Functions									
	T	P	N	F A	AMP	FREQ	P21	F21	Q21	P31	F31	Q31	P42	F42	Q42	P43	F43	Q43	P44	F44	Q44	η	TPR1	TPR2	
18	410	13.0	.084	.084	4.6	-																90.5	345	428	
19	407	13.0	.091	.078	5.4	-																76.2	286	367	
20	409	13.02	.087	.082	3.8	-																83.2	293	369	
21	410	13.05	.087	.136	18.0	60																61.8	630	597	
22	408	13.14	.088	.134	17.6	60	2.25	43	800	1.45	45	700	1.4	60	3450	1.35	60	3450	1.45	60	3500	58.9	630	595	
23	413	13.01	.096	.126	15.4	60	2.4	49	90	1.4	43	70	1.4	63	340	1.3	63	340	1.45	60	345	46.7	662	630	
24	409.8	13.03	.088	.143	22.3	80	2.3	45	85	1.45	44	70	1.35	60	340	1.3	62	342	1.4	62	345	71.3	804	741	
25	410	14.6	.102	.079	5	-	2.25	50	100	1.4	50	90	1.8	58	355	1.75	58	355	1.85	58	355	69	300	357	
26	414	14.5	.093	.087	5.5	-	2.2	52	110	1.35	50	90	1.8	58	350	1.65	55	345	1.85	55	350	82.3	305	360	
27	414	15.4	.098	.098	9.1	60	2.35	50	100	1.4	48	95	1.5	72	355	1.45	70	350	1.55	70	355	60	363	401	
28	410.8	13.74	.091	.105	12.6	50	2.25	50	95	1.4	45	80	1.5	70	352	1.42	62	350	1.52	65	350	70.7	373	410	
29	396	20.3	.132	.062	4.4	-							.8	190	140							68.7	272	310	
30	396	20.3	.127	.065	6.4	160	1.9	45	90	1.2	45	85	1.95	65	350	1.8	65	340	1.95	70	0	75.2	272	310	
31	397.2	21.45	.123	.112	9.7	50	1.85	50	110	1.0	50	90	1.5	55	345	1.45	55	340	1.46	55	340	61.6	975	853	
32	400	22.4	.114	.118	25	100				.9	180	190													
33																									
34	234	19.0	.082	.080	3	-																			
35	235	14.0	.085	.077	5.7	50	2.6	47	115	1.6	44	95	2.0	46	340	1.85	47	350	2.1	47	350	80.3	180	211	
36																									
37																									
38																									
39																									
40																									
41																									
42																									
43																									
44																									
45																									
46																									
47																									
48																									
49																									
50																									
51																									
52																									
53																									
54																									
55																									
56																									
57																									
58																									
59																									
60																									
61																									
62																									
63																									
64																									
65																									
66																									
67																									
68																									
69																									
70																									
71																									
72																									
73																									
74																									
75																									
76																									
77																									
78																									
79																									
80																									
81																									
82																									
83																									
84																									
85																									
86																									
87																									
88																									
89																									
90																									
91																									
92																									
93																									
94																									
95																									
96																									
97																									
98																									
99																									
100																									



TABLE 18. EXPERIMENTAL STUDY RIG DATA (Continued)

TEST POINT 1.6.2  
TEST CONDITION Resonance  
SIN WAVE 7.01

POINT	Y	Rig Condition										Transfer Function										T	TMR1	TMR2
		F	H	P A	AMP	FREQ	F21	F22	F23	F24	F25	F31	F32	F33	F34	F35	F41	F42	F43	F44	F45			
36	235	16.4	.000	.0000	65	45	2.45	44	90			1.6	1.5	35	350	1.4						58.5	218	260
37	235	16.5	.003	.0718	29	55	2.45	45	110			1.4	1.45	55	0	1.4						78.9	225	266
38	236	16.4	.001	.0737	36	55																71.2	270	340
39	206	8.4	.15	.000	No Lifo																	-	155	175
40	202	15.8	.005	.0036	7.6	50																80.6	163	180
41	205	15.2	.008	.0012	10	50																80.8	161	182
42	200	17.0	.100	.0005	26	45																41.7	330	400
43	201	18.0	.018	.0742	5.5	40																66.1	161	186
44	206	18.0	.002	.0045	6.7	50																64.0	160	182

TABLE 18. EXPERIMENTAL STUDY RIG DATA (Continued)

TEST POINT<sup>a</sup> 3  
 TEST CONDITION Flameholder Backlogs Change  
 NEW NUMBER 11.01

POINT	Rig Condition										T	P	H	F A	AMP	FREQ	γ	TPH1	TPH2																																																																																																																																																																																																																																																																																																																																																																																																																																																																																																																																																																																																																																																																																																																															
-------	---------------	--	--	--	--	--	--	--	--	--	---	---	---	-----	-----	------	---	------	------	--	--	--	--	--	--	--	--	--	--	--	--	--	--	--	--	--	--	--	--	--	--	--	--	--	--	--	--	--	--	--	--	--	--	--	--	--	--	--	--	--	--	--	--	--	--	--	--	--	--	--	--	--	--	--	--	--	--	--	--	--	--	--	--	--	--	--	--	--	--	--	--	--	--	--	--	--	--	--	--	--	--	--	--	--	--	--	--	--	--	--	--	--	--	--	--	--	--	--	--	--	--	--	--	--	--	--	--	--	--	--	--	--	--	--	--	--	--	--	--	--	--	--	--	--	--	--	--	--	--	--	--	--	--	--	--	--	--	--	--	--	--	--	--	--	--	--	--	--	--	--	--	--	--	--	--	--	--	--	--	--	--	--	--	--	--	--	--	--	--	--	--	--	--	--	--	--	--	--	--	--	--	--	--	--	--	--	--	--	--	--	--	--	--	--	--	--	--	--	--	--	--	--	--	--	--	--	--	--	--	--	--	--	--	--	--	--	--	--	--	--	--	--	--	--	--	--	--	--	--	--	--	--	--	--	--	--	--	--	--	--	--	--	--	--	--	--	--	--	--	--	--	--	--	--	--	--	--	--	--	--	--	--	--	--	--	--	--	--	--	--	--	--	--	--	--	--	--	--	--	--	--	--	--	--	--	--	--	--	--	--	--	--	--	--	--	--	--	--	--	--	--	--	--	--	--	--	--	--	--	--	--	--	--	--	--	--	--	--	--	--	--	--	--	--	--	--	--	--	--	--	--	--	--	--	--	--	--	--	--	--	--	--	--	--	--	--	--	--	--	--	--	--	--	--	--	--	--	--	--	--	--	--	--	--	--	--	--	--	--	--	--	--	--	--	--	--	--	--	--	--	--	--	--	--	--	--	--	--	--	--	--	--	--	--	--	--	--	--	--	--	--	--	--	--	--	--	--	--	--	--	--	--	--	--	--	--	--	--	--	--	--	--	--	--	--	--	--	--	--	--	--	--	--	--	--	--	--	--	--	--	--	--	--	--	--	--	--	--	--	--	--	--	--	--	--	--	--	--	--	--	--	--	--	--	--	--	--	--	--	--	--	--	--	--	--	--	--	--	--	--	--	--	--	--	--	--	--	--	--	--	--	--	--	--	--	--	--	--	--	--	--	--	--	--	--	--	--	--	--	--	--	--	--	--	--	--	--	--	--	--	--	--	--	--	--	--	--	--	--	--	--	--	--	--	--	--	--	--	--	--	--	--	--	--	--	--	--	--	--	--	--	--	--	--	--	--	--	--	--	--	--	--	--	--	--	--	--	--	--	--	--	--	--	--	--	--	--	--	--	--	--	--	--	--	--	--	--	--	--	--	--	--	--	--	--	--	--	--	--	--	--	--	--	--	--	--	--	--	--	--	--	--	--	--	--	--	--	--	--	--	--	--	--	--	--	--	--	--	--	--	--	--	--	--	--	--	--	--	--	--	--	--	--	--	--	--	--	--	--	--	--	--	--	--	--	--	--	--	--	--	--	--	--	--	--	--	--	--	--	--	--	--	--	--	--	--	--	--	--	--	--	--	--	--	--	--	--	--	--	--	--	--	--	--	--	--	--	--	--	--	--	--



TABLE 18. EXPERIMENTAL STUDY RIG DATA (Continued)

TEST POINT 3  
 TEST CONDITION Flameholder Storage Charge  
 NEW ORDER 11.01

Rig Conditions																			
POINT	I	P	H	F A	AMP	FREQ	°	TPH1	TPH2										
50	407	21.5	.060	.041	15.3	60	101	525	825										
51	408	21.4	.059	.042	15.0	60	103.8	645	830										
52	411	21.4	.058	.072	9.3	60	99.4	505	582										
53	409	21.5	.060	.069	12.6	60	92.9	638	627										
54	408	21.6	.060	.101	9.2	60	-	525	655										
55	411	21.5	.058	.105	10.2	25	-	538	622										
56	410	16.1	.068	.125	19	30	-	790	872										
57	397	22.0	.10	.038	10	65	81.1	381	354										
58	398	22.3	.098	.038	10.3	70	85.9	382	355										
59	398	22.0	.101	.050	10.9	70	79.0	378	347										
60	398	22.0	.103	.048	9.1	30	77.1	378	344										
61	400	22.2	.101	.061	7.2	70	79.9	377	346										
62	401	22.1	.101	.062	6.8	70	79.9	378	347										
63	398	22.2	.102	.079	11.2	60	73.6	374	353										
64	398	22.1	.103	.079	13.5	55	75.1	397	380										



TEST POINT <sup>a</sup>	TEST CONDITION	Flamholder Depth Change
4		12.01

140

TABLE 18. EXPERIMENTAL STUDY RIG DATA (Continued)

TEST POINT 3  
 TEST CONDITION Heated Flameholder (22.5°)  
 RUN NUMBER 13.01

Rig Conditions												
POINT	T	P	N	F A	AMP	FREQ	$\eta$	TR1	TR2			
1	242	14.6	.039	.058	3	-	100	-	-			
2	209	14.5	.042	.051	4	-	105	-	-			
3	207	15.2	.043	.057	3	-	88.1	-	-			
4	214	14.8	.070	.053	3	-	81.6	-	-			
5	296	15.8	.031	.049	10	55	105.5	-	-			
6	395	15.5	.054	.044	5.8	60	98.3	-	-			
7	399	9.8	.110	.045	3	-	19.3	-	-			
8	411	15.3	.080	.040	4	65	85.8	-	-			
9	415	16.5	.060	.043	8.5	65	89.0	-	-			
10	417	16.0	.045	.043	10	60	86.5	-	-			
11	418	21.4	.075	.035	11.2	60	74.2	-	-			
12	422	21.2	.071	.041	11.8	62	83.8	-	-			
13	423	20.8	.076	.045	10.6	60	84.0	-	-			



TABLE 18. EXPERIMENTAL STUDY RIG DATA (Continued)

TEST POINT <sup>a</sup>																								
Turbulent Screens (5%)																								
0.01																								
TEST CONDITION																								
RPM NUMBER																								
Transfer Function																								
Rig Condition																								
Point	T	P	N	F A	AMP %	FREQ	P21	F21	Q21	P31	F31	Q31	P42	F42	Q42	P43	F43	Q43	P44	F44	Q44	T	TPR1	TPR2
45	385	14.1	.076	-.054	4.3	-																86.2	260	348
46	386	14.5	.074	-.081	11.7	60	2.0	50	110	1.25	56	95	1.4	56	345	1.32	56	350	1.45	56	345	73.8	490	520
47	388	14.0	.076	-.117	13.2	40	2.05	43	85	1.5	46	70	1.3	52	335	1.2	52	335	1.2	55	340	68.4	596	608
48	387	13.9	.102	-.092	8.6	50																21.9	295	320
49	400	14.3	.112	-.035	7.0	180																74.2	268	353
50	401	14.8	.109	-.056	15.5	50																81.2	268	360
51	403	14.3	.090	-.079	24	60	1.5	50	101	1.2	62	70	1.15	53	340	1.1	53	345	1.15	55	350	86.5	340	421
52	402	14.0	.109	-.037	2.1	180	8	180	25	8	180	180	85	180	140	95	180	140	1.0	180	140	79.2	255	357
53	403	14.5	.112	-.055	12.4	55																81.7	268	359
54	407	14.9	.102	-.076	20.1	70	1.5	50	105	1.2	50	70	1.1	50	340	1.05	50	340	1.15	50	340	86.1	419	475
55	394	13.1	.078	-.050	3.7	-																70.5	290	365
56	394	14.5	.077	-.076	11	60	1.45	55	120	1.25	55	90	1.45	57	340	1.35	55	340	1.40	55	340	85.3	496	496
57	395	14.3	.079	-.101	14	55				8												66.2	815	715
58	393	13.8	.079	-.118	6.5	-																64.8	420	457
59	398	20.8	.126	-.046	14.9	200																61.3	325	359
60	398	20.6	.120	-.025	11.7	180																74.0	330	367
61	398	20.6	.124	-.037	5	160																84.3	300	350
62	398	20.6	.126	-.036	5	170																82.1	300	350
63	395	21.9	.119	-.046	4	-																77.9	290	352
64	397	21.9	.118	-.046	4.1	-																79.2	292	353
65	396	22.4	.113	-.056	5.4	-																74.6	300	364
66	395	22.5	.110	-.058	5.3	-																78.5	297	369
67	395	22.9	.105	-.072	6.1	50																76.9	297	373
68	395	22.8	.109	-.070	12.5	50																71.2	303	384



TABLE 18. EXPERIMENTAL STUDY RIG DATA (Continued)

TEST POINT 7 TEST CONDITION Turbulent Stream (3%) MM H0002 8.01																							
Big Conditions												Transfer Functions											
Point	T	P	R	P A	AMP %	FREQ	P21	G21	P31	F31	Q31	P42	F42	Q42	P43	F43	Q43	P44	F44	Q44	Y	TPH1	TPH2
68	394	22.6	.109	.078	13.3	60															67.5	308	384
70	397	22.4	.110	.093	8	60															85.5	304	872
71	393	22.4	.112	.090	9.8	60															61.3	307	366
72	238	16.4	.08	.044	4.3	-															-	202	226
73	235	16.3	.08	.034	3.5	-															-	191	218
74	233	15.8	.073	.035	8.9	60	2.1	4.7	1.25	49	95	1.35	350	55	1.25	55	350	1.35	55	345	-	203	220
75	235	15.7	.083	.060	7.0	60															-	207	231
76	234	16.1	.064	.086	7.5	60															-	207	231
77	230	16.1	.071	.078	6.8	60															-	207	231
78	228	16.0	.069	.112	4.4	-															-	211	242
79	227	15.3	.075	.133	4.6	-															-	1020	930
80	228	15.1	.071	.144	4.6	60															-	1112	988

TABLE 18. EXPERIMENTAL STUDY RIG DATA (Continued)

TEST POINT 7  
 TEST CONDITION Turbulent Screen (21)  
 NEW MOSES 8.01

Rig Condition																				
POINT	T	P	N	F A	AMP	PRQ	$\eta$	TPR1	TPR2											
81	397	13.3	.090	.036	3.8	-	-	320	337											
82	399	14.8	.080	.073	8.8	60	60.2	627	542											
83	404	14.5	.087	.084	13.1	60	64.3	470	484											
84	No Data																			
85	407	14.0	.083	.143	8.6	50	-	405	433											
86	389	15.0	.110	.046	4.7	-	-	302	381											
87	391	15.9	.117	.062	7.5	60	49.4	346	407											
88	390	15.6	.106	.093	8.3	65	58.4	339	385											
89	391	16.6	.109	.083	9.6	60	45.2	343	373											
90	239	13.5	.089	.032	4.4	-	-	178	232											
91	238	14.9	.070	.062	4.7	-	-	244	300											
92	239	15.0	.083	.093	2.0	50	63.4	715	595											

TABLE 18. EXPERIMENTAL STUDY RIG DATA (Continued)

TEST POWER  
TEST CONDITION  
NEW NUMBER

8

Gasoline Fuel

11.01

Rig Conditions

POINT	T	P	H	F A	AMP	FREQ	$\gamma$	TR1	TR2
1	230	16.0	.055	.057	6.2	50/180	-	650	394
2	250	15.7	.051	.081	4.5	-	-	1000	710
3	249	15.6	.052	.111	2	-	-	1100	760
4	250	15.7	.054	.123	2	-	-	1100	765
5	255	15.4	.051	.131	3.8	-	-	1102	783
6	252	15.5	.052	.129	7.7	55/170	-	1102	790
7	202	20.7	.054	.054	5.8	60/180	96.4	350	230
8	209	18.3	.067	.061	11	55/180	91	582	271
9	208	17.4	.071	.078	3.4	160	81	817	502
10	208	17.3	.072	.082	4.0	-	84	853	506
11	203	23.1	.035	.057	6	55/180	-	500	500
12	202	25.7	.033	.078	2	-	-	1060	845
13	202	25.7	.036	.105	7	50/180	-	1235	930
14	205	25.7	.031	.126	3	-	-	1220	960
15	387	15.4	.047	.078	3	180	-	220	428
16	401	15.4	.055	.084	3.9	-	-	1025	720
17	403	15.4	.054	.127	3	-	-	1187	835
18	407	15.4	.048	.150	5.2	-	-	1198	839
19	385	18.5	.075	.052	17.3	200	87.4	445	311
20	389	16.1	.082	.084	12.4	180	76.2	617	358
21	386	15.2	.093	.077	4	-	87.5	895	585
22	389	24.1	.050	.042	6.6	60	-	640	385
23	388	24.6	.048	.080	2	-	-	1200	860
24	389	24.3	.047	.096	4.5	-	-	1240	917



**TABLE 18. EXPERIMENTAL STUDY RIG DATA (Continued)**

sig Condition									
POINT	T	P	H	P A	AMP	FREQ	$\gamma$	TPH1	TPH2
1	237	14.7	.085	.048	6.8	-	.8973	-	535
2	248	15.3	.093	.044	-	-	.86.4	-	510
3	237	16.6	.096	.040	-	-	.65.5	-	670
4	236	16.7	.116	.033	36	60	41.9	-	360
5	225	22.2	.082	.033	4.5	-	.58.0	-	460
6	225	23.2	.059	.049	5.6	70	98.3	-	706
7	226	23.2	.062	.046	4.4	-	.80.2	-	215
8	226	23.9	.061	.049	6.3	60	90.6	-	752
9	229	25.0	.055	.062	5.6	60	95.5	-	780
10	417	14.9	.082	.041	10	55	61.7	-	659
11	404	15.2	.027	.063	12	60	71.5	-	780
12	415	16.1	.068	.069	19.8	60	67.5	-	1160
13	426	9.2	.078	.126	-	-	-	-	1160
14	428	16.	.083	.059	17.5	60	41.2	-	1025
15	385	15.8	.121	.060	18.2	65	52.4	-	635
16	393	16.4	.082	.060	6	-	.80	-	590
17	396	16.8	.107	.056	30	60	56.2	-	890
18	398	21.0	.087	.081	7	60	52.5	-	1270
19	398	20.3	.065	.066	5	60	104	-	1200
20	398	18.2	.111	.031	16.5	60	36	-	210
21	391	21.3	.103	.058	6.6	55	84.8	-	590
22	391	22.6	.098	.078	15.5	60	80.1	-	1230

TABLE 18. EXPERIMENTAL STUDY RIG DATA (Continued)

TEST POINT<sup>a</sup> 10  
TEST CONDITION Selected Flameholders  
MS NUMBER 10-01

POINT	T	P	H	F A	AMP	PRQ	γ	TPH1	TPH2	
23	200	15.5	.064	.046	7.7	55	85.1	560	835	↑
24	200	16.2	.058	.063	3.8	60	78.7	1170	840	
25	195	14.2	.065	.049	7.7	50	78.5	480	690	
26	201	8.1	.128	.058	1	-	14.4	-	-	
27	201	15.1	.025	.060	6.6	60	81.1	1120	550	Flameholding
28	185	16.1	.078	.036	16	80	70.9	-	-	Off Viewpoint
29	202	15.5	.053	.062	4.8	-	107	-	-	
30	207	16.1	.049	.092	7.4	60	117	1220	775	
31	200	13.6	.100	.039	2	-	63.5	-	-	
32	221	16.5	.079	.041	6.2	60	96.5	-	-	↓
33	206	26.5	.055	.030	1	60	67.7	620	530	
34	204	26.4	.048	.050	4.2	30	112	1320	1090	
35	200	27.4	.044	.044	2	-	115	1480	1425	
36	206	28.2	.046	.075	17	55	91.7	2050	1400	
37	206	28.7	.045	.087	10	-	102	2050	1650	



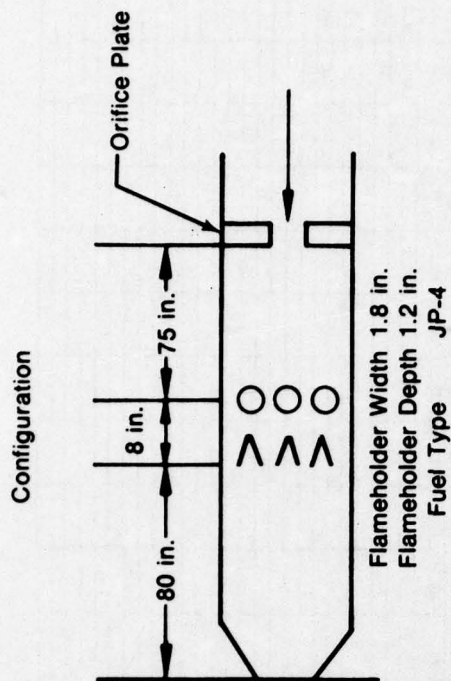
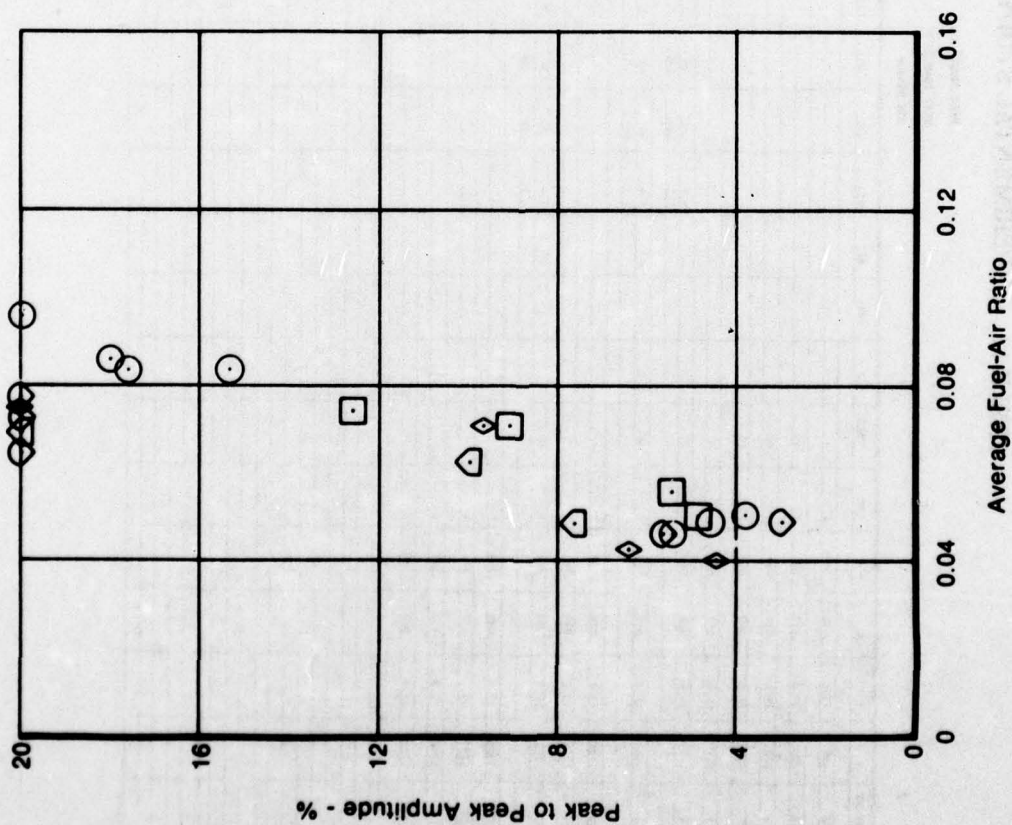
TABLE 18. EXPERIMENTAL STUDY RIG DATA (Continued)

TEST POINT <sup>a</sup>		TEST CONDITION		NEW NUMBER		Transfer Function		Rig Condition		F A		AMP		FREQ		P21	P22	P23	P31	P41	F42	F42	P43	F43	P43	P44	F44	P44	P45	P46	P47	P48	P49	P50	P51	P52	P53	P54	P55	P56	P57	P58	P59	P60	P61	P62	P63	P64	P65	P66	P67	P68	P69	P70	P71	P72	P73	P74	P75	P76	P77	P78	P79	P80	P81	P82	P83	P84	P85	P86	P87	P88	P89	P90	P91	P92	P93	P94	P95	P96	P97	P98	P99	P100	P101	P102	P103	P104	P105	P106	P107	P108	P109	P110	P111	P112	P113	P114	P115	P116	P117	P118	P119	P120	P121	P122	P123	P124	P125	P126	P127	P128	P129	P130	P131	P132	P133	P134	P135	P136	P137	P138	P139	P140	P141	P142	P143	P144	P145	P146	P147	P148	P149	P150	P151	P152	P153	P154	P155	P156	P157	P158	P159	P160	P161	P162	P163	P164	P165	P166	P167	P168	P169	P170	P171	P172	P173	P174	P175	P176	P177	P178	P179	P180	P181	P182	P183	P184	P185	P186	P187	P188	P189	P190	P191	P192	P193	P194	P195	P196	P197	P198	P199	P200	P201	P202	P203	P204	P205	P206	P207	P208	P209	P210	P211	P212	P213	P214	P215	P216	P217	P218	P219	P220	P221	P222	P223	P224	P225	P226	P227	P228	P229	P230	P231	P232	P233	P234	P235	P236	P237	P238	P239	P240	P241	P242	P243	P244	P245	P246	P247	P248	P249	P250	P251	P252	P253	P254	P255	P256	P257	P258	P259	P260	P261	P262	P263	P264	P265	P266	P267	P268	P269	P270	P271	P272	P273	P274	P275	P276	P277	P278	P279	P280	P281	P282	P283	P284	P285	P286	P287	P288	P289	P290	P291	P292	P293	P294	P295	P296	P297	P298	P299	P300	P301	P302	P303	P304	P305	P306	P307	P308	P309	P310	P311	P312	P313	P314	P315	P316	P317	P318	P319	P320	P321	P322	P323	P324	P325	P326	P327	P328	P329	P330	P331	P332	P333	P334	P335	P336	P337	P338	P339	P340	P341	P342	P343	P344	P345	P346	P347	P348	P349	P350	P351	P352	P353	P354	P355	P356	P357	P358	P359	P360	P361	P362	P363	P364	P365	P366	P367	P368	P369	P370	P371	P372	P373	P374	P375	P376	P377	P378	P379	P380	P381	P382	P383	P384	P385	P386	P387	P388	P389	P390	P391	P392	P393	P394	P395	P396	P397	P398	P399	P400	P401	P402	P403	P404	P405	P406	P407	P408	P409	P410	P411	P412	P413	P414	P415	P416	P417	P418	P419	P420	P421	P422	P423	P424	P425	P426	P427	P428	P429	P430	P431	P432	P433	P434	P435	P436	P437	P438	P439	P440	P441	P442	P443	P444	P445	P446	P447	P448	P449	P450	P451	P452	P453	P454	P455	P456	P457	P458	P459	P460	P461	P462	P463	P464	P465	P466	P467	P468	P469	P470	P471	P472	P473	P474	P475	P476	P477	P478	P479	P480	P481	P482	P483	P484	P485	P486	P487	P488	P489	P490	P491	P492	P493	P494	P495	P496	P497	P498	P499	P500	P501	P502	P503	P504	P505	P506	P507	P508	P509	P510	P511	P512	P513	P514	P515	P516	P517	P518	P519	P520	P521	P522	P523	P524	P525	P526	P527	P528	P529	P530	P531	P532	P533	P534	P535	P536	P537	P538	P539	P540	P541	P542	P543	P544	P545	P546	P547	P548	P549	P550	P551	P552	P553	P554	P555	P556	P557	P558	P559	P560	P561	P562	P563	P564	P565	P566	P567	P568	P569	P570	P571	P572	P573	P574	P575	P576	P577	P578	P579	P580	P581	P582	P583	P584	P585	P586	P587	P588	P589	P590	P591	P592	P593	P594	P595	P596	P597	P598	P599	P600	P601	P602	P603	P604	P605	P606	P607	P608	P609	P610	P611	P612	P613	P614	P615	P616	P617	P618	P619	P620	P621	P622	P623	P624	P625	P626	P627	P628	P629	P630	P631	P632	P633	P634	P635	P636	P637	P638	P639	P640	P641	P642	P643	P644	P645	P646	P647	P648	P649	P650	P651	P652	P653	P654	P655	P656	P657	P658	P659	P660	P661	P662	P663	P664	P665	P666	P667	P668	P669	P670	P671	P672	P673	P674	P675	P676	P677	P678	P679	P680	P681	P682	P683	P684	P685	P686	P687	P688	P689	P690	P691	P692	P693	P694	P695	P696	P697	P698	P699	P700	P701	P702	P703	P704	P705	P706	P707	P708	P709	P710	P711	P712	P713	P714	P715	P716	P717	P718	P719	P720	P721	P722	P723	P724	P725	P726	P727	P728	P729	P730	P731	P732	P733	P734	P735	P736	P737	P738	P739	P740	P741	P742	P743	P744	P745	P746	P747	P748	P749	P750	P751	P752	P753	P754	P755	P756	P757	P758	P759	P760	P761	P762	P763	P764	P765	P766	P767	P768	P769	P770	P771	P772	P773	P774	P775	P776	P777	P778	P779	P780	P781	P782	P783	P784	P785	P786	P787	P788	P789	P790	P791	P792	P793	P794	P795	P796	P797	P798	P799	P800	P801	P802	P803	P804	P805	P806	P807	P808	P809	P810	P811	P812	P813	P814	P815	P816	P817	P818	P819	P820	P821	P822	P823	P824	P825	P826	P827	P828	P829	P830	P831	P832	P833	P834	P835	P836	P837	P838	P839	P840	P841	P842	P843	P844	P845	P846	P847	P848	P849	P850	P851	P852	P853	P854	P855	P856	P857	P858	P859	P860	P861	P862	P863	P864	P865	P866	P867	P868	P869	P870	P871	P872	P873	P874	P875	P876	P877	P878	P879	P880	P881	P882	P883	P884	P885	P886	P887	P888	P889	P890	P891	P892	P893	P894	P895	P896	P897	P898	P899	P900	P901	P902	P903	P904	P905	P906	P907	P908	P909	P910	P911	P912	P913	P914	P915	P916	P917	P918	P919	P920	P921	P922	P923	P924	P925	P926	P927	P928	P929	P930	P931	P932	P933	P934	P935	P936	P937	P938	P939	P940	P941	P942	P943	P944	P945	P946	P947	P948	P949	P950	P951	P952	P953	P954	P955	P956	P957	P958	P959	P960	P961	P962	P963	P964	P965	P966	P967	P968	P969	P970	P971	P972	P973	P974	P975	P976	P977	P978	P979	P980	P981	P982	P983	P984	P985	P986	P987	P988	P989	P990	P991	P992	P993	P994	P995	P996	P997	P998	P999	P1000	P1001	P1002	P1003	P1004	P1005	P1006	P1007	P1008	P1009	P1010	P1011	P1012	P1013	P1014	P1015	P1016	P1017	P1018	P1019	P1020	P1021	P1022	P1023	P1024	P1025	P1026	P1027	P1028	P1029	P1030	P1031	P1032	P1033	P1034	P1035	P1036	P1037	P1038	P1039	P1040	P1041	P1042	P1043	P1044	P1045	P1046	P1047	P1048	P1049	P1050	P1051	P1052	P1053	P1054	P1055	P1056	P1057	P1058	P1059	P1060	P1061	P1062	P1063	P1064	P1065	P1066	P1067	P1068	P1069	P1070	P1071	P1072	P1073	P1074	P1075	P1076	P1077	P1078	P1079	P1080	P1081	P1082	P1083	P1084	P1085	P1086	P1087	P1088	P1089	P1090	P1091	P1092	P1093	P1094	P1095	P1096	P1097	P1098	P1099	P1100	P1101	P1102	P1103	P1104	P1105	P1106	P1107	P1108	P1109	P1110	P1111	P1112	P1113	P1114	P1115	P1116	P1117	P1118	P1119	P1120	P1121	P1122	P1123	P1124	P1125	P1126	P1127	P1128	P1129	P1130	P1131	P1132	P1133	P1134	P1135	P1136	P1137	P1138	P1139	P1140	P1141	P1142	P1143	P1144	P1145	P1146	P1147	P1148	P1149	P1150	P1151	P1152	P1153	P1154	P1155	P1156	P1157	P1158	P1159	P1160	P1161	P1162	P1163	P1164	P1165	P1166	P1167	P1168	P1169	P1170	P1171	P1172	P1173	P1174	P1175	P1176	P1177	P1178	P1179	P1180	P1181	P1182	P1183	P1184	P1185	P1186	P1187	P1188	P1189	P1190	P1191	P1192	P1193	P1194	P1195	P1196	P1197	P1198	P1199	P1200	P1201	P1202	P1203	P1204	P1205	P1206	P1207	P1208	P1209	P1210	P1211	P1212	P1213	P1214	P1215	P1216	P1217	P1218	P1219	P1220	P1221	P1222	P1223	P1224	P1225	P1226	P1227	P1228	P1229	P1230	P1231	P1232	P1233	P1234	P1235	P1236	P1237	P1238	P1239	P1240	P1241	P1242	P1243	P1244	P1245	P1246	P1247	P1248	P1249	P1250	P1251	P1252	P1253	P1254	P1255	P1256	P1257	P1258	P1259	P1260	P1261	P1262	P1263	P1264	P1265	P1266	P1267	P1268	P1269	P1270	P1271	P1272	P1273	P1274	P1275	P1276	P1277	P1278	P1279	P1280	P1281	P1282	P1283	P1284	P1285	P1286	P1287	P1288	P1289	P1290	P1291	P1292	P1293	P1294	P1295	P1296	P1297	P1298	P1299	P1300	P1301	P1302	P1303	P1304	P1305	P1306	P1307	P1308	P1309	P1310	P1311	P1312	P1313	P1314	P1315	P1316	P1317	P1318	P1319	P1320	P1321	P1322	P1323	P1324	P1325	P1326	P1327	P1328	P1329	P1330	P1331	P1332	P1333	P1334	P1335	P1336	P1337	P1338	P1339	P1340	P1341	P1342	P1343	P1344	P1345	P1346	P1347	P1348	P1349	P1350	P1351	P1352	P1353	P1354	P1355	P1356	P1357	P1358	P1359	P1360	P1361	P1362	P1363	P1364	P1365	P1366	P1367	P1368	P1369	P1370	P1371	P1372	P1373	P1374	P1375	P1376	P1377	P1378	P1379	P1380	P1381	P1382	P1383	P1384	P1385	P1386	P1387
-------------------------	--	----------------	--	------------	--	-------------------	--	---------------	--	-----	--	-----	--	------	--	-----	-----	-----	-----	-----	-----	-----	-----	-----	-----	-----	-----	-----	-----	-----	-----	-----	-----	-----	-----	-----	-----	-----	-----	-----	-----	-----	-----	-----	-----	-----	-----	-----	-----	-----	-----	-----	-----	-----	-----	-----	-----	-----	-----	-----	-----	-----	-----	-----	-----	-----	-----	-----	-----	-----	-----	-----	-----	-----	-----	-----	-----	-----	-----	-----	-----	-----	-----	------	------	------	------	------	------	------	------	------	------	------	------	------	------	------	------	------	------	------	------	------	------	------	------	------	------	------	------	------	------	------	------	------	------	------	------	------	------	------	------	------	------	------	------	------	------	------	------	------	------	------	------	------	------	------	------	------	------	------	------	------	------	------	------	------	------	------	------	------	------	------	------	------	------	------	------	------	------	------	------	------	------	------	------	------	------	------	------	------	------	------	------	------	------	------	------	------	------	------	------	------	------	------	------	------	------	------	------	------	------	------	------	------	------	------	------	------	------	------	------	------	------	------	------	------	------	------	------	------	------	------	------	------	------	------	------	------	------	------	------	------	------	------	------	------	------	------	------	------	------	------	------	------	------	------	------	------	------	------	------	------	------	------	------	------	------	------	------	------	------	------	------	------	------	------	------	------	------	------	------	------	------	------	------	------	------	------	------	------	------	------	------	------	------	------	------	------	------	------	------	------	------	------	------	------	------	------	------	------	------	------	------	------	------	------	------	------	------	------	------	------	------	------	------	------	------	------	------	------	------	------	------	------	------	------	------	------	------	------	------	------	------	------	------	------	------	------	------	------	------	------	------	------	------	------	------	------	------	------	------	------	------	------	------	------	------	------	------	------	------	------	------	------	------	------	------	------	------	------	------	------	------	------	------	------	------	------	------	------	------	------	------	------	------	------	------	------	------	------	------	------	------	------	------	------	------	------	------	------	------	------	------	------	------	------	------	------	------	------	------	------	------	------	------	------	------	------	------	------	------	------	------	------	------	------	------	------	------	------	------	------	------	------	------	------	------	------	------	------	------	------	------	------	------	------	------	------	------	------	------	------	------	------	------	------	------	------	------	------	------	------	------	------	------	------	------	------	------	------	------	------	------	------	------	------	------	------	------	------	------	------	------	------	------	------	------	------	------	------	------	------	------	------	------	------	------	------	------	------	------	------	------	------	------	------	------	------	------	------	------	------	------	------	------	------	------	------	------	------	------	------	------	------	------	------	------	------	------	------	------	------	------	------	------	------	------	------	------	------	------	------	------	------	------	------	------	------	------	------	------	------	------	------	------	------	------	------	------	------	------	------	------	------	------	------	------	------	------	------	------	------	------	------	------	------	------	------	------	------	------	------	------	------	------	------	------	------	------	------	------	------	------	------	------	------	------	------	------	------	------	------	------	------	------	------	------	------	------	------	------	------	------	------	------	------	------	------	------	------	------	------	------	------	------	------	------	------	------	------	------	------	------	------	------	------	------	------	------	------	------	------	------	------	------	------	------	------	------	------	------	------	------	------	------	------	------	------	------	------	------	------	------	------	------	------	------	------	------	------	------	------	------	------	------	------	------	------	------	------	------	------	------	------	------	------	------	------	------	------	------	------	------	------	------	------	------	------	------	------	------	------	------	------	------	------	------	------	------	------	------	------	------	------	------	------	------	------	------	------	------	------	------	------	------	------	------	------	------	------	------	------	------	------	------	------	------	------	------	------	------	------	------	------	------	------	------	------	------	------	------	------	------	------	------	------	------	------	------	------	------	------	------	------	------	------	------	------	------	------	------	------	------	------	------	------	------	------	------	------	------	------	------	------	------	------	------	------	------	------	------	------	------	------	------	------	------	------	------	------	------	------	------	------	------	------	------	------	------	------	------	------	------	------	------	------	------	------	------	------	------	------	------	------	------	------	------	------	------	------	------	------	------	------	------	------	------	------	------	------	------	------	------	------	------	------	------	------	------	------	------	------	------	------	------	------	------	------	------	------	------	------	------	------	------	------	------	------	------	------	------	------	------	------	------	------	------	------	------	------	------	------	------	------	------	------	------	------	------	------	------	------	------	------	------	------	------	------	------	------	------	------	------	------	------	------	------	------	------	------	------	------	------	------	------	------	------	------	------	------	------	------	------	------	------	------	------	------	------	------	------	------	------	------	------	------	------	------	------	------	------	------	------	------	------	------	------	------	------	------	------	------	------	------	------	------	------	------	------	------	------	------	------	------	------	------	------	------	------	------	------	------	------	------	------	------	------	------	------	------	------	------	------	------	------	------	------	------	------	------	------	-------	-------	-------	-------	-------	-------	-------	-------	-------	-------	-------	-------	-------	-------	-------	-------	-------	-------	-------	-------	-------	-------	-------	-------	-------	-------	-------	-------	-------	-------	-------	-------	-------	-------	-------	-------	-------	-------	-------	-------	-------	-------	-------	-------	-------	-------	-------	-------	-------	-------	-------	-------	-------	-------	-------	-------	-------	-------	-------	-------	-------	-------	-------	-------	-------	-------	-------	-------	-------	-------	-------	-------	-------	-------	-------	-------	-------	-------	-------	-------	-------	-------	-------	-------	-------	-------	-------	-------	-------	-------	-------	-------	-------	-------	-------	-------	-------	-------	-------	-------	-------	-------	-------	-------	-------	-------	-------	-------	-------	-------	-------	-------	-------	-------	-------	-------	-------	-------	-------	-------	-------	-------	-------	-------	-------	-------	-------	-------	-------	-------	-------	-------	-------	-------	-------	-------	-------	-------	-------	-------	-------	-------	-------	-------	-------	-------	-------	-------	-------	-------	-------	-------	-------	-------	-------	-------	-------	-------	-------	-------	-------	-------	-------	-------	-------	-------	-------	-------	-------	-------	-------	-------	-------	-------	-------	-------	-------	-------	-------	-------	-------	-------	-------	-------	-------	-------	-------	-------	-------	-------	-------	-------	-------	-------	-------	-------	-------	-------	-------	-------	-------	-------	-------	-------	-------	-------	-------	-------	-------	-------	-------	-------	-------	-------	-------	-------	-------	-------	-------	-------	-------	-------	-------	-------	-------	-------	-------	-------	-------	-------	-------	-------	-------	-------	-------	-------	-------	-------	-------	-------	-------	-------	-------	-------	-------	-------	-------	-------	-------	-------	-------	-------	-------	-------	-------	-------	-------	-------	-------	-------	-------	-------	-------	-------	-------	-------	-------	-------	-------	-------	-------	-------	-------	-------	-------	-------	-------	-------	-------	-------	-------	-------	-------	-------	-------	-------	-------	-------	-------	-------	-------	-------	-------	-------	-------	-------	-------	-------	-------	-------	-------	-------	-------	-------	-------	-------	-------	-------	-------	-------	-------	-------	-------	-------	-------	-------	-------	-------	-------	-------	-------	-------	-------	-------	-------	-------	-------	-------	-------	-------	-------	-------	-------	-------	-------	-------	-------	-------	-------	-------	-------	-------	-------	-------	-------	-------	-------	-------	-------	-------	-------	-------	-------	-------	-------	-------	-------	-------	-------	-------	-------	-------	-------	-------	-------	-------	-------	-------	-------	-------	-------	-------	-------	-------	-------	-------	-------	-------	-------	-------	-------	-------	-------	-------	-------	-------	-------	-------



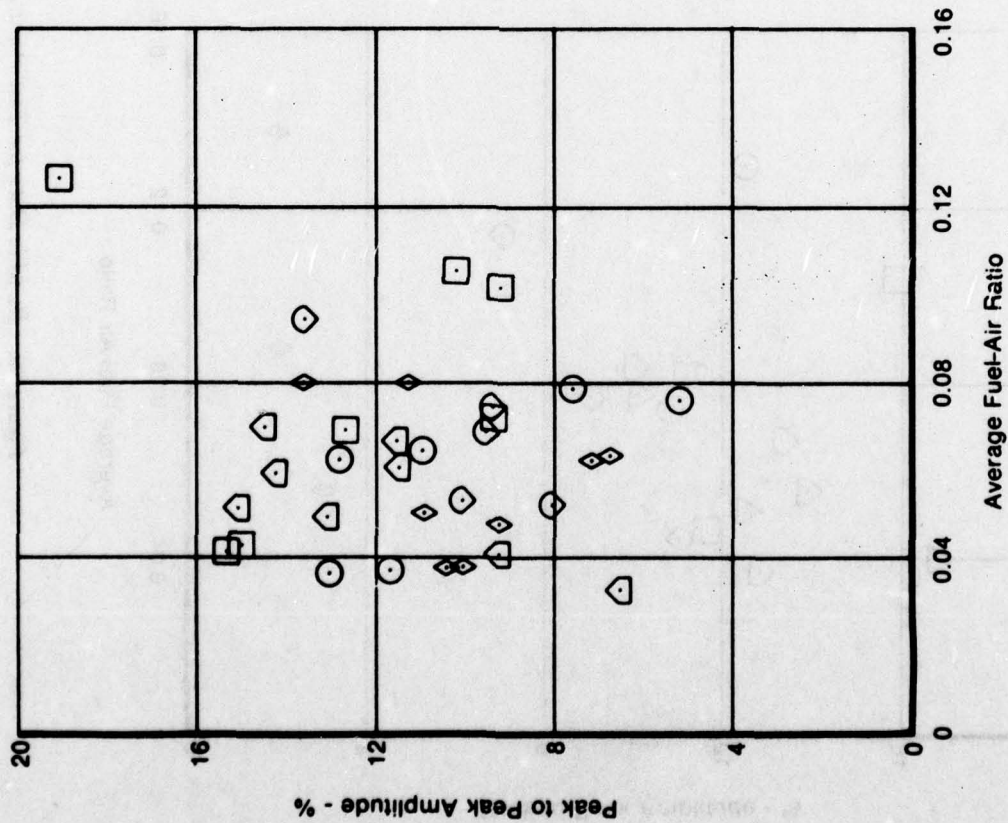
**TABLE 18. EXPERIMENTAL STUDY RIG DATA (Continued)**

[illegible]

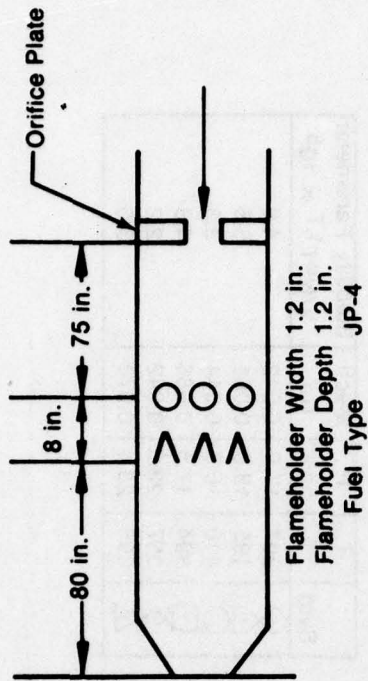


Sym	T °F	P psia	Mach No.	Stability Parameter $V/NPT^{1.7} \times 10^5$
◇	239	14.4	0.083	6.1
○	203	16.6	0.093	6.3
△	410	13.0	0.089	5.2
□	411	13.7	0.091	5.4
○	397	21.5	0.123	4.7

Figure 97. Rumble Data for Test Point Number 1 and 2 — Test Number 7.01



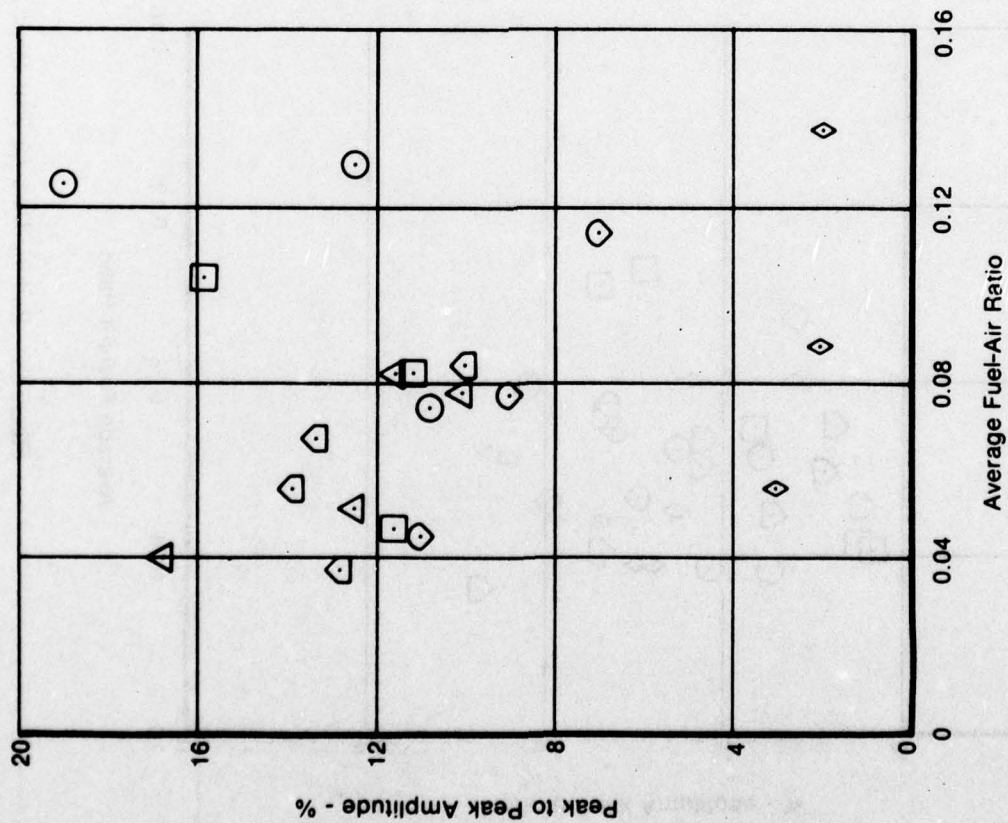
Configuration



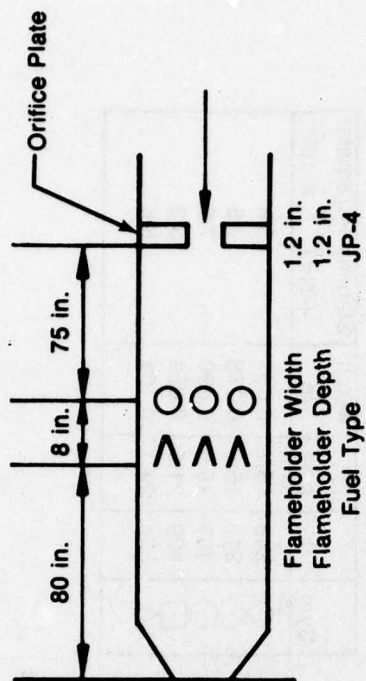
Sym	T °F	P psia	Mach No.	Stability Parameter V/NPT 1.7 x 10 <sup>5</sup>
⊗	248	15.7	0.057	5.6
⊙	213	16.8	0.076	7.5
⊖	407	15.6	0.090	7.0
⊕	409	21.5	0.059	3.3
◇	398	22.1	0.101	5.6

Figure 98. Rumble Data for Test Point Number 3 — Test Number 11.01



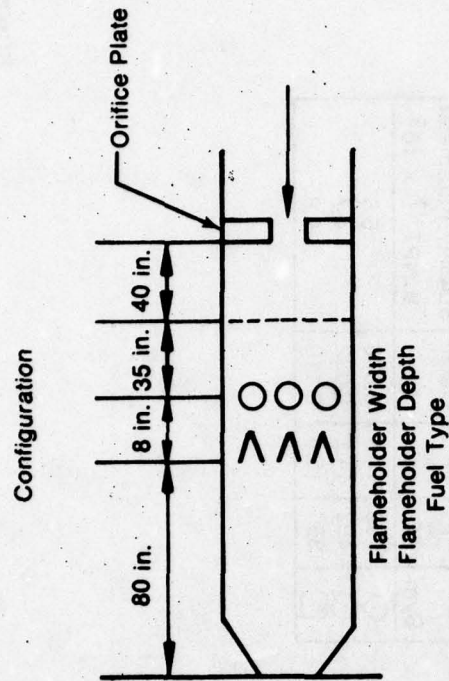
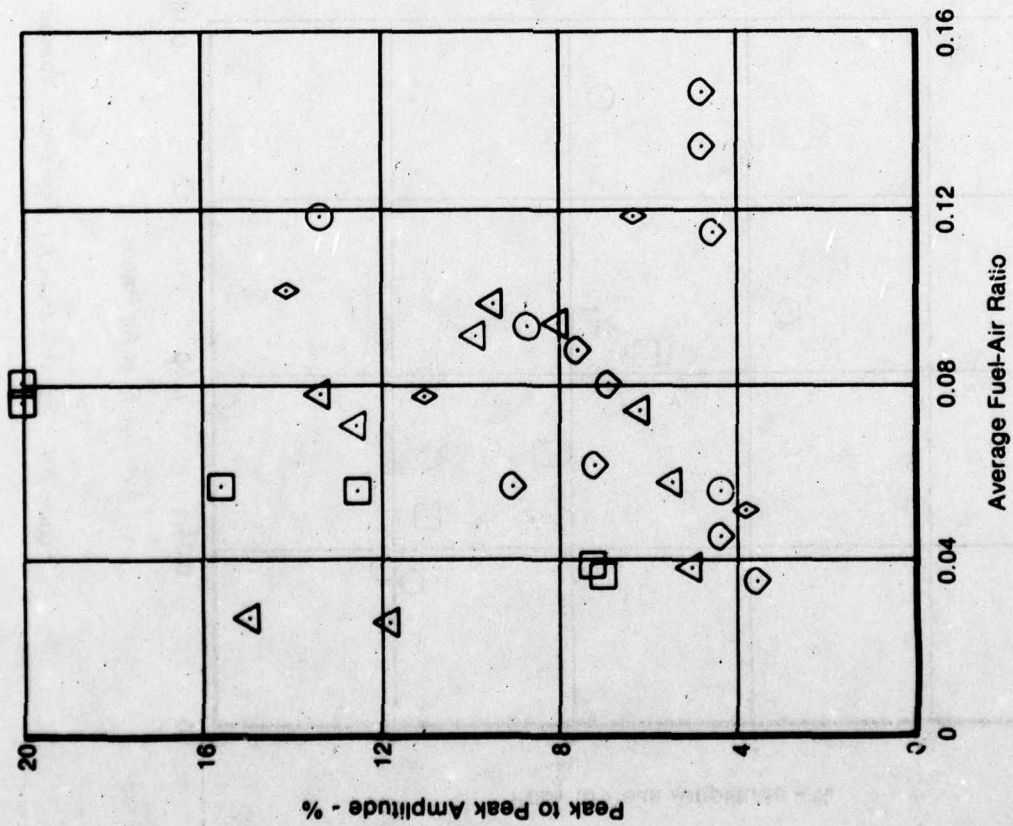


Configuration



Sym	T °F	P psia	Mach No.	Stability Parameter V/NPT <sup>1.7</sup> × 10 <sup>5</sup>
◇	207	17.5	0.042	4.0
◇	195	18.8	0.061	5.5
◇	410	16.3	0.044	3.3
◇	394	17.5	0.068	4.8
◇	397	23.6	0.042	2.2
◇	398	28.4	0.070	3.0

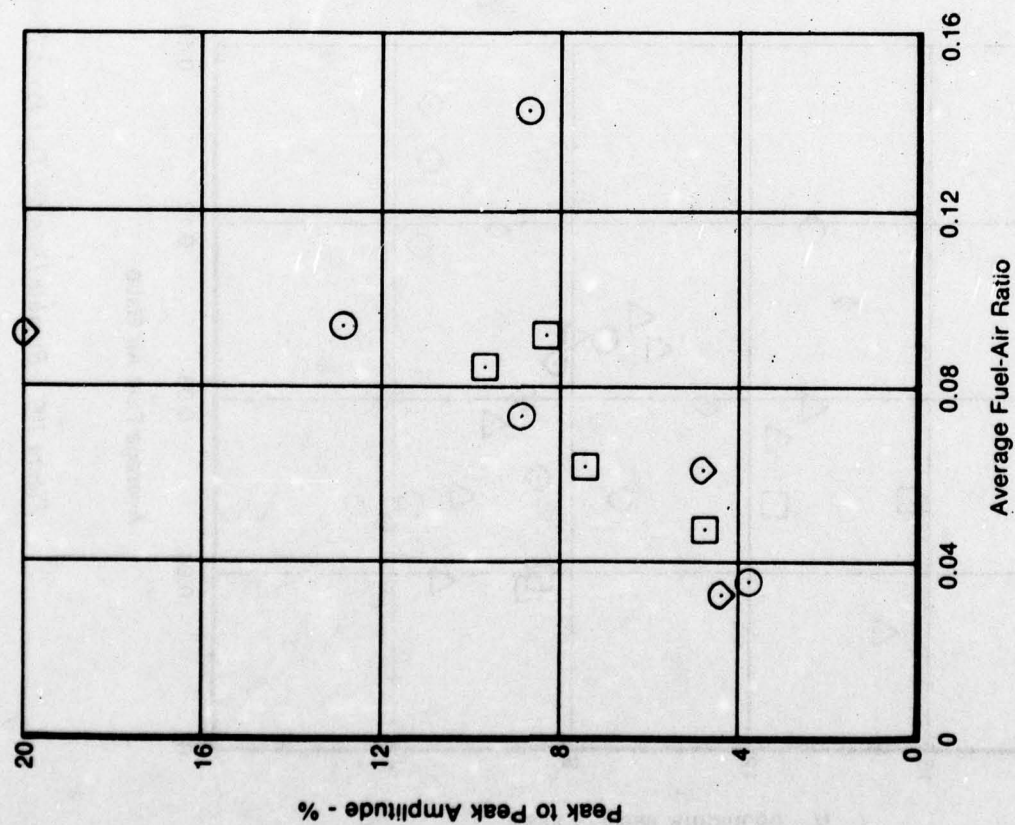
Figure 99. Rumble Data for Test Point Number 4 — Test Number 12.01



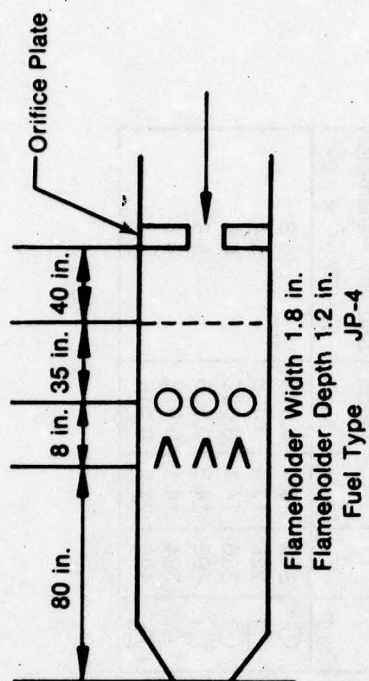
Sym	T °F	P psia	Mach No.	Stability Parameter $V/NPT^{1.7} \times 10^5$
◊	232	15.4	0.070	4.8
△	228	13.4	0.068	5.4
○	386	14.1	0.082	4.5
□	403	14.8	0.106	5.8
◊	394	14.1	0.078	4.6
△	396	21.9	0.116	4.4

FD 140122

Figure 100. Rumble Data for Test Point Number 7 — Test 8.01 (5% ΔP Screen)



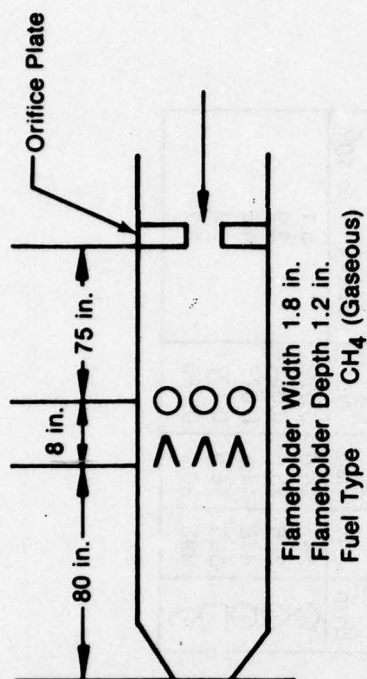
Configuration



Sym	T °F	P psia	Mach No.	Stability Parameter V/NPT <sup>1.7</sup> × 10 <sup>5</sup>
○	239	14.5	0.076	5.5
◌	402	14.2	0.082	4.7
◻	390	15.8	0.110	5.8

Figure 101. Rumble Data for Test Point Number 7 — Test Number 8.01 (2 % ΔP/P Screen)






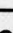



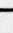
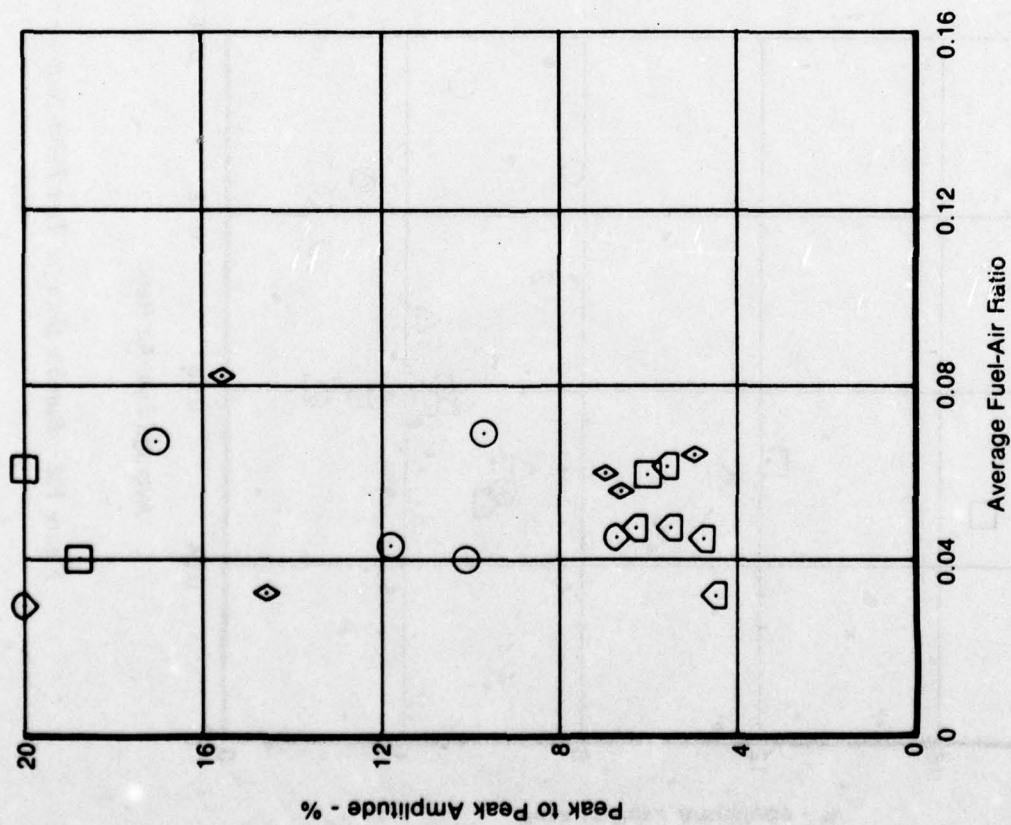
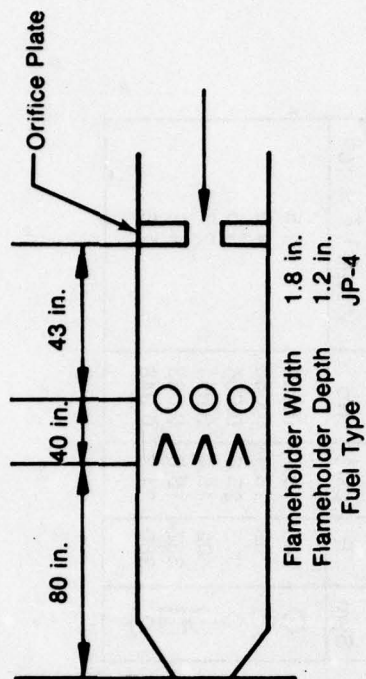
Sym	T °F	P psia	Mach No.	Stability Parameter V/NPT 1.7 × 10 <sup>5</sup>
	248	15.7	0.052	3.5
	209	18.4	0.066	4.0
	203	25.6	0.034	1.5
	402	15.4	0.051	2.7
	387	16.6	0.083	4.2
	389	24.3	0.048	1.6

Figure 102. Rumble Data for Test Point Number 8 — Test Number 11.01 (5%  $\Delta P/P$  Screen)

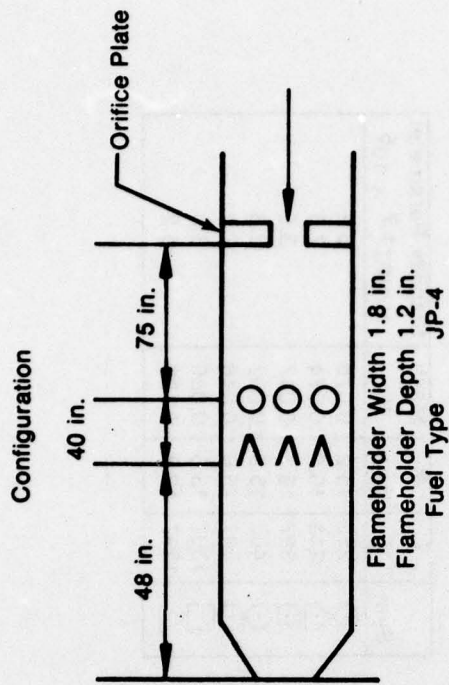
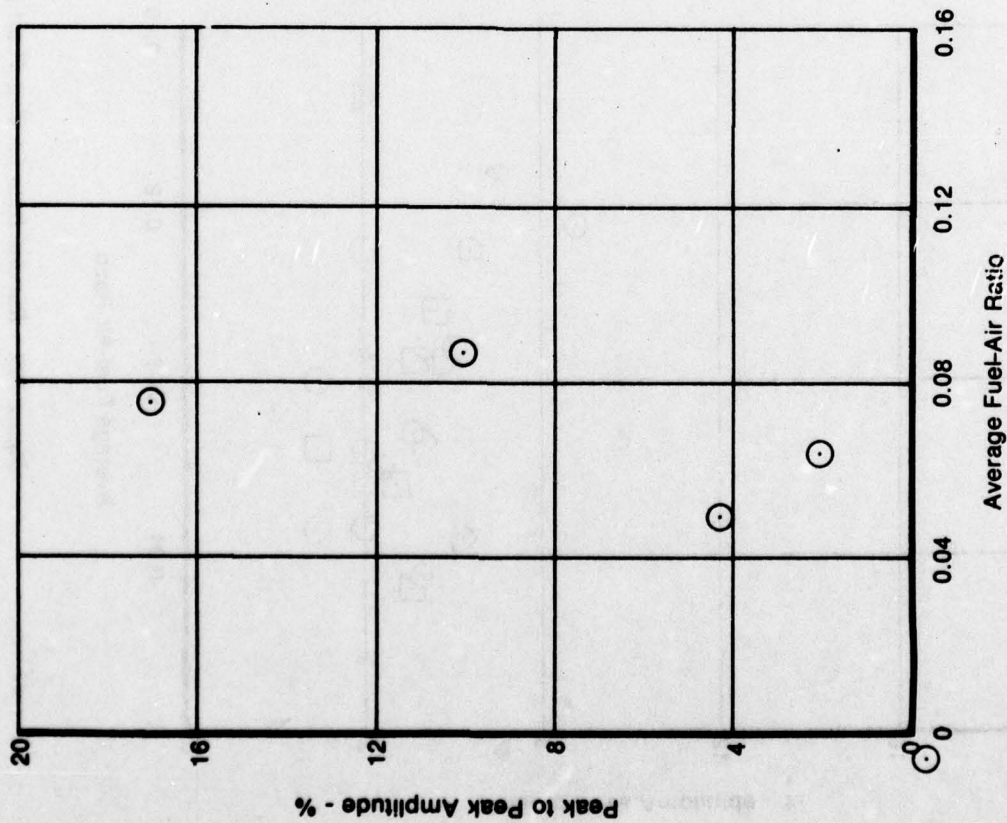


Configuration



Sym	T °F	P psia	Mach No.	Stability Parameter $V/NPT^{1.7} \times 10^5$
◇	242	15.0	0.078	8.1
△	226	23.5	0.064	2.9
○	418	14.3	0.077	4.3
□	395	16.3	0.107	5.4
◇	395	20.9	0.093	3.7

Figure 103. Rumble Data for Test Point Number 9 — Test Number 9.01

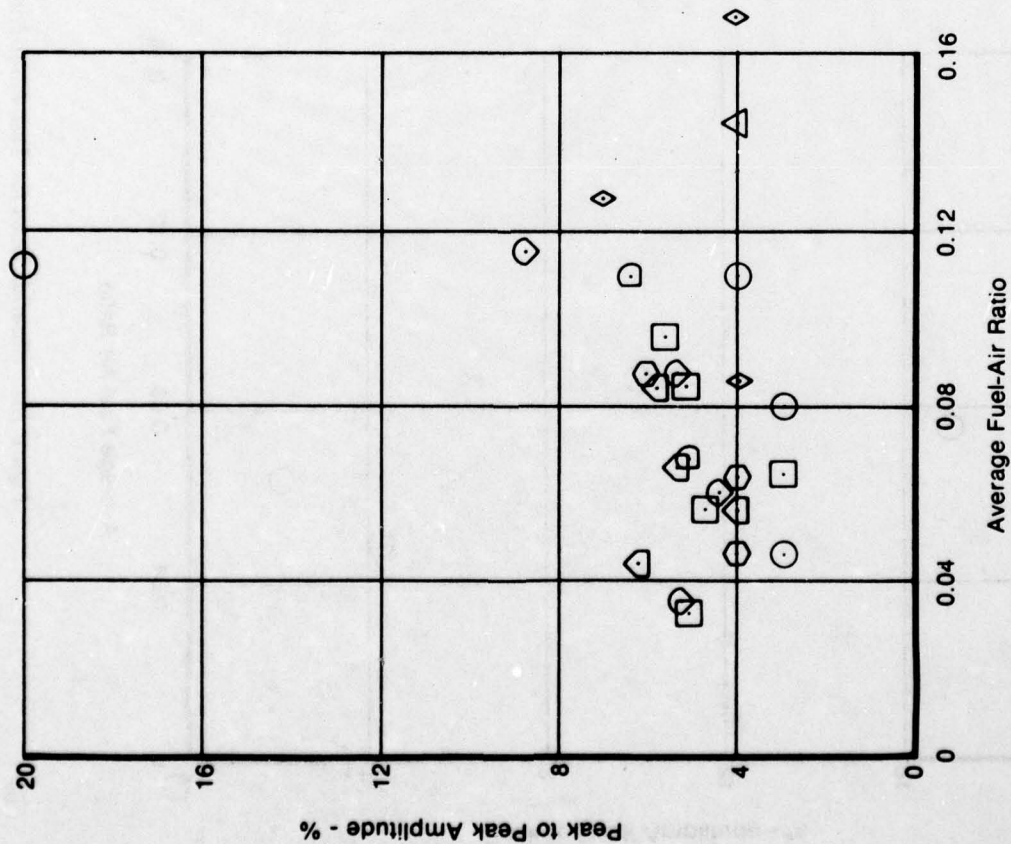


Sym	T °F	P psia	Mach No.	Stability Parameter V/NPT <sup>1.7</sup> x 10 <sup>5</sup>
Q	229	27.7	0.045	1.8

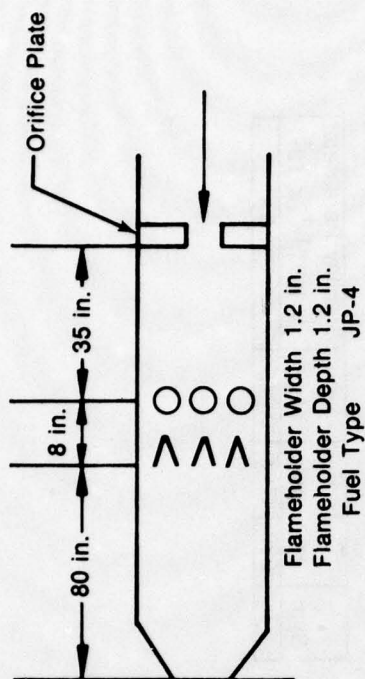
FD 140119

Figure 104. Rumble Data for Test Point Number 10 — Test Number 10.01





Configuration



Sym	T °F	P psia	Mach No.	Stability Parameter $V/NPT^{1.7} \times 10^5$
◇	255	15.2	0.076	6.2
△	213	16.2	0.074	7.5
□	397	16.7	0.047	3.5
○	407	15.9	0.082	6.3
◇	407	25.6	0.046	2.2
△	1307	13.5	0.080	3.0
□	1297	12.8	0.129	5.2

Figure 105. Rumble Data for Test Point Number 11 — Test Number 14.01

## APPENDIX B

### PHASE I — SYSTEM MATH MODEL EQUATIONS

This appendix contains the complete list of system combustion equations used for the rumble model during Phase I when the data were evaluated. A detailed explanation of the assumptions, modeling approach and development of the acoustic equations as well as the combustion equations are included in Section III.C, Task II Formulation of Model.

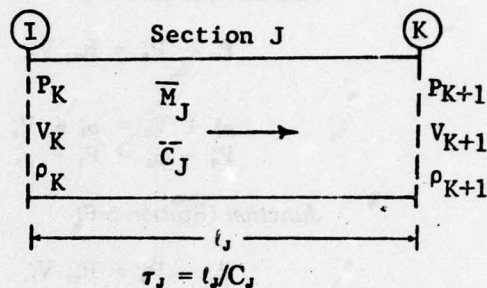
J = section numbers 1, 2, 3, 4, 5, 6

I = upstream station number

K = downstream station number

#### Wave Equations Each Section

J = 1, 2, 3, 4, 5, 6



$$P'_K + \gamma_J M_J V'_K = [P'_I - \gamma_J \bar{M}_J V'_I] e^{\frac{-\tau_J S}{1+M_J}} + \theta_{1J}$$

$$P'_I - \gamma_J M_J V'_I = [P'_K - \gamma_J \bar{M}_J V'_K] e^{\frac{-\tau_J S}{1-M_J}} + \theta_{2J}$$

$$P'_K - \gamma_J \rho'_K = [P'_I - \gamma_J \rho'_I] e^{\frac{-\tau_J S}{M_J}} + \theta_{3J}$$

Note: For J = 5

$$\theta_{1J} = q'_J \frac{\bar{q}}{P} (\gamma-1) \frac{M_J}{S} \left[ e^{\frac{-\tau_J S}{1+M_J}} - e^{\frac{-\tau_J S}{M_J}} \right]$$

$$\theta_{2J} = q'_J \frac{q'}{P} (\gamma-1) \frac{M_J}{S} \left[ 1 - e^{\frac{-\tau_J S}{M_J(1-M_J)}} \right]$$

$$\theta_{3J} = q'_J \frac{q'}{P} (\gamma-1) \frac{\tau_J}{M_J} e^{\frac{-\tau_J S}{M_J}}$$

For all other sections  $\theta_{1J} = \theta_{2J} = \theta_{3J} = 0$

*Upstream Boundary Conditions (Station 1)*

$$\begin{aligned}\rho'_1 + V'_1 &= 0 \\ P'_1 - \rho'_1 &= 0\end{aligned}$$

*Junction (Station 2-3)*

$$P'_2 - P'_3 = R_{23} V'_2, \quad R_{23} = 2 \frac{(P'_2 - P'_3)}{P'_2}$$

$$\begin{aligned}\rho'_2 + V'_2 &= \rho'_3 + V'_3 \\ P'_2 - \rho'_2 &= P'_3 - \rho'_3\end{aligned}$$

*Junction (Station 5-6)*

$$P'_5 - P'_6 = R_{56} V'_5, \quad R_{56} = 2 \frac{(P'_5 - P'_6)}{P'_5}$$

$$\begin{aligned}\rho'_5 + V'_5 &= \rho'_6 + V'_6 \\ P'_5 - \rho'_5 &= P'_6 - \rho'_6\end{aligned}$$

*Downstream Boundary Condition (Station 9)*

$$V'_9 = \frac{1}{2} [P'_9 - \rho'_9]$$

*Input Heat Release Rate*

$$q'_i = q'_{in} e^{\frac{-\tau_i S}{M_i}}$$

*Output Heat Release*

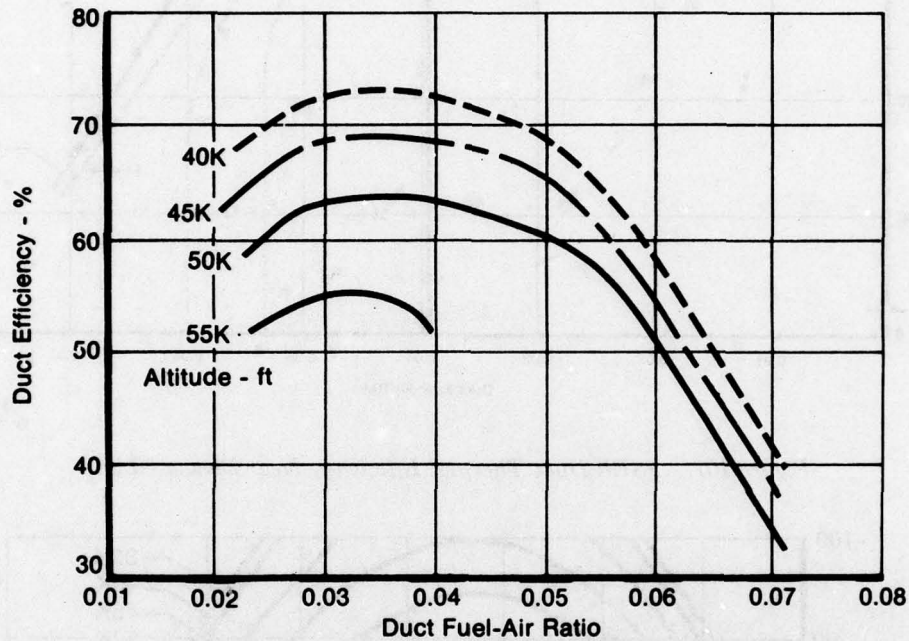
$$\begin{aligned}W'_6 &= \rho'_6 + V'_6 \\ W'_4 &= \rho'_4 + V'_4\end{aligned}$$

$$q'_{out} = W'_6 - \left[ \frac{FA}{T_i} \frac{\partial T_i}{\partial FA} + \frac{FA}{\tilde{\eta}} \frac{\partial \eta}{\partial FA} \right] W'_4 e^{\frac{-\tau_6 S}{M_6}}$$



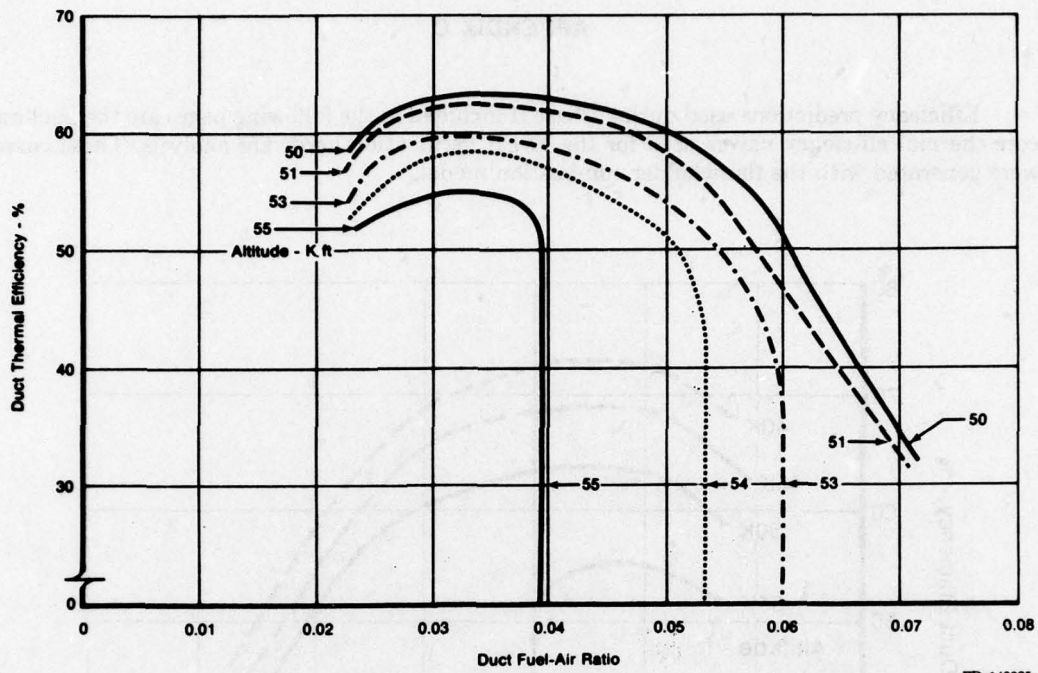
## APPENDIX C

Efficiency predictions used during Phase II included in the following pages are the duct and core thermal efficiency values used for the FSER verification hardware analysis. These curves were generated with the flameholder combustion model.



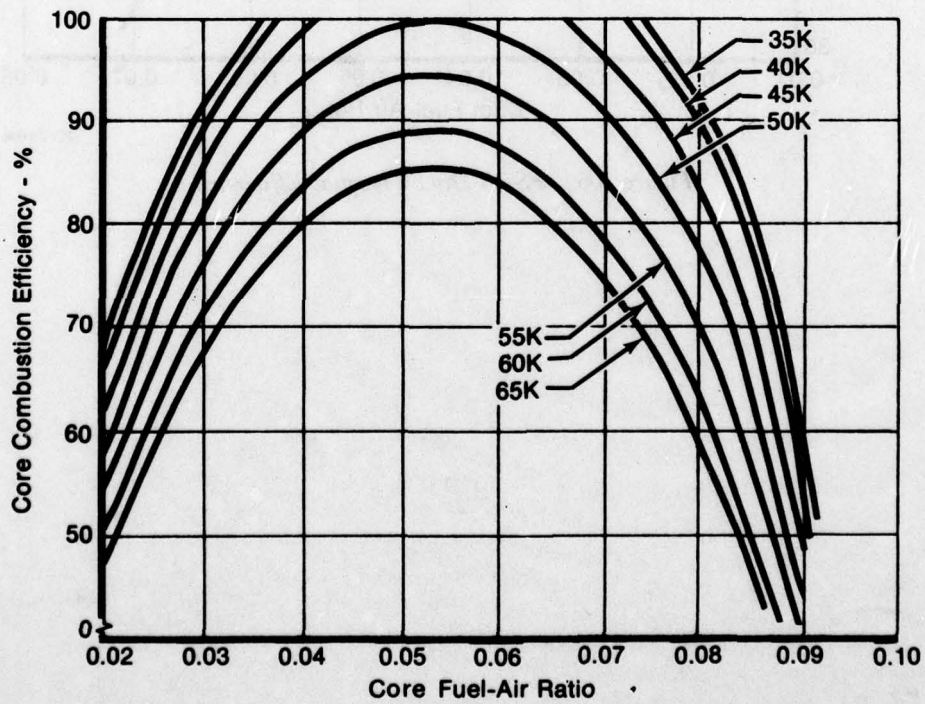
FD 140084

Figure 106. FSER Duct Thermal Efficiency



FD 140085

Figure 107. FSER Duct Thermal Efficiency Near Blowout Limit



FD 140083

Figure 108. FSER Core Thermal Efficiency

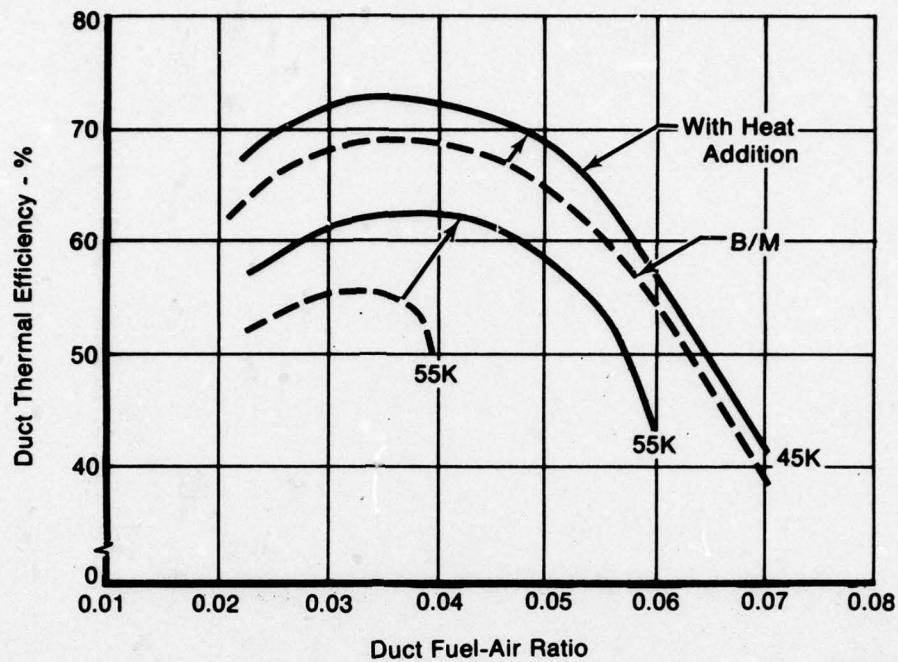


Figure 109. Duct Thermal Efficiency With Heat Addition to Wake of Flameholder

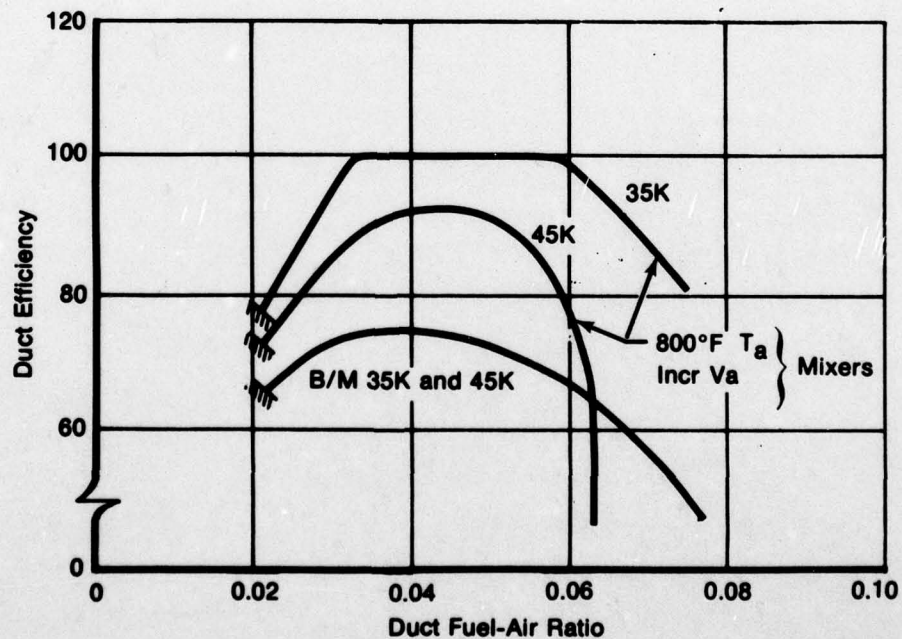


Figure 110. Effect of Mixers on Duct Thermal Efficiency



## APPENDIX D

### 1. DEVELOPMENT OF RUMBLE MODEL EQUATIONS

#### a. General

The augmentor math model consists of a set of time-dependent equations describing the longitudinal dynamics of the flowing air stream and the axially distributed combustion process in the augmentor, coupled with a solution technique for determining stability. These equations are linearized, through the assumption of small perturbations, and transformed from the time-domain to the Laplace transform "S" domain. The solution technique is based upon the Nyquist stability criterion and consists of determining whether the time response of the system to a small disturbance would display oscillatory behavior with a growing amplitude. The result is a determination of stability at a given operating point, regions of operation which will cause rumble, and changes to the augmentor to make it rumble free.

#### b. Development of Acoustic Equations

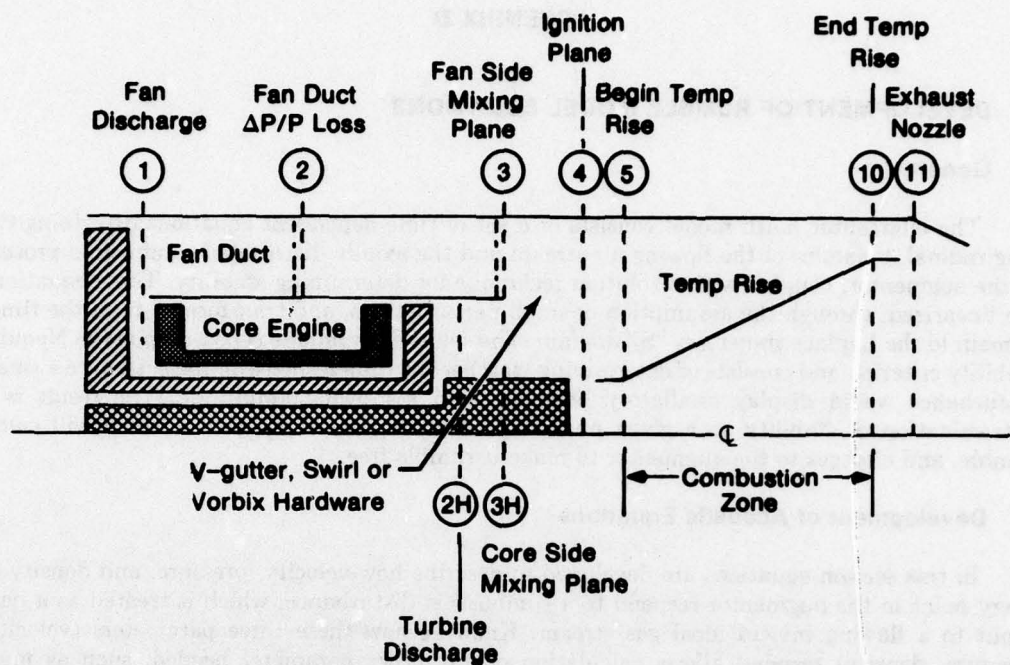
In this section equations are developed to describe how velocity, pressure, and density at every point in the augmentor respond to a combustion disturbance, which is treated as a heat input to a flowing inviscid ideal gas stream. Knowing how these three parameters (velocity, pressure, density) respond allows calculation of any other parameter needed, such as mass flowrate or temperature. The first equations to be developed are the three longitudinal wave equations, which are applicable between boundaries and discontinuities. Then equations for the boundaries and discontinuities are developed. The wave equations plus the boundary and discontinuity equations are referred to as the "acoustic" equations. The "combustion" equations needed to complete the rumble model are developed in part c.

Symbols used below are defined in the List of Symbols. For any section of augmentor with rigid walls and constant cross-sectional area, such as shown in Figure 111, through which an inviscid fluid (viscosity is zero) is flowing, the one-dimensional momentum, continuity, and energy equations are:

$$\begin{aligned}\frac{\partial P}{\partial x} + \rho V \frac{\partial V}{\partial x} + \rho \frac{\partial V}{\partial t} &= 0 \\ \rho \frac{\partial V}{\partial x} + V \frac{\partial \rho}{\partial x} + \frac{\partial \rho}{\partial t} &= 0 \\ q + \frac{PV}{\rho} \frac{\partial \rho}{\partial x} + \frac{P}{\rho} \frac{\partial \rho}{\partial t} &= \rho V \frac{\partial u}{\partial x} + \rho \frac{\partial u}{\partial t}\end{aligned}\tag{31}$$

For an ideal gas, these equations reduce to the following nonlinear wave equations:

$$\begin{aligned}(V+C) \left[ \frac{1}{P} \frac{\partial P}{\partial x} + \frac{\gamma}{C} \frac{\partial V}{\partial x} \right] + \left[ \frac{1}{P} \frac{\partial P}{\partial t} + \frac{\gamma}{C} \frac{\partial V}{\partial t} \right] &= (\gamma-1) \frac{q}{P} \\ (V-C) \left[ \frac{1}{P} \frac{\partial P}{\partial x} - \frac{\gamma}{C} \frac{\partial V}{\partial x} \right] + \left[ \frac{1}{P} \frac{\partial P}{\partial t} - \frac{\gamma}{C} \frac{\partial V}{\partial t} \right] &= (\gamma-1) \frac{q}{P} \\ V \left[ \frac{1}{P} \frac{\partial P}{\partial x} - \frac{\gamma}{\rho} \frac{\partial \rho}{\partial x} \right] + \left[ \frac{1}{P} \frac{\partial P}{\partial t} - \frac{\gamma}{\rho} \frac{\partial \rho}{\partial t} \right] &= (\gamma-1) \frac{q}{P}\end{aligned}\tag{32}$$



FD 146482

Figure 111. Rumble Model Station Identification

The wave equations are linearized by the small perturbation substitutions:

$$\begin{aligned}
 P(x,t) &= \bar{P}(x) + \Delta P(x,t) \\
 \rho(x,t) &= \bar{\rho}(x) + \Delta \rho(x,t) \\
 C(x,t) &= \bar{C}(x) + \Delta C(x,t) \\
 V(x,t) &= \bar{V}(x) + \Delta V(x,t) \\
 q(x,t) &= \bar{q}(x) + \Delta q(x,t)
 \end{aligned}
 \tag{33}$$

Second order terms are neglected in making the substitutions.

To simplify notation, the following substitutions are made which normalize the change in each variable by its steady-state value:

$$P' = \frac{\Delta P}{\bar{P}}, \quad V' = \frac{\Delta V}{\bar{V}}, \quad \rho' = \frac{\Delta \rho}{\bar{\rho}}, \quad q' = \frac{\Delta q}{\bar{q}}
 \tag{34}$$

The linearized version of equations (2) becomes:

$$\begin{aligned}
 (\bar{V} + \bar{C}) \frac{\partial}{\partial x} [P' + \gamma \bar{M} V'] + \frac{\partial}{\partial t} [P' + \gamma \bar{M} V'] + (\gamma - 1) \frac{\bar{q}}{\bar{P}} \beta'_r &= (\gamma - 1) \frac{\bar{q}}{\bar{P}} q' \\
 (\bar{V} - \bar{C}) \frac{\partial}{\partial x} [P' - \gamma \bar{M} V'] + \frac{\partial}{\partial t} [P' - \gamma \bar{M} V'] + (\gamma - 1) \frac{\bar{q}}{\bar{P}} \beta'_a &= (\gamma - 1) \frac{\bar{q}}{\bar{P}} q' \\
 \bar{V} \frac{\partial}{\partial x} [P' - \gamma \rho'] + \frac{\partial}{\partial t} [P' - \gamma \rho'] + (\gamma - 1) \frac{\bar{q}}{\bar{P}} \beta'_z &= (\gamma - 1) \frac{\bar{q}}{\bar{P}} q'
 \end{aligned}
 \tag{35}$$



where:

$$\beta_F' = \frac{1}{(1-M^2)} \left[ P' (1-M-M^2) + \rho' \bar{M} + V' \left\{ \frac{1}{2} + \frac{3}{2} M-M^2 [1 + (1+M) \frac{\gamma}{2}] \right\} \right]$$

$$\beta_G' = \frac{1}{(1-M^2)} \left[ P' (1+M-M^2) + \rho' \bar{M} + V' \left\{ \frac{1}{2} - \frac{3}{2} M-M^2 [1 + (1-M) \frac{\gamma}{2}] \right\} \right]$$

$$\beta_E' = P' + V'$$

Taking the Laplace transform with respect to time, with zero initial conditions, and letting subscripts 1 & 2 stand for the upstream and downstream stations respectively (see Figure 111), the general solution to equations (35) becomes:

$$\begin{aligned} & [P_2' + \gamma \bar{M}_2 V_2'] e^{s \int_0^l \frac{dx}{V+C}} - [P_1' + \gamma \bar{M}_1 V_1'] + \frac{(\gamma-1)}{S} \int_0^l \frac{\bar{q}}{P} \beta_F'(x,s) \frac{d}{dx} e^{s \int_0^x \frac{dx}{V+C}} dx \\ & = \frac{(\gamma-1)}{S} \int_0^l \frac{\bar{q}}{P} q'(x,s) \frac{d}{dx} e^{s \int_0^x \frac{dx}{V+C}} dx \\ & [P_2' - \gamma \bar{M}_2 V_2'] e^{s \int_0^l \frac{dx}{V-C}} - [P_1' - \gamma \bar{M}_1 V_1'] + \frac{(\gamma-1)}{S} \int_0^l \frac{\bar{q}}{P} \beta_G'(x,s) \frac{d}{dx} e^{s \int_0^x \frac{dx}{V-C}} dx \\ & = \frac{(\gamma-1)}{S} \int_0^l \frac{\bar{q}}{P} q'(x,s) \frac{d}{dx} e^{s \int_0^x \frac{dx}{V-C}} dx \quad (37) \\ & [P_2' - \gamma \rho_2'] e^{s \int_0^l \frac{dx}{V}} - [P_1' - \gamma \rho_1'] + \frac{(\gamma-1)}{S} \int_0^l \frac{\bar{q}}{P} \beta_E'(x,s) \frac{d}{dx} e^{s \int_0^x \frac{dx}{V}} dx \\ & = \frac{(\gamma-1)}{S} \int_0^l \frac{\bar{q}}{P} q'(x,s) \frac{d}{dx} e^{s \int_0^x \frac{dx}{V}} dx \end{aligned}$$

In equations (37) the first equation describes downstream running sonic waves of the form  $P' + \gamma \bar{M} V'$ , traveling at sonic speed plus throughflow velocity. The second equation describes upstream running sonic waves of the form  $P' - \gamma \bar{M} V'$ , traveling at sonic speed minus throughflow velocity. The third equation describes entropy waves,  $P' - \gamma \rho'$ , drifting downstream at throughflow velocity.



The entropy waves become more apparent from the expression for the entropy of an ideal gas:

$$\frac{\Delta S}{C_v} = S' = P' - \gamma \rho' \quad (38)$$

The entropy waves are related to temperature by:

$$\gamma T' = S' + (\gamma - 1) P' \quad (39)$$

It is through equation (39) that the drifting hot and cold combustion products, or entropy waves, are accounted for in the rumble model. Temperature changes produced as the entropy waves strike the exhaust nozzle create waves which then travel back upstream at sonic speed.

Equations (37) are not useful until the integrals are evaluated, which will require definitions of  $\bar{V}(x)$ ,  $\bar{C}(x)$ ,  $\bar{q}(x)$ ,  $\bar{P}(x)$  and some assumptions that will allow integration of  $q'(x, S)$ ,  $\beta_f'(x, S)$ ,  $\beta_g'(x, S)$ , and  $\beta_e'(x, S)$ . To complete the solution the augmentor is divided into several "short" sections, each of length  $l$ , for each of which it can be assumed:

- (a)  $\frac{d \bar{P}(x)}{dx} = 0$
- (b)  $\frac{d \bar{T}(x)}{dx} = \text{constant}$
- (c)  $q'(x, t) = q' \left( 0, t - \int_0^x \frac{dx}{\bar{V}} \right)$
- (d)  $\frac{\bar{q}(x)}{\bar{P}(x)} = \text{constant}$

The small static pressure drop in an augmentor justifies assumption (a). A linear temperature rise is also a good approximation, which justifies assumption (b). Assumption (c) is the equation for a "drifting burning particle" releasing heat at a constant volumetric rate as it drifts down the augmentor. A more detailed explanation of this assumption will be provided in part c (Development of Combustion Equations). To justify the constant steady-state heat release rate ( $\bar{q}$ ) consider the steady-state version of the energy equation (third in equations (32)).

$$\bar{V} \left[ \frac{1}{\bar{P}} \frac{d\bar{P}}{dx} - \frac{\gamma}{\bar{\rho}} \frac{d\bar{\rho}}{dx} \right] = (\gamma - 1) \frac{\bar{q}}{\bar{P}}$$

With appropriate substitutions the equation reduces to:

$$\frac{\bar{q}}{\bar{P}} = \left( \frac{\gamma}{\gamma - 1} \right) \frac{R}{\bar{P}} \frac{W}{A} \frac{d\bar{T}}{dx} - \frac{\bar{V}}{\bar{P}} \frac{d\bar{P}}{dx}$$

Since  $\frac{d\bar{P}}{dx} = 0$  and  $\frac{d\bar{T}}{dx} = \text{constant}$ , then

$$\frac{\bar{q}}{\bar{P}} = \text{constant} = \frac{\gamma}{\gamma - 1} \frac{C_p M_1}{l} \left( \frac{T_2}{T_1} - 1 \right) \quad (40)$$

For a "short" section of length  $l$  the integration of  $\beta'_r(x, S)$  in equations (37) can be carried out as follows:

$$\int_0^l \frac{\bar{q}}{P} \beta'_r(x, S) \frac{d}{dx} e^{\int_0^x \frac{dx}{V+C}} dx \approx \frac{\bar{q}}{P} \beta'_r(0, S) \int_0^{l/2} \frac{d}{dx} e^{\int_0^x \frac{dx}{V+C}} dx$$

$$+ \frac{\bar{q}}{P} \beta'_r(l, S) \int_{l/2}^l \frac{d}{dx} e^{\int_0^x \frac{dx}{V+C}} dx$$

Similar treatment allows integration of  $\beta'_G(x, S)$  and  $\beta'_E(x, S)$  in equation (37). To determine how "short" a section must be for the solution to be valid, the resulting rumble model was exercised repeatedly while decreasing the section length (by adding more stations in the combustion zone). As the section length decreases, the result will rapidly approach an exact solution. It was found that section lengths shorter than about 20 inches were unnecessary.

With the above assumptions, equation (37) becomes:

$$[P'_2 + \gamma \bar{M}_2 V'_2 - [P'_1 + \gamma \bar{M}_1 V'_1] e^{-\tau_r S} - (\gamma-1) \frac{\bar{q}}{P} \beta'_{F_1} \left[ \frac{e^{-\tau_r S} - e^{-\tau_{F_2} S}}{S} \right]$$

$$+ (\gamma-1) \frac{\bar{q}}{P} \beta'_{F_2} \left[ \frac{1 - e^{-\tau_{F_2} S}}{S} \right] = (\gamma-1) \frac{\bar{q}}{P} q'_1 \left\{ \bar{M}_1 \left[ \frac{e^{-\tau_r S} - e^{-(\tau_{E_1} + \tau_{F_2}) S}}{S} \right] \right.$$

$$\left. + \bar{M}_2 \left[ \frac{e^{-(\tau_{F_2} + \tau_{E_1}) S} - e^{-\tau_E S}}{S} \right] \right\} \quad (41)$$

$$[P'_1 - \gamma \bar{M}_1 V'_1] - [P'_2 + \gamma \bar{M}_2 V'_2] e^{-\tau_0 S} + (\gamma-1) \frac{\bar{q}}{P} \beta'_{G_1} \left[ \frac{1 - e^{-\tau_{G_1} S}}{S} \right]$$

$$- (\gamma-1) \frac{\bar{q}}{P} \beta'_{G_2} \left[ \frac{e^{-\tau_0 S} - e^{-\tau_{G_1} S}}{S} \right]$$

$$= (\gamma-1) \frac{\bar{q}}{P} q'_1 \left\{ \bar{M}_1 \left[ \frac{1 - e^{-(\tau_{G_1} + \tau_{E_1}) S}}{S} \right] + \bar{M}_2 \left[ \frac{e^{-(\tau_{G_1} + \tau_{E_1}) S} - e^{-(\tau_0 + \tau_E) S}}{S} \right] \right\}$$

$$[P'_2 - \gamma \rho'_2] - [P'_1 - \gamma \rho'_1] e^{-\tau_E S} - (\gamma-1) \frac{\bar{q}}{P} \beta'_{E_1} \left[ \frac{e^{-\tau_E S} - e^{-\tau_{E_2} S}}{S} \right]$$

$$+ (\gamma-1) \frac{\bar{q}}{P} \beta'_{E_2} \left[ \frac{1 - e^{-\tau_{E_2} S}}{S} \right] = (\gamma-1) \frac{\bar{q}}{P} q'_1 \tau_E e^{-\tau_E S}$$

where:

$$\begin{aligned}\tau_F &\equiv \int_0^1 \frac{dx}{V+C} & \tau_G &\equiv - \int_0^1 \frac{dx}{V-C} & \tau_E &\equiv \int_0^1 \frac{dx}{V} \\ \tau_{F_1} &\equiv \int_0^{1/2} \frac{dx}{V+C} & \tau_{G_1} &\equiv - \int_0^{1/2} \frac{dx}{V-C} & \tau_{E_1} &\equiv \int_0^{1/2} \frac{dx}{V}\end{aligned}\quad (42)$$

$$\begin{aligned}\tau_{F_2} &= \tau_F - \tau_{F_1} & \tau_{E_2} &= \tau_E - \tau_{E_1} \\ \beta_{F_1} &\equiv \frac{1}{(1-M_1^2)} \left[ P'_1 (1-\bar{M}_1-\bar{M}_1^2) + \rho'_1 \bar{M}_1 + V'_1 \left\{ \frac{1}{2} + \frac{3}{2} \bar{M}_1 - \bar{M}_1^2 \left[ 1 + (1+\bar{M}_1) \frac{\gamma}{2} \right] \right\} \right] \\ \beta_{F_2} &\equiv \frac{1}{(1-M_2^2)} \left[ P'_2 (1-\bar{M}_2-\bar{M}_2^2) + \rho'_2 \bar{M}_2 + V'_2 \left\{ \frac{1}{2} + \frac{3}{2} \bar{M}_2 - \bar{M}_2^2 \left[ 1 + (1+\bar{M}_2) \frac{\gamma}{2} \right] \right\} \right] \\ \beta_{G_1} &\equiv \frac{1}{(1-M_1^2)} \left[ P'_1 (1+\bar{M}_1-\bar{M}_1^2) - \rho'_1 \bar{M}_1 + V'_1 \left\{ \frac{1}{2} - \frac{3}{2} \bar{M}_1 - \bar{M}_1^2 \left[ 1 + (1-\bar{M}_1) \frac{\gamma}{2} \right] \right\} \right] \\ \beta_{G_2} &\equiv \frac{1}{(1-M_2^2)} \left[ P'_2 (1+\bar{M}_2-\bar{M}_2^2) - \rho'_2 \bar{M}_2 + V'_2 \left\{ \frac{1}{2} - \frac{3}{2} \bar{M}_2 - \bar{M}_2^2 \left[ 1 + (1-\bar{M}_2) \frac{\gamma}{2} \right] \right\} \right] \\ \beta_{E_1} &\equiv P'_1 + V'_1 \\ \beta_{E_2} &\equiv P'_2 + V'_2\end{aligned}\quad (43)$$

For convenience in programming equations (41) on the computer the following identity substitutions were made:

$$\begin{aligned}\beta_{F_1} &= PF_1 P'_1 + RF_1 \rho'_1 + VF_1 V'_1 \\ \beta_{F_2} &= PF_2 P'_2 + RF_2 \rho'_2 + VF_2 V'_2 \\ \beta_{G_1} &= PG_1 P'_1 + RG_1 \rho'_1 + VG_1 V'_1 \\ \beta_{G_2} &= PG_2 P'_2 + RG_2 \rho'_2 + VG_2 V'_2\end{aligned}\quad (44)$$



where by definition:

$$\begin{aligned}
 PF_1 &= \frac{1}{(1-M_1^2)} [1-M_1-M_1^2] \\
 RF_1 &= \frac{M_1}{(1-M_1^2)} \\
 VF_1 &= \frac{1}{(1-M_1^2)} \left\{ \frac{1}{2} + \frac{3}{2} M_1-M_1^2 \left[ 1 + (1+M_1) \frac{\gamma}{2} \right] \right\} \\
 PF_2 &= \frac{1}{(1-M_2^2)} [1 - M_2-M_2^2] \\
 RF_2 &= \frac{M_2}{(1-M_2^2)} \\
 VF_2 &= \frac{1}{(1-M_2^2)} \left\{ \frac{1}{2} + \frac{3}{2} M_2-M_2^2 \left[ 1 + (1+M_2) \frac{\gamma}{2} \right] \right\} \\
 PG_1 &= \frac{1}{(1-M_1^2)} [1-M_1-M_1^2] \\
 RG_1 &= \frac{-M_1}{(1-M_1^2)} \\
 VG_1 &= \frac{1}{(1-M_1^2)} \left\{ \frac{1}{2} - \frac{3}{2} M_1-M_1^2 \left[ 1 + (1-M_1) \frac{\gamma}{2} \right] \right\} \\
 PG_2 &= \frac{1}{(1-M_2^2)} [1 + M_2-M_2^2] \\
 RG_2 &= \frac{-M_2}{(1-M_2^2)} \\
 VG_2 &= \frac{1}{(1-M_2^2)} \left\{ \frac{1}{2} - \frac{3}{2} M_2-M_2^2 \left[ 1 + (1-M_2) \frac{\gamma}{2} \right] \right\}
 \end{aligned} \tag{45}$$

The time constants in equations (42) were evaluated based upon the steady-state throughflow and sonic speed profiles created by the linear temperature gradient.

$$\begin{aligned}
 V(x) &= V_1 \left[ 1 + \left( \frac{T_2}{T_1} - 1 \right) \frac{x}{l} \right] \\
 C(x) &= C_1 \sqrt{1 + \left( \frac{T_2-T_1}{T_1} \right) \frac{x}{l}}
 \end{aligned} \tag{46}$$

Then the time constants in equations (42) become:

$$\begin{aligned}
 \tau_F &= \frac{l/C_1}{\left(\frac{T_2}{T_1} - 1\right)} \frac{2}{\bar{M}_1} \ln \left[ \frac{1 + \bar{M}_1 \sqrt{T_2/T_1}}{1 + \bar{M}_1} \right] \\
 \tau_G &= \frac{l/C_1}{\left(\frac{T_2}{T_1} - 1\right)} \frac{2}{\bar{M}_1} \ln \left[ \frac{1 - \bar{M}_1}{1 - \bar{M}_1 \sqrt{T_2/T_1}} \right] \\
 \tau_E &= \frac{l/C_1}{\left(\frac{T_2}{T_1} - 1\right)} \frac{1}{\bar{M}_1} \ln \left[ \frac{T_2}{T_1} \right] \\
 \tau_{F_1} &= \frac{l/C_1}{\left(\frac{T_2}{T_1} - 1\right)} \frac{2}{\bar{M}_1} \ln \left[ \frac{1 + \bar{M}_1 \sqrt{\frac{1}{2}(1+T_2/T_1)}}{1 + \bar{M}_1} \right] \\
 \tau_{G_1} &= \frac{l/C_1}{\left(\frac{T_2}{T_1} - 1\right)} \frac{2}{\bar{M}_1} \ln \left[ \frac{1 - \bar{M}_1}{1 - \bar{M}_1 \sqrt{\frac{1}{2}(1+T_2/T_1)}} \right] \\
 \tau_{E_1} &= \frac{l/C_1}{\left(\frac{T_2}{T_1} - 1\right)} \frac{1}{\bar{M}_1} \ln \left[ \frac{1}{2}(1+T_2/T_1) \right]
 \end{aligned} \tag{47}$$

This completes the development of the wave equations.

Equations (41) are applied throughout the augmentor between any two stations between which there is no discontinuity. The station designations used for the rumble model are shown in Figure 111. In applying the equations, the general subscripts 1 and 2 are replaced by the actual upstream and downstream station numbers, respectively. Referring to Figure 111 they are applied between stations (1) - (2), (2) - (3), (4) - (5), (5) - (10), and (10) - (11). Between stations (1) through (5) and between stations (10) - (11) there is no heat addition, and so the heat addition terms  $\dot{q}/P$  are set to zero. The heat addition terms for the combustion zone, stations (5) - (10), are discussed in part c.

Discontinuities occur in the pressure drop locations, stations (2) and (3). These are modeled as small incompressible resistive pressure drops of zero length. The continuity and energy equations are so applied.

$$\begin{aligned}
 P_2 - P_3 &\approx \frac{\rho_2 V_2^2}{2} \\
 W_2 &= W_3 \\
 T_2 &= T_3
 \end{aligned} \tag{48}$$

The equations are linearized and normalized as before to yield:

$$P_2' - \left[ 1 - \left( \frac{P_2 - P_3}{P_2} \right) \right] P_3' = \left( \frac{P_2 - P_3}{P_2} \right) (\rho_2' + 2V_2')$$

$$\rho_2' + V_2' = \rho_3' + V_3'$$

$$P_2' - \rho_2' = P_3' - \rho_3'$$
(49)

In applying equations (49) to a given pressure drop the general subscripts 2 and 3 are replaced by the actual upstream and downstream station numbers, respectively. For convenience in programming, equations (49) were combined with the wave equations (41) to eliminate the need for two stations at each pressure drop. It is the combined equations which appear in the rumble model listing.

A junction occurs where the core stream and fan stream enter the augmentor and form the overall augmentor stream (stations (3), (3H), and (4)). Again applying continuity, momentum, and energy:

$$W_3 + W_{3H} = W_4$$

$$\left( \frac{P - P_4}{P} \right) \begin{matrix} \text{FAN SIDE} \\ \text{OR} \\ \text{CORE SIDE} \end{matrix} \approx \left( \frac{W\sqrt{T}}{P} \right)^2 \begin{matrix} \text{FAN SIDE} \\ \text{OR} \\ \text{CORE SIDE} \end{matrix}$$

$$W_3 T_3 + W_{3H} T_{3H} = W_4 T_4$$
(50)

The linearized and normalized versions become:

$$\rho_4' + V_4' = \left( \frac{BPR}{1+BPR} \right) \rho_3' + \left( \frac{BPR}{1+BPR} \right) V_3' + \left( \frac{1}{1+BPR} \right) \rho_{3H}' + \left( \frac{1}{1+BPR} \right) V_{3H}'$$

$$P_4' - \left[ 1 - \left( \frac{P_3 - P_4}{P_3} \right) \right] P_3' = 2 \left( \frac{P_3 - P_4}{P_3} \right) \left( \frac{BPR}{1+BPR} \right) V_3'$$

$$+ \left( \frac{P_3 - P_4}{P_3} \right) \left( \frac{BPR}{1+BPR} \right) \rho_3' + 2 \left( \frac{P_3 - P_4}{P_3} \right) \left( \frac{1}{1+BPR} \right) V_{3H}'$$

$$+ \left( \frac{P_3 - P_4}{P_3} \right) \left( \frac{1}{1+BPR} \right) \rho_{3H}'$$

$$P_{3H}' - \left[ 1 - \left( \frac{P_3 - P_4}{P_3} \right) \right] P_3' = 2 \left( \frac{P_3 - P_4}{P_3} \right) \left( \frac{BPR}{1+BPR} \right) V_3'$$

$$+ \left( \frac{P_3 - P_4}{P_3} \right) \left( \frac{BPR}{1+BPR} \right) \rho_3' + 2 \left( \frac{P_3 - P_4}{P_3} \right) \left( \frac{1}{1+BPR} \right) V_{3H}'$$

$$+ \left( \frac{P_3 - P_4}{P_3} \right) \left( \frac{1}{1+BPR} \right) \rho_{3H}'$$
(51)



AD-A065 144

PRATT AND WHITNEY AIRCRAFT GROUP WEST PALM BEACH FL 6--ETC F/G 21/5  
LO-FREQUENCY AUGMENTOR INSTABILITY STUDY.(U)

DEC 78 P L RUSSELL, G BRANT

F33615-76-C-2024

UNCLASSIFIED

PWA-FR-10397

AFAPL-TR-78-82

NL

3 OF 3

AD  
A065144



END  
DATE  
FILMED  
4 -79  
DDC

The equations are linearized and normalized as before to yield:

$$P_2' - \left[ 1 - \left( \frac{P_2 - P_1}{P_1} \right) \right] P_3' = \left( \frac{P_2 - P_1}{P_1} \right) (\rho_2' + 2V_2')$$

$$\rho_2' + V_2' = \rho_3' + V_3'$$

$$P_2' - \rho_2' = P_3' - \rho_3'$$
(49)

In applying equations (49) to a given pressure drop the general subscripts 2 and 3 are replaced by the actual upstream and downstream station numbers, respectively. For convenience in programming, equations (49) were combined with the wave equations (41) to eliminate the need for two stations at each pressure drop. It is the combined equations which appear in the rumble model listing.

A junction occurs where the core stream and fan stream enter the augmentor and form the overall augmentor stream (stations (3), (3H), and (4)). Again applying continuity, momentum, and energy:

$$W_3 + W_{3H} = W_4$$

$$\left( \frac{P - P_4}{P} \right) \begin{matrix} \text{FAN SIDE} \\ \text{OR} \\ \text{CORE SIDE} \end{matrix} \approx \left( \frac{W\sqrt{T}}{P} \right)^2 \begin{matrix} \text{FAN SIDE} \\ \text{OR} \\ \text{CORE SIDE} \end{matrix}$$

$$W_3 T_3 + W_{3H} T_{3H} = W_4 T_4$$
(50)

The linearized and normalized versions become:

$$\rho_4' + V_4' = \left( \frac{BPR}{1+BPR} \right) \rho_3' + \left( \frac{BPR}{1+BPR} \right) V_3' + \left( \frac{1}{1+BPR} \right) \rho_{3H}' + \left( \frac{1}{1+BPR} \right) V_{3H}'$$

$$P_3' - \left[ 1 - \left( \frac{P_3 - P_4}{P_3} \right) \right] P_4' = 2 \left( \frac{P_3 - P_4}{P_3} \right) \left( \frac{BPR}{1+BPR} \right) V_3'$$

$$+ \left( \frac{P_3 - P_4}{P_3} \right) \left( \frac{BPR}{1+BPR} \right) \rho_3' + 2 \left( \frac{P_3 - P_4}{P_3} \right) \left( \frac{1}{1+BPR} \right) V_{3H}'$$

$$+ \left( \frac{P_3 - P_4}{P_3} \right) \left( \frac{1}{1+BPR} \right) \rho_{3H}'$$

$$P_{3H}' - \left[ 1 - \left( \frac{P_3 - P_4}{P_3} \right) \right] P_4' = 2 \left( \frac{P_3 - P_4}{P_3} \right) \left( \frac{BPR}{1+BPR} \right) V_3'$$

$$+ \left( \frac{P_3 - P_4}{P_3} \right) \left( \frac{BPR}{1+BPR} \right) \rho_3' + 2 \left( \frac{P_3 - P_4}{P_3} \right) \left( \frac{1}{1+BPR} \right) V_{3H}'$$

$$+ \left( \frac{P_3 - P_4}{P_3} \right) \left( \frac{1}{1+BPR} \right) \rho_{3H}'$$
(51)

$$\begin{aligned}
 V_4' + P_4' &= \left[ \frac{\text{BPR} (T_c/T_H)}{1 + \text{BPR} (T_c/T_H)} \right] P_3' + \left[ \frac{\text{BPR} (T_c/T_H)}{1 + \text{BPR} (T_c/T_H)} \right] \\
 &= \left[ \frac{1}{1 + \text{BPR} (T_c/T_H)} \right] P_{3H}' + \left[ \frac{1}{1 + \text{BPR} (T_c/T_H)} \right]
 \end{aligned}$$

For the Swirl augmentor, the momentum equations at stations (3) - (4) and (3H) - (4) are modified to account for the possibility of different pressure drops across the fan and core swirl vanes. The linearized version of the momentum equations for the Swirl augmentor becomes:

$$\begin{aligned}
 P_3' - \left[ 1 - \left( \frac{P_3 - P_4}{P_3} \right) \right] P_4' &= 2 \left( \frac{P_3 - P_4}{P_3} \right) V_3' + \left( \frac{P_3 - P_4}{P_3} \right) \rho_3' \\
 P_{3H}' - \left[ 1 - \left( \frac{P_{3H} - P_4}{P_{3H}} \right) \right] P_4' &= 2 \left( \frac{P_{3H} - P_4}{P_{3H}} \right) V_{3H}' + \left( \frac{P_{3H} - P_4}{P_{3H}} \right) \rho_{3H}'
 \end{aligned} \tag{52}$$

Definition of the upstream and downstream boundary conditions, at the fan and at the nozzle, respectively, will complete the acoustic equations. The fan was assumed to be delivering a constant mass flowrate through the fan OD (defined as that portion of the fan between the fan splitter and fan tip) and through the fan ID (defined as that portion of the fan between the centerline and the fan splitter). It was also assumed that the temperature of the fan discharge flow could be taken as time invariant (also, because of the low Mach number at fan discharge, total and static temperatures can be used interchangeably). To account for the presence of a core engine, and explore any possible attendant interaction with fan duct acoustics, a simple first order lag representation of the core engine was incorporated into the rumble model. The core engine was represented as a compressor delivering constant corrected airflow (corrected to compressor face conditions) into a lumped volume. Flow out of the volume exited through a choked turbine to emerge at station (3H). The resulting transfer function for the core engine is:

$$\frac{W_{3H}'}{P_C'} = \frac{1}{1 + \tau_{\text{CORE}} S} \tag{53}$$

Where:

$$\begin{aligned}
 W_{3H}' &= \text{mass flowrate at station (3H)} \\
 P_C' &= \text{static pressure at the compressor face} \\
 \tau_{\text{CORE}} &= \text{core engine time constant}
 \end{aligned}$$

A default value of  $\tau_{\text{CORE}} = 0.005$  seconds is built into the rumble model. A different value can be input by the user, and is calculated as the mass of air in the core engine volume divided by the mass flowrate of air through the core engine. Proximity of the fan splitter to fan discharge also affects the boundary condition at the fan. Two cases were considered and are built into the rumble model. (See NFSOP.) In the first case, called the "proximate" splitter configuration, the fan splitter is assumed to be so close to fan discharge that no communication can occur between the fan duct and the core engine across the fan splitter. For this case the boundary condition at the fan becomes:

$$\begin{aligned}
 P_C' &= W_{3H}' = 0 \\
 W_1' &= \rho_1' + V_1' = 0 \\
 T_1' &= P_1' - \rho_1' = 0
 \end{aligned} \tag{54}$$



In the second case, called the "remote" splitter configuration, the fan splitter is assumed to be sufficiently remote from fan discharge to allow perfect communication between the fan duct and the core engine across the fan splitter. For this case, the boundary condition at the fan becomes:

$$\begin{aligned} P'_c &= P'_1 \\ W'_1 &= \rho'_1 + V'_1 = -\frac{P'_1}{BPR} \\ T'_1 &= P'_1 - \rho'_1 = 0 \\ W'_{sH} &= \frac{P'_1}{1 + \tau_{CORE} S} \end{aligned} \quad (55)$$

This completes definition of the upstream boundary condition. It is of interest to note that entropy waves are created by sonic wave reflections at the upstream boundary. Since an entropy perturbation is  $S'_1 = P'_1 - \gamma \rho'_1$ , and at the boundary  $\rho'_1 = P'_1$ , then  $S'_1 = (1-\gamma)P'_1$ . A similar argument will show that entropy waves are also created at the pressure drops (Stations (2) and (3)). These are automatically accounted for in the rumble model, but are of minor importance compared to the entropy waves created in the combustion zone by combustion disturbances.

The downstream boundary condition is based upon the presence of a "short" nozzle just downstream of Station (11), for which:

$$\frac{W \sqrt{T_o R}}{A P_o} = \phi(P_R) \quad (56)$$

where:

$$\phi = \frac{\left[ \left( P_R^{\frac{\gamma-1}{\gamma}} - 1 \right) \left( \frac{2}{\gamma-1} \right) \right]^{\frac{\gamma}{2}}}{P_R^{\frac{\gamma+1}{2\gamma}}}$$

$P_R = P_o$  /nozzle throat static pressure

$$P_R \leq \left( \frac{\gamma+1}{2} \right)^{\frac{\gamma}{\gamma-1}}$$

When linearized, the downstream boundary condition becomes:

$$V'_{11} = \frac{1}{2} (P'_{11} - \rho'_{11}) + (KNOZ) P'_{11} \quad (57)$$

where:

$$KNOZ = \frac{\left[ 1 + \left( \frac{\gamma+1}{2} \right) \bar{M}_{11} \right] \left( \frac{P_R}{\phi} \frac{\partial \phi}{\partial P_R} \right)}{[1 - \bar{M}_{11}^2 (1+\gamma)] \left( \frac{P_R}{\phi} \frac{\partial \phi}{\partial P_R} \right)}$$

$$\frac{P_R}{\phi} \frac{\partial \phi}{\partial P_R} = \left[ \frac{P_R^{\frac{\gamma-1}{\gamma}}}{2 \left( P_R^{\frac{\gamma-1}{\gamma}} - 1 \right)} - \frac{\gamma+1}{2(\gamma-1)} \right] \left( \frac{\gamma-1}{\gamma} \right)$$

It is also of interest to note that for choked flow,

$$P_R \geq \left( \frac{\gamma+1}{2} \right)^{\frac{\gamma}{\gamma-1}},$$

then  $KNOZ = 0$  and;

$$V_{11} = \frac{1}{2}(P_{11} - \rho_{11}) = \frac{1}{2}T_{11} \quad (58)$$

substituting from equation (46):

$$V_{11} = \frac{1}{2\gamma} S_{11} + \frac{(\gamma-1)}{2\gamma} P_{11} \quad (59)$$

This equation directly relates how entropy waves, as well as pressure disturbances, striking a choked nozzle will produce a velocity disturbance.

This completes the acoustic equation development. These equations describe the response of pressure, velocity, and density throughout the augmentor to a disturbance in combustion. Development of the corresponding combustion equations, which describe how combustion throughout the augmentor will respond to disturbances in pressure, velocity, and density, is presented in the following section.

### c. Development of Combustion Equations

Development of the combustion equations for the V-gutter flameholder augmentor is presented first. Then the combustion equations for Vorbix and Swirl augmentors are presented.

For the V-gutter flameholder augmentor, two combustion streams, the fan stream and the core stream, are treated. This is necessary to be able to account for the different combustion characteristics of the fan and core streams. The two streams can have different flameholder designs and fuel-air ratios as well as different flameholder approach temperatures and velocities, causing the two streams to have different efficiency vs fuel-air characteristics. In addition, the fan stream is preceded by a long fan duct which can exhibit longitudinal resonance at the low frequencies associated with rumble. The core stream is preceded by a short section terminating at turbine discharge, which is much less responsive at low frequencies.



The basic approach taken for the rumble model was to model combustion disturbances in the fan and core streams independently, accounting for the individual properties of each stream. The resulting two combustion disturbances (calculated as volumetric heat release rate disturbances) were then simply added to form a single overall disturbance. The overall disturbance was then distributed evenly over the total cross-sectional area of the augmentor, which was taken to consist of a single overall stream with mean mixed properties. This approach accounts for the different combustion characteristics of the fan and core streams, while avoiding the complexities associated with a rigorous treatment of the radial as well as the axial distribution of combustion throughout the augmentor.

Experience with modeling the combustion process as a plane heat addition (with all combustion taking place in zero length) had shown that the resulting predictions of rumble were sensitive to the axial location chosen for the plane. Since combustion actually takes place over a distance of 30 to 60 in., it was decided that the axially distributed nature of the burning should be accounted for. This was accomplished by dividing the combustion zone into a number of axial sections, each of length  $\Delta x$ , as explained in part b, (Development of Acoustic Equations).

Combustion equations used in the rumble model are based upon an extension of empirical steady-state processes to the case of time variant flow. A schematic of the steady-state processes is shown in Figure 112. Consider first that the augmentor contains only the fan stream. An identical set of equations will exist for the parallel core stream. Following a particle of air as it moves through the augmentor, the following steps will occur:

- Particle of air picks up fuel as it crosses the spraybar
- Particle drifts at throughflow velocity to the flameholder, Station (4)
- Particle is ignited by the flameholder wake as it drifts from the flameholder, to the beginning of the combustion zone, Station (5) (defined as the location where the bulk fluid temperature begins to rise sharply)
- Particle drifts and burns from Station (5) to the end of the combustion zone, Station (10) (defined as the location where bulk fluid temperature ceases its sharp rise).

It was determined (see equation (40)) that for a linear temperature gradient, the steady-state volumetric heat release rate in the augmentor could be taken as independent of axial position. This implies that at steady state, a particle of fuel-air mixture, drifting and burning through the combustion zone, has a volumetric heat release rate that is independent of axial position. The rate can be computed directly from the flowrate, ideal temperature rise, efficiency, and combustion zone volume of the augmentor.

$$q = \frac{C_p}{v} W T_i \eta \quad (60)$$

For small perturbations, it was assumed that transiently the volumetric heat release rate of a particle could still be taken as independent of axial position, and that equation (60) could be used to compute the rate when  $W$ ,  $T_i$ , and  $\eta$  are referenced to instantaneous approach conditions. The resulting equation will model combustion as though it behaves in a quasi-steady manner. The volumetric heat release rate at any location in the combustion zone will reach the steady-state value corresponding to instantaneous conditions at the flameholder and at the spraybar after a delay. The delay is the time required to purge the old combustion gases and refill with new combustion gases traveling at throughflow velocity.





For the fan stream, instantaneous approach conditions are taken to be the instantaneous conditions at Station (3). Because of the large pressure drop in the fuel spraybar injector, changes in fuel flow in response to augmentor pressure at the spraybar are small compared to changes in airflow. Consequently, fuel flow can be considered constant, and the fuel-air ratio of the particle as it crosses the spraybar is determined by changes in airflow only.

$$FA_{S/B} = \frac{\text{constant}}{W_s} \quad (61)$$

A period of time,  $\tau_{DC}$ , is required for the particle to drift from the spraybar to the flameholder. Therefore, the fuel-air ratio of the particle when it reaches the flameholder can be expressed as:

$$FA_c(t) = FA_{S/B} (t - \tau_{DC}) \quad (62)$$

At the ignition plane (flameholder) the particle has a "potential" volumetric heat release rate of:

$$q_c = \frac{C_p}{v_c} W_s T_{ic} \eta_c \quad (63)$$

The ideal temperature rise is a function of the fuel-air ratio of the particle (effects of approach temperature and pressure are negligible). The efficiency is assumed to be a function of the fuel-air ratio and the approach pressure, temperature, and velocity.

$$T_{ic} = fcn(FA_c) \quad (64)$$

$$\eta_c = fcn(FA_c, P_s, T_s, V_s) \quad (65)$$

The particle crossing the flameholder will begin burning after a time  $t_d/V_s$ , which is the time required to drift from Station (4) to (5) while being ignited. When it begins burning at Station (5), the heat release rate of the particle will be ( $x = 0$  at Station (5)):

$$q(0,t) = q_c (t - t_d/V_s) \quad (66)$$

At some station,  $x$  distance downstream of Station (5), the local heat release rate will become that of the particle after an additional time delay

$$\tau_E = \int_0^x dx/V(x),$$

which is the time required to drift from Station (5) a distance  $x$  at throughflow velocity  $V(x)$ . Then, at a location  $x$  in the combustion zone, the heat release rate will be:

$$q(x,t) = q(0,t - \tau_E) \quad (67)$$

The linearized versions of equations (31) through (35), written in terms of the Laplace transform of the normalized variables are:

$$\begin{aligned} FA'_{s/B} &= -W_s \\ FA'_c &= FA'_{s/B} e^{-\tau_{DC} S} \\ q'_c &= W'_s + T'_i + \eta' \end{aligned} \quad (68)$$

$$T'_{ic} = \left[ \frac{FA}{T_i} \frac{\partial T_i}{\partial FA} \right]_c FA'_c$$

$$\eta'_c = \left[ \frac{FA}{\eta} \frac{\partial \eta}{\partial FA} \right]_c FA'_c + \left[ \frac{P}{\eta} \frac{\partial P}{\partial P} \right]_c P'_s + \left[ \frac{T}{\eta} \frac{\partial \eta}{\partial T} \right]_c T'_s + \left[ \frac{V}{\eta} \frac{\partial \eta}{\partial V} \right]_c V'_s$$

solving for  $q'_c$

$$\begin{aligned} q'_c &= \left[ 1 - \left\{ \left[ \frac{FA}{T_i} \frac{\partial T_i}{\partial FA} \right]_c + \left[ \frac{FA}{\eta} \frac{\partial \eta}{\partial FA} \right]_c \right\} e^{-\tau_{DC} S} \right] W'_s \\ &+ \left[ \frac{P}{\eta} \frac{\partial \eta}{\partial P} \right]_c P'_s + \left[ \frac{T}{\eta} \frac{\partial \eta}{\partial T} \right]_c T'_s + \left[ \frac{V}{\eta} \frac{\partial \eta}{\partial V} \right]_c V'_s \end{aligned} \quad (69)$$

A corresponding equation for the core stream can be directly written by changing subscript "C" to subscript "H," and changing the reference approach station from (3) to (3H).

$$\begin{aligned} q'_H &= \left[ 1 - \left\{ \left[ \frac{FA}{T_i} \frac{\partial T_i}{\partial FA} \right]_H + \left[ \frac{FA}{\eta} \frac{\partial \eta}{\partial FA} \right]_H \right\} e^{-\tau_{DH} S} \right] W'_{sH} \\ &+ \left[ \frac{P}{\eta} \frac{\partial \eta}{\partial P} \right]_H P'_{sH} + \left[ \frac{T}{\eta} \frac{\partial \eta}{\partial T} \right]_H T'_{sH} + \left[ \frac{V}{\eta} \frac{\partial \eta}{\partial V} \right]_H V'_{sH} \end{aligned} \quad (70)$$

The total volumetric heat release rate is formed by adding the heat release rates of the fan and core streams:

$$q_t v_t = Q_t = Q_C + Q_H = q_C v_C + q_H v_H \quad (71)$$

or, in normalized form:

$$q'_t = \left[ \frac{Q_C}{Q_t} \right] q'_c + \left[ \frac{Q_H}{Q_t} \right] q'_H \quad (72)$$

Equation (72) computes the instantaneous volumetric heat release rate of a particle of combined fan stream and core stream fuel-air mixture when the particle reaches the flameholder. The term "potential" is applied because the particle has not yet been ignited. The particle is ignited by the flameholder wake as it drifts a distance  $l_f$  at velocity  $V_s$ . The particle begins releasing the "potential" heat at Station (5), as defined by equation (66). To account for the fact that the core stream has now been added to the augmentor (only the fan stream was originally being considered), so the total heat release of both streams is being treated, equation (66) is re-written as:

$$q(o, t) = q_t (t - t_f / V_s) \quad (73)$$



Linearized:

$$q'(o,t) = q_i (t - t_d / V_d) \quad (74)$$

Equation (74) simply adds a delay into the system which allows tailoring the axial location of the beginning of the combustion zone. For convenience in programming the equations, this delay is added to the drift delay in the combustion zone ( $\tau_E$ ) to form an overall particle drift delay from the flameholder.

$$\tau_Q = t_d / V_d + \tau_E \quad (75)$$

The particle then releases heat throughout the combustion zone as defined by equation (67), the linearized version of which is:

$$q'(x,t) = q'(o, t - \tau_E) \quad (76)$$

Equation (75) was presented in part b, (Development of Acoustic Equations), and used to evaluate integrals in equation (37). The combustion equations require that the following information about the steady-state operating point:

$$\left[ \frac{Q_C}{Q_t} \right], \left[ \frac{Q_H}{Q_t} \right], \left[ \frac{FA}{T_i} \frac{\partial T_i}{\partial FA} \right]_{C,H}, \left[ \frac{FA}{\eta} \frac{\partial \eta}{\partial FA} \right]_{C,H},$$

$$\left[ \frac{P}{\eta} \frac{\partial \eta}{\partial P} \right]_{C,H}, \left[ \frac{T}{\eta} \frac{\partial \eta}{\partial T} \right]_{C,H}, \text{ and } \left[ \frac{V}{\eta} \frac{\partial \eta}{\partial V} \right]_{C,H}$$

The heat release rate ratios  $Q_C/Q_t$  and  $Q_H/Q_t$  are computed in the program from conditions known about each augmentor stream:

$$\frac{Q_C}{Q_t} = \frac{(BPR T_{ic} \eta_C)}{(BPR T_{ic} \eta_C) + (T_{ih} \eta_H)} \quad (77)$$

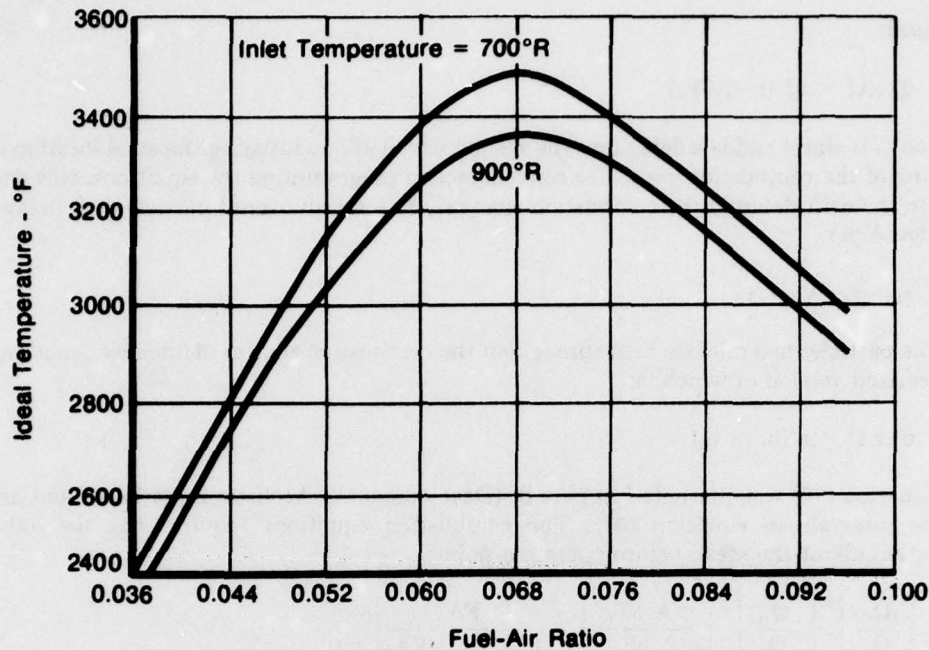
$$\frac{Q_H}{Q_t} = \frac{(T_{ih} \eta_H)}{(BPR T_{ic} \eta_C) + (T_{ih} \eta_H)}$$

The partial derivative terms  $[FA/T_i \partial T_i / \partial FA]_{C,H}$  are computed in the program from a subroutine curvefit of the ideal temperature rise curve. A graphical definition of the term is supplied in Figure 113. The partial derivative terms involving efficiency are computed in the Flameholder Combustion Model and supplied directly to the rumble model. Alternately, they may be computed from empirical data and be input by the user. The graphical definition of terms is similar to that of Figure 113.

This completes the combustion equation development for the V-gutter flameholder model. All of the above equations apply to the Vorbix and Swirl augmentors except as noted below.

For the Vorbix and Swirl augmentors, independent heat release rates for the fan and core streams cannot be identified because of the flow mixing. In addition, the effects of pilot fuel-air ratio on augmentor combustion efficiency must be accounted for. Equation (33) is again applied, but on an overall basis only.

$$q_t = \frac{C_p}{v} W_i T_{i\eta} \quad (78)$$



FD 146483

Figure 113. Ideal Temperature Rise for Constant Pressure Combustion of Hydrocarbon Fuels

The overall fuel-air ratio is computed from total mixed airflow at Station (4).

$$FA = \frac{\text{constant}}{W_4} \quad (79)$$

The overall ideal temperature rise is a function of overall fuel-air. The efficiency is assumed to be a function of overall fuel-air, pilot fuel-air, and pressure at Station (4).

$$T_i = \text{fcn}(FA) \quad (80)$$

$$\eta = \text{fcn}(FA, FAP, P_4) \quad (81)$$

Then for the Vorbix and Swirl augmentors, the instantaneous "potential" volumetric heat release rate of a particle of mixture when the particle reaches Station (4) is:

$$q_i' = \left[ 1 - \left[ \frac{FA}{T_i} \frac{\partial T_i}{\partial FA} \right] - \left[ \frac{FA}{\eta} \frac{\partial \eta}{\partial FA} \right] \right] W_4 + \left[ \frac{FAP}{\eta} \frac{\partial \eta}{\partial FAP} \right] FAP + \left[ \frac{P}{\eta} \frac{\partial \eta}{\partial P} \right] P_4 \quad (82)$$

Equation (82) applies to both the Vorbix and Swirl augmentors, and is equivalent to equation (72) for the V-gutter augmentor. The Vorbix and Swirl augmentors differ in pilot location. The Swirl has the pilot at fan duct exit, so that airflow through the Swirl pilot is proportional to fan duct exit flow,  $W_4$ . The Vorbix has the pilot near midspan, radially, and slightly aft of Stations

(3) and (3H), so that airflow through the Vorbix pilot is proportional to total flow,  $W_4$ . Then, since fuel flow into both pilots is constant:

$$\begin{aligned} \text{Swirl: } FAP' &= -W_3' \\ \text{Vorbix: } FAP' &= -W_4' \end{aligned} \quad (83)$$

For convenience in programming,  $W_4$  can be replaced by:

$$\begin{aligned} W_4 &= W_3 + W_{3H} \\ W_4' &= \left[ \frac{BPR}{1 + BPR} \right] W_3' + \left[ \frac{1}{1 + BPR} \right] W_{3H}' \end{aligned} \quad (84)$$

Substituting (53) and (54) into (52):

$$\begin{aligned} \text{Swirl: } q_i' &= \left\{ \left( 1 - \left[ \frac{FA}{T_1} \frac{\partial T_1}{\partial FA} \right] - \left[ \frac{FA}{\eta} \frac{\partial \eta}{\partial FA} \right] \right) \left( \frac{BPR}{1 + BPR} \right) - \left( \frac{FAP}{\eta} \frac{\partial \eta}{\partial FAP} \right) \right\} W_3' \\ &+ \left\{ \left( 1 - \left[ \frac{FA}{T_1} \frac{\partial T_1}{\partial FA} \right] - \left[ \frac{FA}{\eta} \frac{\partial \eta}{\partial FA} \right] \right) \left( \frac{1}{1 + BPR} \right) \right\} W_{3H}' \\ &+ \left[ \frac{P}{\eta} \frac{\partial \eta}{\partial P} \right] P_i' \end{aligned} \quad (85)$$

$$\begin{aligned} \text{Vorbix: } q_i' &= \left\{ \left( 1 - \left[ \frac{FA}{T_1} \frac{\partial T_1}{\partial FA} \right] - \left[ \frac{FA}{\eta} \frac{\partial \eta}{\partial FA} \right] - \left[ \frac{FAP}{\eta} \frac{\partial \eta}{\partial FAP} \right] \right) \left( \frac{BPR}{1 + BPR} \right) \right\} W_3' \\ &+ \left\{ \left( 1 - \left[ \frac{FA}{T_1} \frac{\partial T_1}{\partial FA} \right] - \left[ \frac{FA}{\eta} \frac{\partial \eta}{\partial FA} \right] - \left[ \frac{FAP}{\eta} \frac{\partial \eta}{\partial FAP} \right] \right) \left( \frac{1}{1 + BPR} \right) \right\} W_{3H}' \\ &+ \left[ \frac{P}{\eta} \frac{\partial \eta}{\partial P} \right] P_i' \end{aligned} \quad (86)$$

Equations (85) and (86) replace equation (72). All other combustion equations are identical to those developed for the V-gutter flameholder augmentor. The partial derivatives in equations (85) and (86) must be computed from empirical data and be input by the user.

This completes development of the combustion equations. For the solution technique, based upon applying the Nyquist criterion to the open loop transfer function (OLTF), the OLTF is formed by renaming  $q_i'$  to  $q_{iN}'$  in equation (74) and by renaming  $q_i'$  to  $q_{OUT}'$  in equations (72), (85), and (86).



## APPENDIX E

### 1. FLAMEHOLDER COMBUSTION MODEL PROGRAM DESCRIPTION

#### a. General

The combustion model performs a multi-streamtube analysis of the flame stabilization and propagation phenomena in a turbofan augmentor. The augmentor is divided into a multitude of equivalent two-dimensional streamtubes with a single flameholder element in each. The program evaluates each streamtube and then mass averages the results.

For each streamtube, the program proceeds from the augmentor inlet towards the exhaust nozzle and evaluates each step in the stabilization and propagation of the augmentor process. The ultimate result is the level of combustion efficiency in that streamtube. The program then performs a small perturbation in velocity, pressure, inlet temperature and fuel-air ratio to evaluate the efficiency slopes.

The final outputs are the fan duct efficiency, the core stream efficiency and the efficiency slopes with respect to the four perturbed variables.

#### b. Modeling Approach

The approach taken for each streamtube is a step-by-step solution to the physical phenomena which determine the flame stability limits of the spraybar flameholder configuration and the subsequent turbulent flame propagation rate. These phenomena include liquid fuel injection, droplet formation, vaporization, fuel impingement onto the flameholder, wake reaction kinetics and turbulent flame penetration.

The approach used is different for the fan duct streamtubes and the core streamtubes. The necessity for different approaches lies in the degree of liquid fuel vaporization between the spraybar and the flameholder. In the core streamtubes, the fuel is virtually totally vaporized in the first few inches by the hot turbine exhaust flow. In the fan duct stream, the much cooler airflow results in only a slight degree of vaporization in the four to six inches typical spraybar-to-flameholder distance.

The core stream analysis is thus done assuming that the fuel at the flameholder is in the vapor phase and the flameholder wake fuel-air ratio is the same as the total fuel-air ratio. This value is used in the kinetics analysis of the wake reaction to evaluate the stability limits.

In the fan duct streamtubes, however, the low level of droplet vaporization yields a vapor phase fuel-air ratio at the flameholder which is well below the lean limit for hydrocarbon fuels. Since the liquid fuel droplets are not capable of entering the flameholder recirculation wake due to their excessive momentum, there must be some other mechanism to provide the necessary wake vapor fuel for stable combustion.

This mechanism in the fan duct streamtubes is the collection of the liquid fuel droplets onto the surface of the flameholders and the vaporization of the resultant liquid film. This evolved vapor recirculates into the flameholder wake with a portion of the droplet evolved vapor fuel to generate the wake vapor fuel concentration.

The streamtube analyses computes the degree of wake reaction at the level of vapor fuel-air ratio appropriate to the streamtube type and approach conditions. For the fan duct cases, this requires a convergent solution between the wake kinetics and the surface vaporization.

Once the flameholder wake reaction level is evaluated, the analysis computes the rate of flame penetration into the free stream as a turbulent flame sheet. This rate is adjusted by the wake reaction level to account for the ignition response in the recirculation zone shear layers. The flame penetration rate is integrated over the available augmentor length to provide the level of streamtube efficiency.

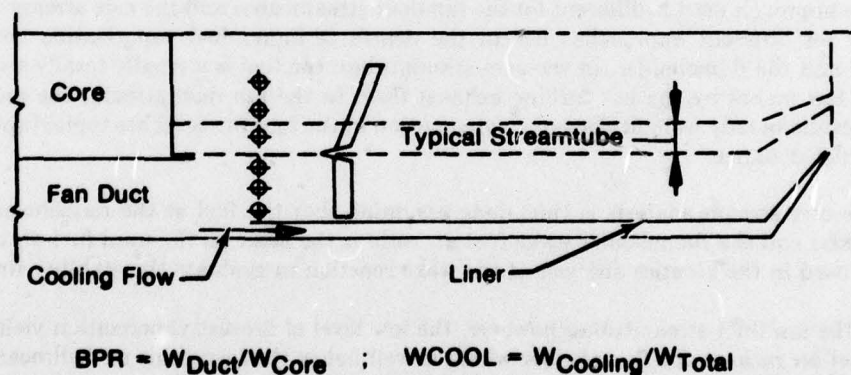
The program thus performs a quantitative evaluation of the phenomenological processes which occur in the turbofan augmentor. The individual calculations are a combination of analytical evaluations and empirical results as required to ensure quantitative accuracy.

### c. Model Description

The combustion model was designed as a complete unit. The program does not require on-line engineering interaction. The combustion model may be run as a separate entity or as a generator for subsequent stability analysis with the rumble model. When exercised alone, the combustion model is an augmentor analysis program and the output is a comprehensive description of the injection, stabilization and flame propagation processes. In this mode, the program is useful as a design tool for conventional turbofan augmentors. The effects of fuel system distribution and V-gutter flameholder tailoring may be determined.

When exercised in conjunction with the stability analysis, a less extensive output is given and the prime purpose of the program is to generate the response of augmentor efficiency to variations in fuel-air ratio and inlet velocity, pressure and temperature.

The augmentor breakdown and specific description of one streamtube is shown in Figure 114. For a single fan duct streamtube, the computer logic is shown in Figure 115. The identified subroutines each evaluate a specific portion of the overall combustion process.

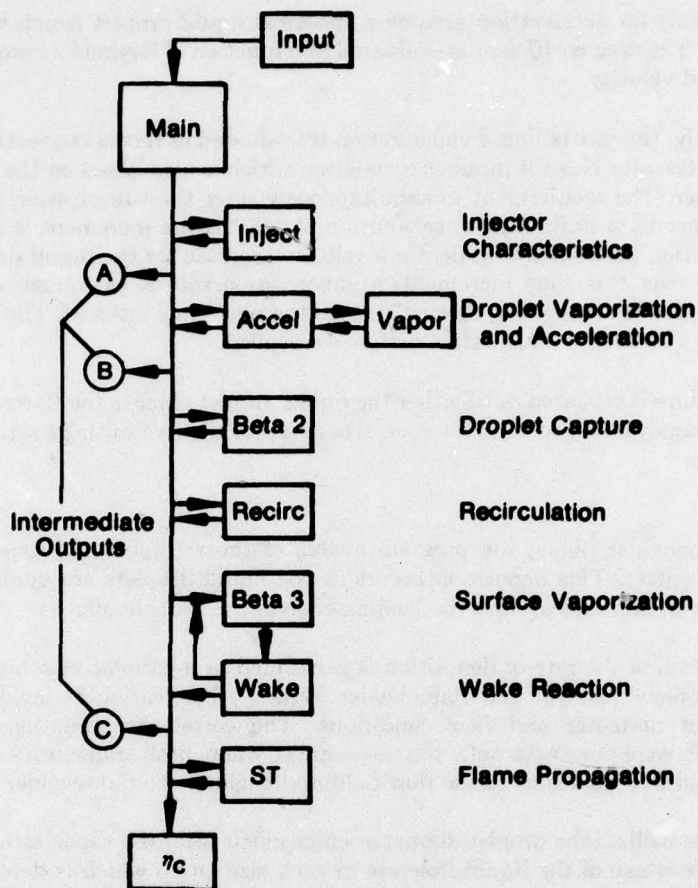


FD 146484

Figure 114. Location of a Core Streamtube in a Turbofan Engine Augmentor

The input requirements for a fan duct streamtube are those to fully describe the approach flow field, geometry of the streamtube and flameholder and the total fuel-air ratio. The execution of one streamtube proceeds as follows:





FD 151094

Figure 115. Single Streamtube Logic Map

#### (1) INJECT

This subroutine evaluates the droplet sizes formed by a variable area spraybar as a function of the injection pressure drop. Five droplet sizes are calculated which represent the cumulative volume versus pressure drop curve for this spraybar type.

This subroutine evaluates the amount of the liquid fuel which is flash vaporized by the injection process. This evaluation is performed as an adiabatic expansion process from the high-pressure spraybar fuel condition to the low-pressure augmentor conditions. The appropriate fuel enthalpy chart is used, keyed by the fuel type input variable.

The liquid flowrate which remains is partitioned equally into the five size groups. The total flowrate is originally calculated from the total fuel-air ratio input and the airflow which is calculated from the streamtube geometry and flow conditions.

#### (2) ACCEL

This program subroutine evaluates the rate of droplet vaporization and acceleration which occurs between the spraybar and the downstream V-gutter flameholder.



The equations for acceleration assume a spherical liquid droplet which is accelerated by drag forces only. The drag coefficient is evaluated as a function of Reynold's number based on the relative air-liquid velocity.

Concurrently, the rate of liquid vaporization is evaluated as forced convection mass transfer utilizing a mass transfer Nusselt number correlation which is also based on the relative velocity Reynold's number. The requirement to simultaneously solve the vaporization and acceleration equations was met by a finite difference solution. A small time increment is selected and the acceleration solution performed to generate a velocity increase for the liquid droplet. Using the average velocity over this time increment, a vaporization rate is calculated and a vaporized fraction evaluated. This sets a new droplet size for the next time interval. The average velocity over this time is also used to calculate a distance travelled.

This procedure is repeated until either the liquid droplet reaches the flameholder or is fully vaporized. This analysis is repeated for each size group of the five initially set.

### **(3) COLLECT**

At the flameholder plane, the program evaluates the rate of liquid deposition onto the surface of the V-gutter. This deposition occurs as the liquid droplets are unable to follow the divergent airflow streamlines around the leading edge of the flameholder.

The evaluation of the rate of deposition is performed as a correlative solution to the point where liquid droplets just hit the flameholder surface. The variables include flameholder geometry, droplet diameter and flow conditions. The correlation equations are based on calculations which were done externally to this program, where limit trajectories were established based on potential flow solutions to the flow field approaching the flameholder.

The program utilizes the droplet diameter which exists after the vaporization evaluation to calculate the percentage of the liquid flowrate in each size group which is deposited on the V-gutter surface. This is done for each of the five size groups. The collection mass flowrate is evaluated from each size group collection percentage and the liquid flowrate in each group at the flameholder.

### **(4) RECIRC**

The gaseous recirculation rate into the flameholder wake is evaluated from a variety of literature sources which present recirculation zone volume and flowrate as a function of flameholder geometry and flow conditions. The program evaluates a "recirculation efficiency" which is the ratio of recirculated mass flow to the flowrate through the area blocked by the flameholder. This typically runs 15 to 25%.

The correlations cover a range of the variables which control the recirculation such as flameholder apex angle, blockage, approach Mach number, and temperature. The result of the subroutine is the recirculation zone. These are used in the analysis of the wake reaction efficiency.

### **(5) WAKE**

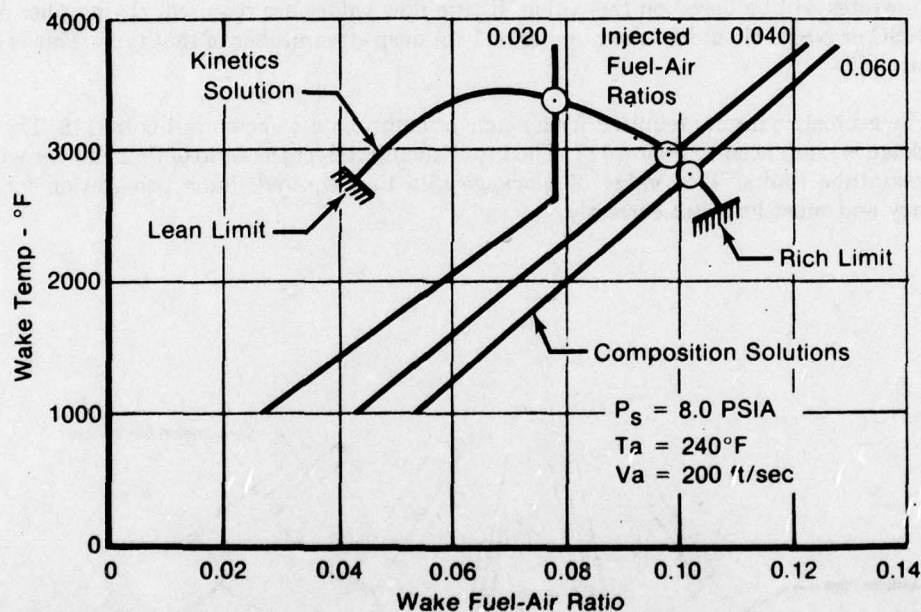
The wake reaction is treated as if it occurred in a well-stirred reactor with volume and entry flowrate as evaluated in RECIRC. The kinetics are assumed to proceed as a single-step, second order conversion process. The kinetics utilize rate coefficients which simulate aircraft fuel behavior. The required inputs are wake volume, wake fuel-air ratio, recirculation rate and inlet conditions of pressure, temperature, etc. The output of the analysis is the wake reaction efficiency and mean wake temperature.

### (6) BETA 3

This subroutine evaluates the degree of vaporization of the liquid film which exists on the flameholder surface. The vaporization process is one of forced convection from the surface into the trailing wake shear layer and heat transfer from the flameholder wake through the flameholder metal into the liquid film. The program utilizes a small element approach using 10 elements on each side of the flameholder. The mass flux and heat flux are evaluated for one at a time starting at the flameholder leading edge. Any liquid left unvaporized is assumed to leave the trailing edge of the flameholder and traverse through the wake shear layers downstream.

The solution of WAKE and BETA3 must be done simultaneously since BETA3 requires wake temperature to find fuel vaporization and the vaporization influences WAKE through fuel-air ratio.

The solution approach is described in part f (Development of the Fan Duct Combustion Equations) of this Appendix with a typical result shown here in Figure 116.



FD 142354

Figure 116. Duct Stream Wake Solution

### (7) FLAME

The turbulent flame propagation downstream of the flameholder uses a small step difference solution with axial profiles of turbulence, flow, etc. The procedure is also discussed in part f of this Appendix.

#### d. Input Requirements and Comments

The model requires as input the physical variables which describe the fan duct and core stream geometry and operating conditions. Since the model functions by repetitive analysis of single streamtubes, the input is required for each different type of streamtube. A different type is one with any input variable different.



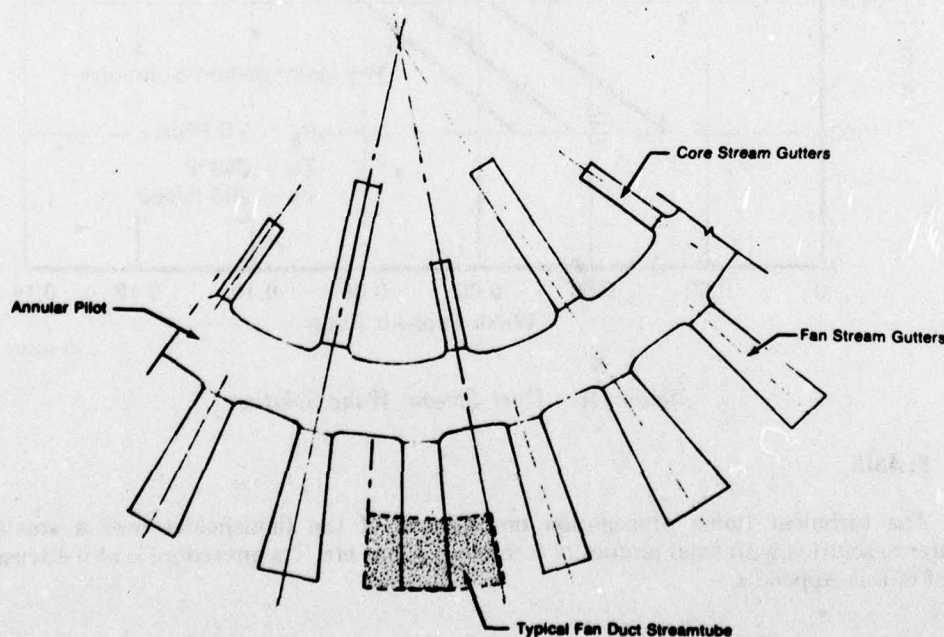
The input requires the following general values in addition to the set-up values of Section II-3.c:

BPR	Actual value. Default to 1.0 if run as a duct burner with no core engine and $WCOOL = \frac{1}{2} \times (m_{cool}/m_{duct})$
M6C	Inlet Mach numbers
M6H	
NTC	No. of types of fan duct streamtubes
NTH	No. of types of core streamtubes
PS6	Inlet static pressure, psia.

Array input is required to describe each streamtube fully. These array values are aerodynamic and geometric. The first array is the number of streamtubes of each type identified in the fan (NSC) or core (NSH) sections. For example, two different flameholder widths with three different fuel-air ratios per width in the fan would require  $NTC = 2$  and  $NSC = 3,3$ .

The program, as currently written, assumes a unit depth streamtube, i.e., 1-in. depth. The mass flowrates will be based on this value. If true flow values are required, the number of each type (NSC or NSH) should be the number of 1-in. deep streamtubes of that type. This is shown in Figure 117.

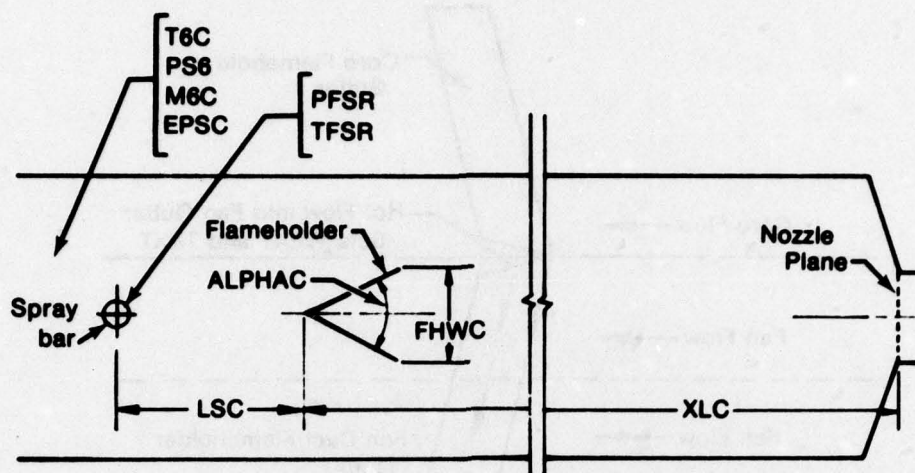
The geometric inputs required for a single streamtube are shown in Figure 118. The value of blockage is referenced to Figure 117. The input should reflect the ratio of flameholder width to the streamtube limits. This value of blockage sets the required flame penetration for 100% efficiency and must be input correctly.



FD 146485

Figure 117. Location of Typical Fan Duct Streamtube





$$TAUC = \frac{FWWC}{\text{Flow Width}}$$

FD 146486

Figure 118. Single Streamtube Geometry and Flow Inputs — Fan

The value of EPSC is the approach turbulence and will affect the flame speed. Unless specific data are available, use a value of 0.04 for a turbofan engine.

The input value for PFSR controls the mean droplet size from the spraying, which has data from a variable area orifice built in. If other values are desired use the equation:

$$d_{50} = 795 \cdot (PFSR - PS6)^{-0.4}$$

to determine the input value of PFSR required to yield a desired mean droplet diameter, in microns. This is the only place where PFSR is used so no disruption occurs if nontrue values are input.

For the aerodynamic inputs, also reference Figure 118, the required input is shown. As previously mentioned, PS6 is assumed to be uniform across the streamtubes.

One input set requires external evaluation. These are the values assigned to WEXT and TEXT in the fan duct streamtubes. The purpose of this input is to account for the influence of hot gas migration down the wake region of the fan duct flameholders from either the core or from a pilot. WEXT is defined as the ratio of this "external" flowrate to the recirculated flowrate. To allow for flexibility in design selection, this input format was selected. The user must evaluate whatever flowrate is expected and calculate WEXT. For use in estimating the recirculated flowrate, assume  $K_1 = 0.25$  and use:

$$\dot{m}_r = K_1 \rho_a V_a N$$

for recirculation rate per inch of flameholder length. Typical values of WEXT are 0.02 to 0.04. TEXT is the temperature of this "external" flowrate. These are shown in Figure 119.

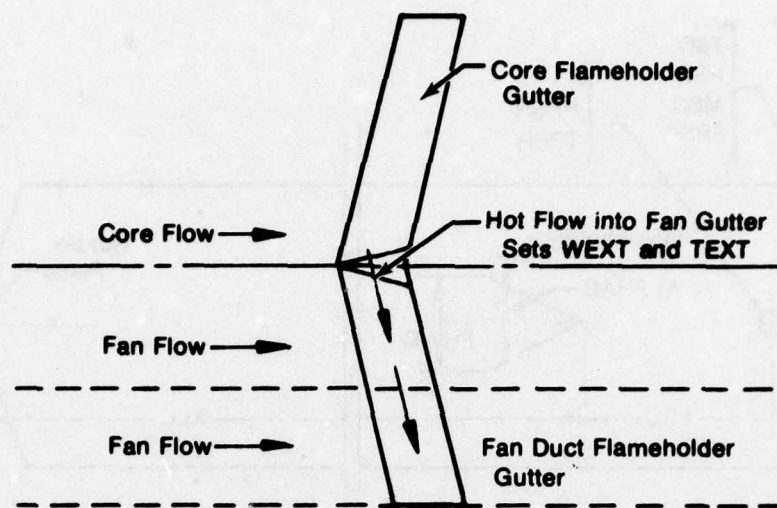


Figure 119. External Heat Addition to Fan Duct Gutters

The liner cooling airflow input, WCOOL, is the ratio of cooling liner air to total engine air. As such the engine bypass ratio is required to evaluate the net available fan duct airflow. If no cooling air is taken from the fan duct or if input fuel-air ratios are based on the true net air available for combustion, input WCOOL = 0.0. If a duct burner is being analyzed and it does have a cooling liner, set a dummy value of 1.0 for BPR and set WCOOL by:

$$WCOOL = \dot{m}_{cooling} / 2 \cdot \dot{m}_{duct \text{ burner}}$$

#### e. Output

The program has two output formats, long and short. The long format presents detailed values for the processes which control the wake vapor-phase fuel-air ratio and flame penetration. The short format essentially presents the overall results. For both, the results are presented as a streamline by streamline analysis with fan and core summaries.

##### (1) Fan Streamtubes

The long format presents the input data for each streamtube and two calculated values. These values are the effective streamtube fuel-air ratio and the effective recirculation temperature. The equations used for these are described in part f of this Appendix.

The output lists the calculated values for the injection process, mean droplet size and flash vaporization, and the influence coefficients,  $\beta_1$ ,  $\beta_2$ ,  $\beta_3$  and  $K_1$ , which control the wake fuel-air ratio.

A word of caution is in order here. If the output is preceded by the warning that the wake temperature iteration has failed, the situation is such that the wake has exceeded the rich limit at the input conditions. Although output is presented, it is not valid and merely represents the limits of the internal convergence search routine. For example, wake temperature will always be 5000°F for a failed case. If a single streamtube is being run, several other error messages will result as the program attempts to interpret zero efficiency. If multiple streamtubes are being run, the program will ignore the failed streamtube in all calculations.



The initial flame speed is the laminar flame speed at the appropriate inlet conditions. The turbulence level is the value induced by the flameholder.

In the stream efficiency section for each streamtube, the following comments are applicable:

1. The ideal temperature use is based on the effective fuel-air ratio.
2. The efficiency is the ratio of flame penetration to streamtube width at the exhaust nozzle.
3. The actual temperature rise is based on 1. and 2. The exit temperature is based on streamtube inlet plus this actual temperature rise.
4. The flowrates are for a 1-in. deep streamtube. The fuel flowrate uses the effective fuel-air ratio.

The fan streamtube summary presents the major items from each streamtube and then the exit average results. The cooling air flowrate ratio is repeated here. Two more values of combustion efficiency are presented and two values of average exit temperature.

The average streamline exit temperature is the mass weighted average of the individual exit temperatures. The chemical combustion efficiency is based on this value for exit and an ideal temperature use based on the average effective fuel-air ratio and average inlet temperature.

The average duct exit temperature includes the mass weighted effect of the liner cooling air being added to the streamtubes at the exhaust nozzle inlet. The average thermal combustion efficiency is based on this exit temperature; the average inlet temperature and an ideal temperature rise is based on the average input fuel-air ratio.

Since engine analysis procedures generally base the fan duct fuel-air on the total duct airflow and use the thermal nozzle inlet averages, the value of thermal combustion efficiency is the one which is used for rumble prediction.

The total flowrate presented here includes the number of each type of streamtube as do all of the above mentioned mass averaged values.

Also note, that at no time are efficiencies ever mass averaged directly. All average efficiencies are based on comparison of the average results of individual streamtubes to the result of the average inlet. That is, the burn-then-mix process is compared to the ideal mix-then-burn process. Since curves of ideal temperature rise exhibit peak vs fuel-air ratio, the average efficiency of two streamtubes, one lean and one rich, may very well be less than either streamtube separately.

## **(2) Core Streamtubes**

Due to the absence of droplet effects, the output is greatly simplified. The wake reaction results are presented as well as initial flame properties. Without liner cooling air there is no fuel-air ratio shift and thus only one efficiency definition. All of the comments in the fan stream apply here except that thermal efficiency is not defined here due to the lack of liner cooling air.

If the message "Aerodynamic Loading exceeds Kinetic Capacity" occurs, the blowout limits were exceeded.



## 1. Development of the Fan Duct Combustion Equations

The equations which are used in the fan duct combustion analysis are highlighted in this section. The reader is referred to the AFAPL TR-78-24 (Contract F33615-76-C-2023) for full details of the analytical development.

The program utilizes the input to set-up and analyze each streamtube as a separate entity. The results are stored for final summation at the completion of the fan duct analysis.

The flow field is first developed from the input:

$$\rho_a = \frac{P_a}{RT_a} \quad (87)$$

$$V_a = M \sqrt{\gamma RT_a} \quad (88)$$

$$W = N/\Gamma \quad (89)$$

$$\dot{m}_a = \rho_a V_a W \quad (90)$$

The streamtube width has been set from the flameholder width and the blockage ratio. Note that the streamtube is assumed to be 1-in. deep. The total flowrates are thus per unit depth. If true total flowrates are desired, the number of streamtubes of each type must be set to reflect the total true depth of that type. For example, if 5 streamtubes, of 4-in. depth each, are input as one type, then set the input number of this type equal to 20.

To account for the removal of air from the streamtube for liner cooling, the input fuel-air ratio is adjusted by:

$$(FA)_{\text{effective}} = (FA)_{\text{input}} \frac{1}{1 - WCOOL \left( \frac{1 + BPR}{BPR} \right)} \quad (91)$$

This increases the fuel-air ratio to reflect the air removal when:

$$WCOOL = \dot{m}_{\text{cooling}} / \dot{m}_{\text{engine}} \quad (92)$$

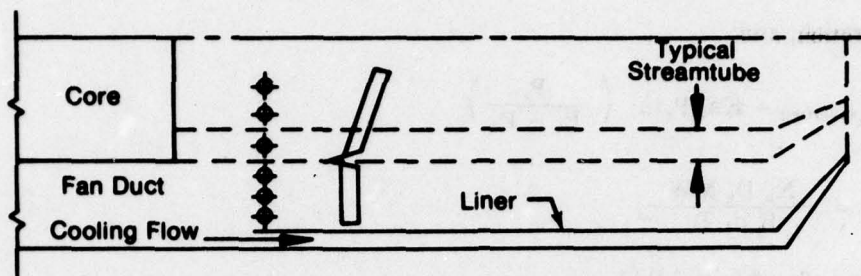
$$BPR = \dot{m}_{\text{duct}} / \dot{m}_{\text{core}} \quad (93)$$

$$\dot{m}_{\text{engine}} = \dot{m}_{\text{duct}} + \dot{m}_{\text{core}} \quad (94)$$

Then

$$\dot{m}_f = \dot{m}_a (FA)_{\text{effective}} \quad (95)$$

This is required since fuel-air ratios are usually based on the total fan duct air flowrates. If true values are known or if no cooling air is used, set  $WCOOL = 0.0$ . Refer to Figure 120 for details.



$$BPR = W_{Duct}/W_{Core} \quad ; \quad W_{COOL} = W_{Cooling}/W_{Total}$$

FD 146488

Figure 120. Location of a Core Streamtube in a Turbofan Engine Augmentor

The injection subroutine divides the fuel into 5 droplet size groups which represent the droplet size vs volume distribution. The curve used is for a variable area pintle injection. The sizes used are:

Group	% Covered	Mean Value
1	0-20	$d_{10}$
2	20-40	$d_{20}$
3	40-60	$d_{30}$
4	60-80	$d_{70}$
5	80-100	$d_{90}$

The curve is a function of the injection pressure drop where:

$$\Delta P_{inj} = PFSR - P_s \quad (96)$$

Any flash vaporization is evaluated from the fuel enthalpy chart assuming adiabatic injection, i.e.,  $\Delta H = 0$

$$H_1 = \text{fcn}(PFSR, TFSR) \quad (97)$$

$$H_2 = \text{fcn}(\% \text{ vaporized}, P_s) \quad (98)$$

The droplet vaporization and acceleration are evaluated by a small time step integration between the spraying and flameholder. The equations are:

$$\frac{dV_t}{dt} = \frac{3}{4} \frac{C_d}{d_t} \frac{\rho_a}{\rho_t} (V_a - V_t)^2 \quad (99)$$

for acceleration, and:

$$\dot{m}_{\text{vaporized}} = K A_s P_s \ln \left( \frac{P_s}{P_s - P_v} \right) \quad (100)$$

$$K = \frac{N_u D_v MW}{R d_l T_s} \quad (101)$$

$$N_u = 2 + 0.6 R_c^{1/2} P_r^{1/3} \quad (102)$$

for vaporization. The evaluation of the liquid temperature follows:

$$h_r = k N_u / d_l \quad (103)$$

$$\dot{q} = h_r A_s (T_s - T_l) \beta \quad (104)$$

$$\beta = \frac{z}{e^z - 1} \quad (105)$$

$$z = C p_v \dot{m}_v / \pi k d_l N_u \quad (106)$$

$$\Delta \dot{q} = \dot{q} - \dot{m}_v \lambda \quad (107)$$

$$\frac{dT_l}{dt} = \frac{\Delta \dot{q}}{m_l C p_l} \quad (108)$$

$$m_l = \rho_l \frac{4}{3} \pi \left( \frac{d_l}{2} \right)^3 \quad (109)$$

$$R_c = \frac{\rho_s d_l (V_s - V_l)}{\mu_s} \quad (110)$$

This procedure is done for each size group until the flameholder is reached and the net fraction vaporized is evaluated

$$\beta_1 = 1 - \left( \frac{\dot{m}_v}{\dot{m}_l} \right)_{\text{at F/H}} \quad (111)$$

The impingement of liquid fuel into the flameholder is evaluated by use of a term  $\beta_2$  where

$$\beta_2 = \frac{\dot{m}_{fc}}{\dot{m}_{l1} \cdot \Gamma} \quad (112)$$

This evaluates the percentage of the liquid fuel exposed to the flameholder which actually collects into its surface. The evaluation procedure is done for each size droplet group by a correlation of  $\beta_2$  vs flameholder size, apex angle, flow velocity and droplet diameter. The correlation is based on evaluations performed by droplet trajectory analysis using the potential flow field aerodynamics. The total impingement flowrate is thus:

$$\beta_2 = \frac{1}{\dot{m}} \sum_{i=1}^n \dot{m}(i) \beta_2(i) \quad (113)$$



or

$$\dot{m}_{r_c} = \beta_2 (1 - \beta_1) \Gamma \dot{m}_r \quad (114)$$

The liquid film vaporization rate is evaluated from the equations for the surface film vaporization caused by heat transfer from the flameholder wake. The surface is broken into ten elements and the vaporization and liquid temperature rise in each is calculated from:

$$\dot{m}_v = C_1 A_s P_s \ln \left( \frac{P_s}{P_s - P_v} \right) \quad (115)$$

$$C_1 = \frac{N_u D_v MW}{R \Delta x T_s} \quad (116)$$

$$N_u = 0.33 R_e^{0.5} P_r^{0.33} \quad (117)$$

$$P_v = \text{fcn}(T_l) \quad (118)$$

$$\dot{q} = \dot{m}_{r_c} C_p \Delta T_l + \lambda \left( \frac{N_u D_v MW}{R \Delta x T_s} \right) P_s A_s \ln \left( \frac{P_s}{P_s - P_v} \right) \quad (119)$$

$$\dot{q} = h_r A_s (T_w - T_{F/H}) \quad (120)$$

$$h_r = N_{u_w} \frac{k}{N} \quad (121)$$

$$N_{u_w} = 0.99 R_e^{0.5} P_r^{0.33} \quad (122)$$

The solution procedure for  $\beta_s$  breaks the flameholder surface into 10 equally spaced increments. The length of each is

$$\Delta x = \frac{1}{10} \frac{N/2}{\sin(\alpha/2)} \quad (123)$$

The fuel collected by the surface is equally divided into the 10 elements on each face of the flameholder:

$$\dot{m}_c(i) = \frac{1}{20} \beta_2 (1 - \beta_1) \Gamma \dot{m}_r \quad (124)$$

Equations (115) to (122) are used for element  $i = 1$  on the surface with  $\dot{m}_{r_c} = \dot{m}_c(i)$  and the fuel temperature is assumed to be the same as the droplet liquid temperature at the flameholder. The fraction vaporized is calculated and the liquid temperature use evaluated. The procedure is repeated using fuel properties evaluated at

$$T_l(i) = T_l(i)_o + \frac{1}{2} \Delta T_l(i) \quad (125)$$

This procedure continues until convergence, i.e.,  $\Delta T_l$  varies less than 1% between passes. Into the next element,  $i = 2$ , the flowrate is set equal to the unvaporized portion of the  $i = 1$  flow and the collection fraction per equation (124).

$$\dot{m}(2) = \dot{m}_c(2) + \dot{m}_c(1) - \dot{m}_v(1) \quad (126)$$

This flowrate initial temperature is set equal to the mass average of the exit temperature from  $i = 1$  and the droplet liquid collection temperature:

$$T_{li}(2) = \frac{\dot{m}_c(2) T_{lc} + [\dot{m}_c(1) - \dot{m}_v(1)] T_{li}(1)}{\dot{m}_c(2) + \dot{m}_c(1) - \dot{m}_v(1)} \quad (127)$$

The solution procedure is separated until all 10 segments are finished. The vaporized flowrate is the sum of all 10 in both sides of the flameholder:

$$\dot{m}_v = 2 \times \sum_{i=1}^{10} \dot{m}_v(i) \quad (128)$$

The fractive vaporized,  $\beta_s$ , is:

$$\beta_s = \frac{\dot{m}_v}{\dot{m}_c} = \frac{\dot{m}_v}{(1 - \beta_1) \Gamma \beta_2 \dot{m}_r} \quad (129)$$

All of the vaporized fuel is assumed to enter the recirculation zone.

From these equations,  $\beta_s$  is a function of the wake temperature. The temperature is a function of the wake fuel-air ratio and recirculation rate. Since  $\beta_s$  strongly influences the wake fuel-air ratio, the solution for wake composition and efficiency becomes a curve intersection procedure.

First we define the recirculation and wake kinetics equations and then the solution procedure.

#### (1) Recirculation:

The wake recirculation flowrate coefficient is defined as:

$$K_1 = \dot{m}_r / \Gamma \dot{m}_a \quad (130)$$

$$\dot{m}_r = \rho_a V_a N K_1 \quad (131)$$

For mass transfer across the recirculation zone boundaries and a homogeneous wake:

$$\dot{m}_r = \frac{\rho_a V_o}{\tau} \quad (132)$$

The wake volume is evaluated as a function of blockage, apex angle, and flow Mach number from literature references as shown in Reference 1. From this:

$$V_o = C_v (L/D)(B/D)N^3 \quad (133)$$

We set

$$\tau' = \frac{\tau V_a}{N} \quad (134)$$

$$\dot{m}_r = \frac{V_a}{N} \frac{\rho_a V_o}{\tau'} \quad (135)$$

Thus:

$$\dot{m}_r = \frac{\rho_a V_a C_v (L/D)(B/D)N}{\tau'}$$

and

$$K_1 = C_v (L/D)(B/D)(\tau')^{-1} \quad (136)$$

By curve fits of  $L/D$ ,  $B/D$  and  $\tau'$  vs  $\alpha$ ,  $N$ ,  $V_a$ , and  $T_a$ , we find the recirculation rate  $K_1$ .

## (2) Wake Reaction Kinetics

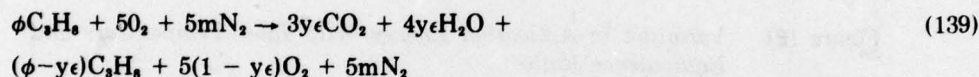
The wake reaction is assumed to be a single-step, second order reactive controlled as follows:

$$-\frac{dm}{dt} = \frac{k}{R^n} x_o^a x_r^{n-a} \frac{e^{-C/T}}{T^{n-0.5}} \quad (137)$$

For a well stirred reactor (wake is assumed to behave as one):

$$\frac{A}{V_o P^n} = \frac{k(m+1)}{R^n y_e} x_o^a x_r^{n-a} \frac{e^{-C/T}}{T^{n-0.5}} \quad (138)$$

For the assumed single-step reaction process postulated here, the reaction mass balance is (for propane fuel):



Also, a linear efficiency vs temperature function is assumed:

$$T = T_a + \epsilon \Delta T_{ideal} \quad (140)$$

From these equations, the stirred reactor loading capability may be written as:

$$\frac{A}{V_o P^n} = \frac{k(m+1)[5(1-y_e)]^a [\phi - y_e]^{n-a} e^{-C/(T_1 + \epsilon \Delta T)}}{R^n y_e [5(m+1) + \phi + y_e]^n [T_1 + \epsilon \Delta T]^{n-0.5}} \quad (141)$$

Based on comparison of predicted results with available stirred reactor data, we use the following values for this reaction:

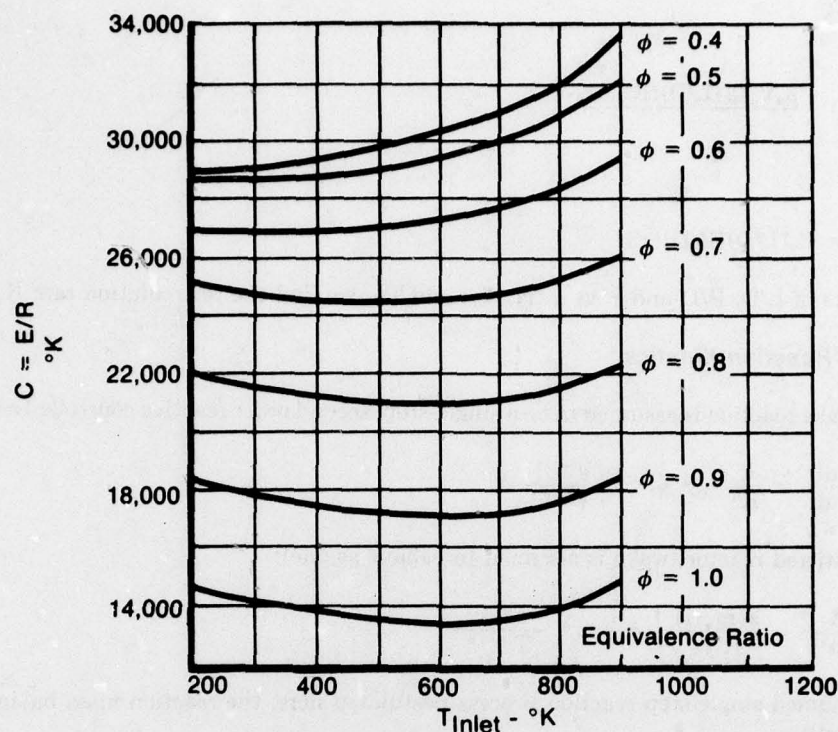
- n: for  $\phi < 1$ ,  $n = 2\phi$   
for  $\phi > 1$ ,  $n = 2/\phi$
- a:  $a = n/2$
- C:  $C = E/R$ , see Figure (121).

This yields:

$$\frac{A}{V_o P^{2.0}} = \frac{1.29 \times 10^{10} (m+1)[5(1-y_e)]^a (\phi - y_e)^a e^{-C/(T_1 + \epsilon \Delta T)}}{(0.08206)^{2.0} y_e [5(m+1) + \phi + y_e]^{2.0} [T_1 + \epsilon \Delta T]} \quad (142)$$

for lean mixtures.





FD 134084

Figure 121. Variation in Activation Energy With Inlet Temperature and Equivalence Ratio

The kinetics solution proceeds by successive iteration between  $\epsilon = 0.999$  and 0.70 to find the wake efficiency where:

$$\frac{A}{V_o P^2} = \frac{K_1 \Gamma \dot{m}_a}{V_o P^2} \quad (143)$$

at a given fuel-air ratio in the wake.

The solution procedure for the wake composition and reaction efficiency proceeds as follows:

1. The wake temperature is varied in steps from 1000 to 5000 $^{\circ}F$  and calculated at each wake.
2. The wake fuel-air ratio is varied from 0.02 to 0.20 and the wake temperature calculated at each fuel-air ratio.

The results of (a) are used in the wake fuel-air ratio equation:

$$FA)_{wake} = FA)_{total} \left\{ \beta_1 + (1 - \beta_1) \frac{\beta_2 \beta_3}{K_1} \right\} \quad (144)$$

This results in two curves which define the wake fuel-air ratio vs wake temperature and wake temperature vs wake fuel-air ratio. A solution technique looks for the intersection of these curves, if it exists. This then defines the stable wake composition solution.

The fan duct gutter wakes may be supplied with hot gasses from an external (to the wake) source such as a pilot region, see Figure 122. If this occurs, the external thermal source is assumed to effectively increase the inlet temperature of the recirculated air-fuel flowrate, i.e.,:

$$\dot{m}_r' = K_1 \rho_a V_a \Gamma + \dot{m}_{ext} \quad (145)$$

$$T_a' = \frac{T_a K_1 \rho_a V_a \Gamma + T_{ext} \dot{m}_{ext}}{\dot{m}_r'} \quad (146)$$

The program then analyzes the behavior at these new conditions as if they were input.

After the wake has been analyzed, the turbulent flame penetration into the free stream is analyzed.

The turbulent flame propagation into the unreacted free stream is initiated in the shear layers of the wake. The model used relates the local turbulent flame speed to the local aerothermodynamic conditions and performs a finite difference integration of the flame front penetration starting in the wake and proceeding to the exhaust nozzle.

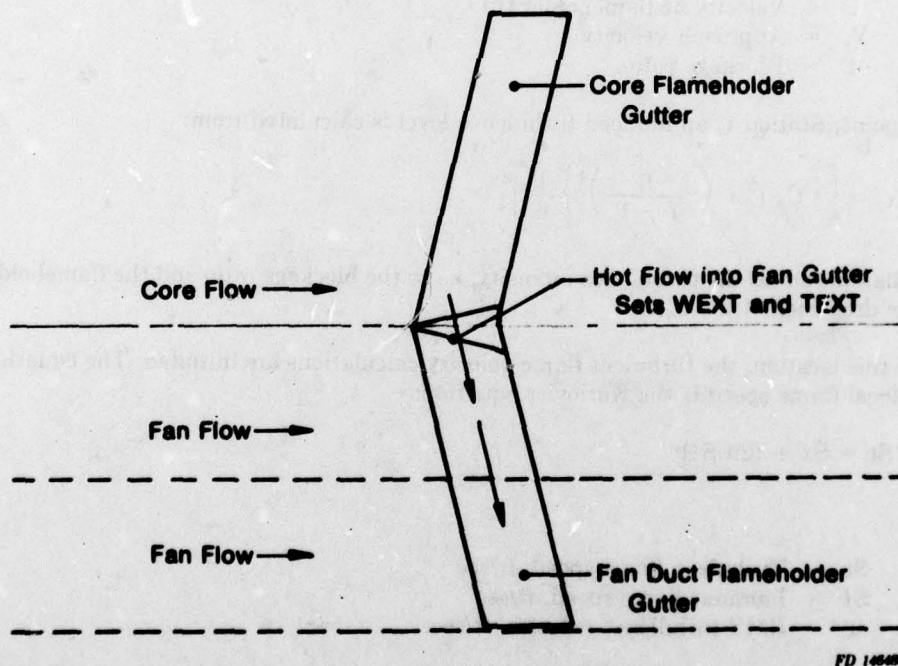


Figure 122. External Heat Addition to Fan Duct Gutters

For the purposes of current analysis, the following assumptions were made:

1. Uniform airflow profiles
2. Uniform fuel-air ratio
3. Incompressible acceleration of free air velocity by the flameholder blockage with no induced profile
4. Known wake size and reaction efficiency
5. Two-dimensional ducted flame.

The schematic of the situation which is analyzed is shown in Figure 123.

The approach flow, at known levels of pressure, temperature, velocity, and fuel-air ratio, is accelerated by the blockage of flameholder to velocity  $U$ , where:

$$U = \frac{V_a}{(1 - \Gamma)}$$

Where:

$U$  = Velocity at flameholder tip  
 $V_a$  = Approach velocity  
 $\Gamma$  = Blockage ratio.

At this point, Station 1, an induced turbulence level is calculated from:

$$\epsilon_o = \left[ \left\{ C_d \Gamma + \left( \frac{\Gamma}{1 - \Gamma} \right)^2 \right\} \frac{1}{6} \right]^{1/2} \quad (147)$$

This equation relates the turbulence intensity,  $\epsilon_o$ , to the blockage ratio and the flameholder zero blockage drag coefficient,  $C_d$ .

At this location, the turbulent flame velocity calculations are initiated. The equation used for the local flame speed is the Karlovitz equation:

$$St = St_l + (2u' St_l)^{1/2} \quad (148)$$

Where:

$St$  ~ Turbulent flame speed, ft/sec  
 $St_l$  ~ Laminar flame speed, ft/sec  
 $u'$  ~ RMS turbulence velocity, ft/sec.

The value of  $u'$  is:

$$u' = \epsilon_o U \quad (149)$$





203

Additionally, the turbulent flame speed initial value is related to the degree of initiation of the flame speed initial value is related to the degree of initiation of the flame front by the wake by the following:

$$St' = St \times \eta_w \quad (150)$$

This generates an effective turbulent flame speed which completely fills the depth of the duct and propagates at the same transverse rate as the full flame speed which does not fill the duct. This arises from the fact that the inefficiencies of the wake reaction generate localized regions where flame front ignition does not occur. This use of a reduced value effective flame speed accounts for this in a two-dimensional model.

The initial value for the augmentor efficiency is the wake reaction level on a mass weighted basis, expressed as an equation this is:

$$\eta_{c_o} = \eta_w \frac{\dot{m}_r}{\dot{m}_a} \quad (151)$$

Where:

- $\eta_{c_o} \sim$  Initial efficiency
- $\eta_w \sim$  Wake efficiency
- $\dot{m}_r \sim$  Wake mass flowrate
- $\dot{m}_a \sim$  Total duct flowrate.

The type of flame utilized in this model is a zero thickness flame which separates a region of unreacted propellants from a region of completely reacted products. From this setup, the average local augmentor efficiency is simply the ratio of the transverse flame penetration,  $\Delta y$ , to the duct width,  $w$ .

To be consistent, the transverse location of the flame front at the initial calculation station is taken to be:

$$\Delta y_o = \eta_{c_o} \cdot w \quad (160)$$

This value is assigned to the first axial station. This is assumed to occur halfway down the length of the recirculation zone. From visual observations of wake stabilized flames, this is the approximate location of transverse flame initiation.

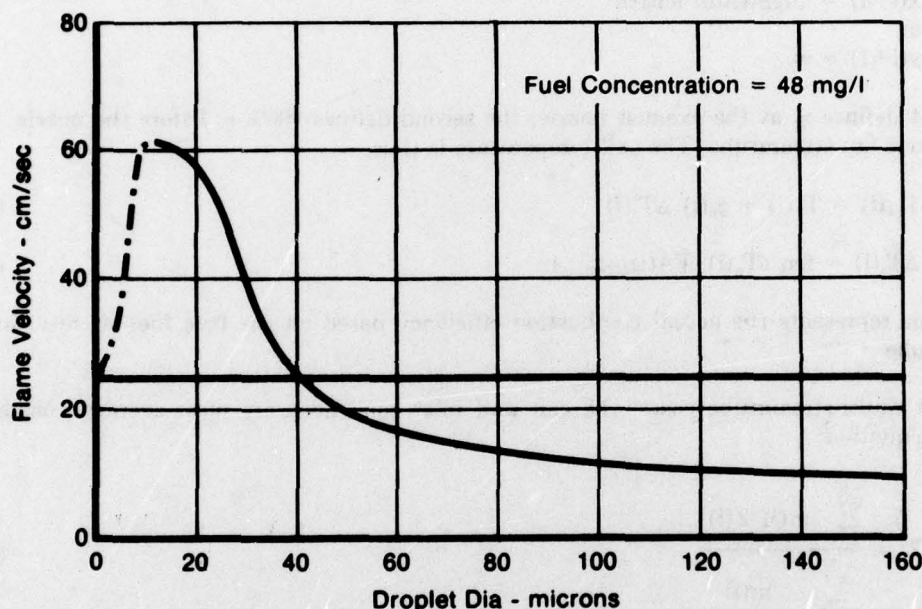
From this location downstream to the exhaust nozzle, the flame front transverse location is calculated by a finite difference integration of the local flame speed. Several axial profiles are introduced as the integration proceeds. These are:

1. The turbulence intensity is decayed from the value generated at the aft flameholder lip at a rate inversely proportional to the square root of axial distance over an effective jet length. The final value is set at the initial turbulence level. The effective jet length is set at  $10 L/D$  where the  $D$  is the open area distance between adjacent flameholders.
2. The velocity of the unreacted fuel-air mixture is retained at the level generated at the flameholder lip. Measured profiles from several ducted flame test rigs support this assumption.



3. A term is introduced which relates the local flame speed to the local average duct combustion efficiency, peaking at 50%. This treats the counteracting influences of reduced heat loss as efficiency increases and the reduced free oxygen concentration. Local rates which roughly follow a sine wave function have been reported from duct data.

An additional term is added to account for the reduction in flame speed of a fuel spray compared to a premixed flame. This term relates the ratio of effective flame speed to premixed laminar flame speed. It accounts for the complicated interactions during flame spreading in an evaporating spray in a simplified manner. The effect of the liquid droplet diameter is shown in Figure 124. The droplet diameter utilized in the analysis will be the mean diameter as it exists at the flameholder trailing edge.



FD 134098

Figure 124. Flame Speed for Monodisperse Tetralin Spray

Analysis of the terms utilized for evaluation of the laminar flame speed term,  $S_l$ , has resulted in the following:

$$S_l = S_l(\phi) \left( \frac{T_a}{540} \right)^{1.5} \left( \frac{\chi_{O_2}}{0.21} \right)^2 \quad (161)$$

where

- $S_l$  = laminar flame speed at 1 atm and 540°
- $\phi$  = equivalence ratio
- $T_a$  = air temperature, °F
- $\chi_{O_2}$  = oxygen mole fraction.

The influence of pressure is indeterminate at this time and has been incorporated as  $\sqrt{P}$  for subatmospheric data and no influence for pressures above 1 atmosphere.



The finite difference solution uses 1-in. increments in axial length as the stepping variable. This sets a time interval:

$$\Delta t = 0.0833/V. \quad (162)$$

The transverse flame penetration distance is thus

$$\Delta y = St \Delta t = y(i+1) - y(i) \quad (163)$$

where  $St$  is evaluated at the conditions of  $x = x(i)$ .

The stepping procedure terminates when either

$$\begin{aligned} x(i+1) &= \text{augmentor length} \\ \text{or} \\ y(i+1) &= w. \end{aligned}$$

The first defines  $\eta_c$  at the exhaust nozzle; the second defines 100%  $\eta_c$  before the nozzle. This defines one fan streamtube. The exit temperature is thus,

$$T_{ex}(i) = T_a(i) + \eta_c(i) \Delta T_1(i) \quad (164)$$

$$\Delta T_1(i) = \text{fcn}(T_a(i), FA(i)_{\text{effective}}). \quad (165)$$

This represents the actual combustion efficiency based on the true fuel-air ratio in the streamtube.

For multi-streamtube cases, the exit and inlet conditions are mass-averaged using the general equation:

$$Z = \frac{\sum_{i=1}^n \dot{m}(i) Z(i)}{\sum_{i=1}^n \dot{m}(i)}. \quad (166)$$

The average input fuel-air ratio and average inlet temperature combine to yield the average ideal temperature rise. The average inlet and exit temperatures yield the average actual temperature use. Thus,

$$\bar{\eta}_c = \frac{\Delta T_{\text{actual}}}{\Delta T_{\text{ideal}}}. \quad (167)$$

This is the chemical efficiency. The thermal exit efficiency assumes that the augmentor liner cooling airflow is included in the average exit temperature,

$$T_{\text{exit}} = \frac{\sum_{i=1}^n \dot{m}(i) T_{ex}(i) + \dot{m}_{\text{cool}} T_a}{\sum_{i=1}^n \dot{m}(i) + \dot{m}_{\text{cool}}}. \quad (168)$$

This reduces the average exit temperature and yields the lower value for thermal combustive efficiency. This value for  $\bar{\eta}_c$  reflects the average exit temperature based on the average input fuel-air ratio based on total fan duct airflow and fuel flow.

Before execution of the core streamtube analysis, the influence coefficients which are required are evaluated. These are of the form:

$$\frac{\partial \eta}{\partial A} \frac{\Delta}{\eta} = Z(\Delta) \quad (169)$$

where  $A = V_a, p_a, T_a$ , and  $FA$ .

They are calculated from a 1% change in the variables and the linear form:

$$\frac{\Delta \eta}{\Delta A} \frac{\bar{A}}{\bar{\eta}} = \frac{\eta_2 - \eta_1}{A_2 - A_1} \cdot \frac{(A_1 + A_2)}{(\eta_1 + \eta_2)} \quad (170)$$

where

$$A_2 = 1.01 A_1. \quad (171)$$

The value of  $\eta_2$  is obtained by execution of the analysis at all the same input as  $\eta_1$ , except  $A_1$  is replaced with  $A_2$ . Thus, the analysis is done once for base and four more times for the  $Z$  factors.

## 2. DEVELOPMENT OF THE CORE STREAM COMBUSTION EQUATIONS

The same basic analysis procedure as accomplished in the duct is used in the core with several major operational differences:

1. There is no cooling air removal from the core streamtubes. Thus, the input fuel-air ratios are used in the analysis.
2. The droplet vaporization rate is so rapid that the fuel exists only as a vapor after a couple inches from the spraybar. This removes the requirement to solve for the wake compositive since it is the same as the input fuel-air ratio.
3. The wake reaction efficiency is solved directly at the input fuel-air ratio and recirculation rates which are calculated the same as the fan duct.
4. There is no droplet size effect in the turbulent flame speed model. The rapid droplet vaporization results in gaseous phase turbulent flame penetration.

The solution for a core streamtube proceeds as follows:

- a. The set-up equations are the same as the fan streamtubes.
- b. The recirculation coefficient,  $K_1$ , is calculated the same way as done in the fan stream. This generates the value of  $A/V_o P^*$  required for the kinetics solution.
- c. The wake reaction kinetics solution is performed at the same value of fuel-air ratio as input for the streamtube.
- d. The turbulent flame penetration solution is the same as for the fan stream except that the droplet correction term is absent. The equation introduces a value for the oxygen concentration,  $\chi_{O_2}$ .



This value is less than the fan duct due to the removal of oxygen by the mainburner combustion process. This vitiation yields:

$$x_{O_2} = 0.21 \frac{(FA)_{mb}}{(FA)_{stoch}} \quad (172)$$

The analysis produces a value of  $\eta_c$  for each streamtube, i, by the same equation as used in the fan:

$$\eta_c(i) = \frac{Y(i)}{w(i)} \quad (173)$$

where  $Y(i)$  is the penetration distance transverse to the flow and  $w(i)$  is the streamtube width.

The exit temperature calculation is different from the fan duct due to the vitiation of the approach airflow and temperature removal in the turbine between the main combustor and the augmentor inlet.

The ideal temperature rise for each streamtube is evaluated by generating a fictitious main combustor inlet temperature. The procedure is as follows:

- a. For known main burner FA and streamtube inlet temperature,  $T_a(i)$ , a fictitious  $\Delta T$ , is read from a curve as in Figure 125.
- b. A fictitious main burner inlet temperature is calculated:

$$T_{mb}(i) = T_a(i) - \Delta T_{fict}(i) \quad (174)$$

- c. An overall fuel-air ratio is calculated:

$$FA_{oa}(i) = FA_{mb} + FA(i) \quad (175)$$

- d. With  $FA = (FA)_{oa}(i)$  and  $T = T_{mb}(i)$ , the overall effective temperature rise is read from the ideal temperature rise curve.
- e. The streamtube exit temperature is

$$T_{ex}(i) = \Delta T_i(i) + T_{mb}(i) \quad (176)$$

- f. The streamtube net ideal temperature rise is thus

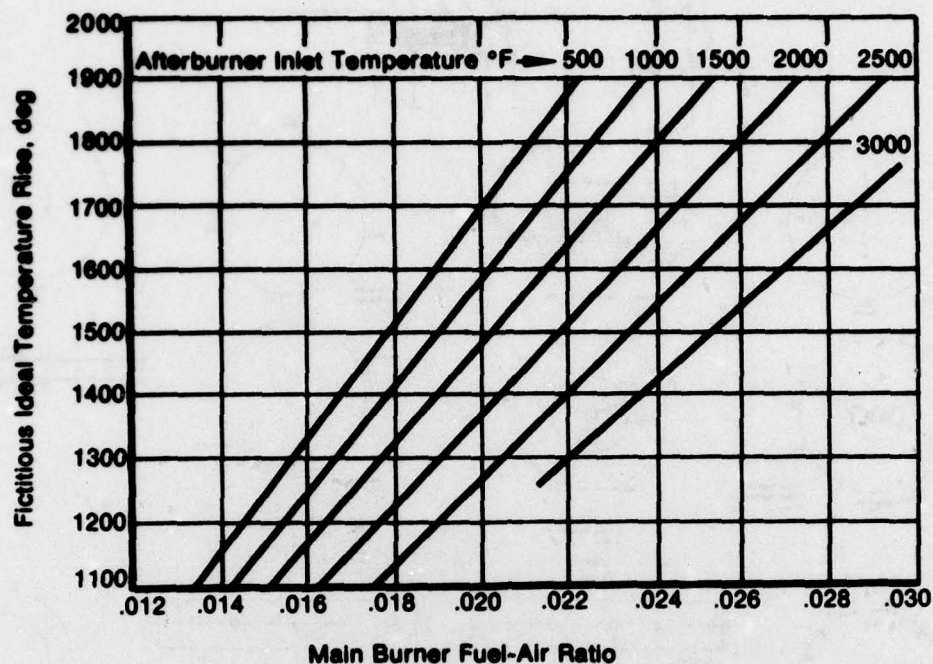
$$\Delta T'_i(i) = T_{ex}(i) - T_a(i) \quad (177)$$

This value is calculated for each streamtube and used exactly as the ideal  $\Delta T$  curve is used in the fan streams. The streamtube exit temperature is:

$$T_{ex actual}(i) = T_a(i) + \eta_c \Delta T'_i(i) \quad (178)$$

The inlet temperatures and fuel-air ratios are mass-averaged as is the exit temperature, using equation (166).





FD 146490

Figure 125. Fictitious Temperature Rise vs Main Burner Fuel-Air Ratio

The overall core efficiency is calculated from steps (a) to (f) using average inlet conditions to yield the average ideal  $\Delta T$  and equations (178) and (166) for the average exit temperature:

$$\bar{\Delta T}_{\text{actual}} = T_{\text{exit}} - T_a \quad (179)$$

$$\bar{\eta}_c = \frac{\bar{\Delta T}_{\text{actual}}}{\bar{\Delta T}_i} \quad (180)$$

The influence coefficients, as shown in equations (169) to (173), are evaluated as was done in the fan.



210

## REFERENCES

1. "Flameholder Combustion Instability Study," Air Force Aero Propulsion Laboratory, AFAPL-TR-78-24, May 1978.
2. Petrien, R. J., J. P. Longwell, and M. A. Weiss, "Flame Spreading from Baffles," *Jet Propulsion*, Feb. 1957, p. 81.
3. Ernst, R. C., "Development of an Augmentor Combustion Model for Low Frequency Instability Prediction (Rumble), Interim Report," Pratt & Whitney Aircraft FTDM 612, 31 December 1974.
4. "Flameholder Combustion Instability Study, Interim Report," Pratt & Whitney Aircraft, FR-8504, 30 April 1977.
5. "Advanced Augmentation System, Final Report," PWA-5261, September 1975.
6. Clements, T. R., "Effect of Swirling Flow on Augmentor Performance, Phase II Final Report," NASA CR 135024, June 1976.
7. "Combined Augmentor Rumble/Flameholder Combustion Model User's Manual for Deck CCD 1144-0.0," Pratt & Whitney Aircraft, FR-9797, 27 March 1978.